DEVELOPMENT OF OPTIMUM WINDOW SIZE IN TROPICAL CLIMATE USING COMPUTATIONAL FLUID DYNAMICS AND EXPERIMENTAL WORKS

By

ALI MOHAMED WAHHAD

Thesis Submitted to the School of Graduate Studies, Universiti Putra Malaysia, in Fulfillment of the Requirements for the Degree of Doctor of Philosophy

June 2016

Abstract of thesis presented to the Senate of Universiti Putra Malaysia in fulfillment of the requirement for the Degree of Doctor of Philosophy

DEVELOPMENT OF OPTIMUM WINDOW SIZE IN TROPICAL CLIMATE USING COMPUTATIONAL FLUID DYNAMICS AND EXPERIMENTAL WORKS

By

ALI MOHAMED A.WAHHAD

June 2016

Chairman : Associate Professor Nor Mariah Adam, PhD
Faculty : Engineering

Windows play an important role in heat transfer and natural ventilation in buildings while allowing many psychological benefits to the occupants. The goal of any office building is to provide a thermally comfortable indoor environment that requires the least energy consumption to maintain throughout the year. One of the energy reduction alternatives that can be incorporated in modern green building design is the installation of efficient windows. The windows should allow thermally acceptable indoor air quality, be operated easily, and have a pleasant design while being energy efficient.

Full-scale measurements were conducted in an office room to analyze the performance of the ventilation system. Air temperature, air velocity, wall temperatures, and humidity were measured. The experimental results together and computational fluid dynamics (CFD) analysis show that ventilation in an office with the model window can remove indoor pollutants efficiently. The thermal comfort prediction used Fanger's method, which was proposed in ISO Standard 7730. Data analysis revealed that the predicted mean vote (PMV) standard equation was thermally neutral.

The objective of this work is to design window sizes for tropical climates using CFD code FLUENT version 6.3 and ANSYS for geometric generation. Input parameters were obtained from an office on the fifth level of a seven-story building; such a building is representative of typical government office buildings in Malaysia and in Hoon, Libya. Input parameters were air temperature, air velocity, and relative humidity. The k-ε for turbulent flow and finite volume method (FVM) with SIMPLE algorithm for treatment of boundary layers was used. The ideal window should create a temperature difference of at least 5 K between indoors and outdoors, with air velocity in the center of room being > 0.01 m/s.

The study examines 36 models of a double-glazed window with three opening windows for controlling fresh air intake flow, i.e., the side-ahead (A), top (B), and bottom (C) opening windows. Of these models, the CFD results of this study showed that a 22% window to wall ratio (WWR) with the (A) opening (height 2 m and width 0.4 m) is the best model in Malaysia. In Libya, 22% window to wall ratio (WWR) with the (A) opening (height 2 m and width 0.8 m) is the best model. The temperature inside the office of the optimum model was 300.1 K, and airflow was 0.36 m/s at 15 cm above the ground office; the outdoor temperature was 307.6 K, and airflow was 0.67 m/s.

Abstrak tesis yang dikemukakan kepada Senat Universiti Putra Malaysia
sebagai memenuhi keperluan untuk Ijazah Doktor Falsafah

PEMBANGUNAN SAIZ TINGKAP YANG OPTIMUM DALAM KAWASAN IKLIM TROPIKAL MENGGUNAKAN DINAMIK BENDALIR PENGKOMPUTERAN DAN EKSPERIMEN

Oleh

ALI MOHAMED A.WAHHAD

Jun 2016

Pengerusi : Profesor Madya Nor Mariah Adam, PhD
Fakulti : Kejuruteraan

Tingkap memainkan peranan penting dalam pemindahan haba dan pengudaraan semulajadi di dalam bangunan, di samping membenarkan banyak manfaat psikologi kepada penghuninya. Matlamat mana-mana bangunan pejabat adalah untuk menyediakan satu persekitaran dalaman termal-keselesaan, yang memerlukan jumlah penggunaan tenaga yang paling kurang untuk mengekalkan keadaan itu sepanjang tahun. Salah satu alternatif pengurangan tenaga yang boleh dimasukkan dalam rekabentuk bangunan hijan adalah pemasangan tingkap cekap. Tetingkap patut dapat membenarkan haba diterima untuk mewujudkan kualiti udara dalaman yang sesuai, mudah dikendalikan dan reka bentuk yang menyenangkan pandangan lagi cekap tenaga.

Satu ukuran skala penuh dibuat di sebuah bilik pejabat untuk menganalisis prestasi sistem pengudaraan. merangkumi suhu udara, halaju udara, suhu dinding, kelembapan relatif. Keputusan eksperimen bersama-sama dengan analisis CFD yang menunjukkan bahawa pengudaraan di pejabat dengan tingkap model mampu keluarkan pencemar dalaman dengan cara yang cekap. Keselesaan haba telah diramal oleh kaedah Fanger yang dicadangkan dalam ISO Standard 7730. Analisis data menunjukkan bahawa ramalar (PMV) adalah headaan neutral terma.

Objektif kajian ini adalah untuk merekabentuk tingkap optimum untuk iklim tropika menggunakan pengkomputeran bendalir dinamik kod FLUENT versi 6.3 dan ANSYS untuk menjana geometri tingkap. Parameter input diperolehi daripada pengukuran di pejabat Aras Lima pada sebuah bangunan tujuh tingkat yang mewakili pejabat kerajaan khusus untuk pejabat awam di Malaysia dan juga bangunan pejabat di Hoon Selatan Libya. Parameter input adalah suhu udara, kelajuaan udara dan kelembapan relative. Kaedah k-ε bagi aliran gelora dan kaedah isipadu terhingga (FVM) dengan algoritma SIMPLE untuk rawatan lapisan sempadan telah digunakan. Tunhgkap unggul mewujudkan perbezaan suhu

sekurang-kurangnya 5K antara dalaman dan luar bangunan dengan kelajuan udara di tengah-tengah bilik > 0.01 m/s.

Kajian ini mengkaji tiga puluh enam model tingkap kaca berlapis dengan tiga tmod bukaan untuk mengawal aliran pengambilan udara segar iaitu sampingan hadapan, (A), ke atas (B), dan kebawah (C) membuka tingkap. Pencarian CFD menghasilkan tetingkap yang 22% kepada nisbah (WWR) dengan (A) pembukaan dinding (ketinggian 2m dan lebar 0.4 m) adalah model yang terbaik Malaysia dan 2m tinggi x 0.8 m lebar terbaik Libya daripada tiga puluh enam model, manakala suhu di dalam pejabat model optimum tetingkap adalah 300,1 K dan aliran udara 0.36 m / s di ke atas 15 cm m dari lantai pejabat apabila ukuran luaran suhu adalah 307K dan aliran udara 0.67 m / s.

ACKNOWLEDGEMENTS

First of all, I give my great thanks to the Most Gracious and Most Merciful, Allah (S.W.T). Without His wish and help, this work would not have been possible. I also would like to express my most sincere appreciation to those who took the time, interest, and effort in guiding, helping, and supporting me throughout the implementation of this work.

I would like to thank Associate Professor Ir. Dr. Nor Mariah Adam and Professor Mohd Sapuan Salit for giving me the opportunity to complete my PhD studies under their valuable guidance, for their useful advice and discussions, for their constant encouragement and guidance, and for co-authoring my publications. Their practical experience and technical knowledge made this research and those publications more interesting and relevant.

Thanks and acknowledgments are meaningless if they are not extended to my parents who deserve my deepest appreciation. I am grateful for the countless sacrifices they made to ensure that I could pursue my dreams and for always being there for me. My real and deepest thanks go to them. Finally, very special thanks go to my wife, my daughters, my sons, my brothers, and my sisters; they are my confidantes and true loves. Their love, support, and encouragement are behind my success.

I certify that a Thesis Examination Committee has met on 21 June 2016 to conduct the final examination of Ali Mohamed Wahhad on his thesis entitled "Development of Optimum Window Size in Tropical Climate using Computational Fluid Dynamics and Experimental Works" in accordance with the Universities and University Colleges Act 1971 and the Constitution of the Universiti Putra Malaysia [P.U.(A) 106] 15 March 1998. The Committee recommends that the student be awarded the Doctor of Philosophy.

Members of the Thesis Examination Committee were as follows:

Barkawi bin Sahari, PhD
Professor Ir.
Faculty of Engineering
Universiti Putra Malaysia
(Chairman)

Kamarul Arifin Ahmad, PhD
Associate Professor Ir.
Faculty of Engineering
Universiti Putra Malaysia
(Internal Examiner)

Renuganth a/l Varatharajoo, PhD
Professor Ir.
Faculty of Engineering
Universiti Putra Malaysia
(Internal Examiner)

Wong Nyuk Hien, PhD
Professor
National University of Singapore
Singapore
(External Examiner)

ZULKARNAIN ZAINAL, PhD
Professor and Deputy Dean
School of Graduate Studies
Universiti Putra Malaysia

Date: 23 August 2016

This thesis was submitted to the Senate of Universiti Putra Malaysia and has been accepted as fulfillment of the requirement for the degree of Doctor of Philosophy. The members of the Supervisory Committee were as follows:

Nor Mariah Adam, PhD
Associate Professor/Ir
Faculty of Engineering
Universiti Putra Malaysia
(Chairman)

Mohd Sapuan Salit, PhD
Professor/Ir
Faculty of Engineering
Universiti Putra Malaysia
(Member)

Mohd Khairol Anuar Mohd Ariffin, **PhD**
Associate Professor/Ir
Faculty of Engineering
Universiti Putra Malaysia
(Member)

BUJANG BIN KIM HUAT, PhD
Professor and Dean
School of Graduate Studies
Universiti Putra Malaysia

Date:

Declaration by graduate student

I hereby confirm that:

- this thesis is my original work;
- quotations, illustrations and citations have been duly referenced;
- this thesis has not been submitted previously or concurrently for any other degree at any institutions;
- intellectual property from the thesis and copyright of thesis are fully-owned by Universiti Putra Malaysia, as according to the Universiti Putra Malaysia (Research) Rules 2012;
- written permission must be obtained from supervisor and the office of Deputy Vice-Chancellor (Research and innovation) before thesis is published (in the form of written, printed or in electronic form) including books, journals, modules, proceedings, popular writings, seminar papers, manuscripts, posters, reports, lecture notes, learning modules or any other materials as stated in the Universiti Putra Malaysia (Research) Rules 2012;
- there is no plagiarism or data falsification/fabrication in the thesis, and scholarly integrity is upheld as according to the Universiti Putra Malaysia (Graduate Studies) Rules 2003 (Revision 2012-2013) and the Universiti Putra Malaysia (Research) Rules 2012. The thesis has undergone plagiarism detection software

Signature: _____ Date: _____

Name and Matric No: Ali Mohamed Wahhad, GS23354

Declaration by Members of Supervisory Committee

This is to confirm that:

- the research conducted and the writing of this thesis was under our supervision;
- supervision responsibilities as stated in the Universiti Putra Malaysia (Graduate Studies) Rules 2003 (Revision 2012-2013) were adhered to.

Signature: _____
Name of Chairman of Supervisory Committee: Associate Professor Dr. Nor Mariah Adam

Signature: _____
Name of Member of Supervisory Committee: Professor Dr. Mohd Sapuan Salit

Signature: _____
Name of Member of Supervisory Committee: Associate Professor Dr. Mohd Khairol Anuar Mohd Ariffin

TABLE OF CONTENTS

LIST OF TABLES

LIST OF FIGURES

LIST OF ABBREVIATIONS

Symbols	Name	Unit
A	Area	m^2
C	Specific heat	J / kgK
d	Thickness of glass	m
C_p	Specific heat	(J/kg K)
g	Standard gravitational acceleration	m/s^2
G_{rL}	Grashof number	
h_c	Heat transfer coefficient of convection	$W/m^2 K$
k	Thermal conductivity	W/ m K
Nu	Nusselt number	
q	Heat flux	W/m^2
Ra	Rayleigh number	
Re	Reynolds number	
Pr	Prandtl number	
t	Time	second
T_∞	Air temperature	^oC
T_{sur}	Surrounding temperature	^oC
Δ_T	Temperature difference	^oC
T_S	Surface temperature	^oC
q	Solar radiation intensity passing through glass	kJ
$q_{CONV.}$	Convection heat flow	W
$q_{rad.}$	Irradiation heat flow	W

SHGC	Solar heat gain coefficient	
SC	Shading coefficient	
VT	Visible transmittance	
V	Volume	m^3
X	Local position along the X-direction	
Y	Local position along the Y-direction	

Greek	**Name**	**Unit**
α	Thermal diffusivity	m^2/s
ρ	Density	kg/m^3
η	Total transmittance	N/m^2
ε	Emissivity of materials	
μ	Dynamics viscosity	N/ms

Subscript	**Name**	**Units**
∞	Ambient	
α	Absorptances of glass window and glass with film	
σ	Stefan–Boltzmann constant	$W/m^2 . K^4$
τ	Transmittance of glass	
ρ	Air density	kg/m^3
V_r	Ventilation rate	
C	Air specific heat	J/kg-K
$T_o - T_i$	Temperature difference	K
Pw	Wind-induced pressure	Pa
C_p	Pressure coefficient	

ρ_u	External air density	kg
v_{ref}	Wind speed at a reference height	m/s
P	External or internal pressure	Pa
$P_{i,o}$	Pressure at a reference level (floor)	
ρ_o	External or internal air density	kg/m^3
g	Gravitational acceleration	m/s^2
H	Height above the reference level	m
PVM	Predicts mean value	
PPD	Predicted percent of dissatisfied	

CHAPTER 1

INTRODUCTION

1.1 Background of the Thesis

As most people spend most (90%) of their time indoors, and often share the same space, knowledge and prediction of conditions in the indoor environment is important for the well -being and productivity of occupants. Moreover windows have a significant effect on the energy performance of a building, and shading devices that have been used for long time to control solar gain and day lighting. Shading windows using coatings has been widely adopted although it has been regarded as a temporary measure, Whaad et al. 2008), and solar radiation tends to increase the surface temperature of the glass Carmody et al. (2000). Window also provide feeling of good being when occupant can look outside yet economically viable to provide thermally comfortable environment Carmody et al. (2000).

Green buildings incorporate passive methods for energy efficiency which is applied at the design phase. Some parameters listed for green building index include energy efficiency initiatives (20%), daylighting (10%) and indoor air quality (29%). These parameters can be linked to window design. Windows are considered as being the site for a predictable thermal radiation. The solar irradiation can exchange through a window during the course of the day. Insulated double or triple glazing; shading devices and orientation of windows can reduce solar heat gain through windows, U.S. Department of Energy, accepted (1997). Today, large government's offices buildings usually have installed large amount of glass windows in the building for cade.

The solar load of direct and diffused solar irradiation that penetrate through the windows are considered to be the source of the external heat load and that depends on many factors such as time of year, time of day an office orientation and installation of solar shading to the windows, the velocity and direction of external wind and in addiction type of window. The external convection may be higher than the internal convection during the summer period especially if large windows are installed in the buildings. Natural ventilation and air conditioning can be used to control indoor temperature and to cool offices in building, ASHRAE Standard 55(2004).

Double glazed windows are assumed to have a greater importance in actual building practice, Oesterle, et al. (2001). An experimental investigation of the novel glass system is designed to overcome the glare and excessing heat gain such that it may improve visual comfort even in spaces with large glazed areas facing east or west, Etzion, et al. (2000). Interface effects of double glazed with ventilation for energy, thermal comfort, ventilation system and energy consumption compared to a single

system without interface glazed has shown promising benefits for green homes and buildings, Wong Nyuk, (2005).
To drive the flow of fresh air through buildings, natural ventilation systems will be effective for this matter and in which these systems rely on natural driving forces, such as wind and temperature difference between buildings and its environment. (Stack effect, pressure effect), both work on the principle of air moving from a high pressure to a low pressure zon, Guohui (2000).

Eftekhari, (1995) measured air velocities and air temperatures in a ventilated single-sided office. The results have shown that high air speeds and low temperatures at floor level and the opposite at head level, which indicates that the fresh and cool air is distributing along the floor in the office. Velocity levels up to 0.4m/s was found at floor level. Rooms with single-sided cross natural ventilation have their effective depth of fresh air distribution which had induced by pressure difference due to room geometry Guobui, G. (2000). This effective depth can be determined by some methods such as a numerical (CFD) technique which is developed for determination of the effective depth of air distribution in rooms with single-sided natural ventilation. The results of such a technique had shown that the effective depth for thermal comfort might not be coincided with that for air quality during the summer. The requirement for thermal comfort is the limiting factor to the effective room depth. The investigation has shown the effectiveness of window opening levels and room heat gains on the air flow rate and effective depth. This technique is effective for temperature climate where temperature difference between indoor and outdoor is high (>5°C), Guohui (2000).

Mokhtarzadeh, Dehghan (2011) performed a numerical study of the rate of heat transfer associated with ventilation at the side and across the room generated by the wind. Examination room was represented by two-dimensional rectangular cavity exposed to an external flow from one side only. The examined room was represented by a rectangular two-dimensional cavity which was exposed to the external flow from one side only.

Schaelin et al., (1992) used two- and three-dimensional CFD techniques in order to simulate the bi-directional flow through large openings in buildings by coupling indoor airflow to the outdoor flow. These researchers focused on the major flow without putting into account the details of flow near the wall, and heat transfer. Recognizing the importance of air flow through the large openings in the natural ventilation of single-sided room, Teh K. and Li, S.L. (1996) studied numerically ventilation rate in a room with an open window with using low-Reynolds-number two-dimensional and turbulence model.

1.2 Problem Statement

The tropical climate like Malaysia has constantly high temperatures and relative humidity and that is due to the location of Malaysia which is close to the equator where the temperature ranges between 25 ℃ to 35 ℃ throughout the year. The mean daily temperature is about 27 ℃ and humidity values may exceed 80%. The climate is highly affected by the two monsoon rains seasons with southwest and northeast monsoon, Rahman (2005).

One passive method of thermal performance in reducing heat load and glare is through the use of double e-Low glazed windows on offices in Libya and with the increase of passive cooling which significantly contributes to energy saving for building operators. Ardalan et al (2015) proposed the window to wall ratio (WWR) as one indicator to determine size of window openings for energy conservation in buildings thus this is one of the criteria chosen for optimum window design. Proposing a better model design of window dimensions using CFD to reduce heat load and glare into offices through the double glazed window in Malaysia can help building professionals in producing green buildings.

Although the use of air conditioning system is necessary to maintain a healthy and productive indoor environment in the tropical and desert buildings it is usually consume a large proportion 0.7025 of the energy cost operating the building. Acquisition of the air conditioning system is also a concern for the building engineers as there are several factors that need to be considered e.g. variable or non-variable volume, choice of refrigerant, sizing, control of particulates etc. There are two problem statements available for this research :(Zain Ahmed, (2008).

i. The buildings in hot dry climate like south Libya has been a serious problem due to the high temperatures, high solar irradiation but low humidity level and low air velocity, Adel Akair and László Bánhidi, (2007). These factors can result to decrease in the indoor comfortable condition in buildings during the hot summer days. The internal heat load can be higher than the external load especially if the building has large windows resulting from high solar irradiation level entering through window during the day time. Solar heat gain through windows can be reduced by insulated glazing, shading devices, orientation of building and type of window, Department of Energy (1997).

ii. Hot humid tropical conditions like in Malaysia, where the high outdoor temperature, high humidity and poor air flow may lead to decrease in indoor comfortable condition in offices. Due to the high intensity of solar irradiation through window causes significant cooling requirements. Large glass wall with two sided openable windows cannot provide good passive ventilation strategy in building. The increase in air velocity inside the office to remove internal heat and large temperature difference between outdoor and indoor can be achieved through passive cooling. The air that is moved through the exchange of indoor with "fresh" outdoor air can provide cooling and act as a heat carrier medium, Abdul Majid Ismail, (2015**)**.

Abdul Rahman and Ismail (2008) reported that the buildings in Malaysia consume about 70% of energy for cooling the indoor environment, and Zain-Ahmed (2008) reported that more than 40% of the energy consumed by the Malaysian buildings can be reduced if energy efficiency as well as application of sustainable technologies for building is implemented. With increasing number of buildings, high fuel cost can push green buildings in Malaysia; to adopt design of suitable window size is logical option to further tap green initiatives.

Roetzel et al (2010) investigated air flow of wind through natural ventilation single-side ventilation. The study recommends that people control natural ventilation is through several parameters, such as windows open type, size of windows, shape of window, and number of the windows and placement, Gratia and De Herde (2004).

The variables that are related to a direct effect in the building thermal environmental analysis consists of ambient air temperature, solar radiation, temperature of surfaces, outdoor humidity, velocity and direction of wind, Katunsky et al. (2013).

Standards Association of Australia presented in clause 4.8 stated that a flow rate of 0.03 m^3/s to 0.04 m^3/s through residential buildings (offices, residences, shops, stores, corridors) was generally suitable for natural ventilation. Rajapaksha (2004) shows that in Malaysia, comfortable indoor temperature should be in the range 25.5^oC to 28^oC. humidity 40% to 60% an optimum air movement 0.3 m/s to 0.5m/s for a naturally ventilated condition. Accordingly ASHRAE standard on thermal comfort in Malaysia could be achieved below 28. 69 C^o, ASHRAE (2012)

Window provides passive strategy to increase indoors ventilation without active use of energy. Cheong (2003) used computational fluid (CFD) PHOENICS software to simulate 3D numerical simulation for the air conditioned lecture hall environment in Singapore. Parameters considered were the field air velocity and air temperature where predicted and measured inside conditions were in great agreement (8.23%). This proves that it is possible to simulate indoor conditions using numerical method for the tropics.

Carlos et al, (2011) used double glazed windows to predict indoor and outdoor environment. The parameters were incident solar radiation, airflow rate and temperature difference between indoor and outdoor. Ooi et al. (2007) used CFD to achieve the maximum comfort for the occupant. The k–ε and Reynolds stress models for turbulent flow were used for the analysis. Jiang and Chen (2002) examined the effective use of natural cross ventilation in buildings. Ayad (1999) applied CFD study of natural ventilation for the room with different opening formations while Jong T. de and Bot G. P. A. (1992) showed full-scale set up to measure window parameters for air flow by one-side opening casement windows. Angalee at el. (2012) investigated wind driven natural ventilation system by using CFD in building with multiple windows. Dahlan et al., (2011) assessed the influences of operative

temperature in three non-air-conditioned multi-store hostels in Malaysia where an operable window-to-wall ratio of 30% was studied by Wang Liping et al., (2007).

Assem and Al-Mumin (2010) investigated the effect of glazing type and other energy conservation measures on the peak power demand of air-conditioning systems for fully glazed government and private office buildings in hot countries. Qiong Li, et al. (2009) used CFD to evaluate the thermal environment in the indoor. To summarize, it is possible to use CFD to predict indoor environment for both naturally and air conditioned situations and that window openings and formation to some extent affect indoor environment of naturally ventilated buildings in the tropics.

Limited studies have been reported for window design in Malaysia yet it is one of the important areas to improve ventilation in naturally ventilated buildings. Therefore for Malaysian conditions the double glazing window is possible to be designed and it is able to have temperature difference between the inside and outside by 6.8^0c with air velocity of 0.36 m/s where distance is 2 m from glass window at 13:20 pm with the use of a computational fluid dynamics (CFD) program (FLUENT version 6.3).

1.3 Objectives of Thesis

The main objective of this thesis is to develop design for window size for naturally ventilated room capable of providing temperature difference between inside and outside temperature by at least $6\,^{o}$C and internal air velocity >0.01 m/s using computational fluid dynamics through 36 window dimensions at 15 cm (skirting height) from the floor.

The specific objectives are as follows:

1. To develop model for window size design under tropical climate condition.
2. To predict pertinent parameters for thermal comfort inside building based on window size.
3. To develop model for optimum window design under tropical climate conditions.

1.4 Scope and Limitations

In order to design optimum window size, the air flow was assumed to be turbulent model (k-ε) difference for window design, Joel H.et al (1999). The indoor ventilation is a major issue and the air temperature, solar radiation, humidity and air velocity are of the most important parameters affecting the natural ventilation inside the buildings. Level 5 of Faculty of Engineering, Universiti Putra Malaysia has been chosen as a standard office room because it represents a typical office size in

Malaysia and away from end effects. The data collection was between June to August 2013. For desert climate an office was selected in Hoon city, South Libya in summer of 2009 and experimental data were used as input variables for the software FLUENT version.

The air flow is limited to the turbulent flow regime. The different models of window to wall ratio (WWR) were 12%, 20%, 22, 32%, 34%, 43%, 51%, 54%, 67% and 84%. Thirty-six models, (head, top and Bottom) opening windows have been chosen.

1.5 Significance of Thesis

This study is about passive strategy to improve thermal comfort in naturally ventilated office or room through window size.

Modern government offices and commercial buildings are equipped with huge heat loads for the air-conditioning systems. In the 1990s, there was a concern about global warming resulted in a resurgence of interest in natural cooling strategies, including the use of solar protections, Allard et.al (1998). The addition of a double-skin decreases the heating loads by 11.3% to 13%. It is observed that the greatest reduction is done by the northern double-skin, indeed, in this case, the southern zones benefit fully from the solar profits which are not filtered by the double-skin and the northern zones are protected by a buffer space, Gratia et.al (2004).

Double-glazed facades are assumed to have a great importance in modern building practices. They have been already a common feature in architectural competitions in Europe; but there are still relatively few buildings in which they have actually been used, and there is too little information on their behavior during operation Zöllner et.al (2002).

1.6 Outlines of Thesis

The thesis is comprised of seven chapters organized in the following way:

Chapter 1: provides the general background of heat transfer and natural ventilation for offices in building and shading for windows; introduces subjects related to this research; defines the problem statement, and research objectives. In addition, it includes the scope and limitation of this research.

Chapter 2: presents literature review: This chapter reviews up-to-date literatures on the subject matter. The chapter also provides the reader with insights of the latest development.

Chapter 3: describes the Materials and Methods used in this research. The experiment is described, which includes a preparation process of a test room conducted in office building located in Libya and Malaysia, Calibration of thermocouple wires for installation of thermocouple wires, windows that are chosen, data collection of air temperature, air velocity, solar irradiation, relative humidity using data-logger, other measuring equipment and a simulation works using commercial software.

Chapter 4: presents results analyses and discussions of the different approaches used in the case studies (experiments and numerical results).

Chapter 5: Optimum Design of Window Configuration, Modelling methodology, analysis of models by CFD, and results and discussion of Numerical Model

Chapter 6: Conclusions and Recommendations: This chapter concludes the findings of each objective and recommends areas for future works.

CHAPTER 2

LITERATURE REVIEW

2.1 Introduction

Wind and solar energy are the most important and amply available natural resources that can be used for natural ventilation in buildings. With proper design, they can represent an alternative technology to reduce energy consumption in buildings and facilitate thermally comfortable and healthy indoor conditions. This chapter describes the principal contents of the reviewed literature in both desert and tropical buildings.

2.2 Heat Transfer through Buildings and Windows

The transfer of heat through buildings depends on many external factors, including weather, orientation of buildings, solar shades of a building, size, design, shape of window, direction, and velocity of the wind Dr. Bin Su, accessed (2014). More heat gain occurs through large windows. The position of the sun is also a major factor in heat gain.

Windows play an important role in the transfer of heat into buildings. They create a psychological atmosphere (daylighting) and to some extent thermal comfort for the building's occupants Hotman J. (2002). Figure 2.1 shows the thermal performance of a glazed window, Ismail (2003).

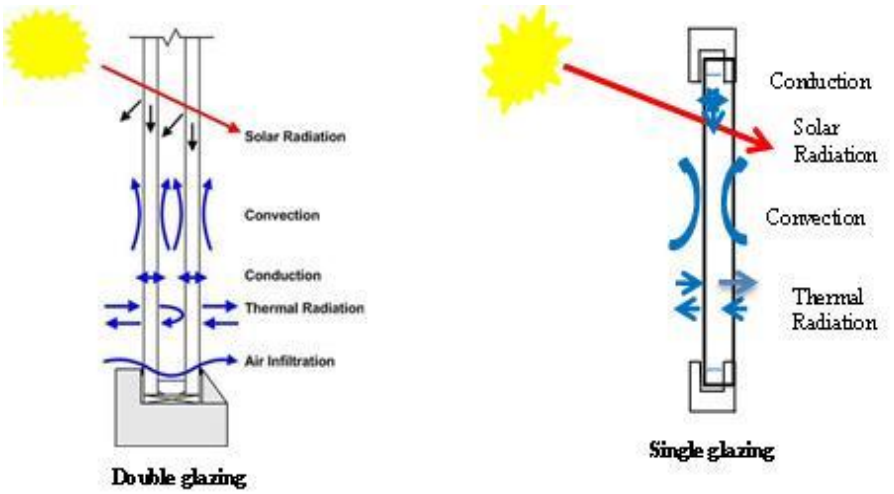

Figure 2.1 : Thermal performances through glazed window (Ismail 2003).

Solar heat gain coefficient (SHGC), shading coefficient (SC), U-factor, and visible transmittance are the best features of thermal performance. These characteristics and

the visible transmittance of daylight play an important role in energy use in buildings. Other important window terminology includes window-wall ratio (WWR) and projection factor (PF), Department of Energy (1997).

2.2.1 Solar Heat Gain Coefficient

SHGC a major characteristic of the incident energy of windows that can control solar heat gain through glass (WINDOWS TECHNOLOGIES). Solar heat is divided into direct and diffuse irradiation. Some of the radiation is transmitted directly through the glass into the building, and some is absorbed from the glass and frame of window; this radiation is also indirectly absorbed into buildings by convection, conduction, and radiation heat transfer (WINDOWS TECHNOLOGIES). Generally, windows with low SHGC values are used in buildings with high air conditioning load, whereas windows that have high SHGC values are used in buildings that need passive solar heating Holman J. (2002).

2.2.2 Shading Coefficient

Windows are installed in buildings for natural ventilation and lighting. Studies have been conducted on improving thermal comfort and health in indoor environments and access to natural light. The window is also the main barrier, albeit a weak one, between inside and outdoor conditions. Presently, high-performance energy efficient window and glazing systems are used to reduce heat and leakage, thereby improving comfort and reducing condensation. High-performance windows are characterized by double or triple glazing, transparent coating, and inert gas between layers of glass. The shading coefficient of heat transfer is the value that identifies one type of thermal performance glass in the building, Hotman J. (2002).

2.2.3 U-Value

The *U*-factor indicates the inverse rate of heat transfer through the window in the unit area and per unit temperature difference. The windows gain heat from the outside during summer and lose heat to the outside during winter. Three heat transfer methods occur through windows. Conduction carries the heat through frame walls and layers of glass. Convection occurs during the transfer of heat between the air and surface glass. Thermal radiation emits heat through glass into the room. These heat transfer modes need to accurately estimate heat loss or gain through the window in the summer. The *U*-factors are typically roughly 0.2 (for multi-paned windows with high-performance coating, low emissivity or low-E, and insulated frames). Low-E coating for glazing, reflective coating, and tinted glass help to reduce the SHGC, Hotman J. (2002).

2.2.4 Visible Daylight Transmittance

Visible daylight transmittance is the percentage of visible light that strikes the glass; this light will pass through the window. Daylight is controlled from direct sunlight;

skylight diffuses natural light into the building. Glazing with high visible transmittance appears relatively clear and provides adequate daylight and views but will create problems with glare. Glazing with low permeability is best used if the visible glare conditions are very strong, but it may be because dim interiors under certain weather conditions. Table 2.1 shows the characteristics of glass type. Good illumination in the building through the window depends on the following three factors; (a) window to floor area ratio (WFR) = (a.b) / (L.W), (b) visible light transmittance of the glazing coating to the total visible light that is incident on the window glazing, and (c) high visual light transmission (VLT) that results in high amounts of daylight entering the building through the glazing window. Double-skin façades, which are used primarily to reduce heating or cooling loads of the building, can also be used for lighting and ventilation, Gratia and Herde (2003).

Table 2.1 : Characteristics of glasses, energy efficiency windows, accepted (2012)

	Glazing type			
	glazed double pane	Tint low-e (e = 0.1)	Clear low-e (e = 0.2)	Reflective low-e
Total solar transmission (SHGC)	0.701	0.377	0.633	0.124
Direct solar transmission	0.604	0.284	0.531	0.058
Light transmission, TV	0.781	0.444	0.721	0.895
U-value (W/($\mathbf{m^2}$K)) (air)	2.711	1.776	1.95	1.638

The rate of heat conduction through the glass window is proportional to the average thermal conductivity, the wall area, and the temperature difference, but is inversely proportional to the glass wall thickness. This scenario is analogous to Ohm's law, in which the electrical resistance is defined as the ratio of the voltage drop across a resistor to the current flow across the resistor and the heat transfer (q). The thermal resistance of the glass against the heat conduction resistance of the wall glass window and the ratio temperature difference (TD) depends on the geometry and thermal properties of the materials Hotman J. (2002).

2.2.5 Heat Transfer Coefficient Calculation

The convective and radiation heat transfer coefficients were calculated in this study by using the following equations Holman, (2001); the properties of air are shown in Table 2.2

$$q = q_{conv.} + q_{rad..} = h_c A(T_s - T_\infty) + \varepsilon\sigma A(T_s^4 - T_{sur.}^4) \qquad (2.1)$$

Where;

q	Total heat flow
q_{conv}	Convection heat flow
q_{rad}	Radiation heat flow

The film temperature is determined as follows: (Holman**,** 2001)

$$T_f = \frac{T_S + T_{sur}}{2} \tag{2.2}$$

Where;

T_f	Film temperature	(K)
T_s	Surface temperature	(K)
T_{sur}	Atmospheric air	(K)

$$\beta = \frac{1}{T_f} \qquad \text{Volume coefficient of expansion} \tag{2.3}$$

Table 2.2 : Properties of air at atmospheric pressure, Holman (2001)

T(K)	ρ (Kg/m^3)	μ x10^5 (kg/m .s)	ν x 10^6 (m^2/s)	K (W/m ^{o}C)	α x 10^4 (m^2/s)	c $_p$ (KJ/kg ^{o}C)	$\boldsymbol{P_r}$
100	3.601	0.6924	1.923	0.00925	0.02501	1.0266	0.77
150	2.368	1.0283	4.343	0.013734	0.05745	1.0099	0.753
200	1.768	1.3289	7.490	0.01809	0.10165	1.0061	0.739
250	1.413	1.599	11.30	0.02227	0.15675	1.0053	0.722
300	1.177	1.8462	15.69	0.02624	0.22160	1.0057	0.708
350	0.998	2.075	20.76	0.03003	0.2983	1.0090	0.697
400	0.883	2.286	25.90	0.03365	0.3760	1.0140	0.689
450	0.783	2.484	31.71	0.03707	0.4222	1.0207	0.683

The rate of heat transfer by free convection from the wall to the room is given by Newton's law of cooling Holman **(**2001).

$$q_{conv.} = h\ \mathrm{A}_s(T_s - T_\infty) \tag{2.4}$$

Where;

$q_{\ conv.}$	Heat transfer of convection	(W)
h	heat transfer coefficient	(W/m^{2}K)
A_s	Surface area	(m^2)
T_s	Surface temperature	(K)
T_∞	Air temperature	

To obtain the Rayleigh number, the following equations can be used on the basis of Holman (2001):

$$R_{al} = Gr_L \Pr = \frac{g\beta(T_s - T_\infty)L^3}{\upsilon\alpha} . \Pr \quad (2.5)$$

Where;

R_{al}	Rayleigh number	
Gr_L	Grashof number	
P_r	Prandtl number	
g	gravitational acceleration	
β	volume coefficient of expansion	
ν	kinematic viscosity	
α	Thermal diffusivity	
L	length of boundary layer	(m)
T_s	Surface temperature	(K)
T_∞	Outside temperature	(K)

Equation (2.5) indicates that transition to turbulence occurs on the wall. The appropriate correlation is then given by Equation 2.6 to obtain

$$N_u = \left\{ 0.825 + \frac{0.327(R_{al})^{\frac{1}{6}}}{\left[1 + (0.492/\Pr)^{\frac{9}{16}}\right]^{\frac{8}{27}}} \right\}^2 \quad (2.6)$$

Hence, heat transfer coefficient of convection is given by Equation 2.7

$$h_C = \frac{N_u k}{L} \quad (2.7)$$

Where;

h_c	Heat transfer coefficient of convection
N_u	Nusselt number
k	Thermal conductivity
L	length of wall

The appropriate correlation for solar radiation passing through a window is then given by Equation 2.8

$$q_{radi} = \varepsilon\sigma \mathrm{A}(T_s^4 - T_{sur}^4) \tag{2.8}$$

Where; $q_{radi.}$ heat radiation of radiation (W)

The conduction heat transfer was calculated with the 1D finite difference methods. Heat transfer coefficients were determined from the thermal balance on the plate glass in transient state. Hence, the total energy is given in Equation 2.9

$$Q_{totl} = Q_{conv.} + Q_{rad} = h\mathrm{A}(T_s - T_\infty) + \varepsilon \mathrm{A}\sigma(T_S^4 - T_{sur}^4), \quad (\mathrm{W}) \tag{2.9}$$

Where;

Q_{totel} Total heat transfer through the windows (W)
$Q_{conv.}$ Heat transfer of convection (W)
$Q_{rad.}$ Heat transfer of radiation (W)

The heat transfer by radiation is evaluated by Equation 2.10

$$h_r = \frac{q_{radi}}{\mathrm{A}(T_S - T_{sur})}, (W/m^2.K) \tag{2.10}$$

Where h_r radiation heat transfer coefficients

Thus, heat transfer h (convection and radiation) can be calculated using the following equation:

$$\mathrm{h} = \mathrm{h_c} + \mathrm{h_r}, (W/m^2.K) \tag{2.11}$$

Where;

h Total heat transfer coefficient
h_c Convection heat transfer coefficient
h_r Radiation heat transfer coefficient

Thus, the total convection heat transfer coefficient of the wall glass is obtained; this coefficient is required for boundary input in the CFD program. The tables that provide Libyan and Malaysian data are presented in Appendices A and E, respectively.

2.3 Natural Ventilation through Buildings

People spend 90% of their time in indoor environments, such as homes, offices, vehicles, and buildings, Awbi (1991). Thus, ventilation has an integral role in the design of buildings, and occupants expect good standards for interior air quality and thermal comfort from windows and window openings. The energy cost of building ventilation is normally 40% less than that of an air-conditioned building, ASHRAE Standard-55 (2012). Natural ventilation, which is either standalone or mixed mode (when combined with a mechanical ventilation system), can provide a comfortable working environment in which low energy consumption is also possible, Heiselberg (2004).

Heat flow rate occurs because of the temperature difference between the interior and exterior of the buildings. Depending on the rate of the air exchange, the following calculation can be obtained as shown in the following equation, Mat and Peter Wouters, (2006):

$$Q_V = \rho\, V_r\, C\, (T_o - T_i) \tag{2.12}$$

Where;

ρ	Air density (kg/m^3)
V_r	Ventilation rate
C	Air specific heat (J/kg-K)
$T_o - T_i$	Temperature difference (K)

2.3.1 Driving Forces for Natural Ventilation

Driving forces for natural ventilation are driven by pressure difference and created by either wind energy on the building or temperature differences (thermal buoyancy or the stack effect) or a combination of both. Building design parameters, such as openings, window type, and fenestration, affect natural ventilation, as does single-sided or cross ventilation. The most important parameter for natural ventilation design inside buildings is the volume of air flow rate through the opening area. For a single-sided ventilation through the head, which has an upper and bottom opening area (A), the volume air flow rate through this area is approximated, Awbi (2003) as shown in the following equation:

$$V = C_d A \sqrt{gh\, \frac{\Delta T}{T_{out}}} \tag{2.13}$$

Where;

V	Air flow volume
C_d	Wind pressure coefficient
A	Opening area
g	Gravitational

h Window height
ΔT Temperature difference
T_{out} Outdoor temperature

2.3.2 Wind-induced ventilation

The wind-induced air flow into a building is affected by the pressure distribution on the building, more specifically at the fenestrations in both the external and internal walls. The air flow is influenced by the distribution of pressure around buildings and in the openings in the building structure. The time-mean pressure because of wind flow or wind away from a surface is calculated based on Equation 2.14, Awbi (2003)

$$p_{wind} = C_p \frac{1}{2} \rho_u v_{ref}^2 \quad (2.14)$$

$$\Delta p_{wind} = C_p \frac{1}{2} \rho_u v_{ref}^2 - P_{inside} \quad (2.15)$$

$$\Delta p_{wind} = (C_{P,windward} - C_{P,Leeward}) C_p \frac{1}{2} \rho_u v_{ref}^2 = \Delta c_p . \frac{1}{2} \rho_u v_{ref}^2 \quad (2.16)$$

$$p_{wind} = C_p \frac{1}{2} \rho_u v_{ref}^2 \quad (2.17)$$

$$P_i = P_{i,o} - \rho_o g H \quad (2.18)$$

$$P_e = P_{e,,o} - \rho_o g H \quad (2.19)$$

Where;

P_{wind} Wind-induced pressure [Pa]
C_p Pressure coefficient
ρ_u External air density [kg/m^3]
v_{ref} Wind speed at a reference height [m/s]
P_i Inside air pressure
P_e External air pressure

The wind on the windward side causes a positive pressure (overpressure) on the windward side but results in a lack of pressure in the leeward and the parallel sides of the building, as shown in Figure 2.2, with reference to the static wind pressure p_{wind} of the opening.

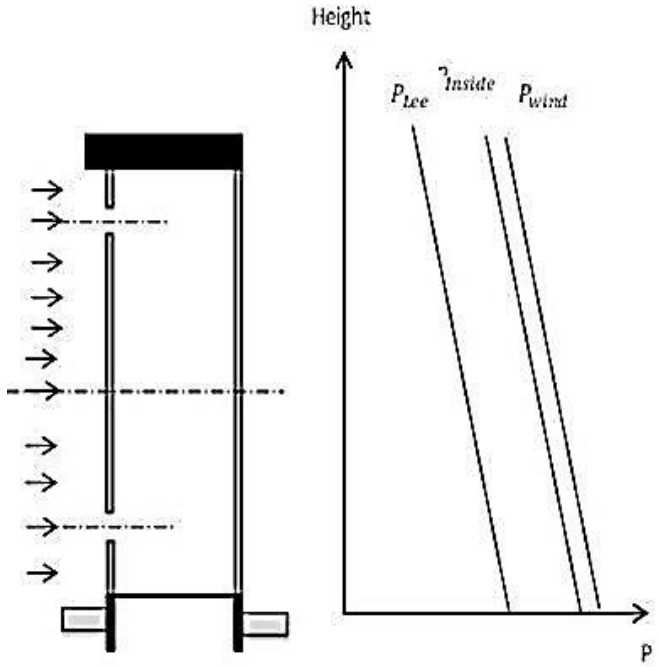

Figure 2.2 : Pressure differences caused by wind on the building, Awbi (2003).

Therefore, the pressure difference caused by buoyancy Δp_s through the opening at height (H) can be calculated by using Equations 2.20 and 2.21

$$\Delta p_s = (P_{exhaust} - p_{inlet}) - gH(\rho_e - \rho_i) \quad (2.20)$$

$$P_i = p_{i,o-}\, \rho_i g\, H \qquad P_e = p_{e,o-}\, \rho_e g\, \mathrm{H} \quad (2.21)$$

Where;
The difference of pressure for the opening of height H1 is obtained from Equations 2.22 and 2.23

$$\Delta P_1 = P_{e0} - P_{i0} = \rho_i g H_1 \frac{T_i - T_e}{T_e} \quad (2.22)$$

$$\Delta P_{H-H} = \rho_i g \frac{T_i - T_e}{T_e} (H_0 - H_1) \quad (2.23)$$

Where;
T_i Inside temperature
T_e External temperature
ΔP_1 pressure difference between outdoors and indoors of H_1
H Building height
g Gravitational constant, 9.8 m/s^2

The sum of driving forces Δp is the total driving forces caused by wind and buoyancy, as shown in Equations 2.24 and 2.25:

$$\Delta P = P_{Wind} + P_{bouyancy} \tag{2.24}$$

$$\Delta P = \Delta P_s + \Delta P_w = (\Delta P_1 = P_{e0} - P_{i0})\,\Delta P_{inlet} + \Delta P_{exhaust} \tag{2.25}$$

Where;

P_{Wind} Wind pressure
$P_{bouyancy}$ Buoyancy pressure
ΔP_s Pressure difference, Pa
ΔP_w Wind pressure difference at the location
P_{e0} External pressure at the height of the location
P_{i0} Interior pressure at the height of the location
ΔP_{inlet} Interior pressure difference at the height of the location
$\Delta P_{exhaust}$ Exhaust pressure difference

The dimensions of the static pressure coefficient parameter C_p are derived from pressure measurements in wind tunnels under reduced-scale models of buildings. The value of C_p at the point on the surface of the building is determined by the geometry of the building, the wind velocity relative to the building, and the exposure (windward or leeward) of the building, Awbi (2003).

Therefore, the pressure difference caused by buoyancy Δp_{wind} across the building is calculated based on Equations 2.26 to 2.28

$$\Delta p_{wind} = P_{exhaust} - p_{inlet} \tag{2.26}$$

$$\Delta p_{wind} = C_{pw}\frac{1}{2}\rho_u v_{ref}^2 - C_{pl}\frac{1}{2}\rho_u v_{ref}^2 \tag{2.27}$$

$$= \frac{1}{2}\Delta C_p \rho_u \tag{2.28}$$

Where;

C_{pw} Windward pressure coefficient
C_{pl} Leeward pressure coefficient
C_p Pressure coefficient
v_{ref} Wind speed at a reference height, [m/s]
ρ_u External air density [kg/m^3]

2.3.3 Buoyancy-induced Ventilation (stack driven)

Buoyancy or stack pressure is due to variation in the air density of different temperatures across the opening at different heights. Differences in temperature occur because of the thermal properties of air at different temperatures. The external pressure and internal pressure distribution can be calculated using Equation 2.29, Awbi (2003)

$$P = P_{i,o} - \rho_o g H \tag{2.29}$$

Where;

P	External or internal pressure [Pa]
$P_{i,o}$	Pressure at a reference level (floor) [Pa]
ρ_o	External or internal air density at a reference level [kg/m3]
g	Gravitational acceleration [m/s2]
H	Height above the reference level [m]
ρ_u	External air density [kg/m^3]

Thus, the pressure difference caused by buoyancy Δp_t through an opening at height H can be calculated as follows, Awbi (2003):

$$\Delta p_t = (P_u - p_i) - gH(\rho_e - \rho_i) \tag{2.30}$$

Where;

P_u	External pressure
p_i	Internal pressure
g	Gravitational acceleration [m/s^2]
H	Height above the reference level [m]
ρ_e	External air density [kg/m^3]
ρ_i	Inside air density [kg/m^3]

If air is incompressible and the temperature difference is not significant when considering the ideal gas law with regard to temperature and density differences, then we can use Equation 2.31, Awbi (2003).

$$\frac{\rho_u - \rho_i}{\rho_i} \cong \frac{T_u - T_e}{T_u} \tag{2.31}$$

Where;

ρ_u	External air density [kg/m3]
ρ_i	Internal air density [kg/m3]
T_u	External air temperature [K]
T_i	Internal air temperature [K]

The air enters and exits the building at a certain height depending on the opening position unlike with the neutral plane in the buildings. The height above the neutral ground is the pressure difference Δp_s= 0, as shown in Equations 2.32 to 2.34, Awbi (2003)

$$\Delta p_t = (P_{u0} - p_{i0}) - gH(\rho_u - \rho_i) = 0 \quad (2.32)$$

$$(P_{exhaust} - p_{inlet}) = gH(\rho_u - \rho_i) \quad (2.33)$$

$$(P_{u0} - p_{i0}) = \rho_o g H_o \frac{T_i - T_u}{T_u} \quad (2.34)$$

Binggeli (2003) stated that the stack effect is the air ventilation system that occurs when hot air exits through the ceiling opening. As hot air rises within the building and out through openings in the ceiling, cold air is infiltrated through the windows and door openings. Considering that hot air is lighter than cold air, the buoyant force causes warm air to rise. The stack effect works better when the air inlet is as low as possible and when the upper level of the building is as large as possible; such scenarios include a multi-space design that reduces the size of the stack effect, Klote (1991).

2.4 Natural Ventilation Strategies

The natural ventilation strategy, which is most suitable for a particular building, can only be reached by careful consideration of a number of factors, such as depth of space with ventilation opening, roof height, mass of thermal exposed to air, building location, heat gain, and climate, Gan (2000). The most widely used natural ventilation method is discussed below.

2.4.1 Cross Ventilation

Cross ventilation is a type of natural ventilation, as shown in Figure 2.4. For successful cross ventilation design, obtaining detailed information on the distributions of air pressure in and around buildings is necessary. Cross ventilation or two opposite-sided of ventilation occurs when wind enters a building from one wall and leaves through openings on the opposite wall.

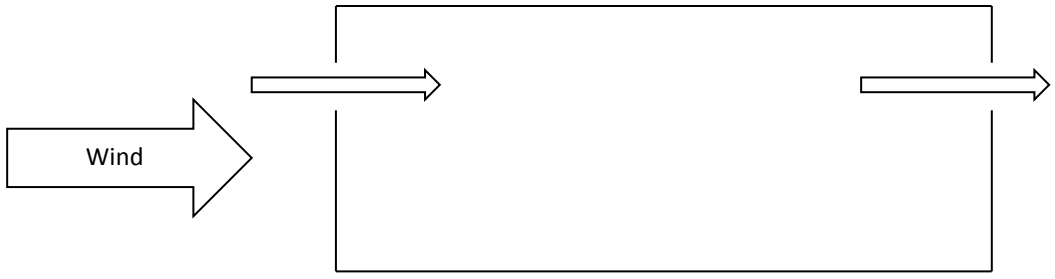

Figure 2.3 : Cross ventilation, Mat and Peter (2006)

In cross ventilation, buoyancy has no effect because the opening is placed at the same height. However, if the openings are at different heights, then thermal buoyancy will affect the flow of air buoyancy and will either work with or against the wind depending on the opening location and the wind direction, Mat and peter (2006).

When natural ventilation is designed to be driven by buoyancy force, the outlet opening is placed in the ceiling to minimize or take advantage of the effect of the wind. This effect in single-sided ventilation with small openings is limited to wind fluctuations or turbulence. The effect of thermal buoyancy ventilation in single-sided ventilation depends on the height of the opening; such an effect causes a difference in temperature between the external and internal environment of the building. These types of opening are used for cross ventilation with small or large openings, such as windows for single-sided ventilation and doors on opposite sides. Cross ventilation is suitable for spaces of depth > 2.5 H and ≤ 5 H, where H is the ceiling height, Awbi (2003).

2.4.2 Stack Ventilation

Stack ventilation is used in buildings that require ventilation rates that are greater than achievable rates using either single-sided or by cross ventilation. This strategy based on the buoyancy is a main driving force; the stack height becomes significant. The stack pressure is determined by the difference between the internal and external temperatures. The position of air inlet and outlet in the building depends on the wind pressure and could assist the stack pressure, reduce influence, or reverse the effect of forcing through to the outside, Awbi (2003).

2.5 Thermal Comfort

Thermal comfort ventilation is required to provide or improve the comfort conditions of building occupants via physiological cooling. Thermal comfort ventilation is often used in hot and humid climates. Thermal comfort has been defined by the American Society of Heating, Refrigerating and Air Conditioning Engineers, ASHRAE (2013) as the mental condition in which satisfaction is expressed with thermal environment standards, ANSI/ASHRAE 55, (2013). Thermal comfort describes a person's psychological state of mind and is usually referred to in terms of whether someone is feeling too hot or too cold, Fanger P.O. (1972).

Air temperature, mean radiant temperature, relative humidity, and air velocity are the four basic environmental variables that define the thermal state of the environment. Combined with the metabolic heat generated by human activity and the clothing worn by a person, these variables provide the six fundamental factors that define human thermal environments, Parsons, K. (2003).

2.5.1 Factors that Affect Thermal Comfort

Six primary factors directly affect thermal comfort. They can be categorized into environmental factors and personal factors. Even if all these factors may vary with time, standards usually refer to a steady state to study thermal comfort, although limited temperature variations are allowed, ISO1984; ASHRAE (2013).

2.5.1.1 Environmental Factors

Operative temperature (T_0)

The operative temperature T_0 is defined as a uniform temperature of a radiantly black enclosure in which a person exchanges the same amount of heat by radiation and convection as in the actual non-uniform environment. On the basis of CSN EN ISO 7738, T_0 is derived from

$$t_0 = t_a + (1 - A)\,(t_r - t_a) \tag{2.36}$$

Where;

t_a Air temperature (℃)

t_r Temperatures mean radiant (℃)

A Heat transfer coefficient

Coefficient (A) is calculated from the following equation, CSN EN ISO 7738:

$$A = 0.73\, V^{0.2} \tag{2.37}$$

The air velocity of an environment affects the heat transfer coefficient. When the air velocity increases, the coefficient of heat transfer by convection increases and the Coefficient of heat transfer by radiation had changes.

Mean radiant temperature

The radiant temperature is related to the amount of radiant heat transferred from a surface, and it depends on the material's ability to absorb or to emit heat, which is also known as its emissivity. The mean radiant temperature depends on the temperatures and emissivity of the surrounding surfaces. The mean radiant temperature experienced by a person in a room with streaming sunlight varies based on how much of their body is exposed to the sun, Fanger (1972). Figure 2.5 shows a typical comfort chart constructed by Fanger. This chart shows the effect of air relative velocity on optimum mean radiant temperatures at various air temperatures. The value of mean radiant temperature, t_r (℃), can be calculated by the following equation, Fanger (1972):

$$T_{mr} = T_1\ A_1\ + T_2\ A_2 + T_2\ A_2 + T_3\ A_3 + \ T_4\ A_4 / (A_1\ + A_2\ +\ A_3\ + A_4\ ) \tag{2.38}$$

Where;

T_{mr}	Mean radiant temperature (℃)
T_2 T_2 T_2 T_2	Surface temperature (℃)
$A_1A_2A_3A_4$	Surface area (m)

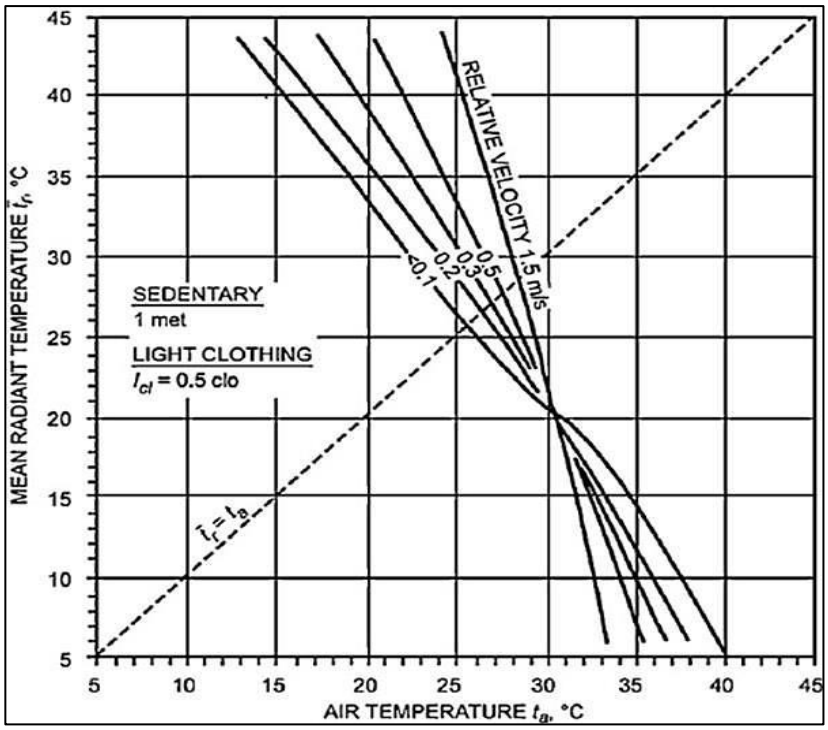

Figure 2.4 : Comfort charts by Fanger (1972).

Air Velocity

ANSI/ASHRAE Standard 55(2013) defined air speed as the rate of air movement at a point without considering direction. Air speed is the average speed of the air to which the body is exposed with respect to location and time.

Relative humidity

Relative humidity (RH) is the ratio of the actual amount of water vapor in the air to the amount of water vapor that the air could hold at a specific temperature and pressure. The human skin is fairly efficient at sensing heat and cold. The wetness of skin in different areas also affects perceived thermal comfort. Humidity can increase wetness on different areas of the body, thereby leading to a perception of discomfort. The recommended RH is 50% to 70%, ASHRAE Standard 55, (2013).

2.5.1.2 ASHRAE Requirements

Metabolic rate

The ASHRAE 55- Standard,(2013) defines metabolic rate as the level of transformation of chemical energy into heat and mechanical work by metabolic activities within an organism; the rate is usually expressed in terms of unit area of the total body surface. Metabolic rate is expressed in met units, which are defined as 1 met = 58.2 W/m^2. The surface area of an average person is 1.8 m^2. ASHRAE Standard 55 provides a table of metabolic rates for a variety of activities, as shown in Appendix H.

Clothing insulation

The amount of thermal insulation worn by a person has a substantial effect on thermal comfort because it influences heat loss and, consequently, thermal balance. The type of material and the clothing are dependent on air movement and relative humidity; these factors can decrease the insulating ability of the material. In this study, 1 clo is equal to 0.155 m^{2}K/W and a table of clothing insulation is shown in Appendix H.

2.5.2 Models for Thermal Comfort

2.5.2.1 Predicted Mean Vote (PMV)

The predicted mean vote (PMV) is the predicted mean vote on the thermal sensation scale of a large population exposed to a certain environment. PMV is derived from the physics of heat transfer combined with an empirical fit to sensation. PMV establishes a thermal sensation based on steady-state heat transfer between the body and the environment and assigns a comfort vote to that amount of sensation. PPD is the predicted percent of dissatisfied people at each PMV Fanger (1972). PMV changes from zero in either the positive or the negative direction. PMV is an index that predicts the mean value of the votes of person on the seven-point thermal sensation scale based on the heat balance of the human body, as shown in Table 2.3.

Table 2.3 : Seven-point thermal sensation scale, (ASHRAE (2012)

+3	Hot
+2	Warm
+1	Slightly warm
0	Neutral
-1	Slightly cool
-2	Cool
-3	Cold

Thermal balance is influenced by physical activity and clothing, as well as the following environmental parameters: air temperature, mean radiant temperature, air velocity, and air humidity. If these factors are measured or estimated, then the thermal sensation for the body can be predicted for the whole body, as calculated by the PMV equations in Appendix H.

2.5.2.2 Predicted Percentage Dissatisfied (PDD)

Predicted percentage dissatisfied (PDD) is a quantitative measure of the thermal comfort of a group of people in a particular thermal environment. The PDD index provides information on thermal discomfort by predicting the percentage of persons who feel too warm or too cool in an environment. The use of these indices as the basis for this method results in consistency between Standard 55-2013 and ISO Standard 7730. The PPD can be obtained from the PMV, as shown in Appendix H.

2.5.3 Indoor Air Quality

Ventilation and shading can help control indoor temperatures and remove indoor airborne pollutants from indoor sources. Natural ventilation can also improve indoor air quality by reducing indoor pollutants. Natural ventilation reduces the level of contaminants and improves indoor air quality (IAQ). The use of ventilation to reduce indoor air pollutants should be carefully evaluated where outdoor sources of pollutants, such as smoke or refuse, are nearby. Outdoor air is an important factor in promoting good air quality. Moreover, air quality inside buildings such as homes, offices, and schools, where people spend a large part of their life, is an essential determinant of healthy life and well-being.

Pollutants in the indoor environment can increase the risk of illness. Although most buildings do not have severe indoor air quality problems, even well-run buildings can sometimes experience episodes of poor IAQ (United States Environmental Protection Agency, (1970). Natural ventilation can improve IAQ by reducing pollutants.

2.6 WWR

WWR is the ratio of the window area to the total wall area in a particular interface. The British Local Government Board bylaws in the 1920s and London Building Acts 1894 to 1909 required a WWR of 10%. The area includes the total area of the window and the surface wall area, as shown in Figure 2.6. In Malaysia, the Uniform Buildings bylaws of 1984 specify a minimum window-to-floor area ratio of 1/20. The WWR for the given façade will be (a x b)/ (H x W). The visible light transmittance (VLT) of glazing is the ratio of visible light to be transmitted through the glass to the total visible light that falls on the glazing. The ratio of glazing area to floor area for daylighting must be 10% to 25% as prescribed by Gutherie (1995).

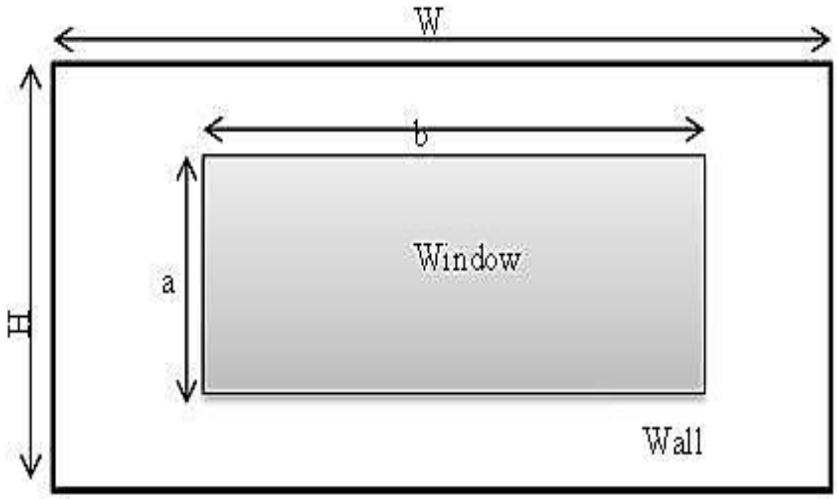

Figure 2.5 : Wall and window dimensions used to calculate WWR.

2.7 Characteristics of Ideal Window

The design of the ideal window depends on the optimization of many factors and the functions that follow the weather conditions and shape of a building. The selection of the correct window requires specific advantages between different energy consumption performances and the decreased heat gain in the tropics. Reducing the SHGC of windows has a significant effect on inside comfort level. Low-E provides lower solar heat gain for windows and rejects a greater amount of incident solar irradiation. Three main types of energy flow occur through the windows.

1. Insulation heat flow through material of window is commensurate with temperature difference and is inversely related to heat resistance (R value) of heat that penetrates inside an office. Aluminum and vinyl frames have good insulation value, high impact resistance, and good resistance to corrosion (WBDG).
2. Visible transmittance is the amount of visible light in the visible part of the spectrum that passes through the glazing material. The low-E cover must reduce SHGC without reducing the view from visible transmittance.
3. The flow of air through buildings is used to improve indoor thermal comfort and reduce energy use by equipment such as air conditioning systems, ASHRAE, (2012).

One way to reduce this demand is improvement of the design of windows. In the tropics, the entrance of solar radiation through the windows can be controlled in a spectrally selective manner. Such an approach reduces the energy used for air conditioning and raises the comfort level in rooms, Durrani, et al (2004). Table 2.5 shows a comparison model of the window with other references, ASHRAE, (2013).

Table 2.4 : Comparison of window requirement in different references

References	Δ_T	Indoor Air Velocity	Window to wall ratio
ASHRAE Standard (USA)	28.69	V= 0.15 m/s to 0.50 m/s	-
Dahlan et al 2011 (Malaysia)	Δ_T= 2 K	V= 0.3 m/s	30%
Wang Lipling 2007 (Singapore)	Δ_T= 4.2 C	V=.04 m/s	24%
Reference office in Malaysia on thermal comfort	27.8 C	V=0.36	22%

2.8 Purpose of Design Window

The main design consideration of windows is mostly the thermal performance. Evaluation of each variable, especially in the commercial, industrial, and institutional buildings, is usually based on three basic options: glazed façade systems, curtain wall systems, and manufactured or pre-glazed windows. Other differences should be considered, especially in aspects related to appearance, cost, customization, manufacture, and installation.

Weather and building type are given conditions in window design. The orientation of the window controls the daylight, size, and type of window, as well as the shading systems and frame type that can be processed. The window design must be optimized to achieve thermal comfort in naturally ventilated buildings and to reduce solar heat gains inside the building, ASHRAE (2013).

The purpose of this study is formulate a new design for window dimensions by using CFD on data of a naturally ventilated office in Malaysia, thereby obtaining a smaller temperature difference, providing the building with daylight, and controlling air flow through the window. Ultimately, thermal comfort is improved and energy costs are reduced. The opening window has three modes of movement (front opening, top opening, and bottom opening) with an air flow gap of 10 cm on all sides.

2.9 Computational Fluid Dynamics (CFD)

ANSYS, which includes CFD analysis tools, is widely used and well validated (ANSYS Fluent and ANSYS CFD). It is available separately or included in the ANSYS CFD bundle. Considering solver robustness, speed, development, knowledge, and experience, advanced modeling capabilities can provide reliable results for fluid dynamics and create high-quality visualizations and estimation. The computation in this study was performed on the commercial CFD software FLUENT 6.3. The CFD tools provide detailed knowledge of air flow type, temperature distribution, and air velocity inside a closed space. Thus, mathematical application

models have become popular because of accurate and acceptable CFD results, as well as relatively low-information equipment and labor costs. CFD is a computer-based tool for numerically simulating the behavior of systems that involve heat transfer, fluid flow, and other physical procedures. The specified boundary conditions of the region are determined by finding the equations of fluid over a region of interest. In industry, CFD can solve many systems and is more cost effective than other experimental investigations. The effects of geometrical parameters on office room were investigated via CFD. This software solves the Reynolds-averaged Navier–Stokes (RANS) equation for finite volume method formulation. Two turbulence models were chosen for this study, namely, k-ε-realizable model for hot-dry climate simulation and k-ε-RNG model for humid–warm climate simulation and modeling.

2.9.1 Turbulence Flow (Laminar Flow and Turbulent Flow)

The uniform speed fluid hits the front edge of the flat plate, and the laminar boundary layer begins to develop. The flow in this region is highly predictable. After a certain distance, small chaotic oscillations begin to develop in the area of the fluid; the flow is begins to transition to turbulence and eventually becomes quite turbulent. The transition between these three regions can be defined in terms of the Reynolds number. The Reynolds number is the ratio of momentum forces to viscous forces and consequently quantifies the relative importance of these two types of forces for given flow conditions Purcell, (1977).

$$\mathrm{Re} = \frac{\text{intertial forces}}{\text{viscous forces}} = \frac{\rho\, v\, L}{\mu} = \frac{v\, L}{\nu} \qquad (2.39)$$

Where;

v Characteristic velocity scale (m/s)
L Characteristic linear length (m)
ν Kinematic viscosity of the fluid (m^2/s)
μ Dynamic viscosity of the fluid ($\nu = {}^{\mu}/_{\rho}$) (m^2/s)
ρ Fluid density (kg/m^3)

Laminar and turbulent flows can be characterized and quantified using Reynolds number

N_R < 4000 laminar flow

N_R > 4000 turbulent flow

The flow of the fluid can be completely predicted by solving steady-state Navier–Stokes equations, which predict the velocity and the pressure fields. RANS modeling parameters determine the average flow time, such as the average air speed and temperature, via the turbulence model. RANS modeling requires less time, and it solves the average flow parameters. Therefore, RANS CFD modeling is most

commonly used in many industrial applications and to simulate natural ventilation in buildings (ANSYS, FLUENT, 6.3).

Many models are used to predict the turbulent viscosity, such as the standard k-ε model, k- ε RNG model, realizable k- ε model, and k- ω model. In this study, turbulent flow was used. The RNG-based k-ε turbulence model and the k-ε model are popular for industrial applications because of their good convergence rate and relatively low memory requirements. The model focuses on the mechanisms that affect the turbulent kinetic energy (per unit mass) k-ε.

The RNG-based k-ε turbulence model is derived from the instantaneous Navier–Stokes equations by using renormalization group (RNG) methods. The analytical derivation results in a model that has constants that are different from those in the standard k-ε model, as well as additional terms and functions in the transport equations for k and ε (Fluent Inc.).

2.9.2 Turbulence Models

2.9.2.1 Standard k- ε Model

The standard k-ε model in FLUENT within this class of models has become a workhorse of practical engineering flow calculations. The standard k-ε model has robustness, economy, and reasonable accuracy for a wide range of turbulent flows in industrial flow and heat transfer simulations. The standard k- ε model is based on model transport equations for the turbulence kinetic energy (k) and its dissipation rate (ε). These equations are shown in Equations 2.40 and 2.41.

$$\frac{\partial}{\partial t}(\rho\, k) + \frac{\partial}{\partial x_i}(\rho\, k u_i) = \frac{\partial}{\partial x_j}\left[(\mu + \frac{\mu_t}{\sigma_k})\ \frac{\partial_k}{\partial x_j}\right] + G_k - \rho\varepsilon + S_k \qquad (2.40)$$

And

$$\frac{\partial}{\partial t}(\rho\, \varepsilon) + \frac{\partial}{\partial x_i}(\rho\, \varepsilon u_i) = \frac{\partial}{\partial x_j}\left[(\mu + \frac{\mu_t}{\sigma_\varepsilon})\ \frac{\partial_\varepsilon}{\partial x_j}\right] + G_{1\varepsilon}(\frac{\varepsilon}{k})\ G_k \qquad (2.41)$$

The turbulent viscosity μ_t is computed by combining (k) as shown in Equation 2.42

$$\mu_t = \rho\, C_\mu\, (\frac{k^2}{\varepsilon}) \qquad (2.42)$$

In these equations, G_k represents the generation of turbulence kinetic energy because of the mean velocity gradients. $C_{1\varepsilon}, C_{2\varepsilon}, and\ C_\mu$, are constants. $\sigma_{k,and\ \sigma_\varepsilon}\ \sigma_k$, and σ_ε are the turbulent Prandtl numbers for k and ε, respectively. S_k and S_ε are user-defined source terms. The model constants in the standard k-ε model have the following default values:

$$C_{1\varepsilon} = 1.44,\quad C_{2\varepsilon} = 1.92,\quad C_\mu = 0.09,\ \sigma_k = 1.0,\ \sigma_\varepsilon = 1.3 \qquad (2.43)$$

2.9.2.2 RNG k- ε Model

The RNG k-ε model using statistical technique was derived from the theory of renormalization. This model is similar to model k-ε standing but includes certain improvements. It contains additional terms in its equations to improve the accuracy of rapidly strained flow and the effects of turbulence in a swirl on the RNG k-ε model accuracy and swirling flow. The RNG theory offers an analytical formula for turbulent Prandtl numbers, whereas k-ε standard criteria are modeled by the user with the use of constant values. However, the effective use of this feature does not depend on the appropriate treatment in the near-wall region. The derivative turbulence model of instantaneous Navier–Stokes equations uses RNG methods. As a result, a derivation analytical model that is different from those in the standard k-ε-based constants on the model RNG is obtained. Additional terms and functions are present in the transport and equations for k and ε.

2.9.2.3 Realizable k-ε model

The realizable model satisfies certain mathematical constraints on the Reynolds stresses, which is consistent with the physics turbulent flows. Neither the standard k-ε model nor the RNG k-ε model is achievable. The realizable k-ε and standard k-ε models manifest in two important but different ways. The realizable k-ε model contains an alternative formulation for the turbulent viscosity and transport equation for the dissipation rate k, which has been derived from an exact equation of the mean square vortex fluctuation. The realizable k-ε model is based on model transport equations for the turbulence kinetic energy (k); its dissipation rate (ε) equations are presented in Equations 2.44 and 2.45, FLUENT 6.3 User's Guide (2006).

$$\frac{\partial}{\partial t}(\rho\,\varepsilon) + \frac{\partial}{\partial x_i}(\rho\,\varepsilon u_j) = \frac{\partial}{\partial x_i}\left[\left(\mu + \frac{\mu_t}{\sigma_\varepsilon}\right)\frac{\partial_\varepsilon}{\partial x_j}\right] + \rho G_1 S_\varepsilon\left(\frac{\varepsilon}{k}\right) G_{3\varepsilon}\, G_b + S_\varepsilon - \rho\, C_2\left(\frac{\varepsilon^2}{k+\sqrt{\nu\varepsilon}}\right) \qquad (2.44)$$

$$C_1 = \max\left[0.43, \left(\frac{\eta}{\eta+5}\right)\right] \text{ and } \quad \boldsymbol{\eta} = S\left(\frac{k}{\varepsilon}\right) \qquad (2.45)$$

In this equation, G is the generation of turbulence kinetic energy because of buoyancy, $C_{1\varepsilon}$ and $C_{3\varepsilon}$ are constants, σ_ε is the turbulent Prandtl number for ε, and S_ε is a user-defined source term. The difference between the realizable k-ε models is that C_μ is no longer constant. It is computed from Equation 2.45

$$C_\mu = \frac{1}{\left(A_{0+A_S}\left(\frac{kU^*}{\varepsilon}\right)\right)} \qquad (2.46)$$

2.9.3 CFD Modeling Process

The general modeling procedure to solve any CFD problem is shown in Figure 2.7. The commercial software GAMBIT 2.4.6 and FLUENT version 6 were used. In CFD terminology, the domain is decomposed into sub-domains through grid or mesh generation. All CFD codes contain the following three main elements:

1) A pre-processor, which is used to input the problem geometry, generate the grid, define the flow parameter, and the boundary conditions to the code.
2) A flow solver, which is used to solve the governing equations of the flow subject to the provided conditions.
3) A post-processor, which is used to massage the data and show the results in a graphical and easy-to-read format.

The majority of these CFD programs is based on the solution of Navier–Stokes equations, energy equations, mass and concentration equations, and transport equations for turbulent velocity and its scale. The numerical solution of all these equations in three dimensions has been applied to air flow and heat problems in buildings. Franke et al. (2010) provided guidelines for best practices and applied them to urban flows. These guidelines, which are described briefly here, are a collection of results from previous initiatives in the field of CFD in general. The guidelines focus on applications of statistical steady-state RANS equations for situations with neutral stratification without dispersion modeling.

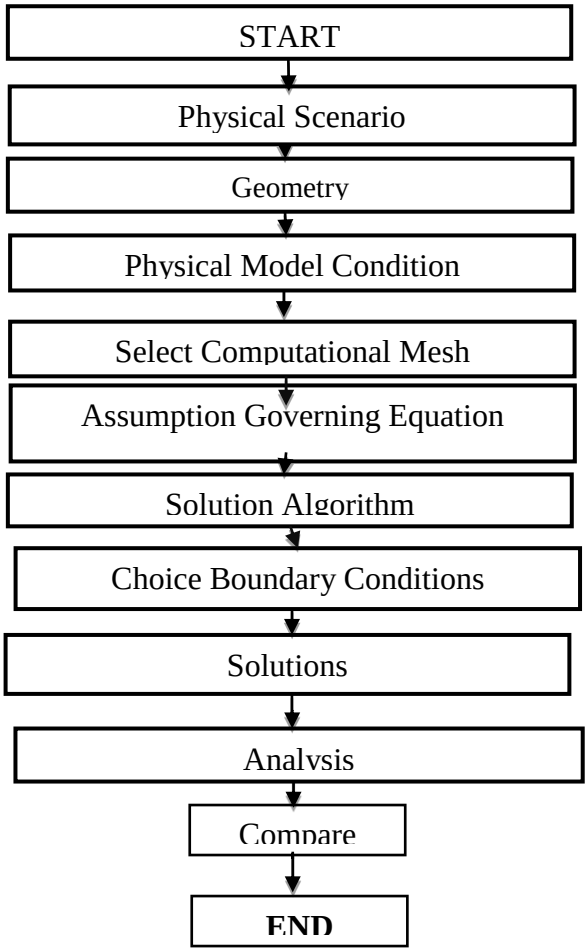

Figure 2.6 : General modeling processes, Venturino and Rubini (1995).

The computational domain of the post-processing stage could be helpful to find the results. For any physical system, mass, momentum, and energy are the applicable preservation laws, Ferziger and Peric (1999).

2.9.4 Fluid Properties

A significant step in the preparation of the model is to determine the physical and material properties. The medium flow of the system is the air. The property analysis of air for this analysis is taken from the opening window, which has a dynamic viscosity 1.7894 e-0.5 (kg/ m$-s$), density 1.2225 (kg.m^3), C_p1006.43 (j/kg-K) and thermal conductivity (w/m-k). These values are assumed constant for all the simulations. Operating pressure specifications affect the account in different ways in different flow regimes. Absolute pressure is the sum of the operating pressure and the pressure gauge. Corrected operating pressure, *P*op = 101977.85 pa, is used in simulation from Holman J. (2002).

2.9.5 Numerical method

2.9.5.1 Equations of motion

For all flows, CFD-FLUENT solves conservation equations for mass and momentum. Conservation of divergence is the system of equations that govern the time-dependent 3D fluid flow and heat transfer of a compressible Newtonian fluid. The governing equations are solved with the following assumptions:

1. Heat transfer and fluid flow are in steady state and 3D.
2. Fluid is turbulent flow, incompressible, and single phase.
3. Temperature independence is the physical properties of the fluid flow and heat.

On the basis of the above assumptions, the energy, momentum, and continuity equations for this study can be written as stated by Hung et al. (2012):

Conservation of mass (continuity equation)

When taking U, V, and W, as the velocity components in the x, y, and z directions, respectively, (ρ) the fluid density, (t) the time, and the rate of increase in (ρ) within the control volumes dx, dy, and dz equal the net rate of influx of mass to control volume, as seen in Equations 2.47 and 2.48:

$$\frac{\partial u}{\partial x} + \frac{\partial v}{\partial y} + \frac{\partial w}{\partial z} = 0 \tag{2.47}$$

$$\frac{\partial \rho}{\partial t} + \frac{\partial}{\partial x}(\rho U) + \frac{\partial}{\partial y}(\rho V) + \frac{\partial}{\partial z}(\rho W) = 0 \tag{2.48}$$

Conservation of momentum (Navier–Stokes equations)

Applying the law of conservation of momentum in the x, y, and z directions obtains the following equations:

The X-momentum equation

$$\rho_f \left(u \frac{\partial u}{\partial x} + v \frac{\partial u}{\partial y} + w \frac{\partial u}{\partial z}\right) = - \frac{dp}{dx} + \mu \left(\frac{\partial^2 u}{\partial x^2} + \frac{\partial^2 u}{\partial y^2} + \frac{\partial^2 u}{\partial z^2}\right) \tag{2.49}$$

The Y-momentum equation

$$\rho \left(u \frac{\partial v}{\partial x} + v \frac{\partial v}{\partial y} + w \frac{\partial v}{\partial z}\right) = - \frac{\mathrm{dp}}{\mathrm{dy}} + \mu \left(\frac{\partial^2 v}{\partial x^2} + \frac{\partial^2 v}{\partial y^2} + \frac{\partial^2 v}{\partial z^2}\right) \tag{2.50}$$

The Z-momentum Equation

$$\rho\left(u\,\frac{\partial w}{\partial x}+v\,\frac{\partial w}{\partial y}+w\,\frac{\partial w}{\partial z}\right)=-\frac{dp}{dx}+\mu\left(\frac{\partial^2 w}{\partial x^2}+\frac{\partial^2 w}{\partial y^2}+\frac{\partial^2 w}{\partial z^2}\right) \quad (2.51)$$

Internal energy equation

The conservation of thermal energy in the volume controls dx, dy, and dz states that the net increase in internal energy in the volume control is equal to the net flow of energy via convection in addition to the net inflow by thermal and mass diffusion. The energy equation per unit volume is presented in Equation 2.52.

$$\frac{\partial}{\partial t}(\rho\bar{T})+\frac{\partial}{\partial x}(\rho U\bar{T})+\frac{\partial}{\partial y}(\rho V\bar{T})+\frac{\partial}{\partial z}(\rho W\bar{T})=\frac{\partial}{\partial x}\left(\frac{\Gamma(\partial\bar{T})}{\partial x}\right)+\frac{\partial}{\partial y}\left(\frac{\Gamma(\partial\bar{T})}{\partial y}\right)+\frac{\partial}{\partial z}\left(\frac{\Gamma(\partial\bar{T})}{\partial z}\right) \quad (2.52)$$

ρ Effective density
c_p Heat capacity
μ Dynamic viscosity
k Thermal conductivity
T Temperature of coolant (℃)
Γ Diffusion coefficient, which is μ/σ and $\sigma = \mu c_p/\lambda$ is the Prandtl number for a fluid.

2.9.5.2 Grid Generation using CFD

The GAMBIT is a single integrated pre-processor tool for CFD analysis used for mesh generation. It enables the user to generate a grid in structured and unstructured hexahedrons, pyramids, and prisms, as well as assigns boundary zones to the grid. A combination of structured and unstructured cells was generated for domains in this study. The critical zones are those near the window surfaces. The geometry mesh used in the Libyan and Malaysian simulation grids is a conjugate heat transfer and air flow analysis.

Slah Driss et al. (2016) presented the validation heat ventilation and thermal comfort evaluation in a room via the CFD model. RANS modeling used the k–ε turbulence model. Numerical results were obtained for the temperature distributions, the airflow patterns, and the turbulence characteristics inside the building.

Li Yang et al. (2014) used CFD numerical simulation to analyze the air velocity and indoor temperature of a room mounted with wall air conditioning units in a summer climate. Results showed that the air conditioning system could use indoor heat to provide good indoor thermal comfort and air velocity in activity areas where people sit and stand.

James Lo and Novoselac (2013) explored the use of localized air flow to divide an open office without partition walls. The study used the CFD model to simulate air flow in an office and to address indoor air quality. The experiment was validated by CFD simulation; temperature differences between occupied and unoccupied areas reached up to 2 ℃. Simulation results achieved significant energy savings (approximately 12% of total cooling energy) and indicated that occupancy-based air conditioning can effectively remove contaminants from indoor sources.

Ardalan et al. (2015) reviewed research on applications of passive design strategies for natural ventilation in tropical climates. They found that ventilation openings, WWR, and building orientation should be applied in future buildings.

Wong P. et al. (2008) analyzed the various CFD parameters for thermal comfort with various configurations of double-glazed façade to determine a new type of double-skin interface configuration; this configuration will provide thermal comfort indoors in hot and humid climates, thereby facilitating natural ventilation of skyscrapers. This analysis was carried out with different ambient temperatures, different wind speeds, and different orientations of the double-skin façade at different periods throughout the day.

Jennifer et al. (2008) proposed a four-step computational method that used both CFD and coded radiation calculations to determine airflow and heat transfer through the window. The experimental work was tested on a full-scale dual-airflow window system, which was used to obtain various indoor and outdoor air and window surface temperatures for validating the computer method. They used FLUENT to model conduction and convection within the window system and radiation from the inner and outer surfaces of the window system. The difference between the computed air and surface temperatures and the measurement data was generally less than 1 K; the new computational method was validated and recommended for further use in hour-by-hour energy simulations by an energy simulation program.

Whaad et al. (2010) presented the effects of selected shading devices (silver coating, blinds, tinted coating, and clear glass at 6 mm) on office room temperature distribution with a glass window in a tropical climate. The thermal effects of glass with different shading devices were dependent on their optical properties (reflectance, absorption, and transmittance).

Abdul Rahman and Ismail (2008) reported that buildings in Malaysia consume roughly 70% of energy for cooling the indoor environment. Zain-Ahmed (2008) also reported that more than 40% of the energy consumed by the Malaysian buildings can be reduced if energy efficiency and sustainable technologies is applied in building ventilation. Thus, passive design is evitable for energy efficiency as stated by Siewa C. et al. (2011), who classified physical passive designs into five major groups to optimize the application of natural ventilation within building zones. The categories of physical designs were air wells, façade designs, ventilation

openings, corridors and shadings, and partitions. Natural ventilation by cross flow occurs when wind enters into a building from one or more openings on one side and leaves through one or more openings on the opposite wall. The wind-driver ventilation depends on the indoor wind velocity, direction of wind, and configurations of openings, as well as building layout and orientation.

Olufowobi and Adenuga (2012) provided the basic approach to create window sizes mainly to facilitate the promotion of the movement of air in the classroom in hot humid weather. The analysis enables the development of guidelines for designing windows in the classroom to create thermal comfort.

James et al. (2011) examined the effects of hypothetical apartments in a building on natural ventilation by solving the cross ventilation rate; agreement was found between the CFD model and experimental measurements. Jiang Yi and Chen Q. (2003) used measurements and CFD simulations to achieve single-sided natural ventilation and buoyancy of natural ventilation with large openings. The measurement data are used to validate CFD models. The two models, along with the RANS equation were used for modeling and simulating large eddy simulation (LES). The CFD models determined air temperature, air velocity, and rate of ventilation to develop prediction models in which the LES was in better agreement with the measurement data than those calculated by the RANS model.

Ayad Samir S. (1991) applied the CFD technique to study natural ventilation for the room fitted with different opening formations. The verification of the model was compared with the results of 2D steady flow around a square cylinder immersed for an extended period in the atmospheric boundary layer with the corresponding measurement values. The results include mean air velocity and air pressure distribution near the building and inside the room. The results consider tanker average speed, stream lines, the distribution of pressure around the building, and vector medium speed. In the results, the turbulent eddy viscosity inside the room is simplified.

Guohui and Gan (2000) introduce the effective depth of fresh air distribution in rooms under single-sided natural ventilation using a numerical CFD technique. The effective depth was based on the room air flow pattern, air temperature, and local mean age of air. Results showed that the effective depth for thermal comfort may not coincide with that for air quality, in which the requirement for thermal comfort in summer is the limiting factor for the effective room depth. The investigation also showed the effects of window opening levels and room heat gains on the air flow rate and room effective depth.

Hassan et al. (2007) investigated the wind effects of window combinations by examining ventilation characteristics in buildings via CFD results and experimental work. In this study, single-sided ventilation with two adjacent openings on the far right and far left are given better natural ventilation than the center location.

Selkowitz (2004) suggested that the assessment of the adequacy of natural ventilation should be based on the air velocity inside the unit rather than simply the amount of air changes per hour because the human body reacts more to air flow rather than just air quality. The results considered the average minimum air speed per day in the room was 1 m/s in providing an acceptable level of natural ventilation for a climate or community.

Roetzel et al. (2010) investigated single-sided natural ventilation air flow for a test room and integrated distribution of air flow and thermal comfort in the room. The study suggests that people's control of natural ventilation is dependent on several parameters, such as type of window opening, window size, window shape, number of windows, and placement. These parameters can better reflect the individual characteristics of specific weather and building use.

Christine Walker et al. (2011) analyzed similarities between a scaled down model of building and CFD with air as the working fluid for natural ventilation driven by buoyancy to analyze air movement and velocity values. This type of investigation was also performed by Bangalee et al. (2012), who investigated wind-driven natural ventilation systems by CFD in buildings with multiple windows. The simulation for cross and single-sided ventilations used (RNG) k– ε turbulence model, and comparison with an experimental result. The CFD model is applied on the physical mechanism of the air movement. The results are shown as a vector average speed, size, magnitude of velocity, distribution of pressure, pressure coefficient, and the effect of the incoming wind speed both inside and outside the building. This method can be accepted for this work because of similar window conditions.

Stavrakakis et al. (2008) studied natural ventilation for cross openings at non-symmetrical locations. Two measurement arrangements were examined for noon and afternoon hours under a warm and mild summer; included factors are air temperature and velocity measurements in the chamber. A CFD technique has been applied to the simulation work. Three models, standard, RNG k–ε, realizable k–ε models were used in CFD. RNG k–ε was implemented in a comparatively better model, particularly for temperature predictions of the RNG k–ε and the realizable' k–ε models. Thus, this formation is important for selecting the appropriate model for this work.

Anastasia et al. (2013) investigated cross natural ventilation for building buoyancy assisted by wind through CFD and laboratory simulation. Three initial Froude numbers that correspond to the three different types of ventilation, namely, displacement, transitional, and mingling ventilation, were examined by the effect of the outlet opening position. Full-scale analyses through the 3D unsteady RANS equations in conjunction with the energy equation and the turbulence model RNG k-ε were used to solve the problem.

Ramponi and Blocken (2012) conducted CFD simulation of cross ventilation. The outdoor and indoor wind flow for buildings with effects of computational parameters was examined. They studied a series of 3D steady RANS simulations, and the geometry included middle–windward and middle–leeward openings.

Hajdukiewicz et al. (2013) verified and validated the CFD model of a highly-glazed meeting room in the Engineering building. Comprehensive field measurements were conducted in real time with supported CFD model generation and validation. A previously proposed formal calibration methodology served a guide toward the creation of the final CFD model, which showed satisfactory agreement with the field measurements.

Monterey and Blockenhas (2013) presented a systematic evaluation of the 3D steady RANS CFD to predict the average wind pressure distributions on the windward surfaces and leeward of a mid-rise building with and without balconies. Results show that steady RANS can reproduce the mean wind pressure distribution across the windward façade of the building. The average deviations from the wind tunnel measurements are 12% and 10% for the building with and without balconies, respectively.

Dahlan et al. (2011) assessed the influences of operative temperature in three non-air-conditioned multi-story hostels in Malaysia with an operable WWR of 30%. The measured rooms were recorded with and without an operating ceiling fan from May until July 2007. The temperatures recorded among all the hostels ranged from 29 ℃ to 30 ℃ because of the high mean outdoor temperature, which ranged from 32.2 ℃ to 32.8 ℃.

Jong and Bot (1992) used a full-scale setup to measure for air flow by single-sided opening casement windows. Experimental results confirm the validity of the approach in describing the outflow of air and the inflow of this type of window when fully opened. The work also shows that the ratio of height to length of the window played an important role. The air properties are described, and such description can be a useful tool to predict the rate of ventilation in buildings that contain this type of window. The Standards Association of Australia was used in Clause 4.8, which stated that a flow rate of 0.03 m^3/s to 0.04 m^3/s through residential buildings (offices, residences, shops, stores, and corridors) was generally suitable for natural ventilation.

Wong and Li (2007) examined the effectiveness control methods for buildings by using passive climate and conducted field measurement and computational simulation. Their results show that the best orientation of the building is north/south and that the highest surface temperature of external walls occurred at a middle floor instead of a high floor. They also found that east and west external walls can reduce the heat gain from solar radiation. The shading device of the window helps to reduce the cooling load and save energy. Results indicate considerable energy and

cost savings and also indirectly lower workload on the environment, because energy use always corresponds to the production of waste materials Wong et al. (2003).

Chen (1996) compared five different k–ε models, including the standard k–ε, the LR k–ε, and the RNG k–ε model. He recommended only the RNG k–ε model for simulations of indoor air flow and noted that the performance of the other models was not stable.

Rouaud and Havet (2002) showed that the standard k–ε and the RNG k–ε model effectively predict the main features of the flow in clean rooms. They also claimed that the RNG k–ε appears more suitable, whereas the standard k–ε model overestimates turbulent diffusion.

Gebremedhin and Wu (2003) evaluated five RANS models (the k–ε, RNG k–ε, LR k–ε, k–ω, and the RSM) with the code (PHOENICS 1999). On the basis of convergence and computational stability criteria, they concluded that the RNG k–ε model is the most appropriate for characterizing the flow field in a ventilated space.

Vasanth et al. (2013) studied the standard k–ε model, RNG k–ε model, realizable k–ε model, and standard k–ω model to simulate the experiments. Results show that the standard k–ε model facilitated the CFD simulation of the experimental results.

Shafqat Hussain et al. (2012) evaluated the prediction of indoor air flow and temperature distributions. They tested turbulence models for various thermal conditions in two existing buildings by using RANS modeling. The resultant steady-state governing equations were solved using FLUENT. The numerical results for a particular time of day were compared with the experimental data. The performance of two-equation turbulence models (the standard k-ε, RNG k-ε, realizable k-ε, standard k-ω, and SST k-ω models) is better that of the one-equation model (Spallart–Allamaras) and that among the two-equation models.

Ayad (1999) used CFD to study the characteristics of ventilation for a room with various opening configurations. The model is verified by comparing the results of 2D steady flow with experimental values. These analyses have been taken as a reference model to allow computational domain atmospheric air to flow across the room. Sinha et al. (2002) analyzed air distribution in a room numerically with or without the effects of buoyancy to the entrance or different outlet configuration of the rooms under cross ventilation. Telebany et al. (1985) and Dascalaki et al. (1996) experimentally investigated natural ventilation in single-sided ventilation. Etheridge (2001) presented charts for the design of non-dimensional natural ventilation for two rooms with one-sided cross-ventilation. Mokhtarzadeh et al. (1990) and Papakonstantinou et al. (2000) focused on the analysis aspects of ventilation in a single-sided room via CFD. Tahir Ayata et al. (2005) investigated via CFD the

potential of using natural ventilation as a passive cooling system in new building designs in a moderate climate.

2.10 Conclusion

An examination of window design for natural ventilation using scientific methods is needed. The literature shows that CFD is preferable because it can be used for many natural ventilation situations. The WWR is used as one design criterion based on (Dahlan, N.D et al. (2001) and Wang et al. (2007). In this research, the 3D CFD code used FLUENT 6.3 to predict temperature distribution and air velocity, but its application was limited to research related to windows in desert buildings and ventilated buildings. The K-epsilon turbulent model followed Ooi et al. (2007), Jeol et al. (1999), Nohora H.B. (2005), Yongsan et al. (2007), Bangalee (2012), Cheong et al. (2003), Stavrakakis et al. (2008), and Anastasia et al. (2013). Furthermore, the height to length ratios of window dimensions is based on Jong and Bot.

CHAPTER 3

EXPERIMENTAL AND NUMERICAL SETUP

3.1 Introduction

The methodology adopted for this thesis comprises field measurements in Hoon City, Libya and the Faculty of Engineering lecture office at the Univeristi Putra Malaysia. The basic data were used to evaluate the PMV and PPD. The field data for Malaysia were used as the input parameter to design windows with the optimum size for natural ventilation in an office by using CFD. The Libyan data were used to validate the results for the Malaysian site using the same 36 models and to check the optimum design for the Libyan site.

3.2 Experimental Setup (Libya)

Data were collected in 2009 to determine the air flow and temperature profile inside an office in a modern air-conditioned building in a desert. Field experiments were conducted in the south of Libya, specifically in the city of Hoon in the province of Al-Jufrah. The focus was on air temperature distribution, air velocity circulation, and the temperature difference between outdoors and indoors. These parameters were judged by using an appropriate simulation technique.

3.2.1 Building Description and Tested Office

The study was conducted on a four-story air-conditioned building, which is an administrative office center built in 2002. This building is representative of Libya's regional development. The building is in Hoon City, Al-Jufrah province, Southern Libya, which lies at 29° 7' N latitude and 15° 65' E longitude 300 km south of the Mediterranean coast. The research was undertaken when the weather was hot and dry during the summer season in the inland region that is primarily desert.

The complex includes 2 main buildings, 14 office buildings, and a conference hall; the site is roughly 14.2 hectares. The conference hall facilitates functions of the regional secretariat. It contains a comprehensive conference and concert hall that can accommodate 600 people, as well as multi-purpose spaces, a library, and maintenance facilities. The main buildings are blocks of four floors with entrance courtyards and halls that form a welcoming spatial group.

The building shows the use of large glass areas to create a distinct functional entity that resembles a closed main square that is surrounded by wall-like building masses that protect against sun and desert winds. The external walls are made up of concrete that consist of two sides, each of which is 20 cm thick. Between these sides is polyurethane foam that is 5 cm thick; the foam prevents the entry of heat into the

office. The aluminum double-glazed windows consist of green tinted glass and sunscreen. The main doors, railings, and sunshades are made of stainless steel. The ground office is covered with marble; the internal and external walls are painted white, which reduces the effect of solar radiation on the exposed surface. The types of buildings are shown in Figure 3.1, and the test office is shown in Figure 3.2.

The tested cellular office was located on the third floor and windows face north to 20 ° E. Its interior dimensions are 4.50 m × 3.80 m × 3.20 m (length × width × height) with a 30% floor area.

Figure 3.1 : Buildings in Hoon, Libya (Source: Al-Jufrah administration).

The vertical double green low-E window dimensions are 2.36 m × 2.36 m × 14 mm (length × width × thickness), as shown in Figure 3.2; the schematics are shown in Figure 3.3.

Figure 3.2 : Test cellular office.

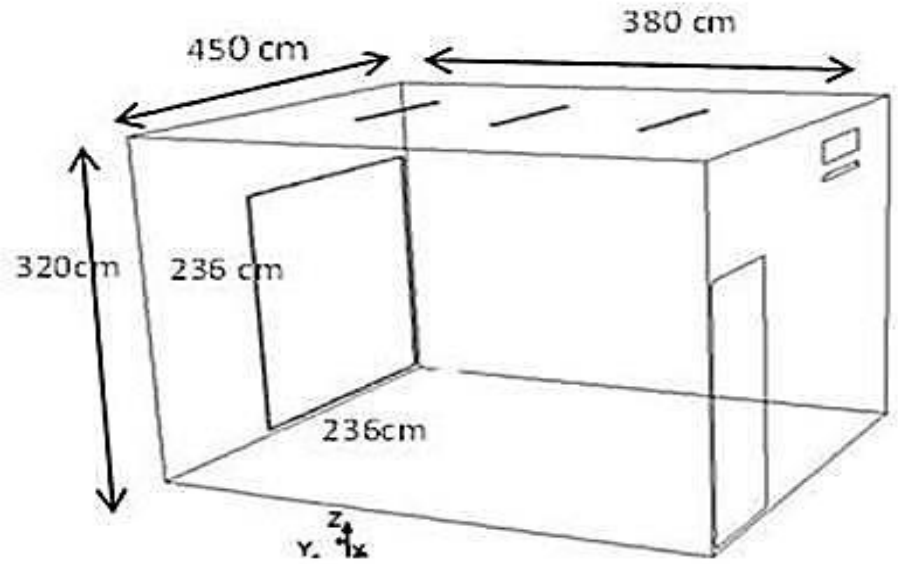

Figure 3.3 : Schematic of the test office.

3.2.2 Installation and Calibration of Thermocouple Wires

The accuracy level of the measuring elements is one of the important requirements to carry out measurement tasks in the experimental system. The type K thermocouple wires were calibrated before data collection. Calibration is the process of establishing accurate readings for a measuring device. To test thermocouple wires, an ice bath was used as the reference temperature. The ice bath maintains the water temperature (reference temperature) to within 0.1 ℃. This approach is the simplest and most widely accepted calibration method.

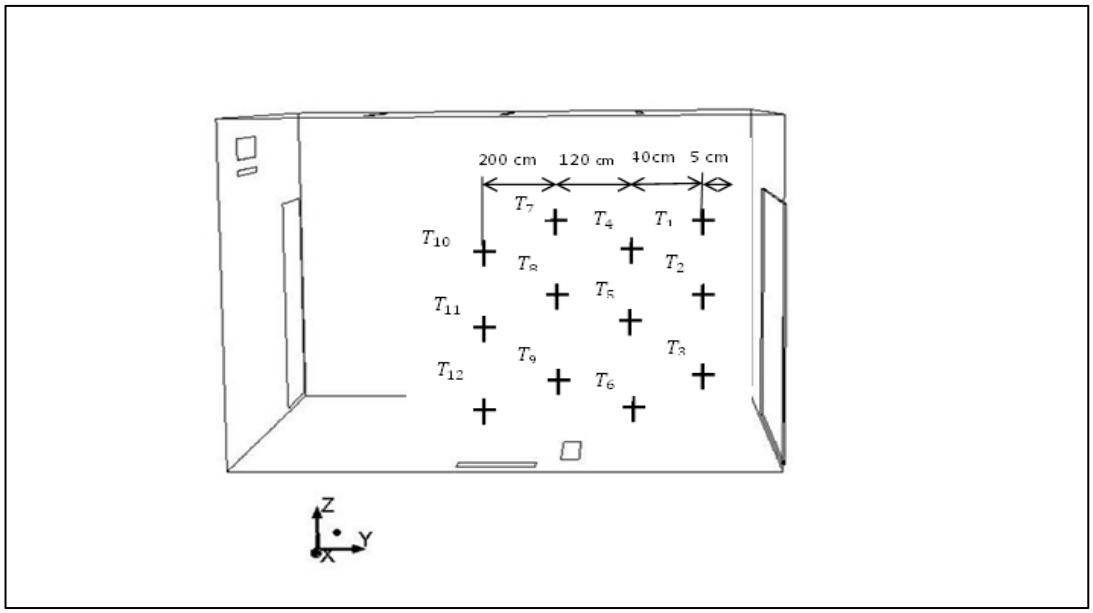

Figure 3.4 : Locations of thermocouple wires in the Libyan office.

Figure 3.5 : Locations of thermocouple wires above the window of the Libyan office.

3.2.3 Field measurements

3.2.3.1 Outdoor measurements

Solar heat gain, relative humidity, wind velocity, and dry and wet bulb ambient temperatures were facilitated by the Libya Meteorological Department (LMD) at Hoon. The station was located in an open space without any buildings,

approximately 300 m from the test building. The measurements provided to the station were taken every 3 hours. The weather station provided essential data to support the development of computational models (CFD). The measurement data are shown in Appendix A.

3.2.3.2 Data Collection

The experimental measurements were conducted between July to September 2009, which is the hottest period of the year in Libya. Sarah L. et al. (2006) conducted a field study to monitor the dust distribution for a year from three regions across Libya. Their field measurements were taken from July, August, and September.

The air conditioner was operated from 8:30 am to 6:00 pm. Its temperature was controlled to between 16 and 18 ℃. The temperature stability and equilibrium was established gradually roughly 30 minutes after the air conditioner was activated. The continuous collection of the data was carried from 09:00 to 18:00. All measured signals were channeled to a nearby data logger station at one-second intervals. Data from the data logger were uploaded to a PC using software provided by the data logger company. The data acquisition system for acquiring thermocouple temperature included a relative humidity sensor that consisted of a programmable data logger (D80 and 85). Online transfer was possible through the type T thermocouple wires to a portable PC, as shown in Figures 3.5 and 3.6.

In this study, the measurement data are solar irradiation, air temperature, temperature on double glass surfaces, and air velocity inside the test office. The data were collected for three months; the collected data are shown in Appendix B.

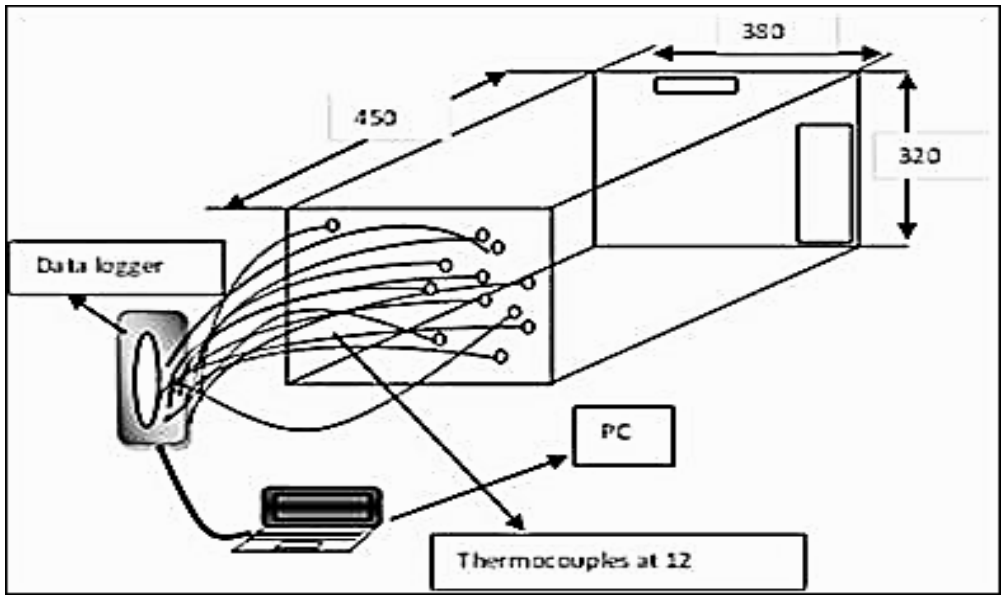

Figure 3.6 : Thermocouples in 12 locations in the office.

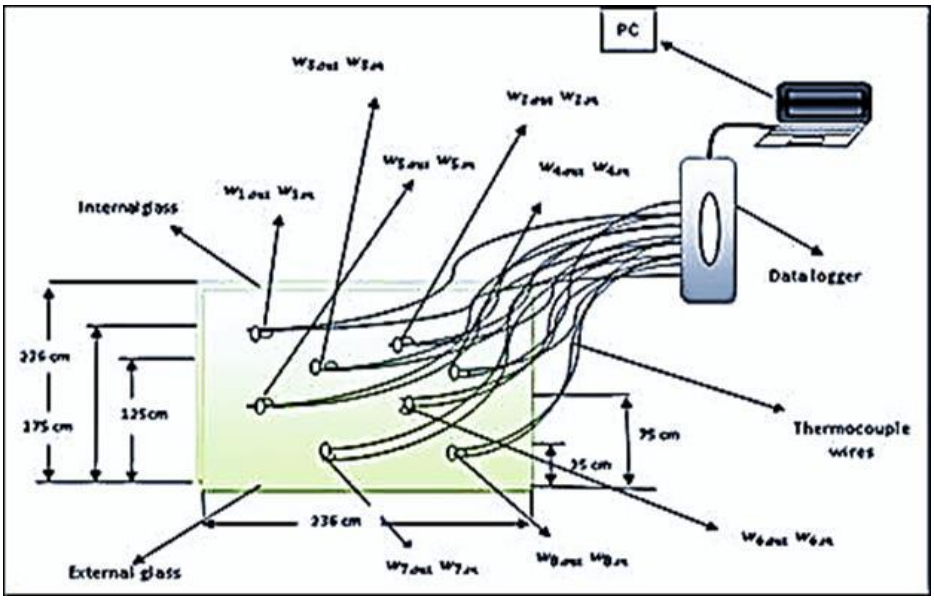

Figure 3.7 : Thermocouple placement on surfaces of double-glazed window.

Temperature measurement arrangements, including 16 thermocouples, were placed at eight segments of the center glaze outer surface and eight segments of the center glaze inner surface (6 mm). These arrangements measure the surface temperature (Figures 3.5 and 3.6). The experimental design is presented in Table 3.1.

Table 3.1 : Design of experiment in the Libyan work

Shapes of building	Materials	Time	Points
Types of administrative Centre Air-conditioner buildings in Desert Country	✓ Air-conditioner an Office ✓ Double glazing window	9 am 12 noon 15 pm 18 pm	✓ Twelve thermocouples (1 to 12), distance (0.5 cm, 40 cm, 120 cm and 200 cm) from window, show Figure 3.4. ✓ Eight points on the outer center surface and eight on the inner center surface, show Figure 3.6.

3.2.4 Measuring Equipment and Materials

Materials and equipment required for the experimental studies in Libya and used in both measurements are summarized in Table 3.2.

3.2.4.1 Thermocouple wires

In this study, type (T) thermocouple wires were selected to measure the temperature within the range of –40 ℃ to 1200 ℃. Thermocouple wires are flexible, reliable, and easy to use; they are widely accepted for temperature measurements in the field.

Table 3.2 : Materials and equipment

Item	Measuring sensor	Uncertainty	Specification	Location
Glass surface temperatures and Air temperatures	Thermocouple wires of type 'T'	+1.0%	40 o C to 1200 o C	Indoor
Irradiations flux	pyranometer		30 °to 70 ℃.	indoor
Humidity	model HX92A sensor	+/- 2.5% RH		Indoor
Data logger D80 and D85 With laptop computer	(40-channel logger) to collect data		logged at 1-min Intervals	Indoor
Wood angles	To make test rig			Indoor
Double glass window	inner surface (clean glass) outer surface (e-low glazed glass)			Outer and inner

3.2.4.2 Pyranometer

The LP02 pyranometer is a common solar radiation sensor that measures the solar radiation inside the office, as shown in Figure 3.8. The pyranometer can be used outdoors under the sun and indoors with solar simulators. Its orientation depends on the application and may be horizontal, and it can be connected directly to commonly used data logging systems.

3.2.4.3 Data Logger D80

Data logger records environmental parameters such as temperature, relative humidity, wind speed and direction, light intensity, water level, and water quality over time. Figure 3.9 shows two types of data loggers, namely, D80 and D85. To improve the accuracy of thermocouples, they may be calibrated by a calibration lab. In this particular scenario, a calibration lab provided a certificate that identifies calibration data at certain temperatures.

Figure 3.8 : Pyranometer sensor (LP02).

To apply these corrections in the calibration data logger, a polynomial must first be generated. The technique involves calculating polynomial equations for account adjustments.

Figure 3.9 : Data loggers D80 and D85.

3.2.4.4 HX92A Sensor

The HX92A sensor, as shown in Figure 3.10, is protected by a stainless mesh-type filter that can be removed easily for cleaning. The sensor is used to measure humidity inside an office

.

Figure 3.10 : HX92A sensors for measuring humidity.

3.3 CFD Simulation (Libya)

CFD has become a helpful tool for designers. The commercial CFD software ANSYS-FLUENT 13.0 was used based on the finite volume of the simulation approach for the measurements in Libya. This technique involves the application of CFD and has achieved considerable success in office design; its performance advantages in analysis were observed by Franke (2010). The study involves modeling and simulation to solve fluid dynamic problems using CFD in three dimensions. The CFD solver FLUENT 6.3 was used to simulate temperature distribution and air flow in the office. Modeling and simulation were carried out by using FLUENT 6.3. The software was chosen because of its simplicity and user friendliness, and because it does not require extra modules.

3.3.1 Physical Model and Assumptions

3.3.1.1 Physical Model

The study subject is a four-story air-conditioned office building in the administrative center, as shown in the schematic diagram of office design in Figure.3.11. The tested office was located on the third floor of a reinforced concrete building. The office dimensions are 4.5 m × 3.80 m × 3.20 m (LWH), as shown in Figure 3.12. Double vertical glass overlooks the northern facade of the building; the dimensions for each layer are 2.36 m × 2.36 m × 6 mm (length, width, thickness) for each layer, and the space between the two surfaces is 20 mm.

The exterior walls face the east and north, whereas the interior walls face the west and south. The exterior walls are made of reinforced concrete, and they are double walls, each of which has a thickness of 20 cm. Figure 3.13 shows the flowchart for the methodology adopted for this research.

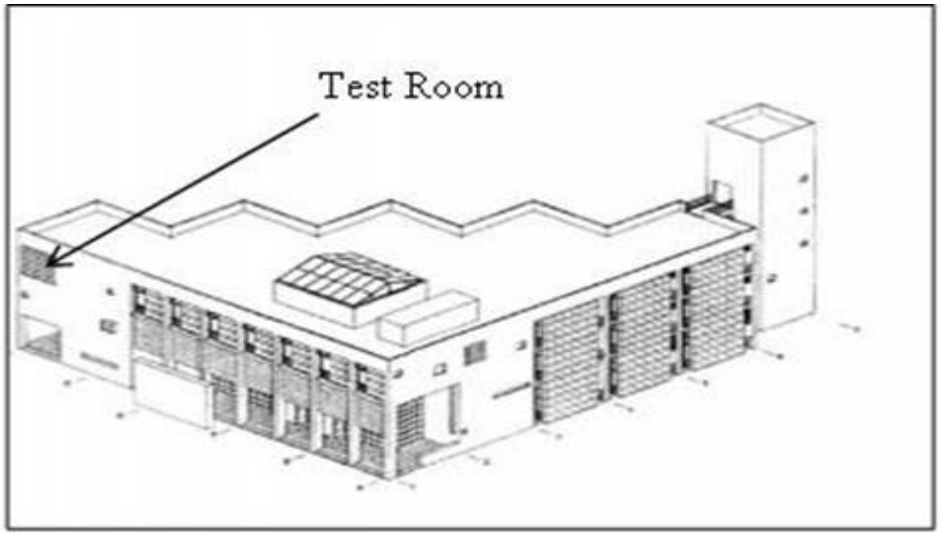

Figure 3.11 : Sketch of the building.

The space between the two walls is filled with polyurethane foam as an isolating material with a thickness of 5 cm. The office floor is covered with a marble material. The internal and external faces of the walls are painted white. An air conditioner blower was installed asymmetrically in the office and was located on the south-facing wall.

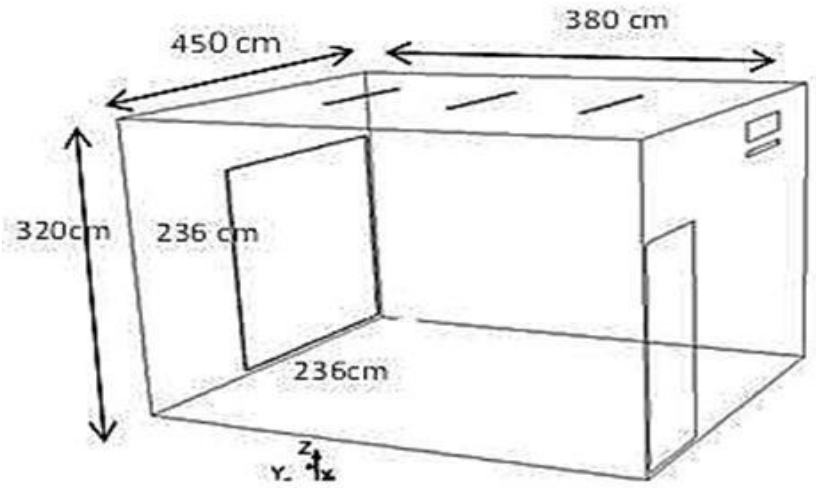

Figure 3.12 : Sketch of the office room model.

The distance between the air conditioner and both the ceiling and ground is 0.15 and 3 m, respectively. The room is illuminated by three sets of twin fluorescent lights. The main goal of this study is to evaluate the internal distribution of temperatures starting from the window to the opposite end of the room, as well as to evaluate the temperature difference between the outdoors and the indoors of the office.

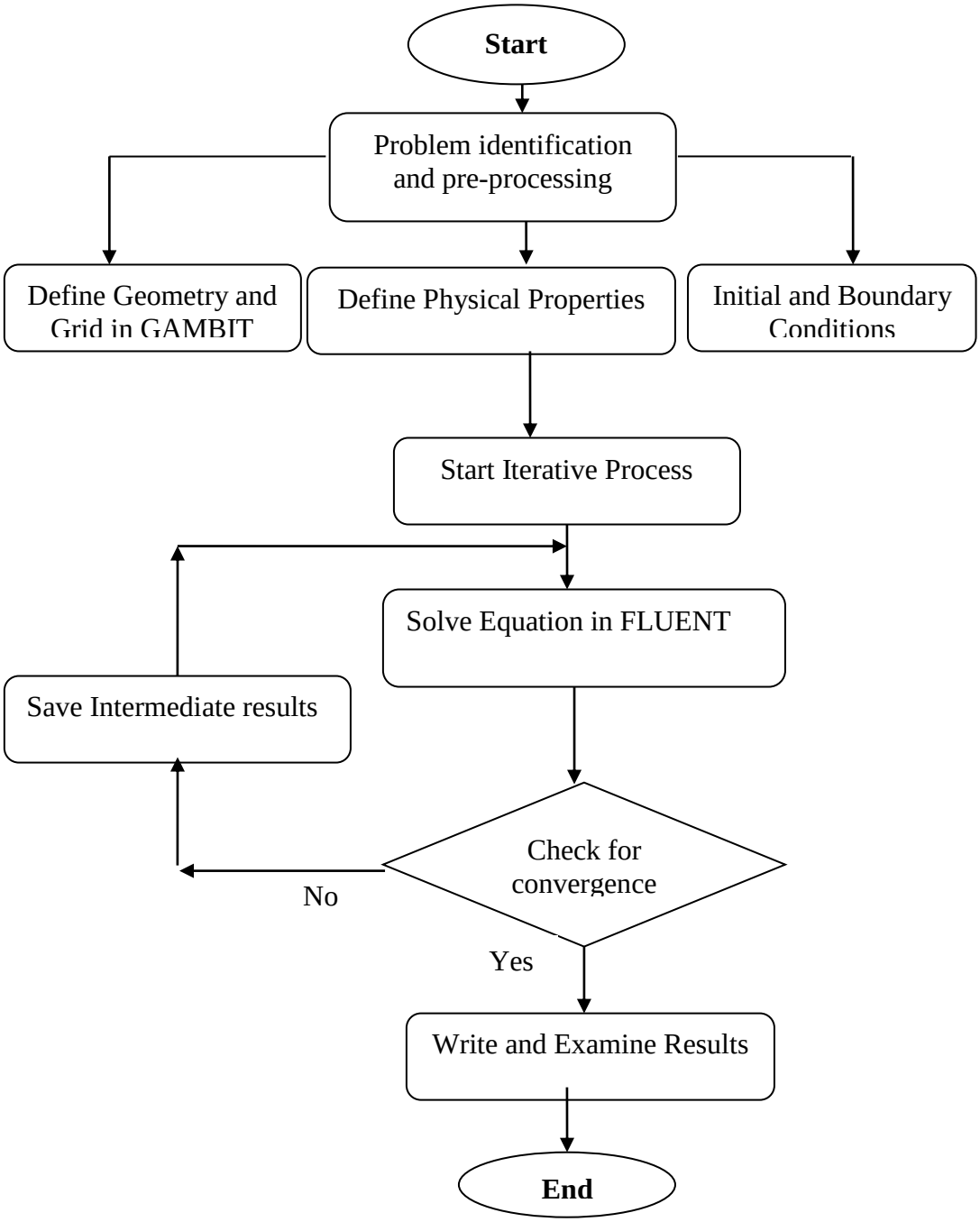

Figure 3.13 : Stepwise flowchart of CFD analysis of the Libyan office.

3.3.1.2 Governing Equations

3.3.1.3 Code Validation

Code validation is important in any numerical work because the assurance of numerical code is valid with other previous works, thereby facilitating further implementations. The code validation should obtain results that are identical or very close to those of previous studies. Its capabilities and its limits are well understood. The code validations of this study depend on two numerical papers based on Cheong K. (2003) in which PHOENICS was used for 3D numerical simulation of an office environment inside a thermal air-conditioned lecture hall in the summer. The velocity and air temperature field data were simulated in an air-conditioned room. Numerical simulation has shown close agreement with the experimental data as indicated by an analysis and comparison of the maximum accuracy error of 8.23% between the measurement and simulation results. Ooi et al. (2007) analyzed temperature and velocity distribution over various virtual planes for different locations of the air conditioner blower to achieve maximum comfort for the occupant. The k–ε and Reynolds stress models for turbulence flow were used for the analysis.

3.3.1.4 Boundary Conditions

The boundary conditions are significant for the numerical solution of this problem. The type and the numerical values should be selected carefully especially for the turbulence amount. The air inlet the outlet of the air conditioner and the wall of boundary conditions are the main areas of interest in this study. The CFD model boundary conditions were provided by the experimental measurements of the wall temperatures. Figure 3.14 shows the surface boundary conditions used in the CFD simulation based on the experimental work. The summary of indoor loads in the test office is shown in Table 3.3.

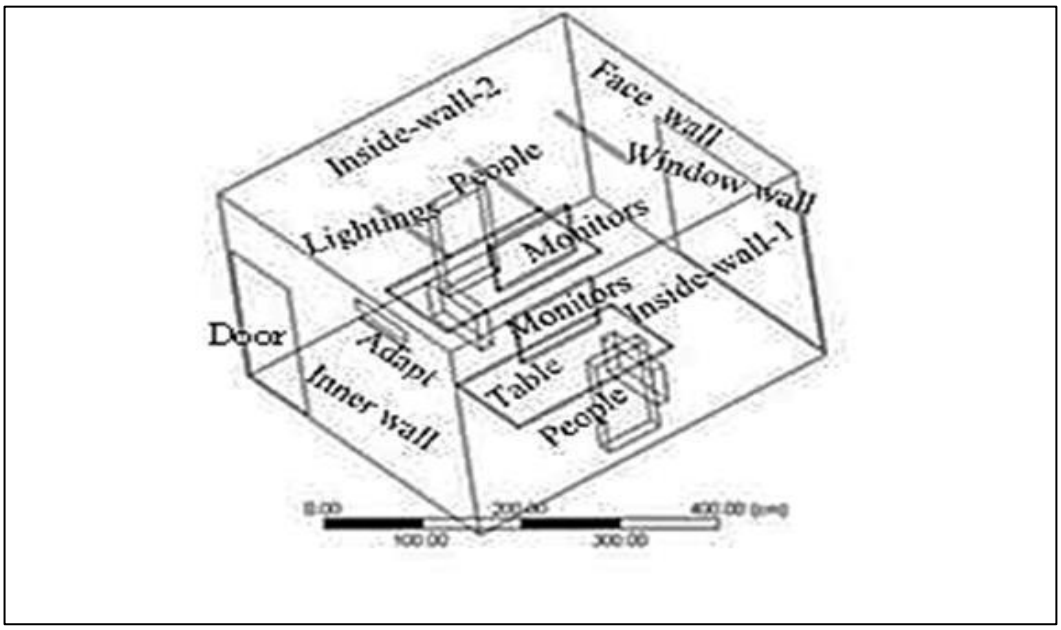

Figure 3.14 : Surface boundary conditions of the office.

Table 3.3 : Boundary conditions of the Libyan office

Boundary	Type	Count	Heat transfer	
Face wall	Wall	1	T= 297K	Measurements, 2009
Window wall	Wall	1	T= 296K	Measurements, 2009
Outer glazed window	Wall	1	heat transfer coefficient	Measurements, 2009
Inner clear glass window	Wall	1	T= 300 K	Measurements, 2009
inside-wall-1	wall	1	T= 298 K	Measurements
inside-wall-2	wall	1	T= 298K	Measurements
Inner wall	Wall	1	T= 298K	Measurements
Computers	blocks	2	Heat flux 75 w/m^2 x 2	ASHRAE.2012
Monitors	Wall	2	Heat flux 10 w/m^2 x 2	ASHRAE.2012
Lightings	blocks	3	Heat flux 120 w/m^2 x 3	ASHRAE.2012
People	People	2	80 w x 2	ASHRAE.2012
Inlet air flow (adapter)	vent	1	T= 293 K	Measurements, 2009
Outer air flow (adapter)	open	1	T= 296 K	Measurements, 2009
Table	Wall	2	Ignorant	
Door	Wall-close	1	Ignorant	
ceiling	Wall	1	297 K	Measurements,2009
floor	Wall	1	300 K	Measurements.2009

The coefficient of heat transfer through window ranged between 1.8 w/K to 2.2 w/K (Appendix A). The volume conditioner properties of the blocks are shown in Table 3.4.

The geometry mesh used in this study is a conjugate heat transfer and air flow analysis that includes two partitions. The first partition has 402270 cells and 832613 faces; the second partition has 404059 cells and 828626 faces. The total partitions have 806329 cells. Different types of cells can be used for meshing.

Table 3.4 : Volume conditioner setting for properties of blocks

Code	ANSYS-FLUENT 13.0
Turbulence model	RNG (renormalization group) k-ε model
Algorithm	Steady state (SIMPLE)
Analyzed area	4.5m ×3.80m ×3.20m +2.36m x 2.36m x0.32m
Convection and radiation term scheme	QUICK Scheme
Wall boundary condition	Standard log-low, adiabatic
Cells of mesh	806329

3.3.1.5 Geometry Mesh

Tetrahedron, hexahedron, and prism dimensional cells are available for meshing. The hexahedron cell was chosen because of its homogeneity with the office model (CFD). Non-uniform grids were used for the consideration of positions with large gradients of solution variables (air velocity and temperature). The three types of grid spacing are 15 cm (coarse), 10 cm (medium), and 7.5 cm (fine). The non-uniform grids were used in consideration of the positions with large gradients of solution variables (air velocity and temperature). Grid refinement occurs on the window surface in the presence of heat source, and the mesh was tested independently (Figure 3.15).

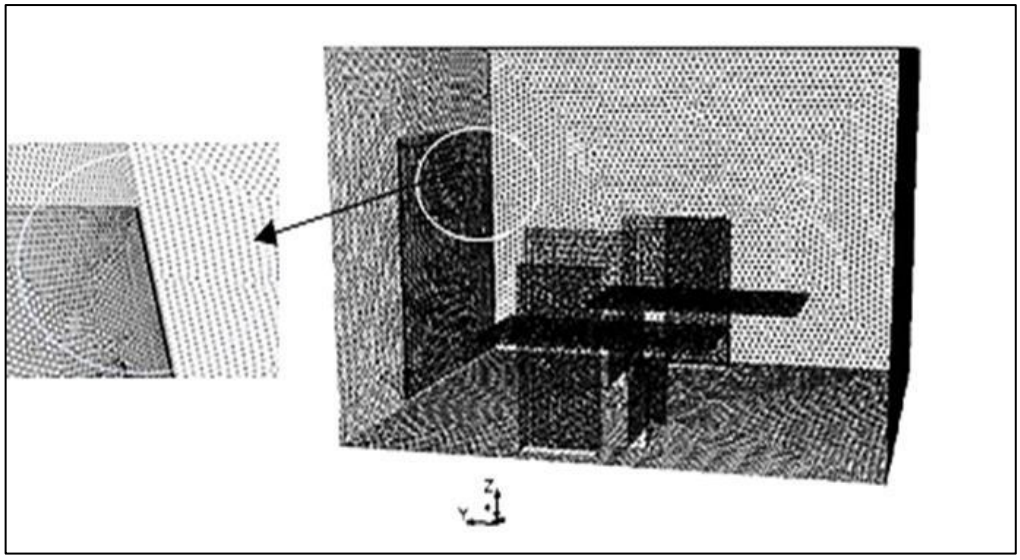

Figure 3.15 : Grid mesh generation

3.4 Experimental Work and Numerical Simulation (Malaysia)

In this section, air velocity and temperature within an office with cross natural ventilation through windows was determined inside an office in the Faculty of Engineering administrative building of Universiti Putra Malaysia. The fifth-floor office was chosen because its layout and size are typical for the office of a Malaysian government official. The office can be used as a reference to model dimensional analysis of double-glazed windows. The effects of these parameters on temperature distribution and air flow velocity from a window were judged using an appropriate simulation technique (CFD).

3.4.1 Experimental Work

The analysis of the Malaysian office was completed via a combination of measurements with experimental work to focus on specific areas.

3.4.2 Description of the Building and the Selected Office

The field measurement was conducted in the Faculty of Engineering of Universiti Putra Malaysia. The seven-story building was built in 2005 and is geometrically facing and oriented at 22 ° from north to the true east. It is located between the ground floor workshop in the north and a lake in the south. The shape of the building is cuboid, as shown in Figure 3.16.

Figure 3.16 : Test window of the office of the Engineering faculty at UPM

The height of the building was roughly 29.6 m from ground to top of the building, and the height from the ground to the fifth floor was 19 m. Figure 3.17 shows the plan of the fifth floor of the building. The diagram shows that the east and west walls of the office are adjacent to other offices; the north wall is located in the exterior, whereas the south wall is located on the corridor. The temperature data

were recorded by using thermocouple wire throughout the daily cycle (8 am–4:40 pm). Measured parameters include surface glazed window temperatures and interior temperatures.

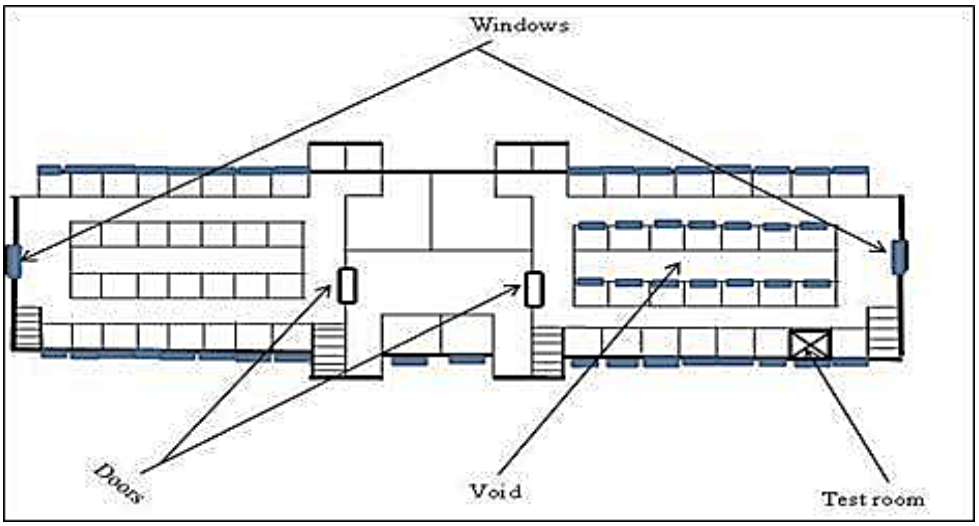

Figure 3.17 : Schematic view of the fifth floor of the building

Temperature measurement arrangements include four thermocouple wires placed near the opening window at the center of the office near the door and surface windows; these were used to measure the temperature. The experimental design is presented in Table 3.5.

Figure 3.18 Test lecture office

Table 3.5 : Design of experiment in the Malaysian work

Shapes of building	Materials	Time	Points
Types of building	✓ Air-velocity ✓ Temperature	(solar time) From 8:00 To 16:40 pm	✓ Installation thermocouples wires distance (0.05 m, 1m, 2 m and 3.85) from ✓ Surface windows. ✓ External Temperature, air velocity and humidity

3.4.3 Measuring Equipment and Materials

3.4.3.1 Installation of Thermocouple Wires

Experimental data for natural ventilation of the Malaysian office were measured. The main factors for driving forces of natural ventilation are temperature, air velocity, wind direction, and relative humidity. The outdoor conditions are a significant factor when studying natural ventilation. The measurements included both outdoor and indoor data conditions.

3.4.3.2 Measuring Equipment

The materials and equipment required for performing the experimental studies and used in measurements are shown in Figure 3.19 and Table 3.6.

Figure 3.19 : Measuring equipment.

Table 3.6 : Materials and Equipment

Item	Measuring sensor	Uncertainty	Specification	Location
Single Glass surface temperatures and Air temperatures	Thermocouple wires of type 'T'	+1.0%	40 o C to 1200 o C	Indoor
Irradiations flux	pyranometer		30 °to 70 ℃.	indoor
Data logger D80 With laptop computer	To collect data		logged at 1-min Intervals	Indoor
To measure air velocity	Velometer AVM 440		Accuracy with max reading of 30 m/s	Outdoor and Indoor
Measure wall	Infrared thermometer			Indoor
For software and data analyses	Laptop			
To measure air temperature and air humidity inside the office	thermo-hygrometer			Indoor

3.4.4 Field Measurements of UPM Test Office

The field measurement from the measurement data were used as input data for simulation of a tropical office. The dimensions of the single office in this study were 2.85 m × 3.80 m × 2.60 m. Data loggers were stationed at three different points in the indoor environment to record air temperature.

3.4.4.1 Outdoor Measurements

Typical meteorological measurements included the daily average for one year (2013) from Meteorological Station Malaysia. This station is located in Petaling Jaya, Kuala Lumpur, and it provides essential data to support the development of computational models (CFD) for entire simulations. The meteorological station measures wet bulb temperature, dry bulb temperature, relative humidity, global radiation, wind velocity, and direction. The average relative humidity does not vary considerably throughout the year and is lowest in July (74.3%) and highest in November (83.1%). The average wind velocity in the city is 5.0 m/s. The average dry bulb air temperature was lowest in January (27.0 ℃) and highest in June (29.2 ℃). The average wet bulb air temperature was lowest in January (24.1 ℃) and highest in June (25.8 ℃). The average wind velocity near the experimental building was lowest in January (5.01 m/s) and highest in May (10.8 m/s); the table of the data is shown in Appendix C. The outdoor temperature was measured by using the

Velocicalc Model 9545A. The outdoor wind direction was recorded from Meteorological Station Malaysia and applied in CFD.

3.4.4.2 Indoor Measurements

The data acquisition system for acquiring thermocouple air temperature (T) used thermocouple wires and a data logger (D80). The measurements of indoor air temperature at opened windows and the opened door were taken at a one-minute interval. The measurement installation of thermocouple wires for air temperature, surface of windows, and air velocity inside the office is shown in Figure 3.20. Two measures of air velocity (inlet and outlet) near opened windows provided the components of inlet air velocity and outlet boundary condition for the CFD model; the measurement setup for (V) air velocity (m/s), relative humidity (%), and (P) pressure indoors and outdoors was measured by using Velocicalc Model 9545A. The thermocouple wires were installed on glazed surfaces of windows and in four various positions inside the office (Y):, 0.05 m near the opened window (inlet) at 1 m, in the center of the office at 2 m, 3.80 m near the opened door (outlet), and 1.5 m from the floor level (Z) at the level of a sitting person (0.6). The accuracy of thermocouple wires was calibrated in the laboratory, and a certificate was provided to indicate the calibration details for certain temperatures. The outlet temperature was measured using Velocicalc Model 9545A, which was used to measure ambient temperatures, outdoor relative humidity, and outdoor air velocity. The measurements were conducted with an accuracy of ± 0.5 ℃. The velocimeter AVM 440 has an accuracy of 1.5% and max reading of 10.6 m/s. The CFD model validation of indoor air temperatures was conducted from four points within the office. The first point consisted of measurements of outdoor and indoor environmental conditions on August 2013 with a specific focus on seven sequential days.

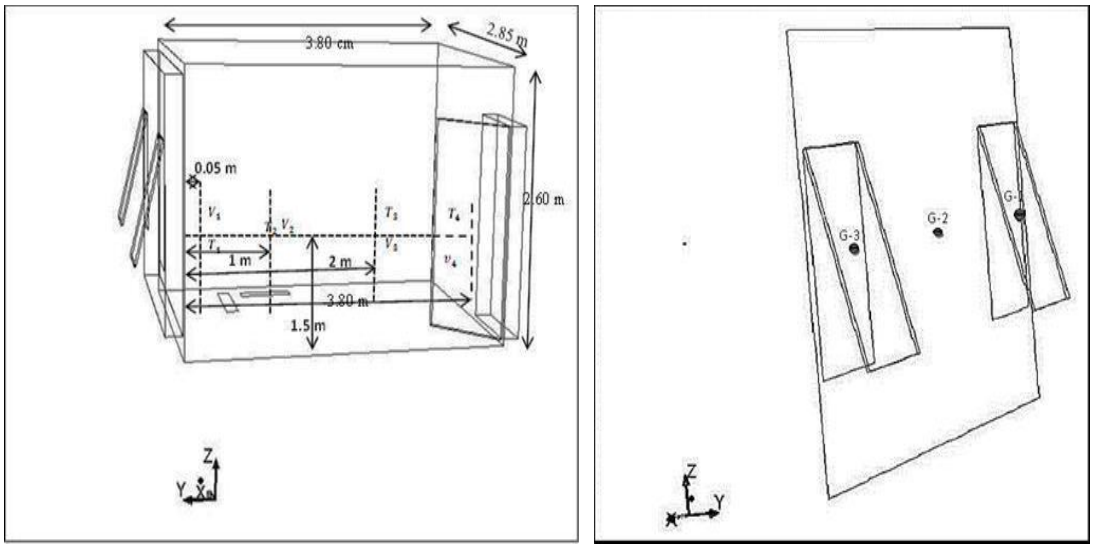

Figure 3.20 : Location of thermocouples in the test room.

The full-scale field measurements were taken from the start to the end of August 2013. During the measurement period (August 22, 2013), the outdoor environment was measured from 8:00 am to 4:40 pm by using the velocimeter AVM 440 to check ambient temperature, wind speed, and relative humidity. Solar irradiance (W/m^2) was measured using a pyranometer senor (LP02).

3.4.5 Experimental Work for Best Window Model Size

The experimental data were used to verify the window model. The experiments were performed in the Malaysian model office, which had dimensions of 2.85 m $\times$ 3.80 m $\times$ 2.60 m. The total air volume is 28 m^3. The east and west walls of the office are adjacent to other offices; the north wall is exterior, whereas the south wall is located on the corridor. The two double-glazed windows used for testing were mounted in the center

of the front wall with dimensions of 0.52 m $\times$ 1.15 m. The test windows were of the same size, and the opening mechanism is shown in Figure 3.21. The measurement devices for performing the experimental studies are listed in Table 3.7.

Figure 3.21 : Measuring equipment

The basic characteristics of the measurements in the office are as follows:
Air Velocities: Steady-state velocity measurements were obtained at three locations, namely, near the window, the center of the office, and near the door. The accuracy of the measurements was determined at $\pm$0.025 m/s for velocities in August 2013.

Table 3.7 : Measuring items

Item	Measuring sensor	Uncertainty	Specification	Location
Thermocouple wires of type 'T'	Double glazed surface temperatures and Air temperatures	+1.0%	**40°** C to **1200°** C	Indoor
Pyranometer	Solar radiation		30 °to 70 ℃	Indoor
Data logger D80 With laptop computer	To collect data		logged at 1-min Intervals	Indoor
Velometer AVM 440	To measure air velocity		Accuracy with max reading of 30 m/s	Outdoor and Indoor
Infrared thermometer	Measure wall			Indoor
Lux meter	To measure light level			
Pelican Case 1120	To measure average air velocity and humidity			Indoor
Laptop	For software and data analyses			
Thermo-hygrometer	To measure Average air temperature And air humidity inside the office			Indoor

Air and wall temperatures: Steady-state air temperatures measurements were measured at three locations with thermocouple wires. The side wall temperatures, ceiling, and floor of the model office room were fixed. Layers of double-glazed windows were measured by thermocouple wires. The accuracy of the temperature measurements was determined at 0.1 and 0.125 ℃ for the thermocouple wires. Typical meteorological measurements included the daily average for one year from the Malaysian meteorological station. Instantaneous measurements of outdoor air temperatures, air velocities, and humidity were used.

Measuring Equipment

The materials and equipment used in experimental data for the verification of window model are shown in Figure 3.22.

Figure 3.22 : Required materials and equipment.

3.5 Numerical Setup (CFD) Malaysia

At the Malaysian office, CFD simulation was conducted by using commercial CFD software. The air flow and stratification of air temperature were simulated in a naturally ventilated room occupied by one person in the office.

3.5.1 Physical Model

The reference office model uses large glass areas with dimensions of 230 mm × 259 mm. Two 6 mm thick glazed windows can be opened. The dimensions of both inlets of windows were 1.14 m x 0.52 m, as shown in Figure 3.23. The windows were coated with a thin silver film to reduce heat from solar radiation.

3.5.2 Geometry Mesh

The geometry was created in 3D for the office on the basis of technical drawings and field measurements, thereby comprising the details in the CFD model. The office geometry mesh used in the study is shown in Figure 3.24.

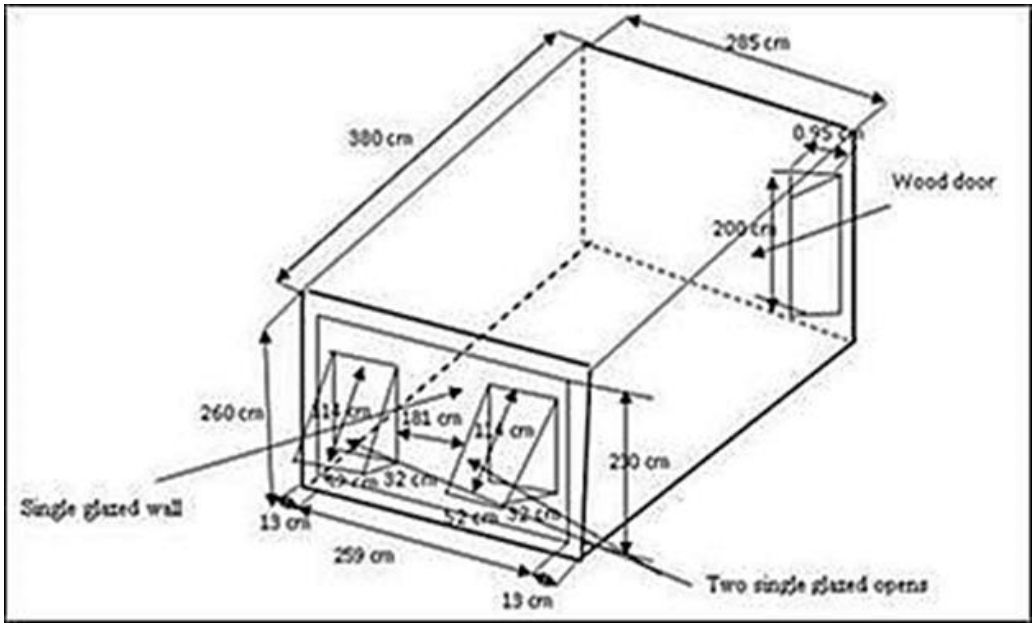

Figure 3.23 : Physical model of the Malaysian test office.

An unstructured hybrid mesh of element generator with the adaptive mesh refinement algorithm was used automatically; this mesh allows a highly accurate representation of the boundary conditions. The use of the mesh can reduce numerical errors and improve the consistency of cross-domain solving. The numerical grid consists of approximately 39030 unstructured elements, and a hexahedron-type mesh was used for the shapes of windows, office, corridors, tables, computers, and humans. The total number of mesh cells for the office room is 1066636.

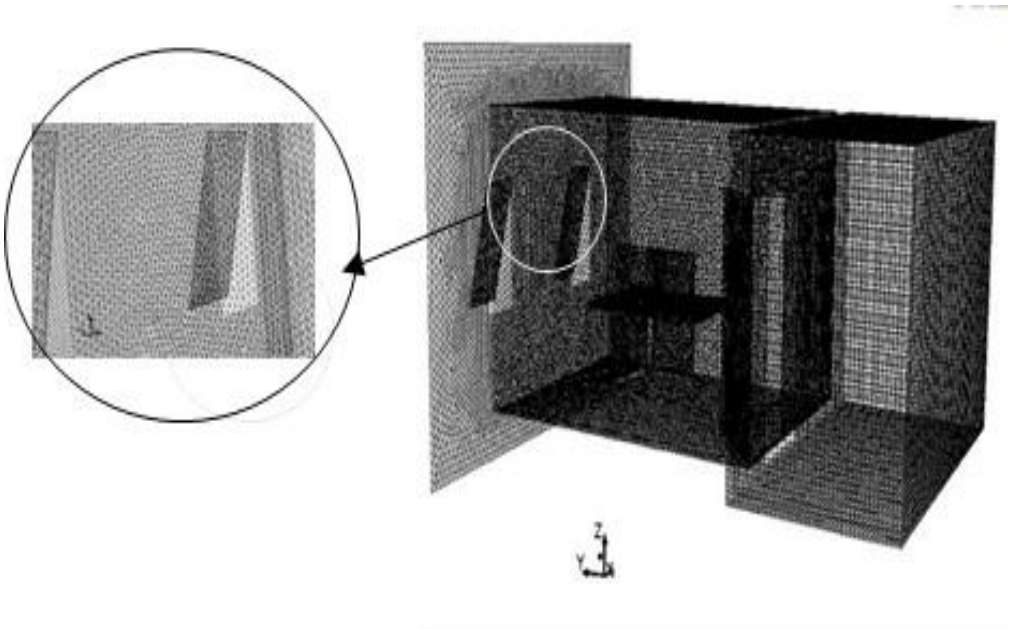

Figure 3.24 : Mesh model: Office model view, Front glazed window wall.

3.5.3 Boundary Conditions

Specification of boundary conditions is essential for a realistic simulation result. A general rule to apply in establishing realistic boundary conditions is to follow mass and energy conservation. The measurement data were collected to support CFD simulation during field measurements in the test office on August 22, 2013. Outdoor weather conditions and the speeds of the indoor air and the air temperature were monitored throughout the day. The office room is a highly glazed space with two windows and a glazed wall that covers the majority of external walls. The windows of the office face north to 22^{o} east; the radiation model was included in the CFD simulation. The boundaries of this model indicate that the boundary conditions are specified for the simplified computational domain. The geometry used in the computations is approximately the same with the original geometry, as shown in Figure 3.25. The outdoor air entered through the northeast facing window (window gap) and exited through the southwest-facing door. Two air velocity components were at the center of the gap (X component, horizontal and parallel to the window; Y component, vertical). The boundary conditions for air velocities measured between 0.15 and 0.23 m/s with ambient temperature measured between 30.6 and 34.9 ^{o}C. The heat source within the office washes a person working on his computer. The temperature from the person was assumed 310 K, and the generated heat flux was 68 W/ m^2 for the seated person, ASHRAE (2012). The heat flux by the computer and monitor is set equal to 75 and 10 W, respectively, ASHRAE (2012). The surface temperature of the glazed window wall and windows that face the front of the office ranged between 304 and 306 K, that of the internal side walls was 298 K, and that of the floor and ceiling was 300 and 299 K, respectively. The door, chairs, and table were assumed to be adiabatic, Hajdukiewicz, (2013). The emissivity and diffuse fraction of all surfaces inside the office were assumed to be 0.9 and 1.0, respectively (FLUENT 6.3 User's Guide).

The measurement period was from 8:00 am to 4:40 pm; this period was applied in the CFD simulation. The average values provided the boundary conditions and data validation of the model. Table 3.6 shows the summary of boundary conditions for the CFD model of the office. The office has a high-glazed exterior wall, with two openable windows, and most of the walls were covered with a silver coating. Thus, the radiation model was included in the CFD simulation. The single office has large glazed windows that cover all external walls. Thus, the solar radiation mode is included in the CFD simulation, and strong air temperatures indoors are under predicted.

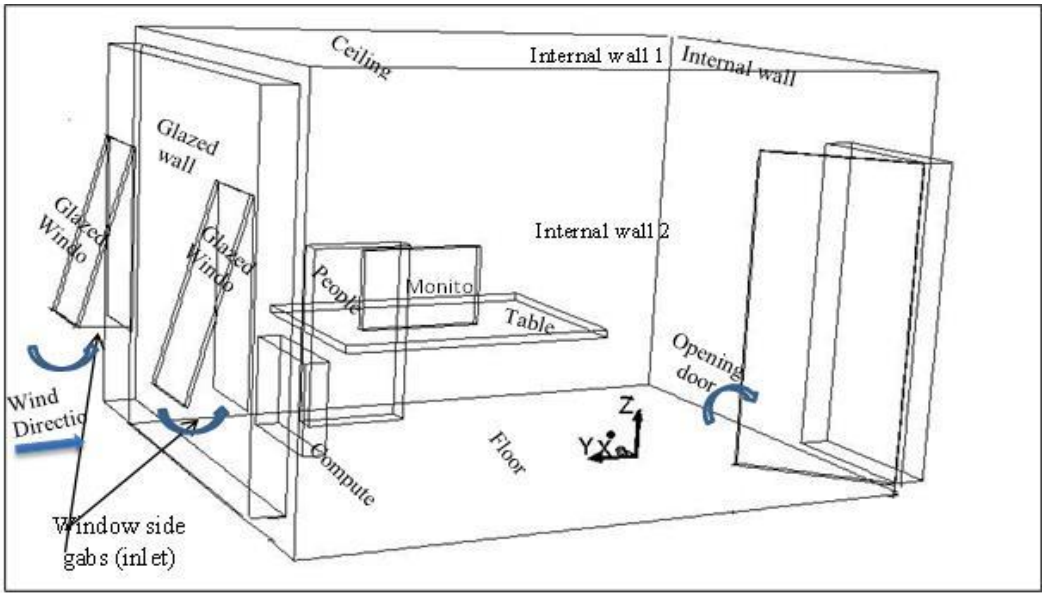

Figure 3.25 : Boundary conditions of the test office.

Table 3.8 : Boundary conditions for the CFD model

Boundary	Type	Heat transfer	Mass & momentum	Radiation
Window gap	Inlet	T_o = 303.6 (K)	V_x=0.67 (m/s) V_y=0.74 (m/s)	
Outdoor	Outlet (opening)	T_o = 307.8 (K)	$P_{relative}$ = 0	ε = 0.9 DF = 1.0
Computer + Monitor	Wall	Heat flux=75w +10W		
Internal sides walls	Wall	T_{wall} = 298 K		ε = 0.9 DF = 1.0
People sitting	Wall	generate heat = 68 W/m^2 T=310 K		ε = 0.9 DF = 1.0
Ceiling of Room	wall	T_{wall} = 298 K		ε = 0.9 DF = 1.0
Floor of Room	Wall	T_{wall} = 300 K		ε = 0.9 DF = 1.0
Internal sides walls	Wall	T_{wall}= 298 K		ε = 0.9 DF = 1.0
The door, Table and chair	wall	Adiabatic		ε = 0.9 DF = 1.0
Glazed Window wall	wall	T_{wall}= 304 K		ε = 0.9 DF = 1.0
Glazed Windows	wall	T_{wall}= 306 K		ε = 0.9 DF = 1.0

3.5.4 Justification of Solution Convergence

The convergence process in FLUENT is monitored by the residual of different variables, such as 3D velocities, energy, area, and weighted average surface temperature. The solution does not converge until all the residuals fall below certain values. In this study, the recommended values by Jianhua (2010) are used. All the residuals criteria are set to 10^3 except for the energy, which is set to10^6. Verifying conservation of mass and energy is also necessary after the solution is converged. A value within 1% of the difference balance of mass and energy experience is acceptable. The mass flow rate and the rate of heat transfer in FLUENT indicates that the imbalance in both cases results in a very small number of analytical and simulation CFD solutions, thereby supporting the convergence of simulation.

3.5.5 Turbulence model

Iterations are used in CFD to solve the solutions to the RANS equation and the mass conservation equation. The RNG k –ε model is used in the simulation because several studies (Chen Q. 1995) show that the model is appropriate for indoor flow modeling. Following the equation, Nielsen (2009) is used in numerical calculations for the RNG k – ε model (CFD, FLUENT V 6.3)

$$\frac{\partial}{\partial t}(\rho\emptyset)+\frac{\emptyset}{\emptyset x_j}\left(\rho U_j\,\emptyset\right)=\frac{\partial}{\partial x_j}\left(\Gamma_\emptyset\frac{\partial\emptyset}{\partial x_j}\right)+S_\emptyset \quad (3.1)$$

Where;
t is the time
ρ is the air density (kg/m^3)
Ø is the transport variable, such as enthalpy, concentration of contaminant, velocity, Ø the uj (J=1,2….)

For three components of momentum, Ø for k is the kinetic energy of turbulence, Ø the ε is the dissipation rate of turbulence energy, Ø the T is the temperature, Ø the c is the contaminant concentration, X_j is the coordinate, $\Gamma_\emptyset$ is the effective diffusion coefficient, and $S_\emptyset$ is the source term.

Given that RNG $k-\varepsilon$ model is valid only for a high Reynolds number, transport variables near the wall should be calculated by standard wall functions; full buoyancy effects are also chosen in the turbulence modeling. The following equations are used in the wall function (CFD, FLUENT V. 6.3):

For air velocity

$$U=\left(\frac{\tau}{\rho}\right)^{0.5}*\frac{1}{K}\log\left(\frac{Y}{y^*}E\right) \quad (3.2)$$

For kinetic energy of turbulence

$$k=\frac{1}{C_u^{0.5}}\left(\frac{\tau}{\rho}\right) \quad (3.3)$$

For dissipation rate of turbulent kinetic energy

$$\varepsilon=\left(\frac{\tau}{\rho}\right)^{\frac{3}{2}}*\frac{1}{k'y} \quad (3.4)$$

For temperature (Holman, 2002)

$$q=h_c\,A\,(T_w-T) \quad (3.5)$$

Where;
U is the velocity parallel to the wall
τ is the total shear stress
k' is the von Karman constant
y is the distance between the first grid node and the wall
E is an integration constant
y* is a length scale

q is the heat flux
h_c is the convective heat transfer coefficient
T_w is the wall temperature
T is the temperature of the coolant (℃)
In this study, the Reynolds number was calculated following Purcell (1977) in Chapter T, thereby obtaining (828553). Thus, this study uses turbulent flow.

3.6 Optimization of Models

Windows play an important role in energy performance and must therefore be chosen carefully. The selection of glazing type along with WWR is important to achieve a desirable indoor environment and energy consumption. The window contributes to heat gain or heat loss and day lighting; the quality of glazing and size of windows should be decided.

The study involved the design of an optimized WWR via the CFD method for the fifth floor in the Faculty of Engineering at UPM with differently sized windows on the northeast façade. Figure 5.1 shows the flowchart for the methodology adopted for this study, and Table 5.1 presents the input and output data for this thesis.

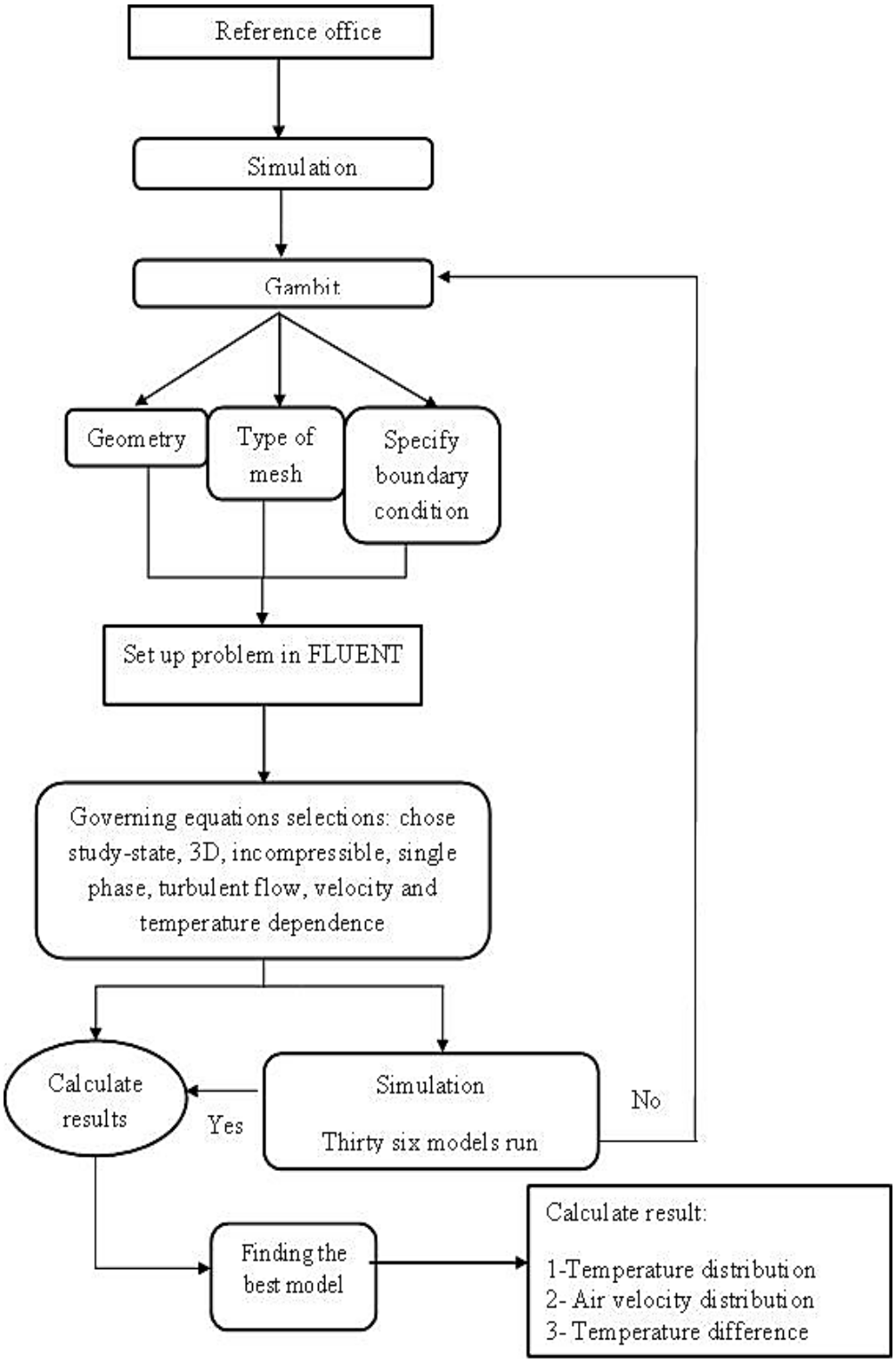

Figure 3.26 : Methodology flowchart

3.7 Summary

In this chapter, the methodology, the experimental setup, the measuring equipment, and data collection from the research conducted in Libya and Malaysia are described. The experimental parameters are used to measure air temperature, air velocity distribution, and the temperature difference between the outdoor and indoor environments for an office that uses an air-conditioned office and a naturally ventilated office. Temperature differences within the office were also measured. These parameters were judged by using an appropriate simulation technique. In this study, numerical computation by CFD via FLUENT 6.3 software was carried out to help solve the governing conservation equations.

CHAPTER 4

RESULTS AND DISCUSSION

4.1 Experimental Results (Libya)

The results of the experiments in Libya together with the measurement data were compiled then tabulated and presented graphically. The internal and external air temperatures, inner and outer glass temperatures, velocity, and relative humidity were measured.

4.1.1 Outdoor Environment Results

The highest ambient temperature in the hot desert at summer season ranges from 38 ℃ to 45 ℃. The climate was hot-dry throughout summer and very cold during winter. During winter, rainfall rarely occurs, and snow occasionally occurs.

Figure 4.1 shows the annual and fluctuations of average outdoor environmental parameter and the relationships between ambient air temperature (AT), relative humidity (RH), and air velocity (AV), from the Meteorological Department of Libya (MLD). Higher temperatures are observed during the summer season from June to mid-September. The relative humidity rises and falls opposite to the ambient temperature, which is low in the winter and high in the summer months. The solar radiation gradually increases from 308 (W/m ²) to 808 (W/m ²), which peaks between June to August. The average velocity speeds (see curve), was more or less constant or increased slightly between 5 m/s to 6 m/s. The measurement results for the meteorological station are presented in Appendix A.

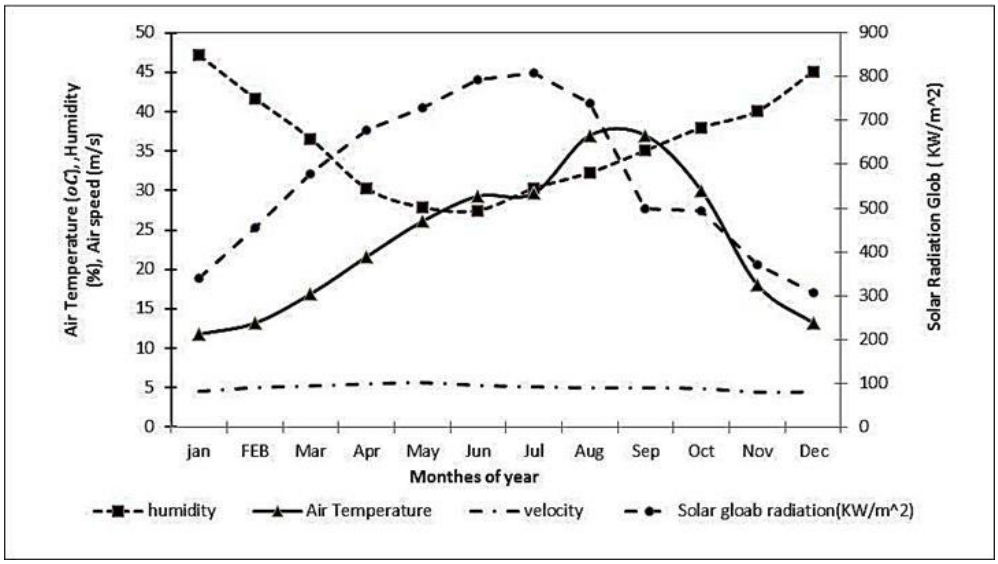

Figure 4.1 : Graph of the annual climate data in Southern Libya (MLD 2009).

Figure 4.2 shows the climate variables throughout August 2009 in Hoon, Libya; the figure shows the average dryness and wetness for summer days. The design condition for the indoors is the average maximum dry temperature of 32.9 ℃, which was observed on August 16 and 31. The minimum average dry temperature was 27.5 ℃. The average air velocity fluctuated between 5.1 m/s to 12.2 m/s with 49% humidity. The measurements data in August are presented in Appendix A.

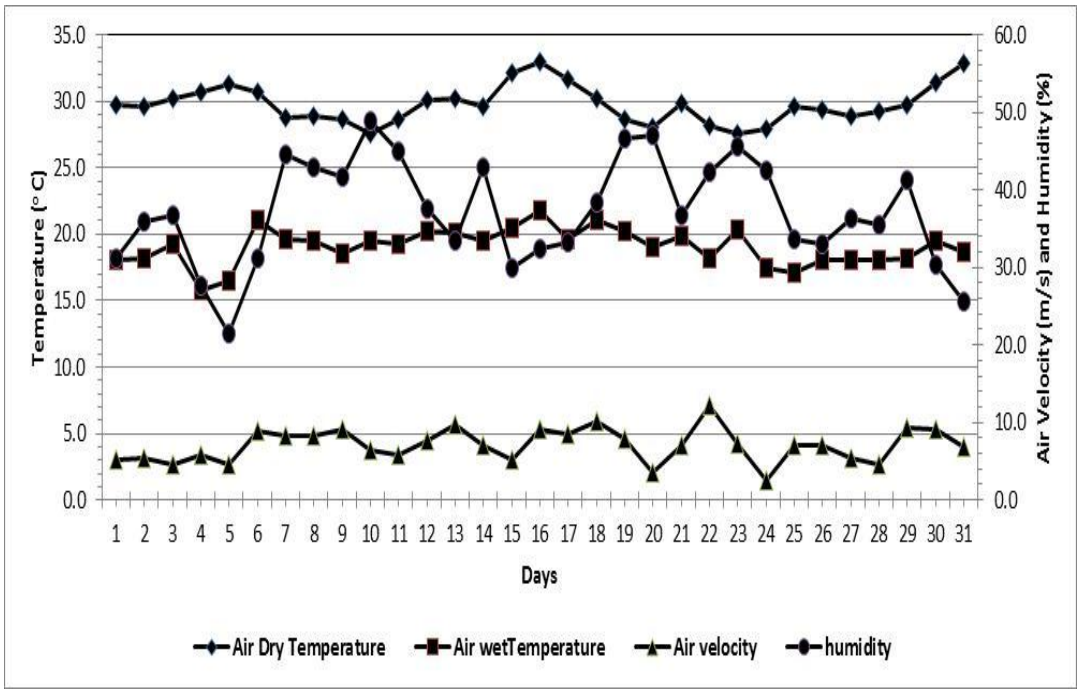

Figure 4.2 : Graph of climate data in Southern Libya, MLD (2009).

Weather data for Hoon were obtained from the meteorological station. Figure 4.3 shows the hourly climate variables for a typical day in August 2009 in Southern Libya. The curves show hourly measurements of dry and wet temperatures, as well as air velocity and humidity for summer days. In summer, the maximum temperature ranged between 38 and 39 ℃ between 12:00 pm to 3:00 pm, respectively; the minimum temperatures are 32 and 37 ℃ at 9:00 am and 6:00 pm, respectively. The measurement data are presented in Appendix A.

Figure 4.3 also shows hourly data for wind velocity and humidity in summer days. The maximum wind velocity is 5 m/s at 9:00 am and 6:00 pm and varies inversely with ambient temperature. The absolute humidity is low and falls with a relatively ambient temperature that ranges from 18% to 33%.

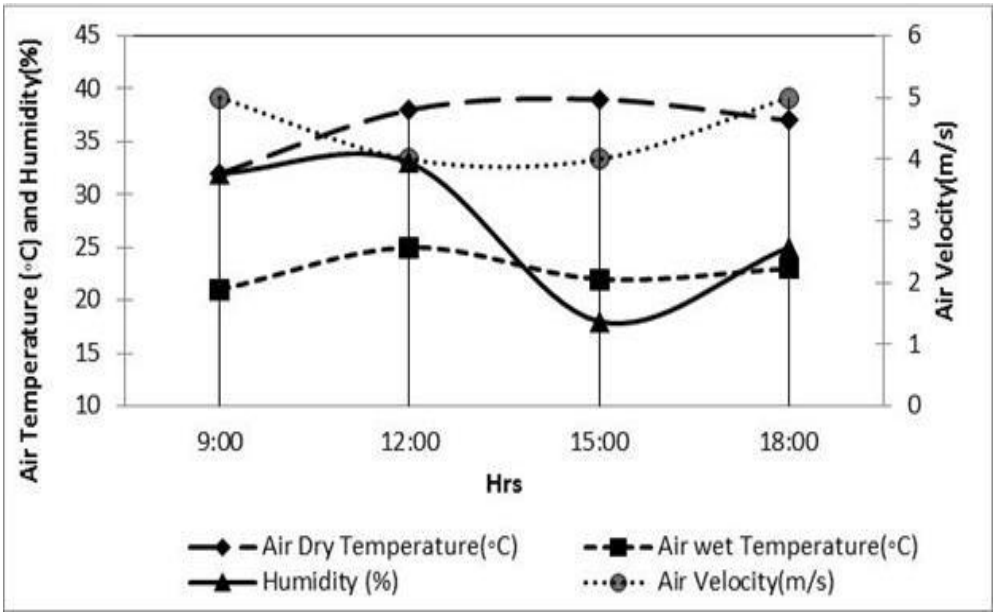

Figure 4.3 : Graph of climate data from the Libyan station, MLD (2009).

4.1.2 Indoor Environment Results

The air conditioner in the office building in Hoon operated from 8:30 am to 6:00 pm. The air conditioning temperature was controlled between 16 and 18 ℃. The temperature stability was established gradually roughly 30 minutes after the air conditioner was activated.

4.1.2.1 Temperature Changes within the Office

The office room temperature attained a maximum of 23.4 ℃ at 9:00 am. Results show that the internal air temperature was lower than the external air temperature during the summer. The northeast orientation of the façade showed that the solar rays overcame the fenestration system within one hour; the solar rays during summer significantly affected the internal temperatures. Figure 4.4 shows the distribution of air temperature at 12 points (P1 to P12) within the test office. Figure 4.5 shows solar irradiation within the office. The measurement data are presented in Appendix B.

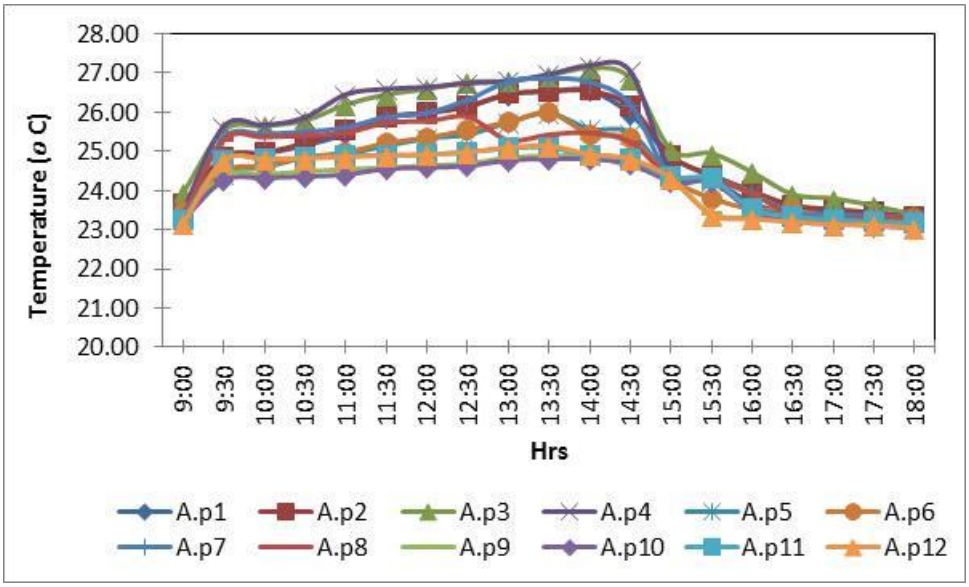

Figure 4.4 : Distribution temperature of the office (August 15, 2009)

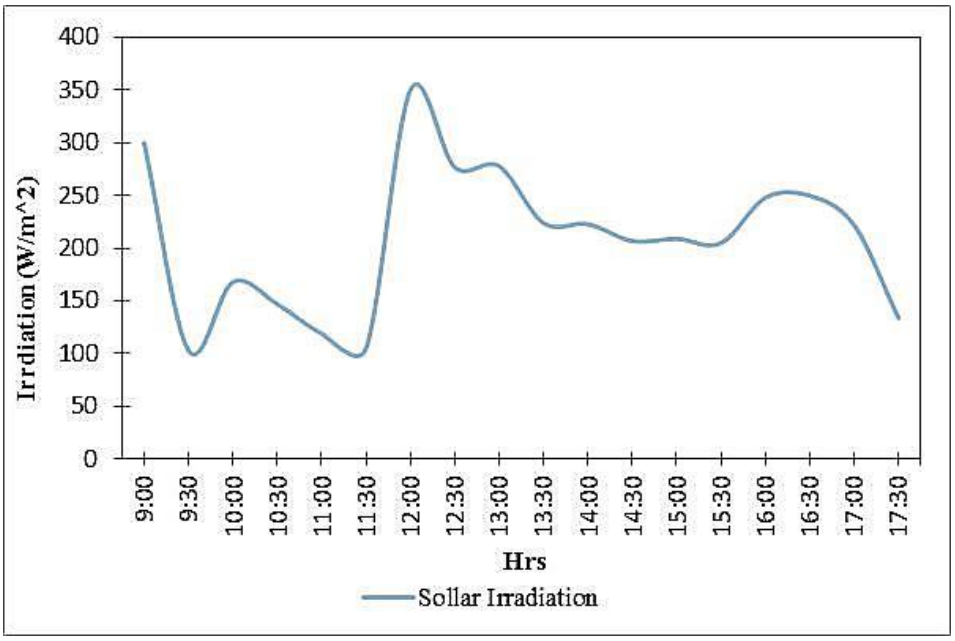

Figure 4.5 : Solar irradiation within the office (August 15, 2009)

Temperature increased from 9:00 am to midday and decreased at 4:00 pm. The average temperature reading was taken at 12:00 pm. The distance of the measuring device was 5 cm from the top of the window. The distance from the top of the window was 5 cm and was 200 cm from the office center. The curve shows temperature fluctuations from the window 5 cm to 200 cm at the office center. Figure 4.6 shows the average internal temperature 5 cm to 200 cm from the window. Internal surface temperature varied from 28.6 ℃ and 24.4 ℃ to 24.8 ℃ in the office room when the air conditioning was being used. The measurement data are presented in Appendix B.

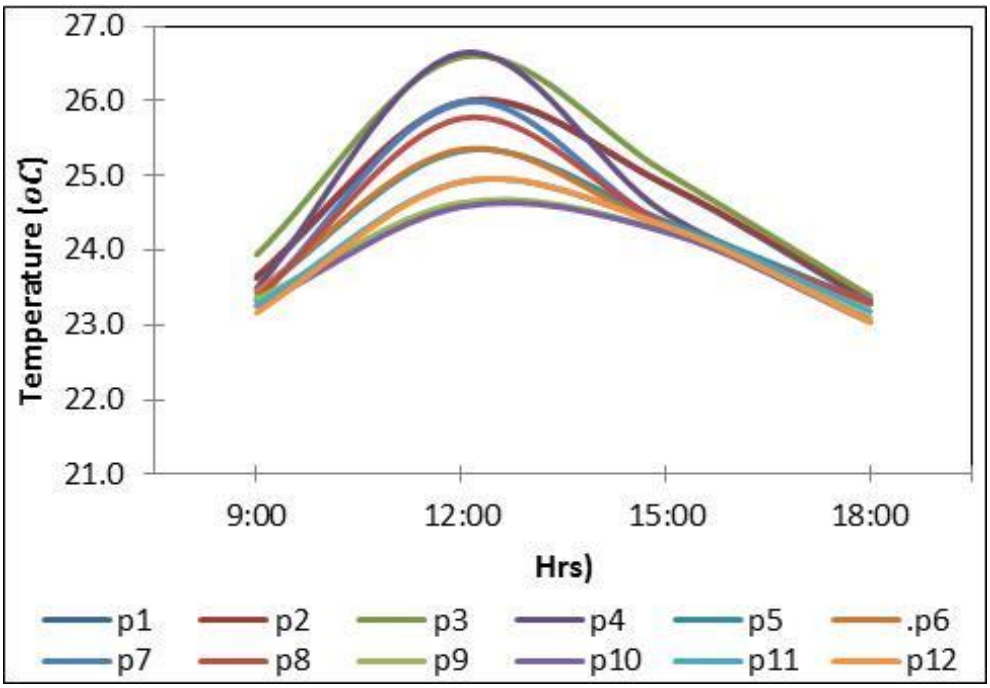

Figure 4.6 : Average internal temperature (August 15, 2009).

4.1.2.2 Horizontal Temperature Distribution

Figure 4.7 shows the average temperature in the office at a horizontal distance of 5 cm from the window to the center of the office at a distance of 200 cm at 12 noon. The figure also shows the average temperature curve 28.6 ℃ at 5 cm from the window, 24.6 ℃ at 50 cm, 24.4 ℃ at 100 cm, and 24.8 ℃ at 200 cm. The air temperature near the window (5 cm) was high because of the absorption and emission of heat from the window. Table 4.1 shows the average horizontal air temperature from the window.

Table 4.1 : Average horizontal temperature with varying distance

Distance (cm)	Average interior temperature (℃)
0.5	28.6
0.50	24.6
100	24.4
200	24.8

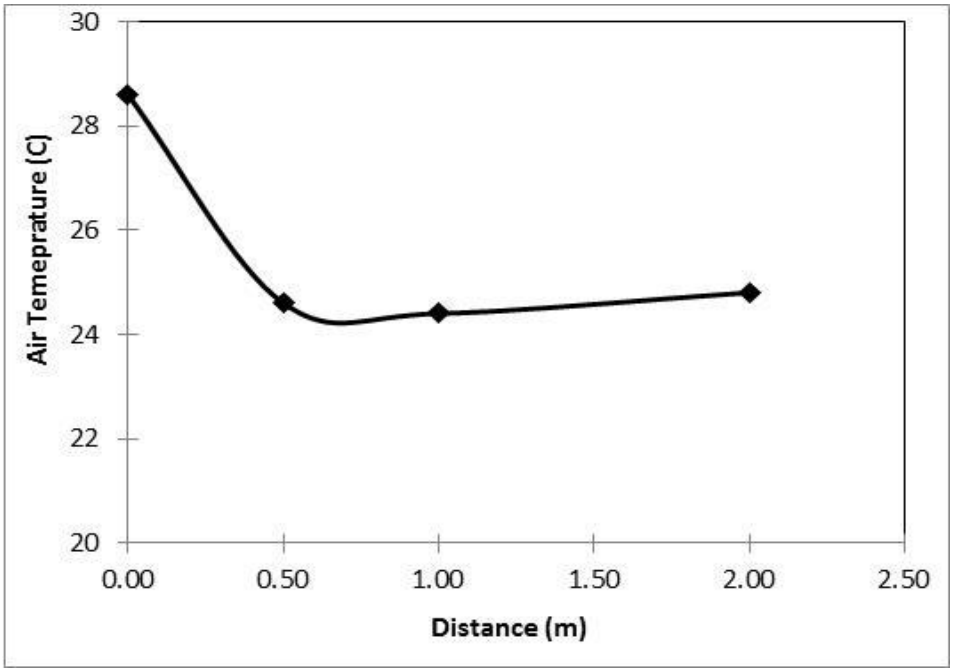

Figure 4.7 : Average internal temperature (August 15, 2009)

4.1.2.3 Vertical Temperature Distribution

Figure 4.8 shows the average temperature reading in the office at a vertical distance of 0.5 m from the floor to the ceiling at a distance of 2 m at 12 noon. The figure also shows the average temperature curve of 24.7 ℃ at 0.50 m above the floor, 24.6 ℃ at 1 m, and 24.3 ℃ at 2 m. The curve shows a slight temperature increase in the floor; this increase was lower in the ceiling. The measurement data are presented in Appendix C.

The temperature rose from 9:00 am and at 1:00 pm, then became stable at the summit from 1:00 pm until 4:00 pm. The temperature gradually reduced because of the high flow of solar irradiation in the desert from sunrise to sunset.

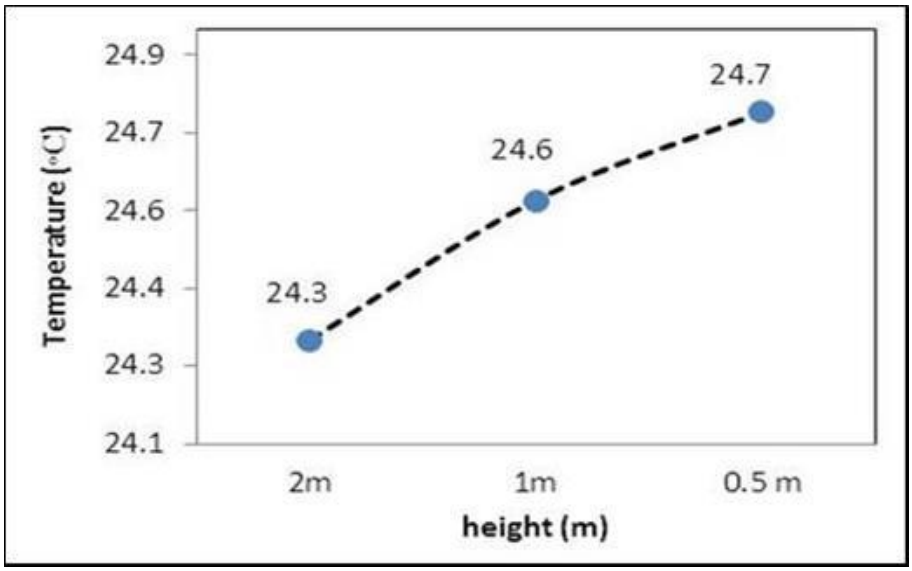

Figure 4.8 : Average internal air temperatures with vertical temperature.

The part of the direct solar irradiation that is incident at the double-glazed window wall is reflected toward the office until it reaches 37 ℃ outside and 23 ℃ inside by 6:00 pm, as shown in Figure 4.9. The measurement data are presented in Appendix B.

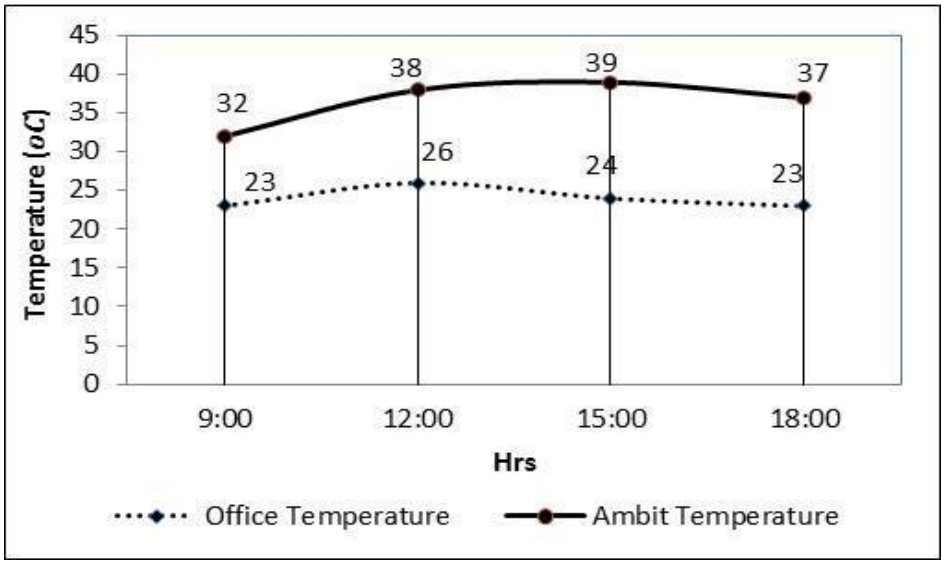

Figure 4.9 : Average internal air temperature and ambient temperature.

4.1.2.4 Temperature Difference between External and Internal Office

The temperature difference between internal and external air was roughly 9 ℃ to 15 ℃ at approximately 9:00 am and 3:00 pm in the desert when the double-glazed window was installed, as shown in Figure 4.10. The observed data are presented in Appendix C.

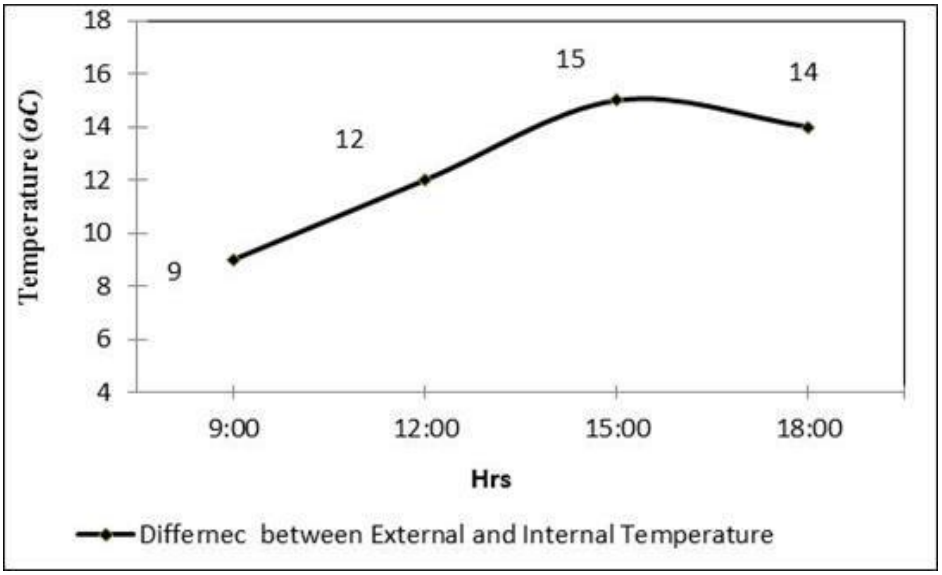

Figure 4.10 : Temperature difference between external and internal office.

4.1.2.5 Average Temperature above Inner Glazed Window

In addition to orientation, the classification affects surface temperatures and the construction material. The double glass (low-E) has good insulation properties, and the concrete shows the best results in a desert (dry-hot) climate. Figures 4.11 and 4.12 show the temperature and distribution of the inner and outer surface layers of glass temperature for eight points in the glass center (W1-in to W8-in) as well as the inner glass layer and eight points in the glass center (W1-out to W8-out). For the outer glazed (low-E) layer, the flow rate through glass in steady state was the highest (W5-in) in the center of the inner clear glass and at the point (W6-out) for the outer glazed layer. The measurement data are presented in Appendix C.

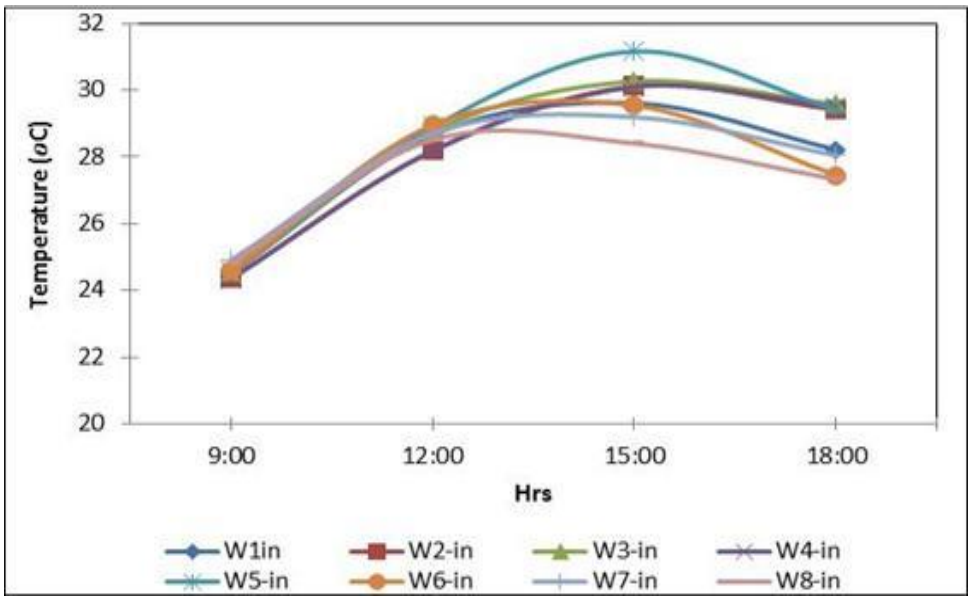

Figure 4.11 : Average temperatures above the inner glazed window.

Figure 4.13 shows the fluctuation curve of average surface temperatures of outer and inner glass windows. Maximum temperatures were observed above the outer glazed window, and the highest temperature was recorded at 12 noon and at 3:00 pm up to 42 ℃. The inner surface temperature was lower than the outer surface glass temperature because of the office cooling system. The measurement data are presented in Appendix C.

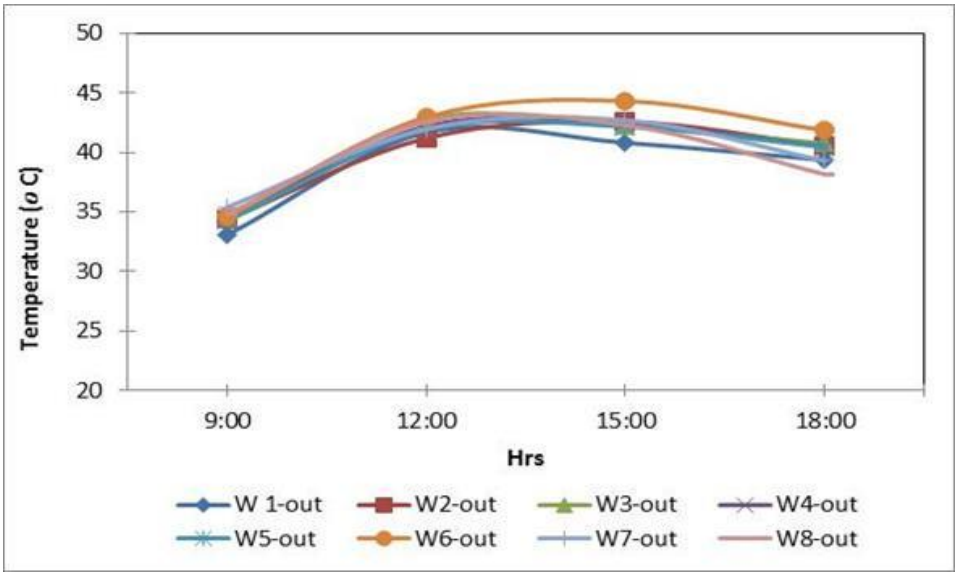

Figure 4.12 : Average temperatures above the outer glazed window.

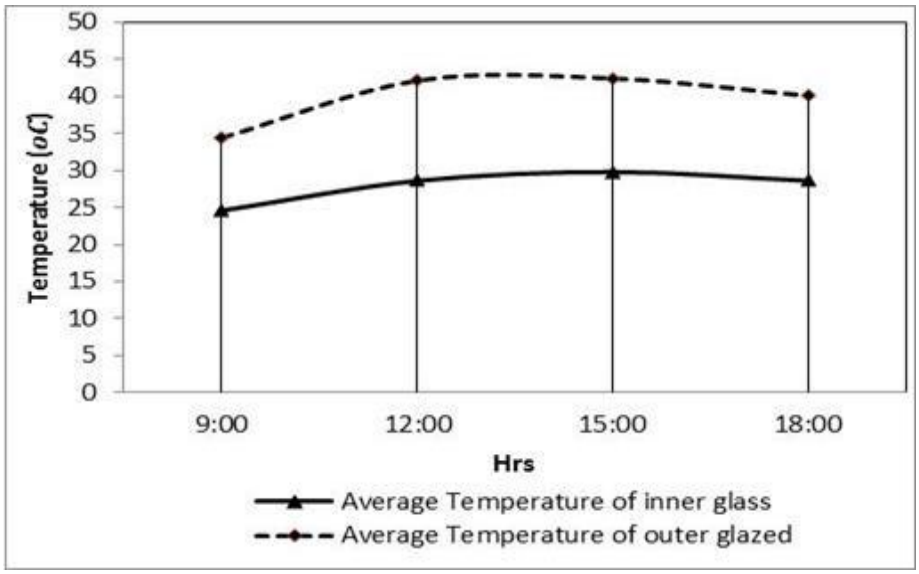

Figure 4.13 : Average air temperatures above the inner and outer glazed glass windows.

4.1.2.6 Temperature Difference between Inner and Outer Glazed Windows

Different temperature ranges between outer and inner glass with fluctuations are shown in Figure 5.12. The greatest temperature difference was observed between the inner and outer zone of the glass window from 9^{o} C to 15^{o} C. Different temperature ranges between the outer and inner region with fluctuations are shown in Figure 4.14. The measurement data are presented in Appendix C.

The highest temperature difference was observed between the inner and outer part of the glass window from $9\ ^{o}$C to $15\ ^{o}$C. The data of different temperatures between the glass are presented in Appendix C.

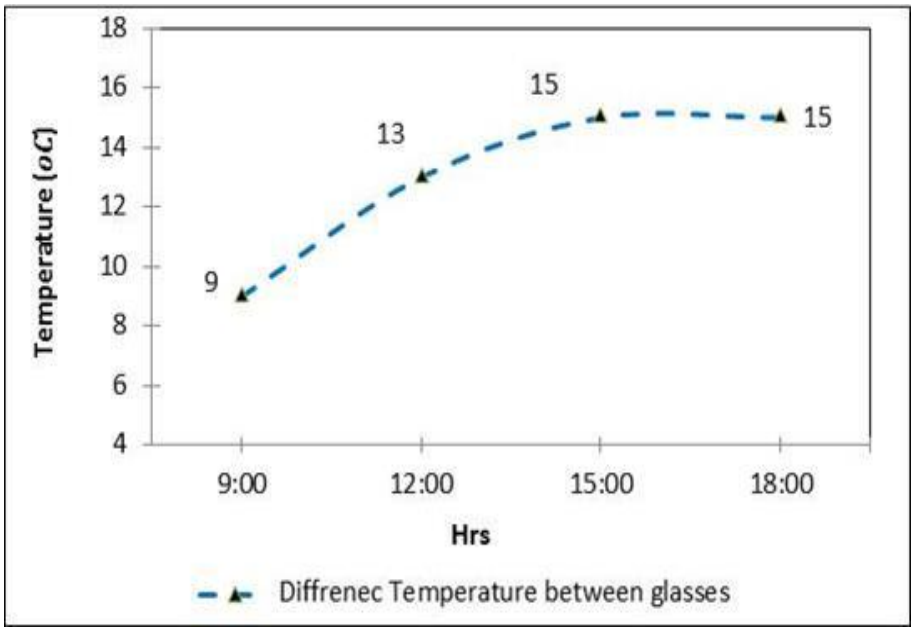

Figure 4.14 : Temperature difference between inner and outer glazed glass (Gap).

4.1.2.7 Convective and Radiation Heat Transfer Coefficient of Windows

The outer convective and radiation heat transfer coefficients were calculated as shown in Figure 4.15. The equations to calculate heat transfer coefficients near the window are presented in Chapter 3. The data of convective and radiation heat transfer coefficients are presented in Appendix C.

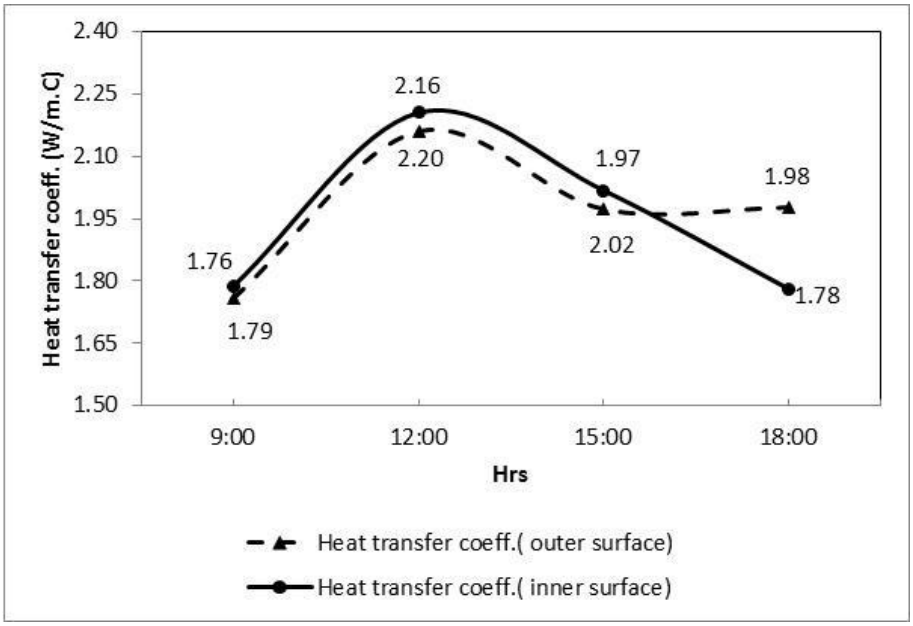

Figure 4.15 : Heat transfer coefficients (outer and inner windows).

4.2 Numerical Results (Libya)

The CFD simulation package used in this study is FLUENT version 6.3. The simulation procedure is conducted as follows to obtain simulation results.

4.2.1 Temperature Distribution

Figure 4.16 illustrates the average temperature distribution in the office using CFD simulation. Temperature stratification, which covered almost the entire office, as well as averages were between 298 and 299 K within the office. The temperature difference between the outdoor and indoor environments was approximately 9 K to 13 K. The temperature difference between the ceiling and the ground was approximately 1.4 K. The temperature of the inner surface of the window was relatively low at roughly 299.8 K to 302.5 K. The temperature of the outer surface of the window was approximately between 302 and 311 K. The temperature difference between the outer and inner surfaces varied from 9 K to 15 K. Figure 4.6 also shows the horizontal temperature distribution from the window surface to the center of the office. Measurements were obtained from different positions (0.5, 1, 1.5, and 2 m) from the window during the cooling period. The temperature difference between distance 0.5 and distance 2 m had a maximum value of approximately 2 K at 12 noon.

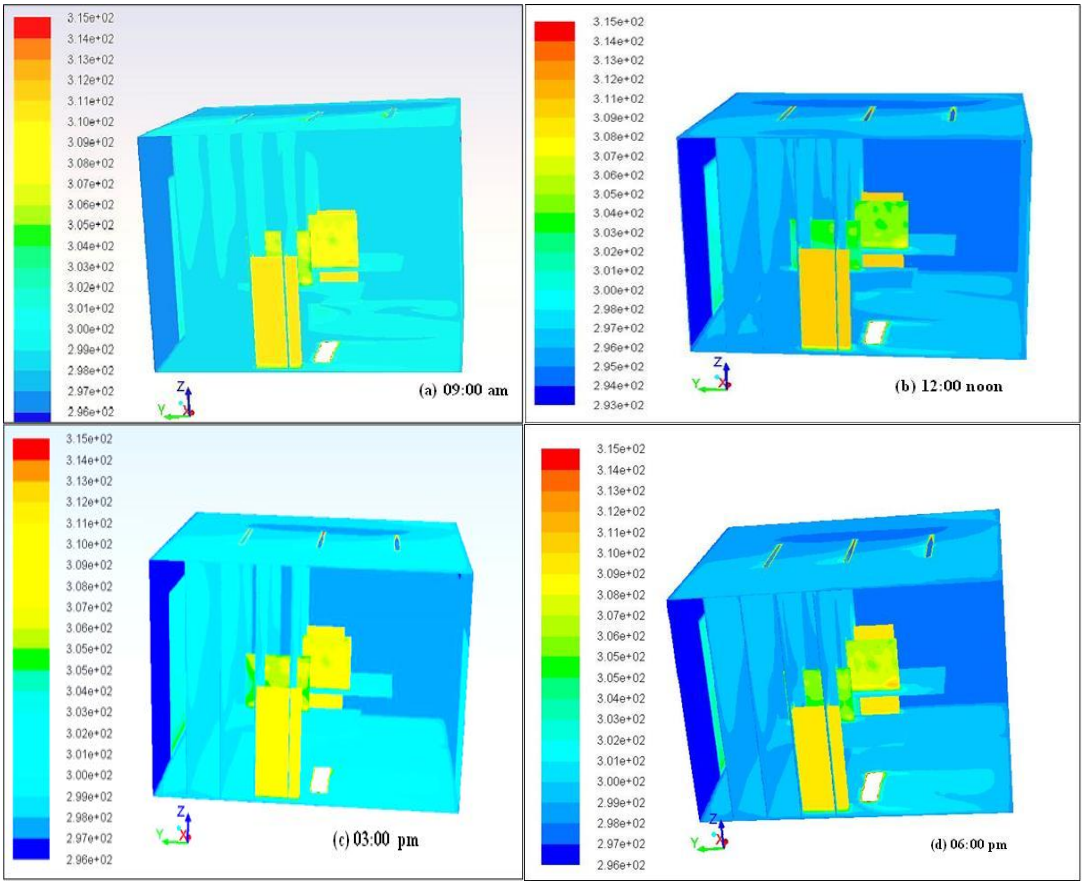

Figure 4.16 : Average temperatures by CFD (9 am, 12 noon, 3 pm, and 6 pm).

For thermal comfort, the occupied condition was from 0.5 m to 1.5 m from the window because of the cooled air from the cooling panel of the air conditioner. The air temperature was lower near the glass window and slightly higher at a distance of 1 m from the glass window.

4.2.2 Airflow Distribution

The Figure 4.17 shows the air flow distribution based on estimates by CFD. Airflow near the air conditioner was 1.1 m/s to 1.3 m/s. A downward flow was observed close to the windows because of emitted heat, and the low air flow velocity was less than 0.3 m/s.

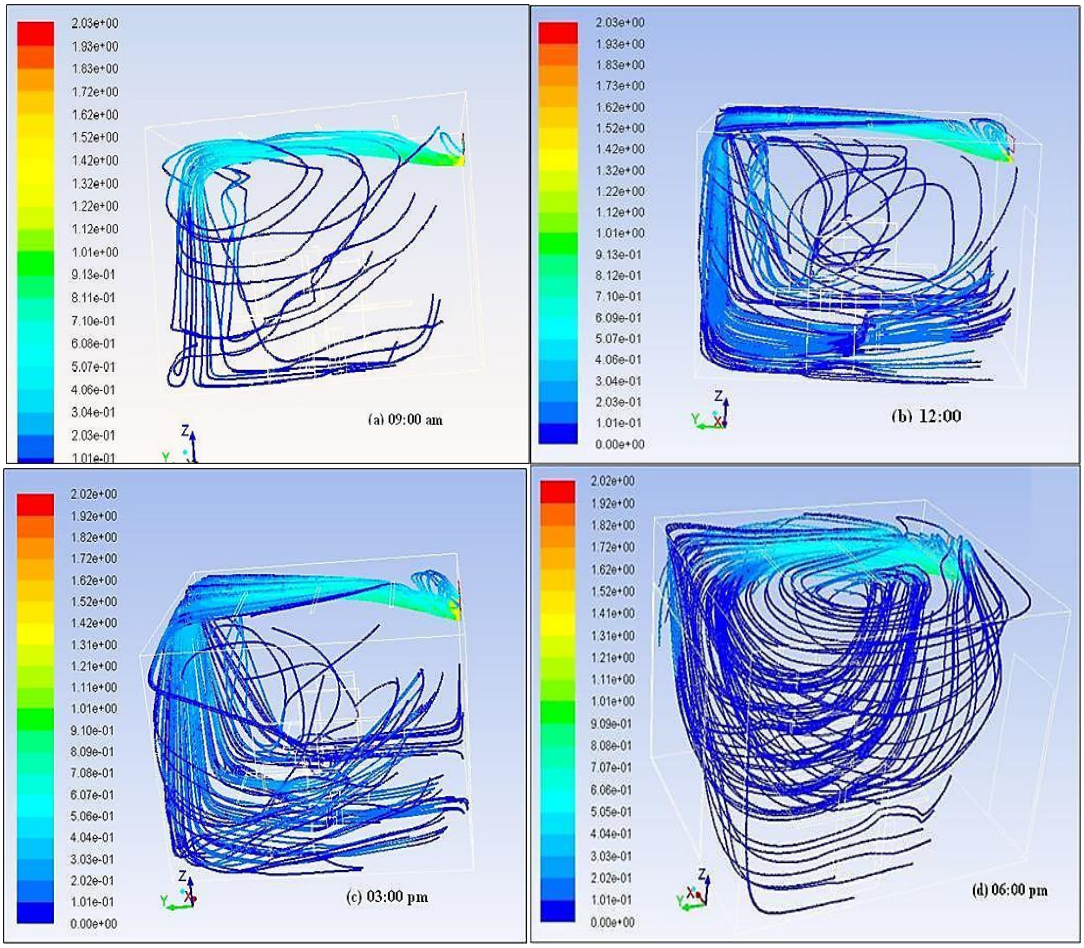

Figure 4.17 : Average air velocities by CFD (9 am, 12 noon, 3 pm, and 6 pm).

4.2.3 Comparison between Experimental and CFD Results

The experimental results were compared with the theoretical results of the measured temperature profiles. Figure 4.18 shows the comparison of average temperatures in the room. The theoretical and experimental values showed significant agreement.

The average relative error varied from 0.3% to 0.7%, which was minuscule and acceptable for engineering applications. The data are presented in Appendix B.

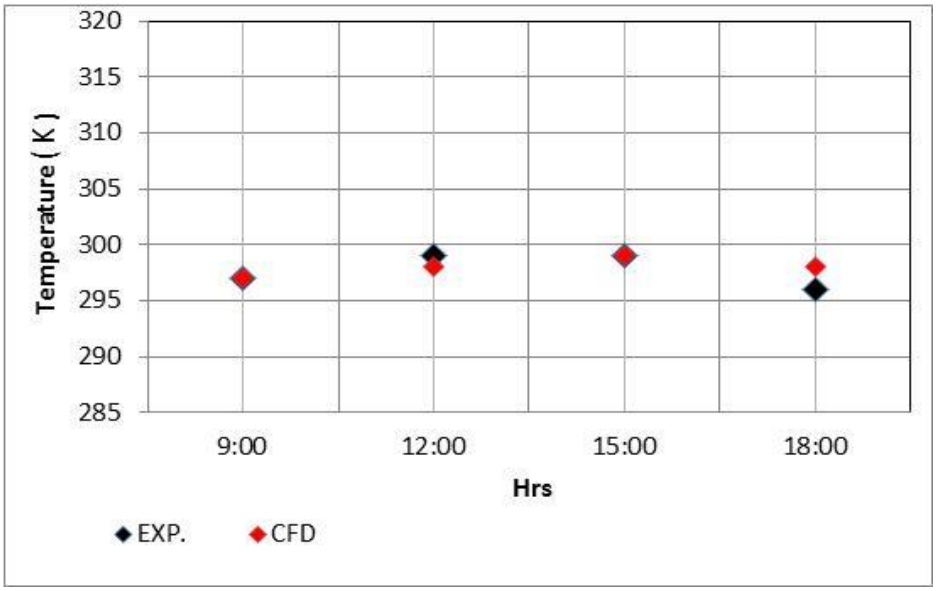

Figure 4.18 : Comparison between experimental and CFD results.

Figure 4.19 illustrates the comparison of the experimental and theoretical average air temperature profiles of internal and external window surfaces. At 12:00 pm and 3:00 pm, the highest temperatures were 315 K on the outer surface and 300 K on the inner surface. The data are presented in Appendix C.

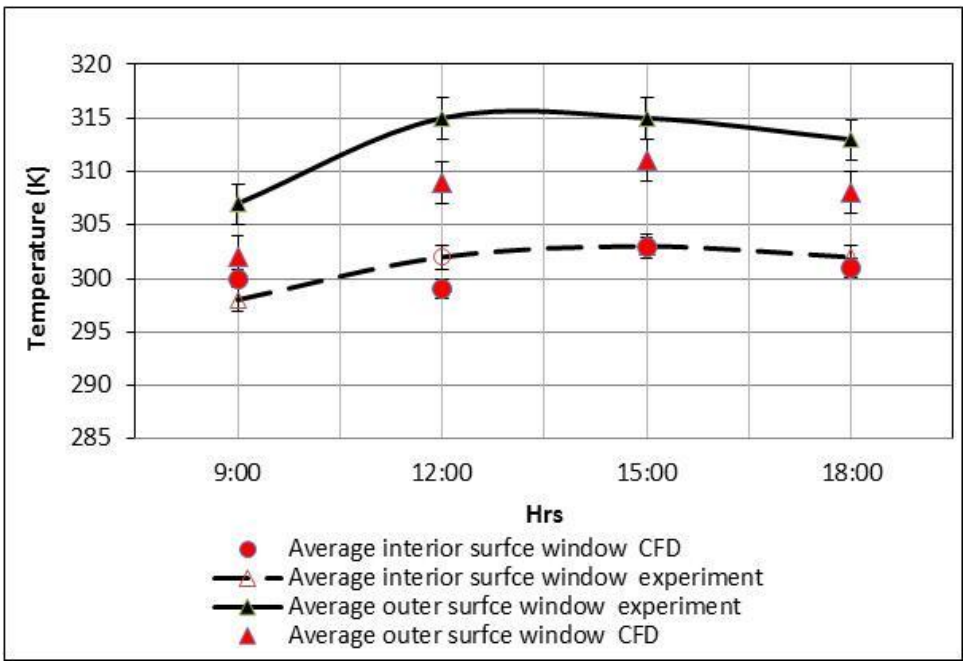

Figure 4.19 : Comparison between experimental and CFD results of double-glazed window.

Figure 4.20 presents a comparison of the experimental and theoretical temperature differences between outdoor and indoor environments. At 12:00 pm, only one mark appeared because of the applicability of the experimental result to the theoretical result, such as the occurrence of overlapping. The highest temperature difference was observed at 6:00 pm. The data are presented in Appendix C.

Figures 4.21 and 4.22 illustrate the comparison of the experimental and theoretical results of the average inner and outer heat transfer coefficient, respectively. At 12:00 pm, only one mark appeared because of the applicability of the experimental result to the theoretical result, such as the occurrence of overlapping. The highest temperature difference was observed at 3:00 pm. The data are presented in Appendix C.

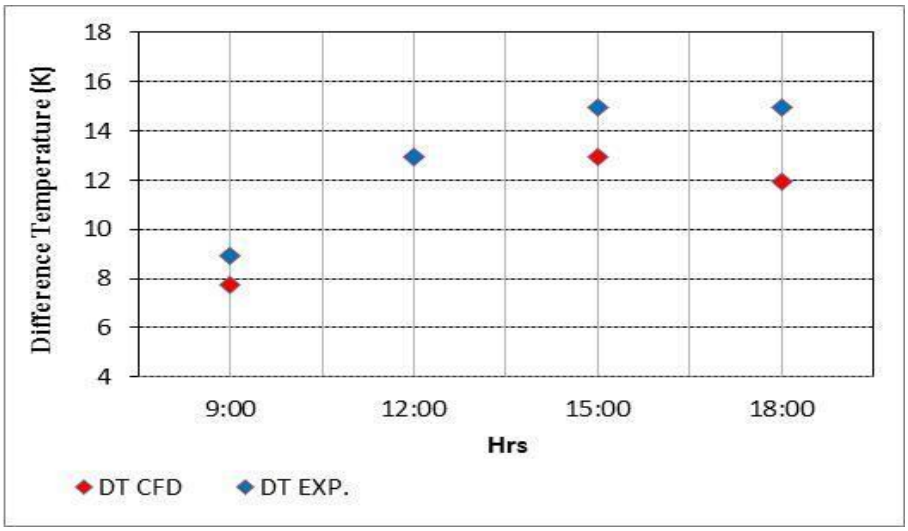

Figure 4.20 : Comparison between outdoor and indoor temperatures.

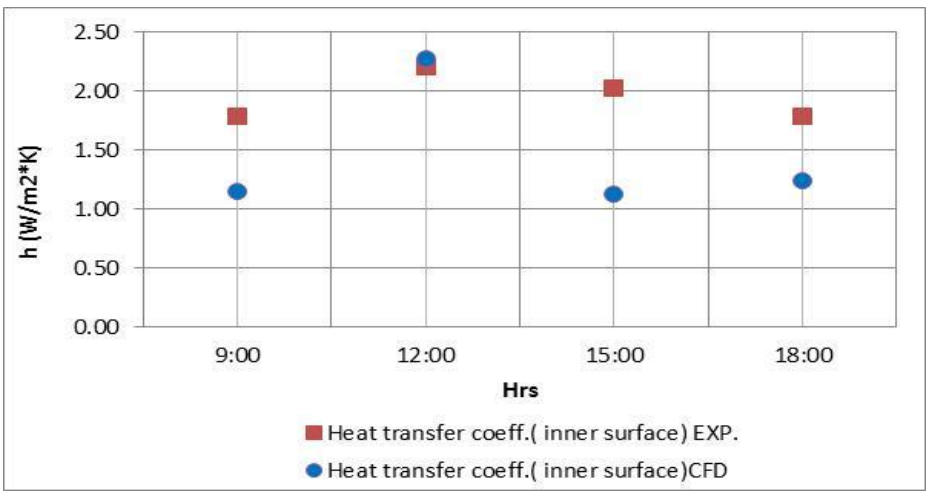

Figure 4.21 : Comparison of experimental and CFD results of inner heat transfer.

Figure 4.23 illustrates the comparison between the experimental and theoretical results of the average heat transfer flux. The highest heat flux was observed at 1200 h. The data are presented in Appendix C.

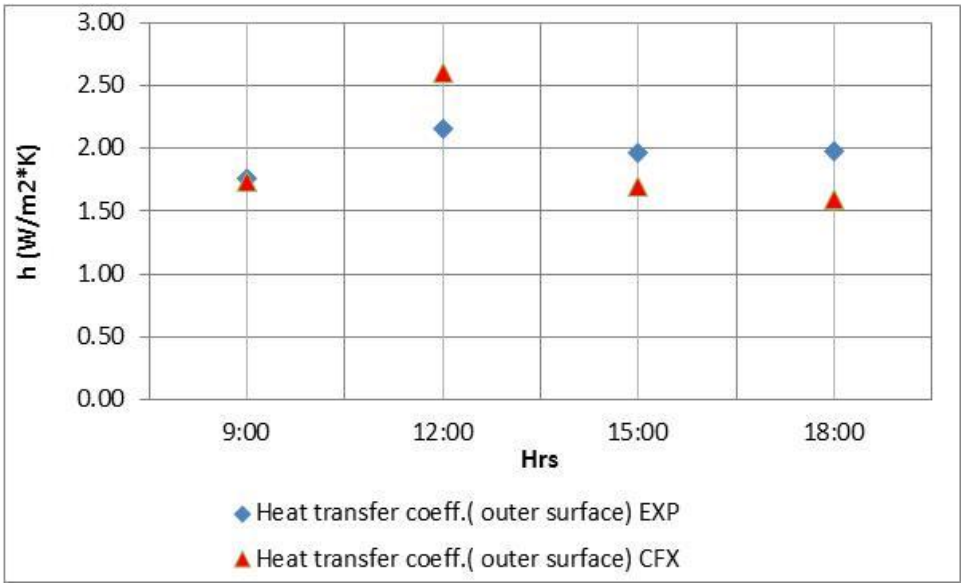

Figure 4.22 : Comparison of experimental and CFD results of outer heat transfer.

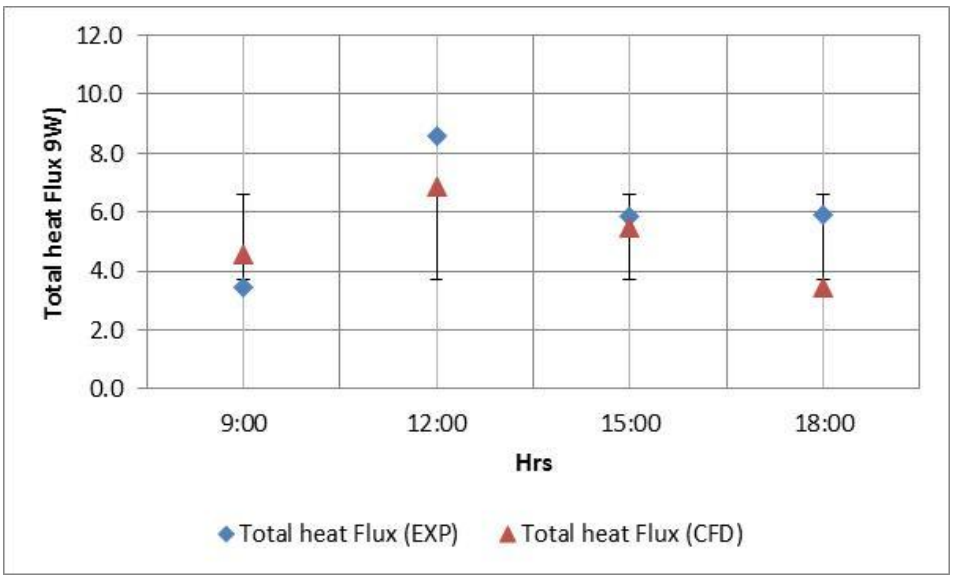

Figure 4.23 : Comparison of experimental and CFD results of heat transfer flux.

4.3 Experimental Results (Malaysian Work)

4.3.1 Outdoor Measurements of the Meteorological Station

Full-scale field measurement results of outdoor conditions were taken from a meteorological station in Kuala Lumpur (2013) for the test reference year). The climate data indicate that the average mean wet and dry temperature was 25^{o}C and 30^{o}C, respectively. The average relative humidity during the year was 82.6%, as shown in Figure 4.24. The temperature increased to 30^{o}C, and humidity was at 78% in August. The average outdoor air wet and dry temperature as well as humidity for each month in Kuala Lumpur is presented in Appendix D.

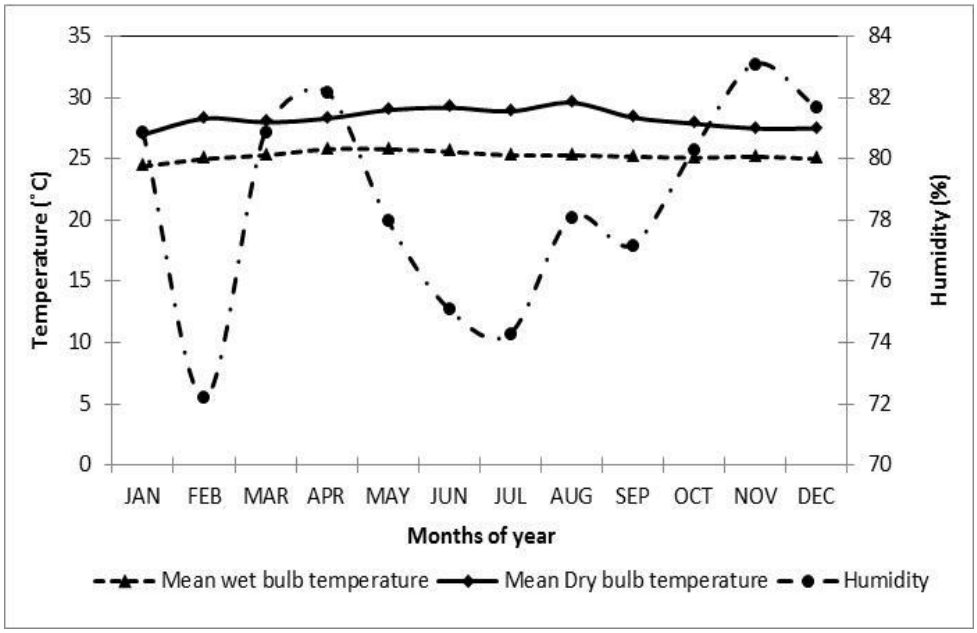

Figure 4.24 : Relative humidity and mean wet and dry temperature in 2013.

Figure 4.25 shows the annual and fluctuations of average dry air temperature and global radiation. The average dry air temperature was the highest in August (30^{o} C). The global radiation gradually decreased from 18.59 (MJm^{-2}) to 17.81 (MJm^{-2}) and peaked between June to August. The measurement results for the meteorological station are presented in Appendix D.

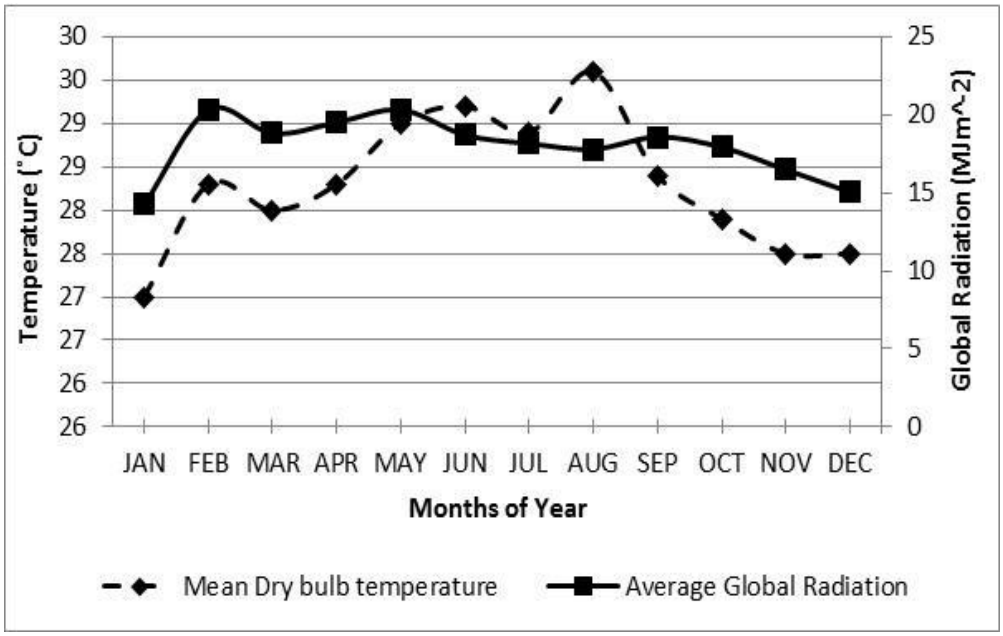

Figure 4.25 : Average dry air temperature and global radiation (2013).

The table in Appendix D and Figure 4.26 show the fluctuation between average air direction and average air velocity in August. The minimum air velocity was at 5.5 m/s on August 18 and the maximum value was at 13.5 m/s on August 31, whereas the average air velocity on August 2 (measurement day) was 10.6 m/s and the wind direction was70^{o}.

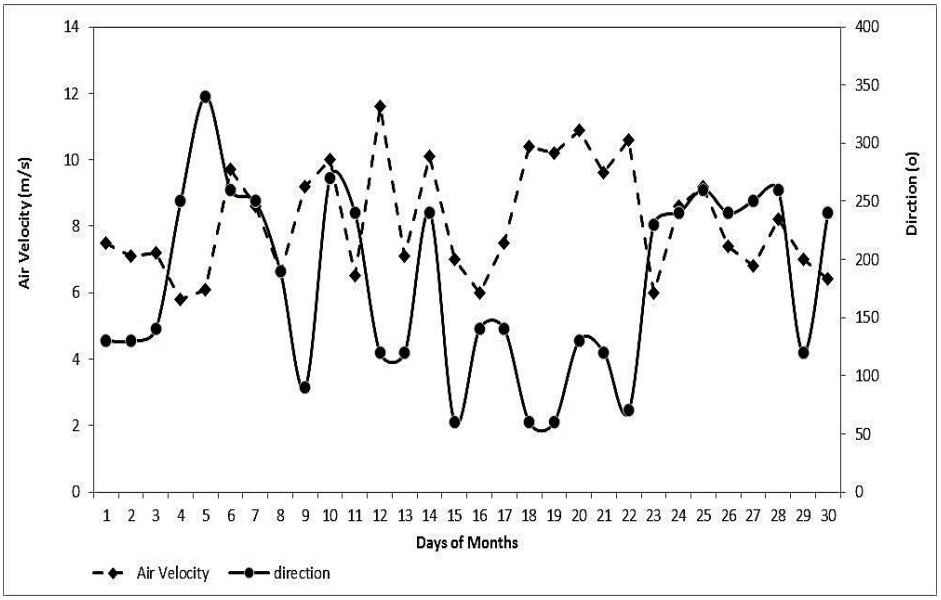

Figure 4.26 : Average air direction and average air velocity in August (2013).

Figure 4.27 illustrates the climate variables throughout August 2013 in Kuala Lumpur. The figure presents the average dry and wet temperatures, relative humidity, and air velocity for the designated days. The maximum average dry temperature is 30^{o}C, and the minimum average dry temperature is 26.6^{o}C. The average air velocity fluctuates between 5.5 m/s to 13.5 m/s, and the maximum average humidity is 85.1%. The measurements during August were obtained from the meteorological station. The measurement data are presented in Appendix D.

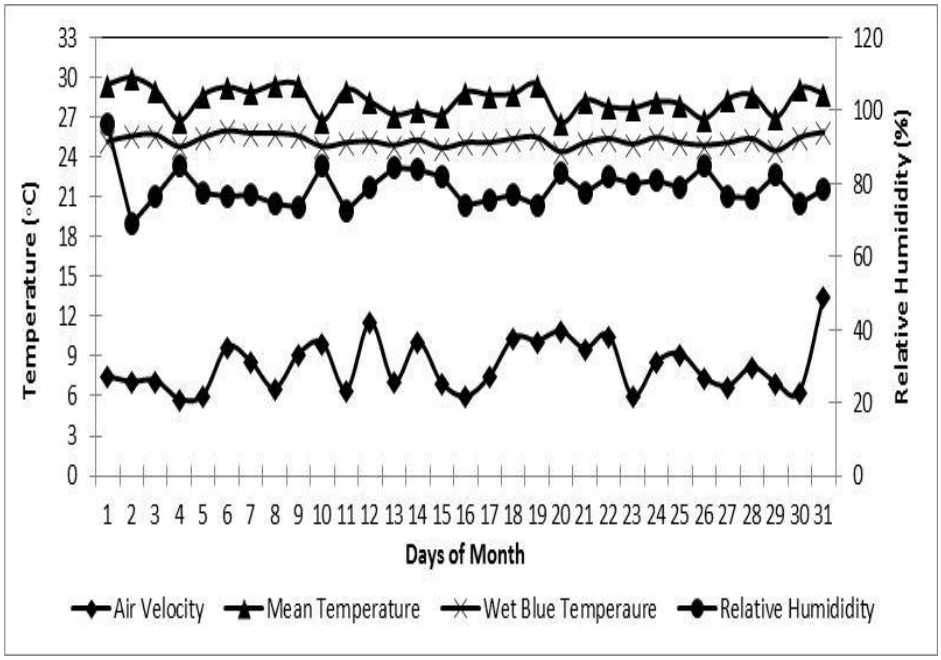

Figure 4.27 : Temperatures, humidity, and air velocity (August 22, 2013).

4.3.2 Outdoor Measurement Results of Field Study

The outdoor and indoor measurement conditions and results during measurement periods in August are presented in Appendix E. Table 4.2 shows the outdoor results on August 22, 2013 at solar time 8:00 am to 4:40 pm.

Figure 4.28 shows the relationship and the fluctuations between ambient temperature and external solar radiation at various times of day. The ambient temperature increases linearly with the solar radiation and tends to settle to a constant outdoor temperature of 34.6°C and solar radiation of 750.4 W/m² from 1:20 pm to 2:00 pm.

Table 4.2 Outdoor measurements (August 22, 2013)

Solar Time	Ambient Temperature (C)	Wind speed (m/s)	Relative Humidity (%)	Solar Irradiance (W/m^2)
8:00	30.5	0.98	69%	201.4
8:40	30.7	0.89	64%	203.2
9:20	31.2	0.87	54%	388.4
10:00	31.3	0.83	57%	405.7
10:40	31.7	0.65	55%	412.9
11:20	32.4	0.72	57%	525.2
12:00	32.8	0.67	54%	674.3
12:40	33.7	0.78	57%	702.1
13:20	34.6	0.67	60%	750.4
14:00	34.1	0.83	65%	840.2
14:40	33.8	0.81	64%	726.7
15:20	33.6	1.18	70%	441.5
16:00	33.7	0.94	75%	358.8
16:40	32.6	0.64	69%	255.3

The opposite occurs with low values of solar irradiation and with 203 W/m^2 at 8:00 am; thus, the temperature decreases slightly. Moreover, with low levels of irradiation, low temperatures become lower in the open air in the early morning.

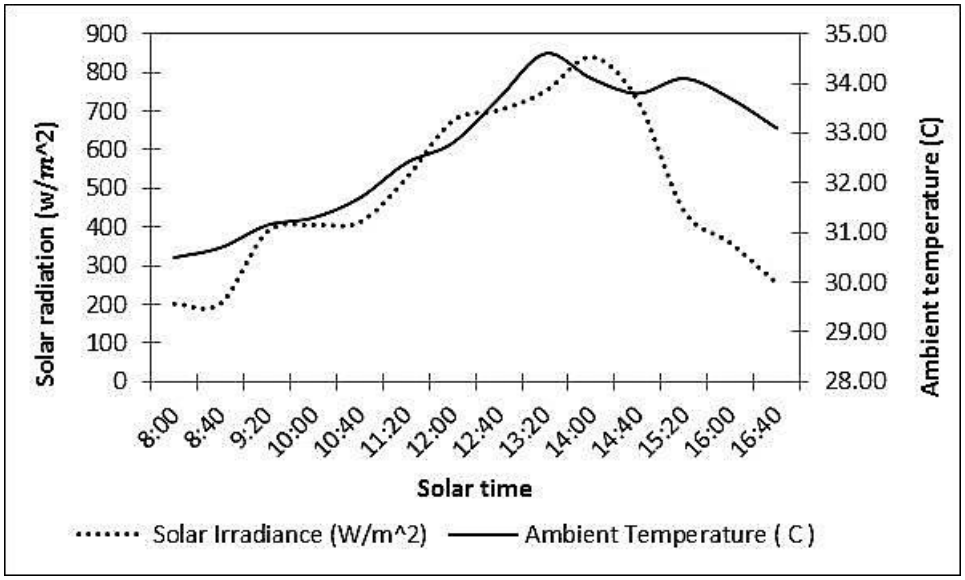

Figure 4.28 : Outdoor environment measurements

The relationship between ambient temperature and air velocity of outdoor environment is inversely related. An increase in air velocity decreases the ambient temperature, as shown in Table 4.4 and Figure 4.29.

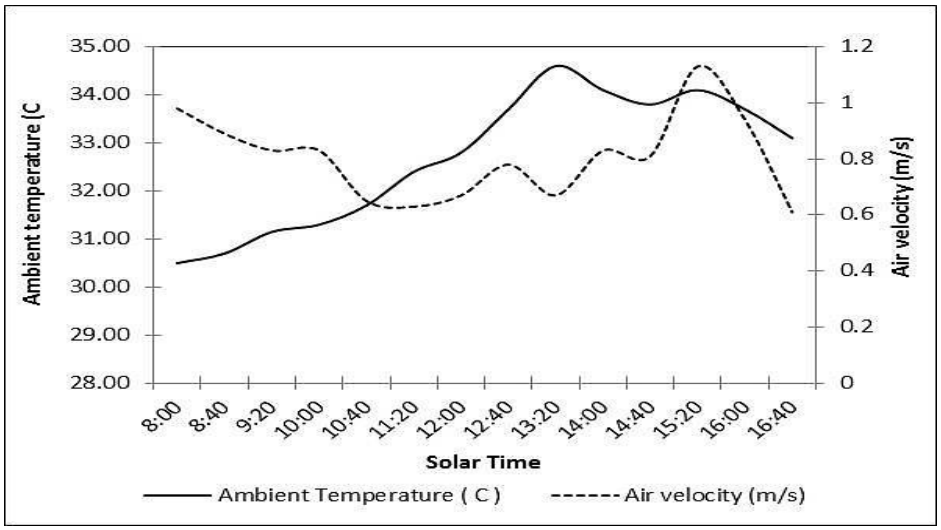

Figure 4.29 : Outdoor environment measurement

The peak air velocity was at 3:20 pm and lower air velocity was at 12:00 pm, whereas the peak relative humidity was at 10:00 am.

Figure 4.30 indicates the fluctuations between relative humidity (%) and air velocity (m/s) with the temperature variation (o_C). The ambient temperature showed an inverse relationship with air velocity, but relative humidity mostly remained constant, except early in the morning when it increased.

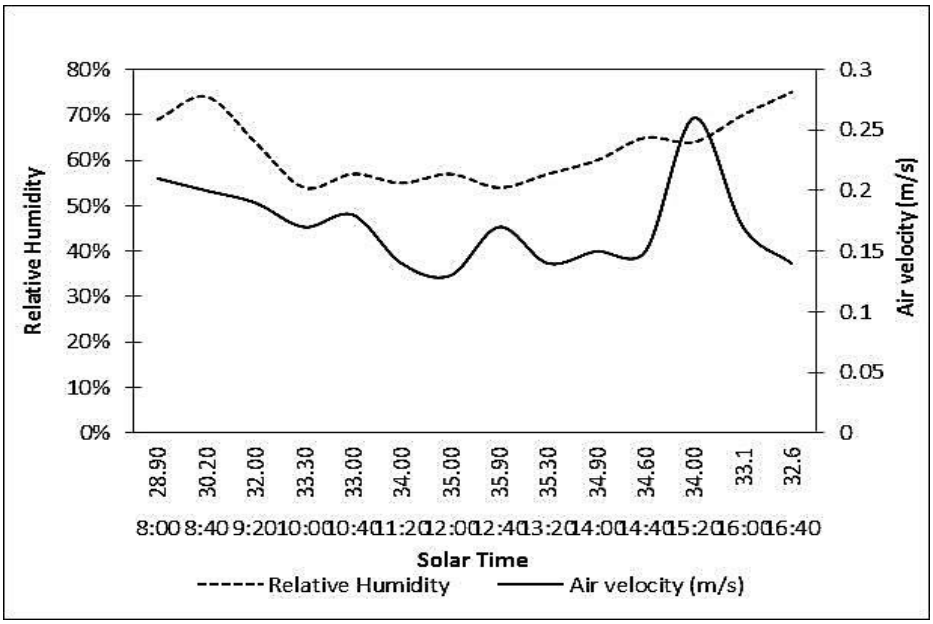

Figure 4.30 : Outdoor humidity and air velocity with temperature variation.

4.3.3 Indoor Measurement Results of Field Study in Malaysia

At the Malaysian office, temperature and air velocity measurements were conducted at various solar times, with two windows opened to facilitate air flow inside. Table 4.3 shows indoor measurements of the surface temperatures above the glazed windows and the glazed wall as well as the average indoor temperature, humidity, wind speed, and air pressure. Figure 4.31 shows the fluctuations between surface temperatures that are above the glazed windows, glazed wall, and average ambient temperature.

Table 4.3 : Indoor Measurements (August 22, 2013)

Solar Time	Glazed window (G-1)	Glazed wall (G2)	Glazed window (G-3)	Aver. Indoor Temperature (C)	Relative Humidity (%)	Wind speed (m/s)	Air Pressure
8:00	32.5	31.4	31.7	30.5	55	0.24	0.01048
8:40	34.6	31.8	34.1	30.6	53	0.14	0.02341
9:20	35.2	33.3	34.7	30.9	49	0.17	0.03841
10:00	34.6	33.6	33.8	31.1	45	0.15	0.03552
10:40	33.4	33.8	32.1	31.1	46	0.22	0.05427
11:20	32.7	33.8	33.3	31.3	46	0.17	0.05051
12:00	33.3	34.2	33.1	31.2	55	0.25	0.02541
12:40	34.3	35.7	34.7	31.3	44	0.20	0.04741
13:20	35.9	36.1	35.4	31.2	41	0.15	0.03671
14:00	35.4	34.8	34.6	31.2	49	0.15	0.02441
14:40	34.6	34.3	33.8	31.2	46	0.20	0.02234
15:20	34.4	33.7	33.8	31.0	49	0.27	0.01254
16:00	33.2	33.6	32.8	30.8	47	0.19	0.01048
16:40	32.7	32.9	32.5	30.2	53	0.12	0.01048

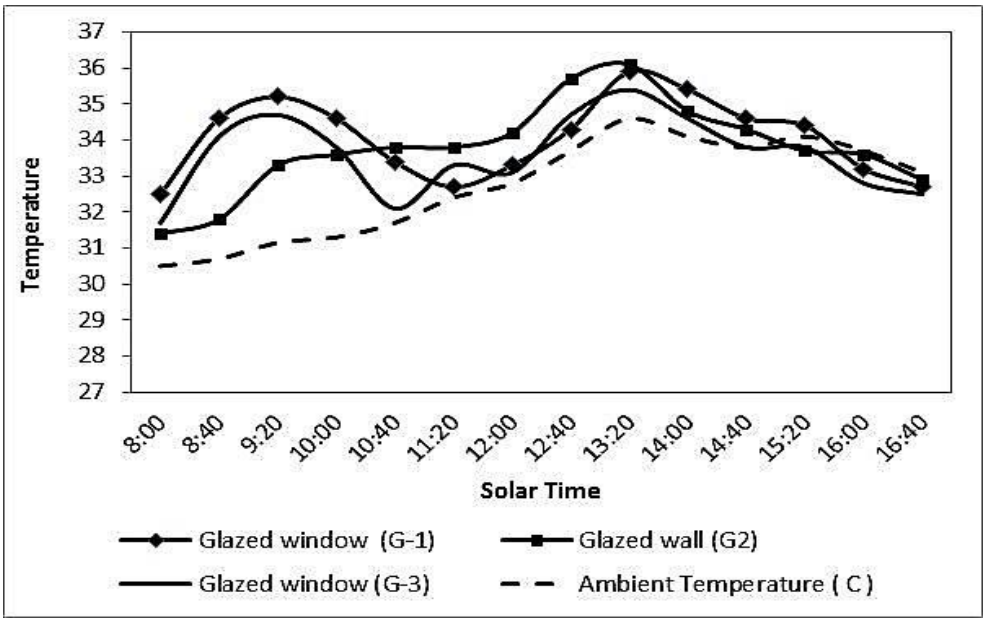

Figure 4.31 : Measurement of indoor environment.

Figure 4.32 shows the fluctuations between relative humidity and air velocity inside the office. The air temperature outside the office was 34.6°C at solar noon (1:20 pm), whereas high air temperature inside the office was 31.9 °C at midday. The air velocity inside the office was between 0.14 to 0.27 m/s, and higher air velocity that reached a maximum of 0.27 m/s was observed at 8:00 am. The curves of relative humidity (%) and air velocity were parallel and linear, and the highest air velocity was 0.26 m/s when the air temperature in the office was 30.98°C.

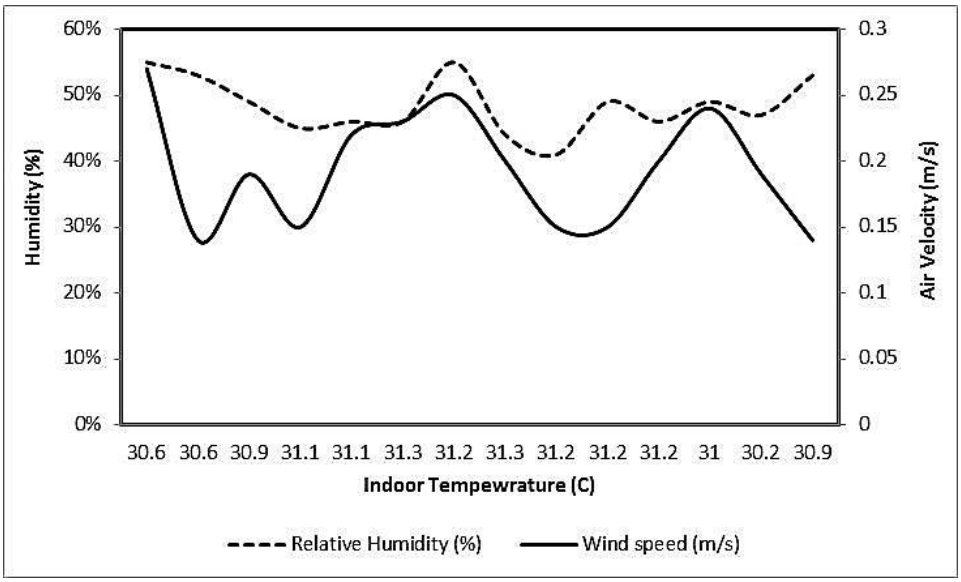

Figure 4.32 : Humidity and air velocity with air temperature inside the office

Figure 4.33 shows the typical diurnal variation of the indoor temperature against the outdoor temperature. The graph indicates that the average indoor temperature was between 30.15^{o} C and 31.25^{o} C, and was significantly below the outdoor temperature at 1:20 pm. Furthermore, the outdoor temperature reached a peak at 35^{o}C.

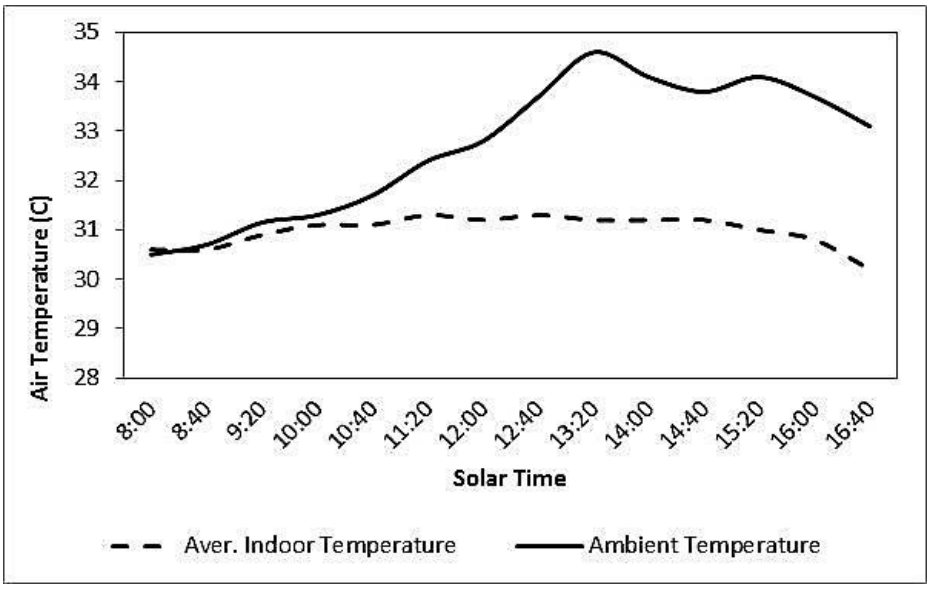

Figure 4.33 : Internal and external temperature (August 22, 2013).

Figure 4.34 illustrates the outdoor and indoor humidity and air temperature of the office. The humidity in the office was generally lower than that outdoors; relative humidity outdoors increased at 8:00 am because of a decrease in outdoor temperature. Indoor humidity started increasing at 2:40 pm until 4:40 pm given a decrease in temperatures in the evening.

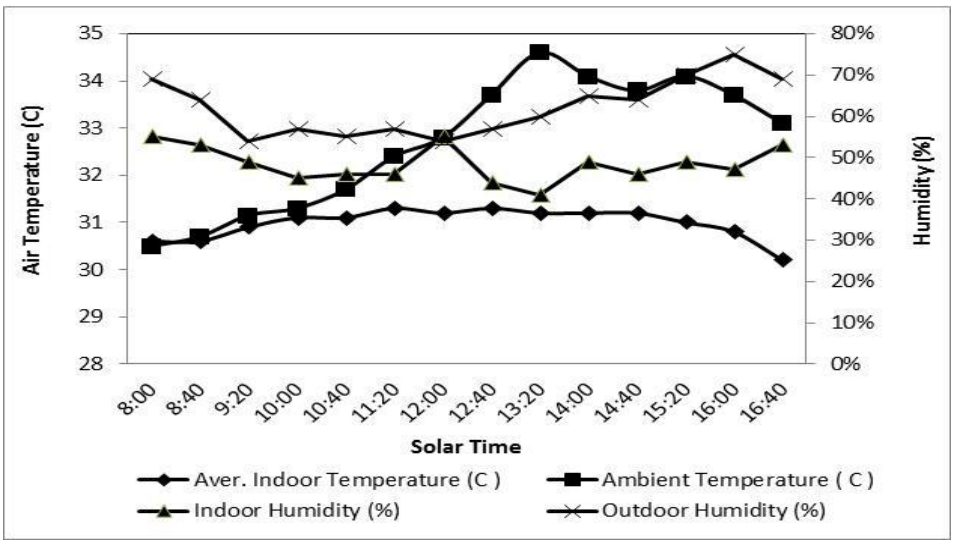

Figure 4.34 : Indoor and outdoor temperature, and humidity (August 22, 2013)

Table 4.4 and Figure 4.35 show a horizontal distribution of temperature within an office with the distance from the window to inside the office. The locations of points (T-1, T-2, T-3, and T-4) are shown. The peak temperature was $32.50^{o}C$ at 1:20 pm near the window opening (T-1).

Table 4.4 : Horizontal distribution temperature with distance from window

Solar Time	T-1	T-2	T-3	T-4	Average Temperature
8:00	31.86	30.04	29.94	29.86	30.56
9:20	31.98	31.40	30.70	30.19	30.96
11:20	32.14	31.45	31.15	30.47	31.25
13:20	32.50	31.16	30.76	30.29	31.19
15:20	31.87	31.26	30.76	30.30	30.98
16:40	31.78	31.37	30.70	30.3	30.20

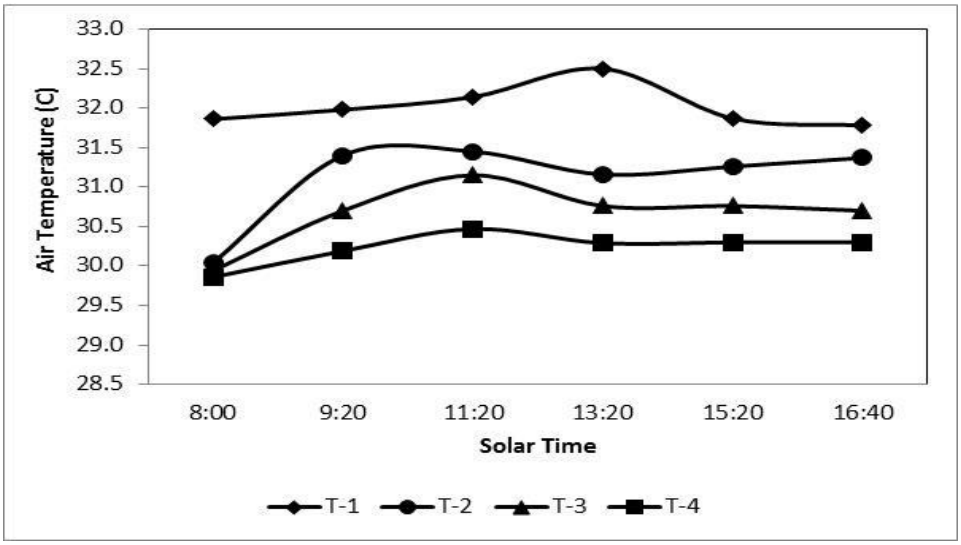

Figure 4.35 : Horizontal temperature distributions with distance from window.

Table 4.5 and Figure 4.36 show the horizontal distribution of velocity inside the office with distance from the window. The measurement point's installations are shown in Figure 4.20. The average velocity within the office was between 0.15 and 0.24 m/s, and peak velocities occurred in the inlet near the window. The peak velocity occurred in the morning at 8:00 am with a value of 0.27 m/s.

Table 4.5 : Horizontal temperature distribution velocity with distance

Solar Time	V-1	V-2	V-3	V-4	Average Velocity
8:00	0.23	0.22	0.20	0.22	0.27
9:20	0.21	0.15	0.18	0.20	0.19
11:20	0.18	0.12	0.15	0.16	0.23
13:20	0.16	0.11	0.15	0.15	0.15
15:20	0.21	0.18	0.20	0.21	0.24
16:40	0.18	0.175	0.15	0.18	0.14

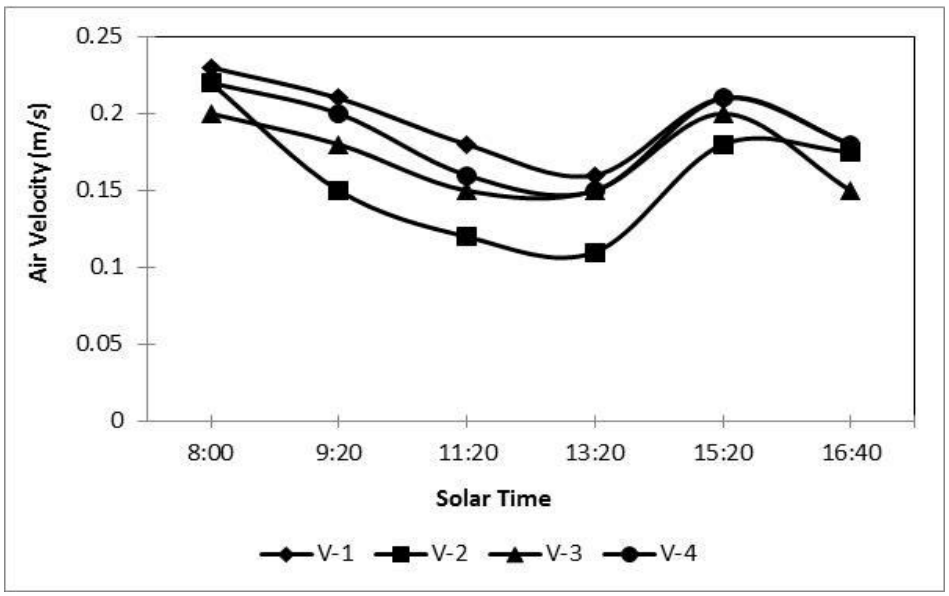

Figure 4.36 : Horizontal air velocity distributions with distance from window.

Table 4.6 and Figure 5.37 illustrate fluctuations of vertical pressure distribution pressure at four measurement points within the office with solar time. The peak pressure was at 9:20 am and 3:20 pm at values between 0.035 Pascal to 0.040 Pascal.

Table 4.6 : Horizontal distribution of pressure with distance from window

Solar Time	P-1	P-2	P-3	P-4	Average Pressure
8:00	0.018	0.010	0.016	0.015	0.0146
9:20	0.034	0.003	0.005	0.014	0.0139
11:20	0.011	0.007	0.015	0.011	0.0110
13:20	0.015	0.009	0.010	0.011	0.0112
15:20	0.040	0.026	0.040	0.035	0.0352
16:40	0.012	0.008	0.008	0.009	0.0095

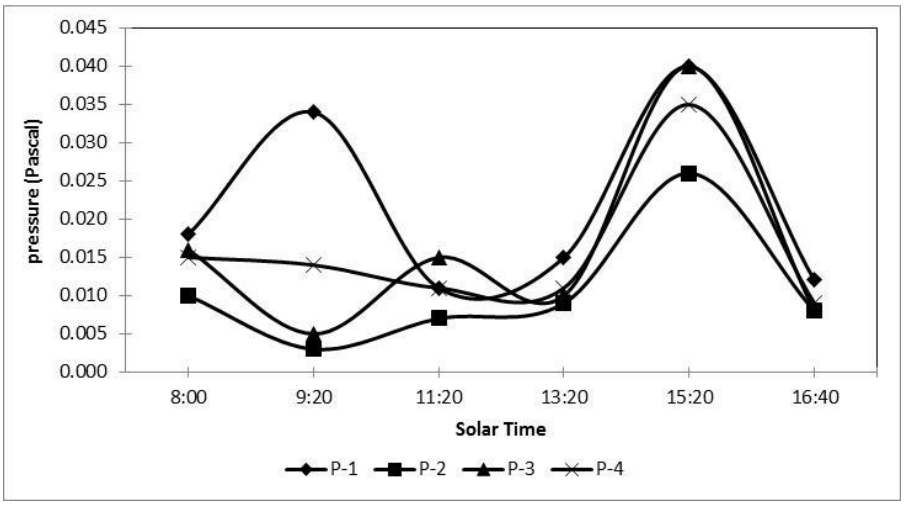

Figure 4.37 : Horizontal distribution of pressure with distance from window.

Table 4.7 and Figure 4.38 show the fluctuations of outlet and inlet wind velocity that occurred near the window and surface of the façade wall.

Table 4.7 : Outdoor and inlet wind velocity near the window

Solar Time	Inlet Velocity	Outlet Velocity
8:00	0.39	0.98
9:20	0.34	0.83
11:20	0.32	0.63
13:20	0.25	0.67
15:20	0.30	0.63
16:40	0.33	0.61

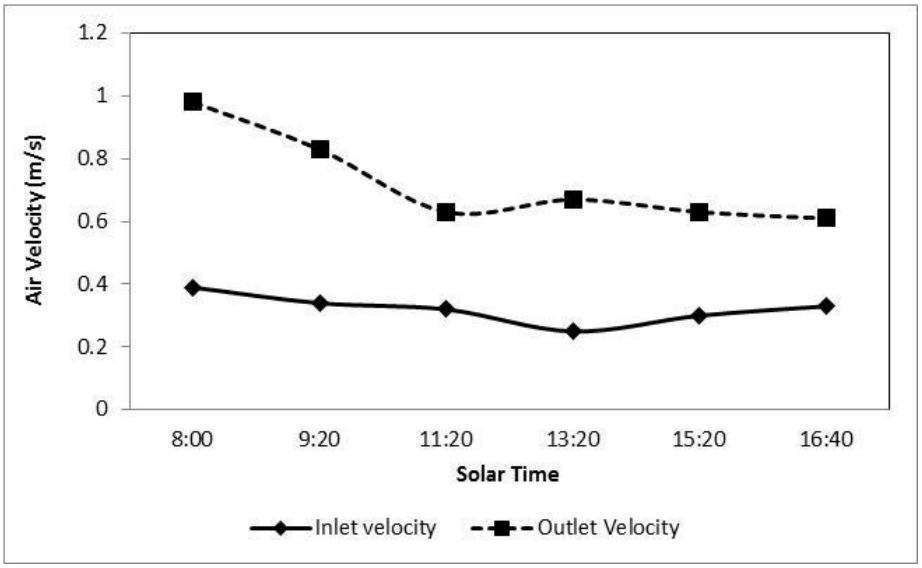

Figure 4.38 : Inlet and outdoor air velocity

Table 4.8 and Figure 5.39 show the differences of temperature obtained by measurements inside the office. The maximum temperature difference during the daytime on August 22, 2013 was approximately 3.7 °C. The solar radiation absorbed by the window results in a temperature difference between the outdoors and the indoors, thereby increasing the air temperature inside the office.

Table 4.8 : Temperature difference between ambient and indoor temperatures

Solar Time	Ambient Temperature	Average Indoor Temperature	Difference Temperature
8:00	30.5	30.5	0.0
8:40	30.7	30.6	0.1
9:20	31.2	31.0	0.2
10:00	31.3	31.1	0.2
10:40	31.7	31.1	0.6
11:20	32.4	31.3	1.1
12:00	32.8	31.2	1.6
12:40	33.7	31.3	2.4
13:20	34.8	31.1	3.7
14:00	34.1	31.2	2.9
14:40	33.8	31.2	2.6
15:20	34.1	31.0	3.1
16:00	33.7	31.0	2.7
16:40	33.1	30.9	2.2

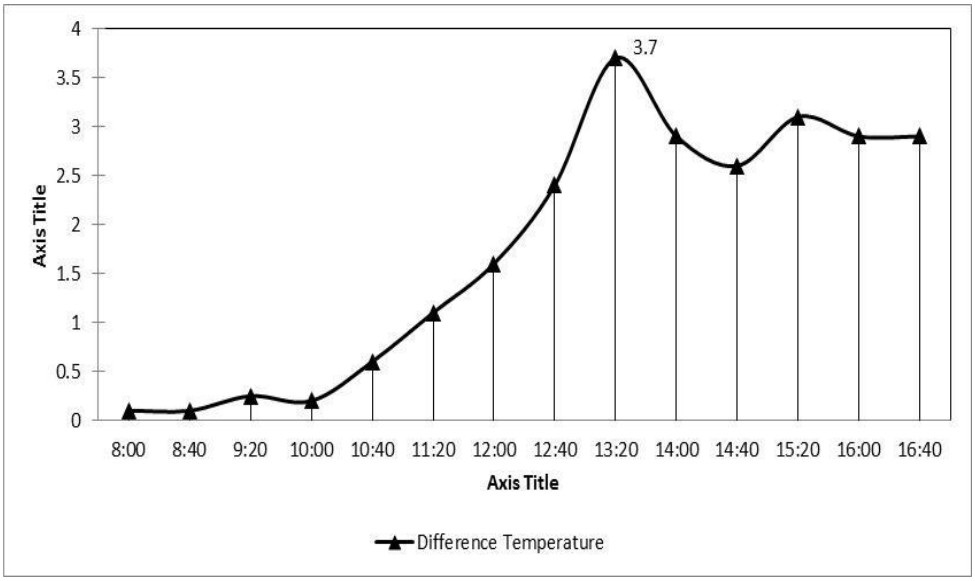

Figure 4.39 : Temperature difference between outdoor and indoor environments.

Figure 4.40 shows a comparison of temperature differences on August 16, 20, and 22, 2013. The maximum differences of temperature during the mentioned days were between 3.4^{o}C and 3.7 ^{o}C, whereas the minimum readings occurred in the morning and reached between 0.3 and 2.1^{o}C.

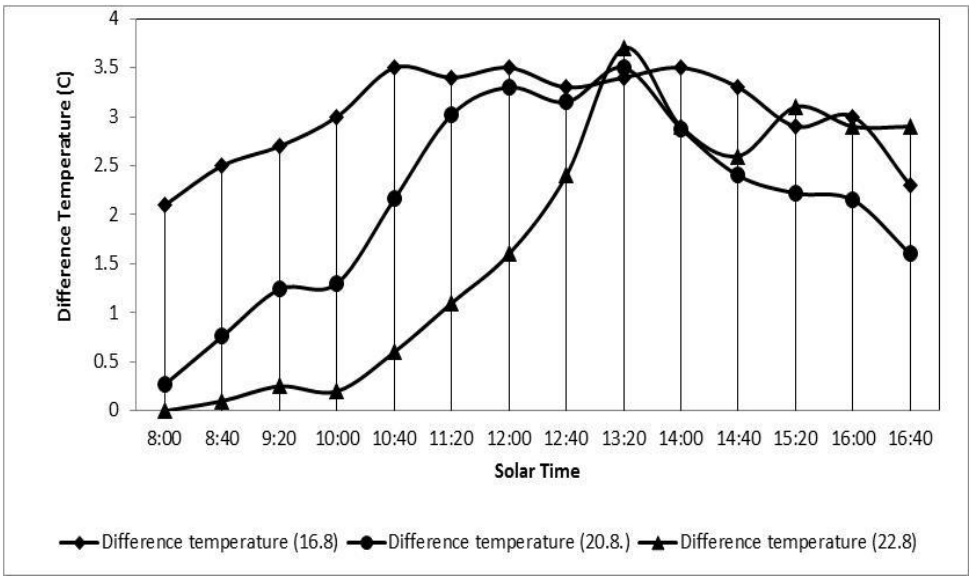

Figure 4.40 : Temperature differences for three days.

4.3.4 Verification of Measurement Results

Temperature and air velocity measurements were performed at solar noon of the office, with two windows opened to facilitate air flow inside the office. Table 4.9 shows the indoor measurements of the surface temperatures above the glazed windows, as well as the average indoor temperature, humidity, wind speed, and air pressure. Figure 4.41 shows fluctuations in average outdoor and indoor wind velocities in the office.

Table 4.9 : Indoor parameter measurements

solar Time	Ambient Temp.	Average indoor Temp.	outdoor velocity	Average Indoor Velocity	Indoor humidity	outdoor humidity	Lux
12:00	33.1	28.4	0.66	0.26	56%	55%	180.2
12:40	33.5	28.7	0.76	0.34	42%	44%	132.5
13:20	34.4	28.8	0.82	0.33	53%	42%	100.7
14:00	33.7	28.5	1.17	0.30	45%	47%	100
14:40	33.3	28.4	0.93	0.22	56%	45%	113.9

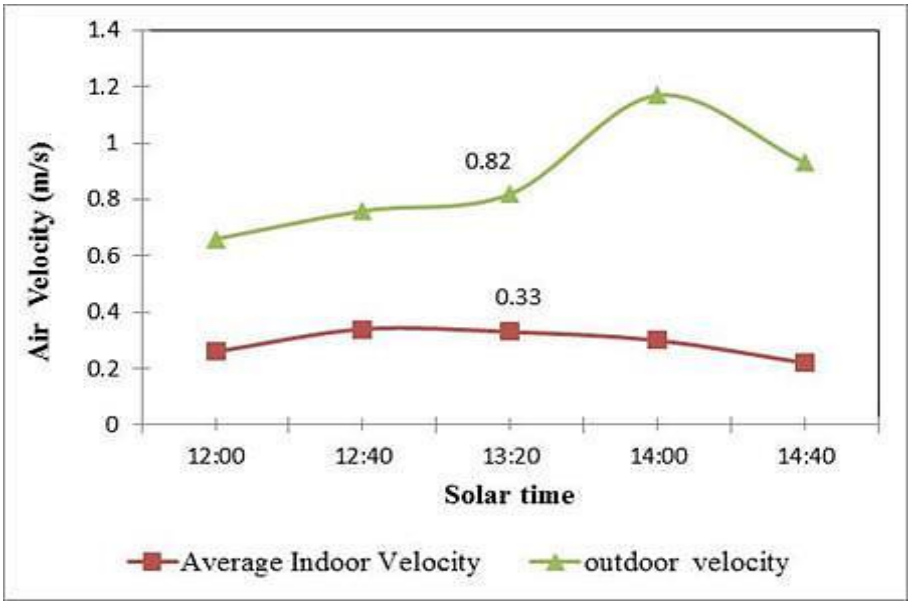

Figure 4.41 : Average air velocities inside the office.

Figure 4.42 shows the average distribution of ambient temperatures inside the office from 12 noon to 2:40 pm. The peak temperature inside the office was 28.8^{o}C at 1:20 pm.

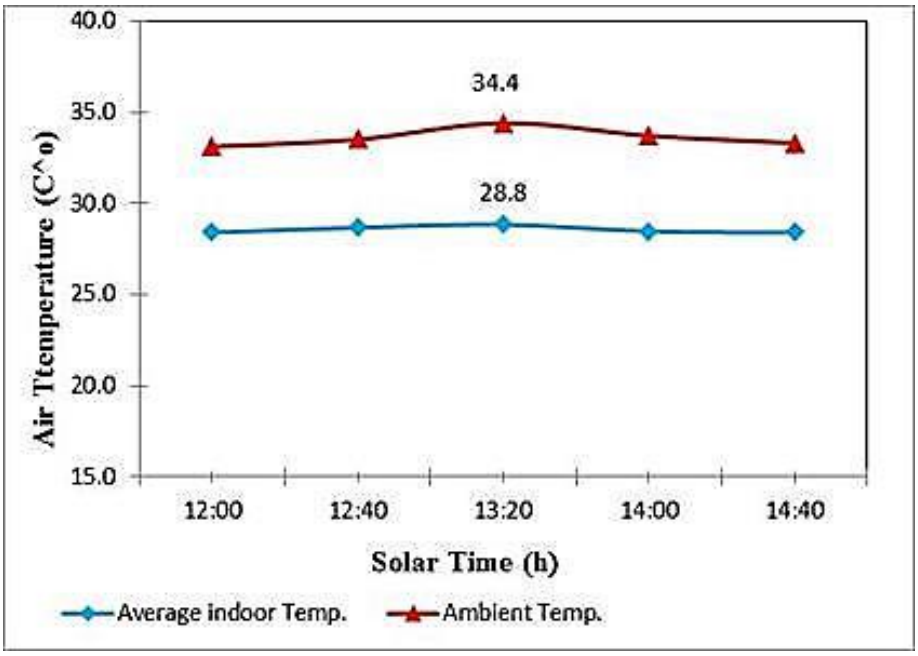

Figure 4.42 : Average air temperatures outside and inside the office.

Figure 4.43 shows the temperature differences in the office. The maximum temperature difference during the daytime was approximately 5.6 ℃. The solar radiation reflection through the double-glazed window reduces the WWR,

consequently reducing the air temperature inside the office and reducing the temperature difference.

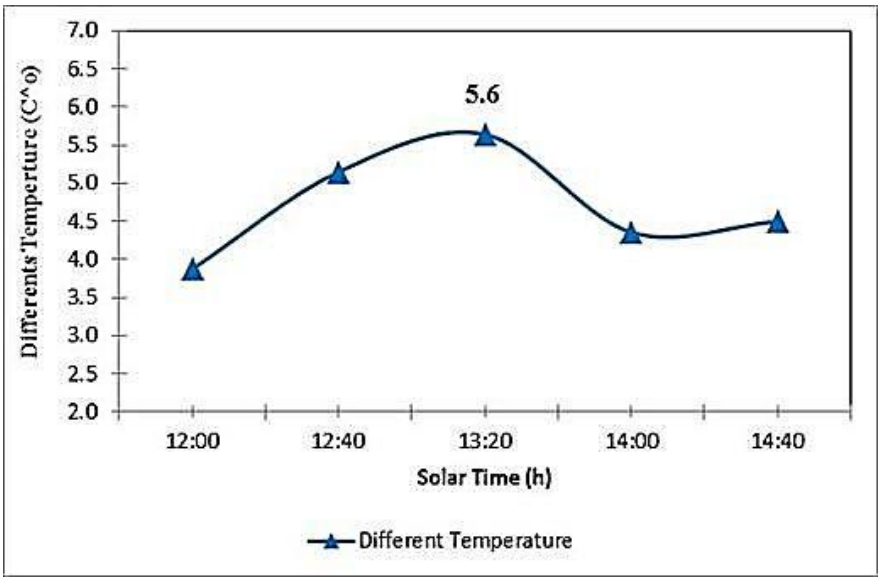

Figure 4.43 : Temperature difference between outdoor and indoor environments.

Figure 4.44 illustrates the outdoor and indoor humidity. The humidity in the office was generally lower than that outdoors. The indoor humidity began to increase at 2:40 pm because of the decrease in temperatures in the evening.

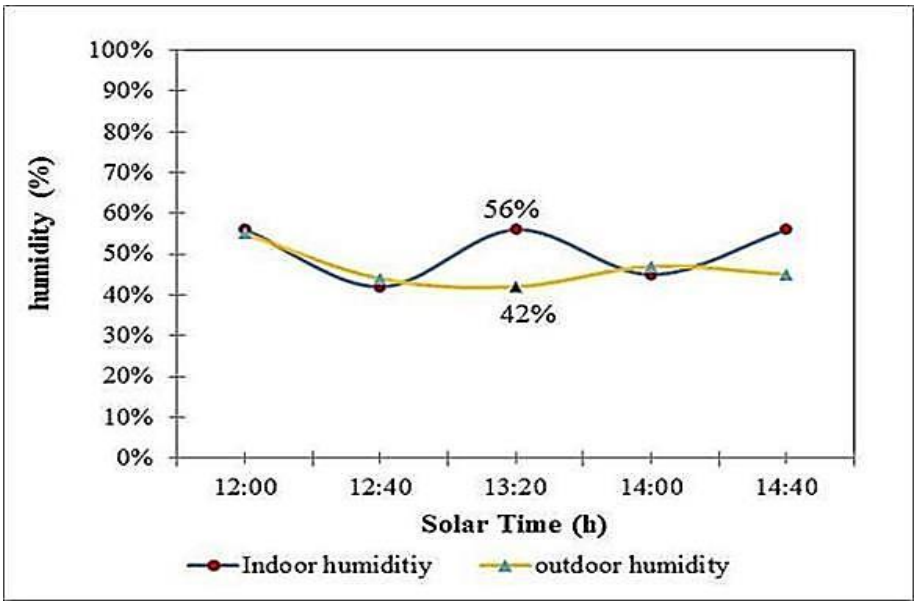

Figure 4.44 : Indoor and outdoor relative humidity.

Figure 4.45 shows the level of natural lighting inside the office from 12 pm to 2:20 pm, where the light intensity was between 100.2 lux to 180.2 lux.

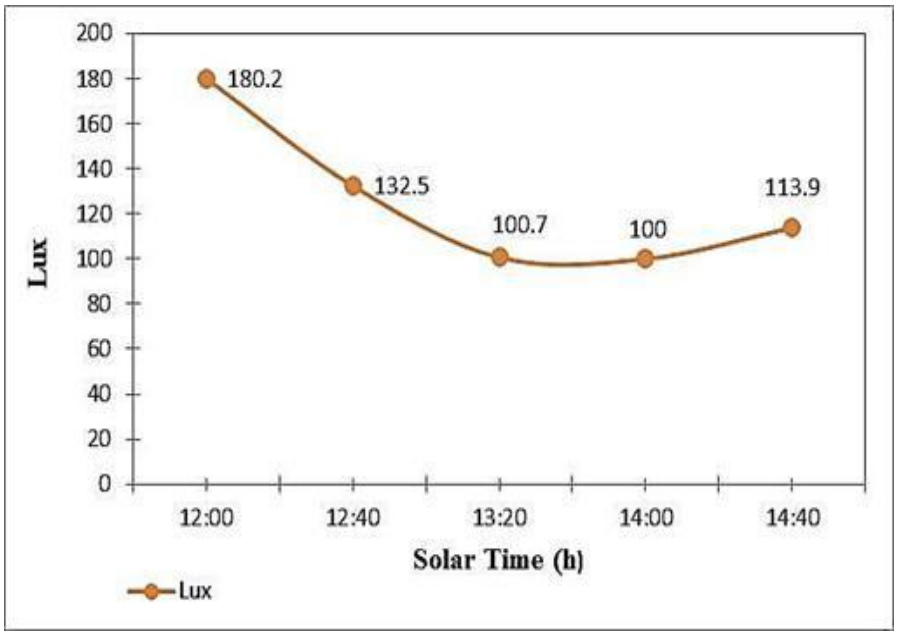

Figure 4.45 : Level of lux inside the office.

4.4 Numerical Results (Malaysia)

Natural ventilation depends entirely on the circumstances that surround the building. Wind velocity, wind direction, and air temperature may change significantly at each hour. This study is predicated on the effect of wind speed and air temperature in all cases. The inlet flow through windows that are installed in the front wall and the outlet flow within the office and corridor were in a steady-state condition by cross ventilation.

4.4.1 Grid Independence Test

The grid independence test is determined by testing the independence of hexagonal cells in each office and windows in the cross section by a series of tests with different numbers of cells to obtain the more suitable mesh for the current geometry.

Three mesh cells are used in this study; the results for these cells are shown in Figure 4.46. Results of 210.000, 1.050.000, and 1.810.000 grids for velocity and temperature are almost at equal grids. A computational cell with 1.050.000 was used for all the numerical results because calculating the results for this grid requires less time compared with that for 1.810.000 grids

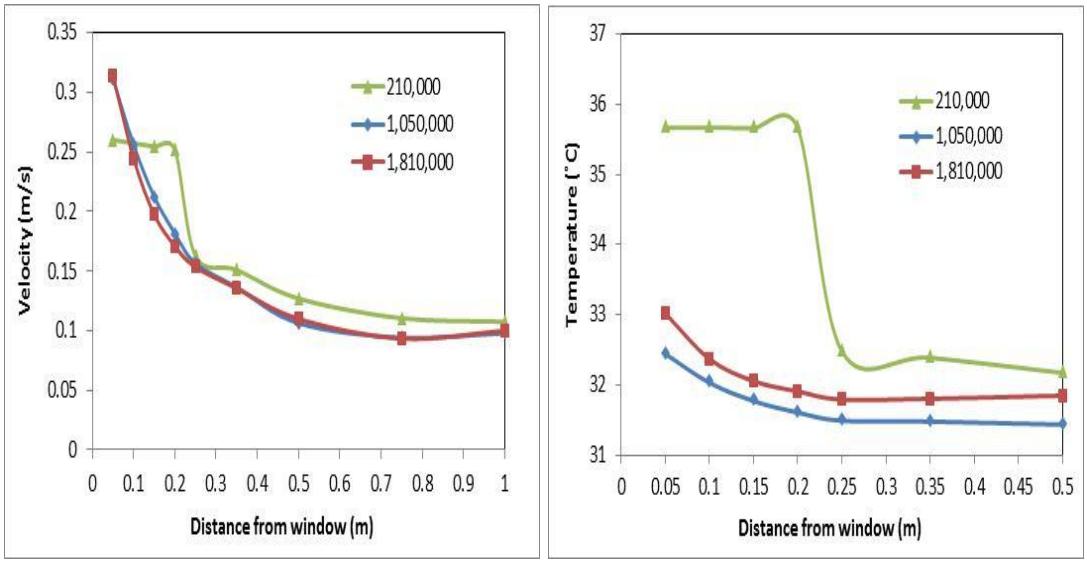

Figure 4.46 : Grid independence tests of velocity and temperature.

4.4.2 Interpretation of Contours of Total Temperature Distribution

CFD results were simulated using test office data over different solar times. Figure 4.47 shows the simulated temperature inside the office along the ZX plane with solar time from 8:00 am to 4:40 pm. The results are almost nearly the same with all models, and each model is slightly different from the other. The figures indicated that the average temperatures simulated inside the office ranged from 303 K to 304 K when the outside temperatures were between 303 K and 306 K for all solar times. The lower average temperature was in the early morning at 8:00 am; higher temperature inside the office that reached 304.7 K was observed at solar noon (1:20 pm). The temperature in the corridor was lower than that which is normally obtained in an office; the difference in temperature ranges from 0.1 K to 0.5 K. The temperatures on the side walls, with values between 1 K and 2 K, were lower than those in the middle of the office. The temperature within the office was slightly higher at 8:00 am, 9:20 am, and 11:20 am because of the emission of solar radiation and heat from the glass wall.

Figure 4.48 shows the temperature distribution at a height of 1.50 m from the office floor through the whole length of the office. The CFD results of temperature distribution in the office are summarized in Table 4.10. Temperatures near the side wall were between 299.6 K and 302 K. The average temperatures inside the office were 303 K to 304 K at all times.

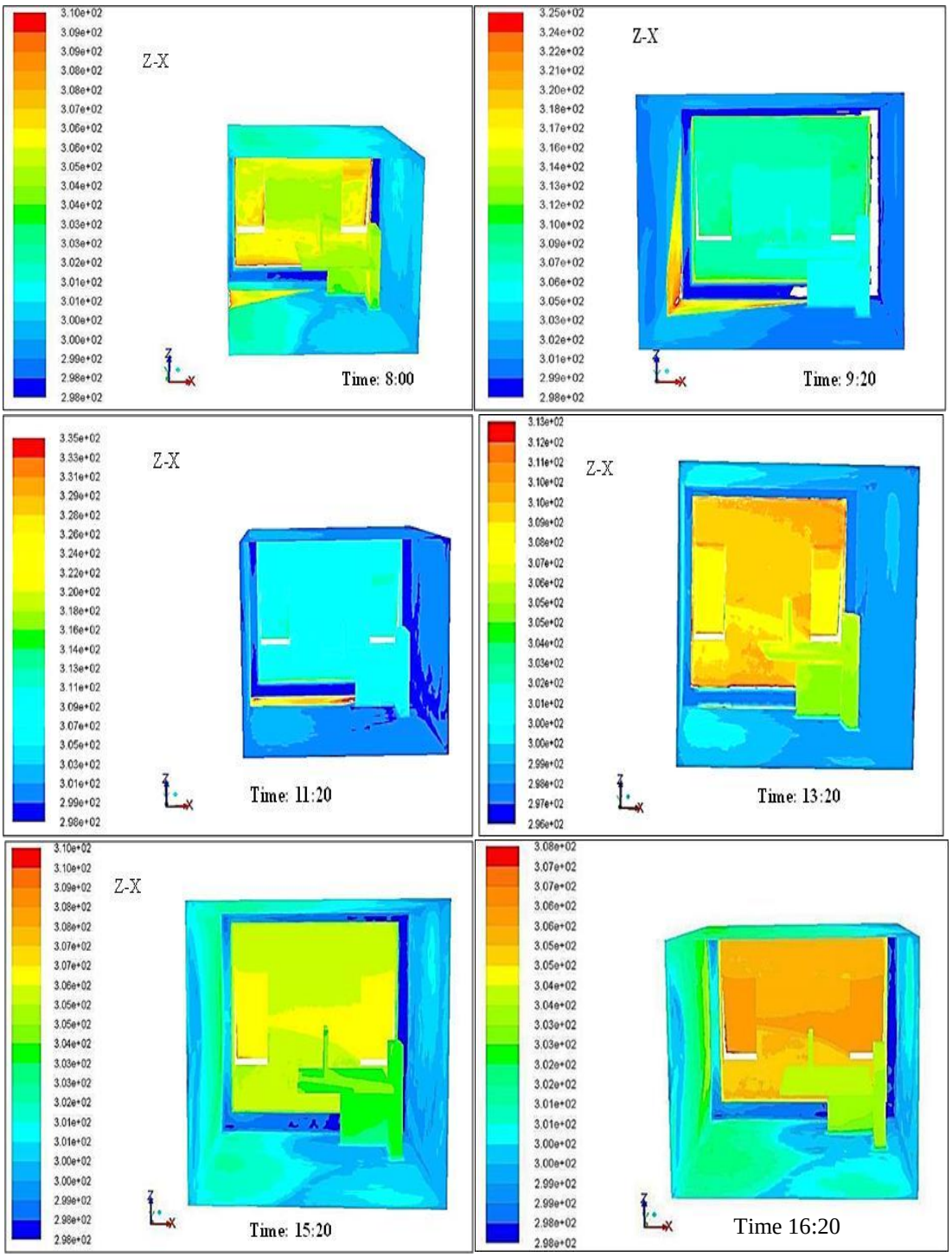

Figure 4.47 : Temperature distribution of office walls (CFD).

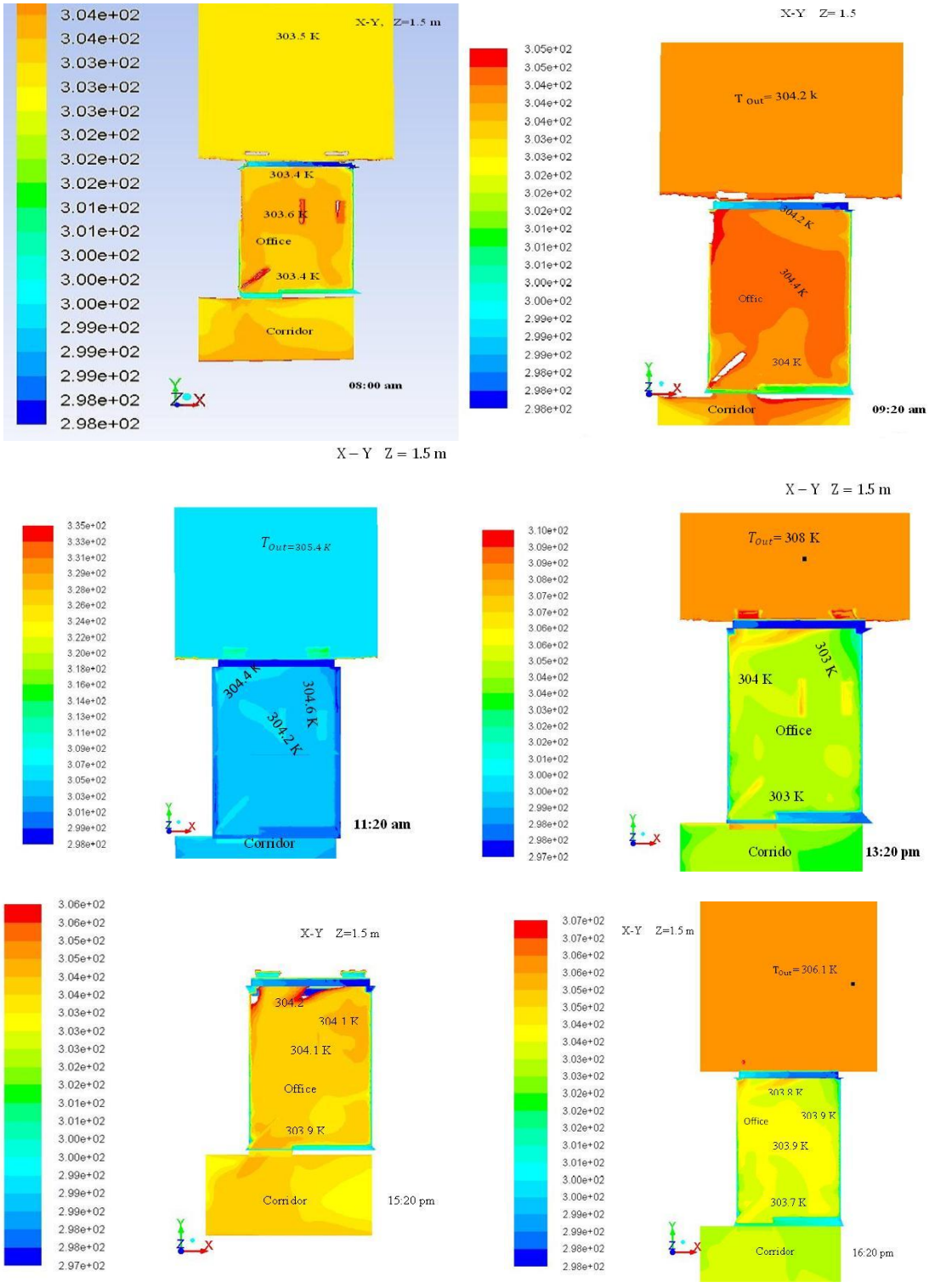

Figure 4.48 : Temperature distributions within an office above 1.5 m from the floor.

Table 4.10 : Temperature distribution (CFD) in an office above 1.5 m from the floor

Solar Time	Y=0.05m	Y=1.5m	Y-2m	Y=3.85 m	Windows	glass wall	Wall sides	Outdoor
8:00	303.4 k	303.2 k	303.6 K	303.4 k	306 k	299.7 k	303 k	303.5 k
9:20	304.2 k	304.5 k	304.4 k	304 k	309.4	307.9	302.4 k	304.2 k
11:20	304.6 k	304.7 k	304.6 k	304.2 k	311 k	308.5 k	300.7 k	305.4k
13:20	304.8 k	304.8 k	304.8 k	304.3 k	309.1 k	309.4 k	299 k	308 k
15:20	304.2 k	304.1	304.1	303.9 k	300 k	306.5	300 k	307 k
16:40	303.8 k	303.9 k	303.9 k	303.7 k	306.2	305.5	300.8 k	306.1 k

4.4.3 Interpretation of Contours of Air Velocity Distribution

Figures 5.49 and 4.50 shows the velocity distributions inside the office when wind comes from the northeast direction and perpendicular to the exposed wall, in which the average wind velocity was 0.6 m/s. The CFD simulation periods are 8:00 am, 9:20 am, 11:20 am, 1:20 pm, 3:20 pm, and 4:40 pm on August 22, 2013. The results are similar with all models, although the air flow fields of each model are slightly different from each other. The model indicated that the areas in front of the inlet and at the side of walls showed high wind speed.

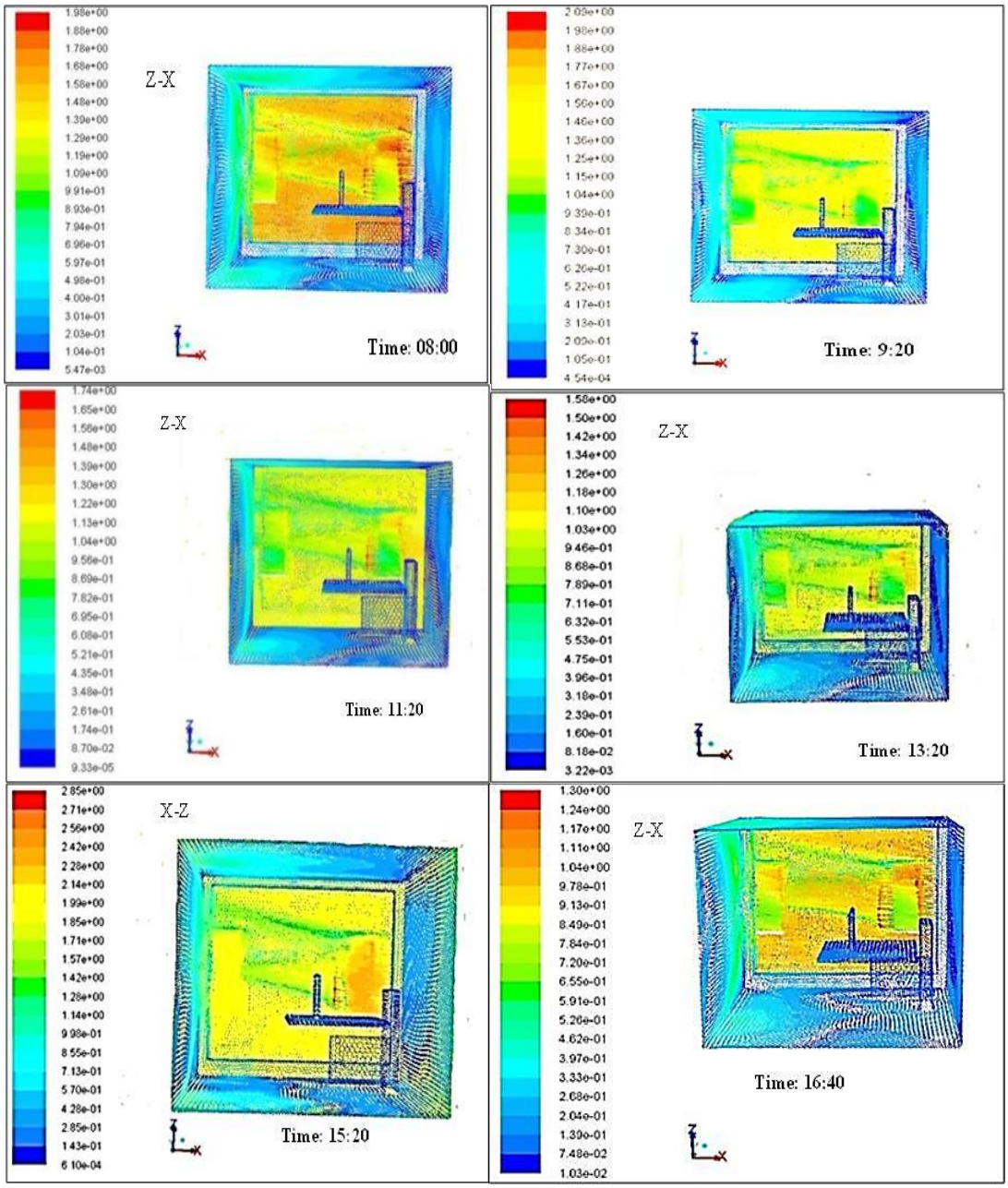

Figure 4.49 : Air velocity distributions of office walls (CFD).

Figure 5.51 illustrates that the temperatures simulated at 8:00 am were 303.6 and 305 K at distances of 50 and 100 cm, respectively, from the window opening. The temperature at the floor of the office and near the table ranged from 301 K to 303 K, whereas the outside air temperature at 8:00 am was 307.6 K.

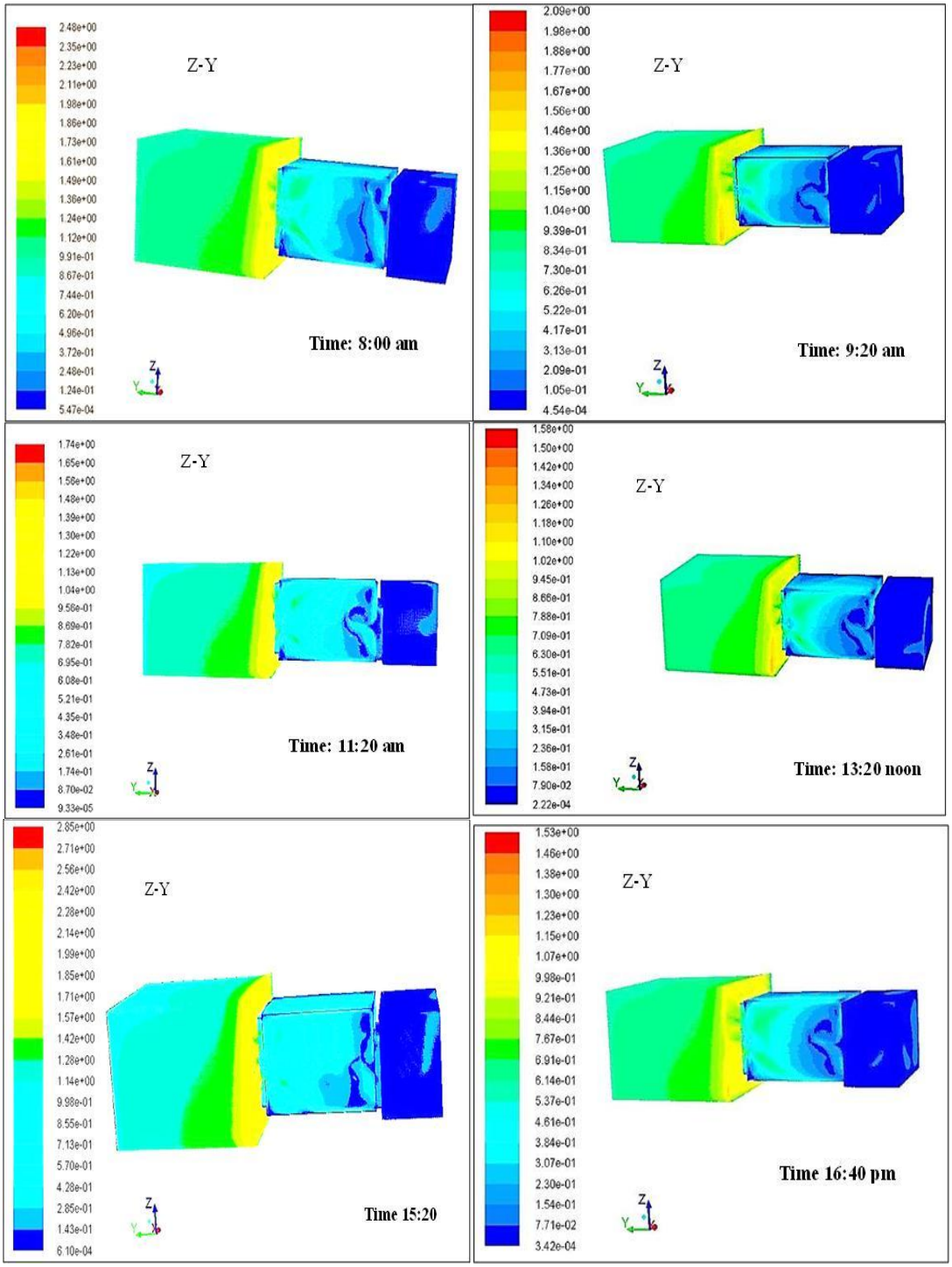

Figure 4.50 : Air velocity flow through windows.

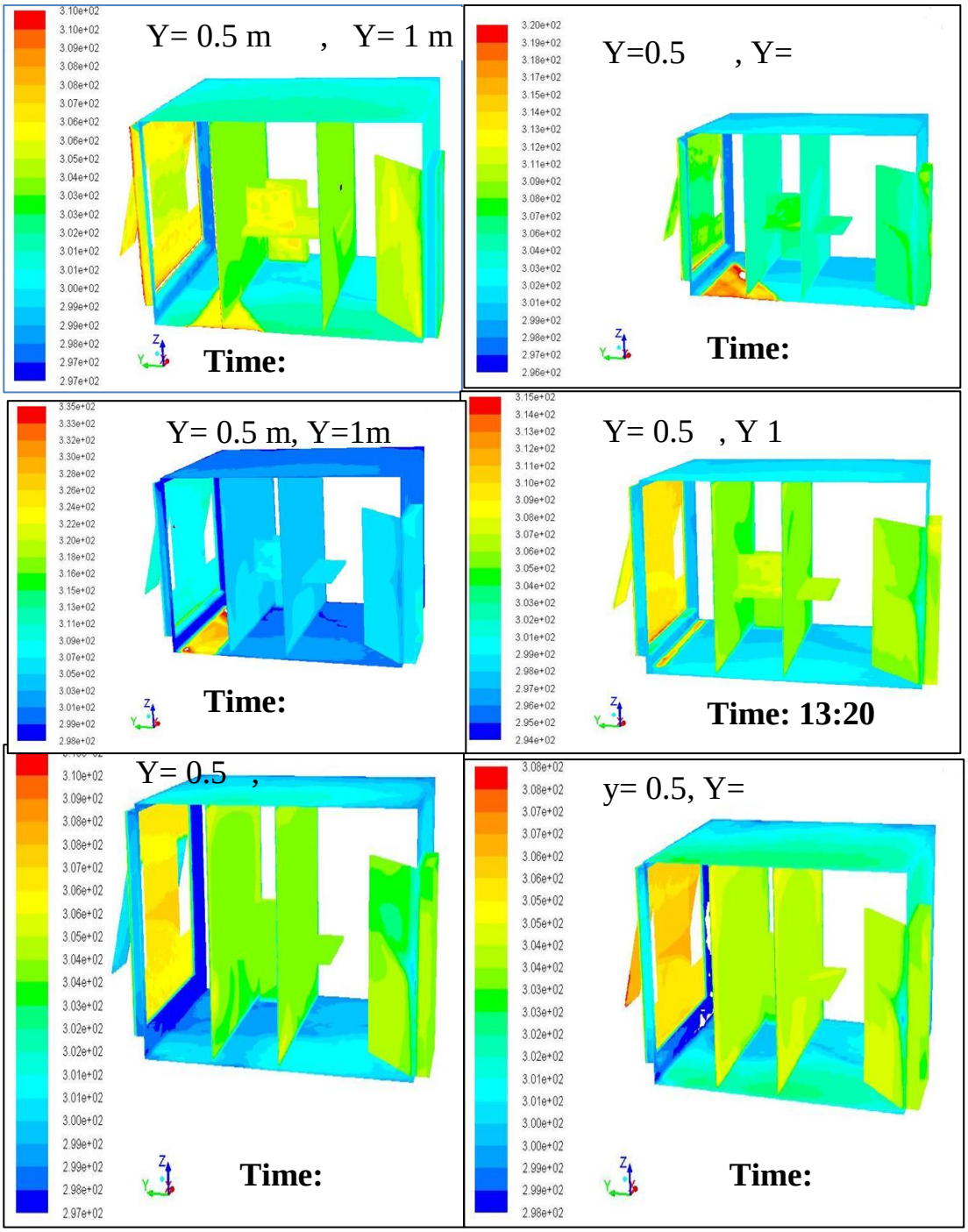

Figure 4.51 : Average temperature distributions with distance in an office (CFD).

4.4.4 Comparison between Experimental Data and Numerical Results

In this study, airflow and air temperature measurements data are validated by using the computational method via experimental measurements in a full-scale test office. The experimental results and the numerical results with solar times are compared.
Temperature Profiles

Figure 4.52 shows a comparison between numerical results (CFD) and experimental results of indoor and average outdoor temperatures and their relationship with solar time. The predicted temperatures are linearly related with measured experimental values. The figure shows that the numerical (CFD) results agreed well with the experimental results, thereby confirming that the CFD simulations are acceptable and achievable.

Table 4.11 shows the average temperatures from experimental measurements and numerical (CFD) results. The percentage of accuracy between the numerical and experimental measurements was 0% to 0.02%.

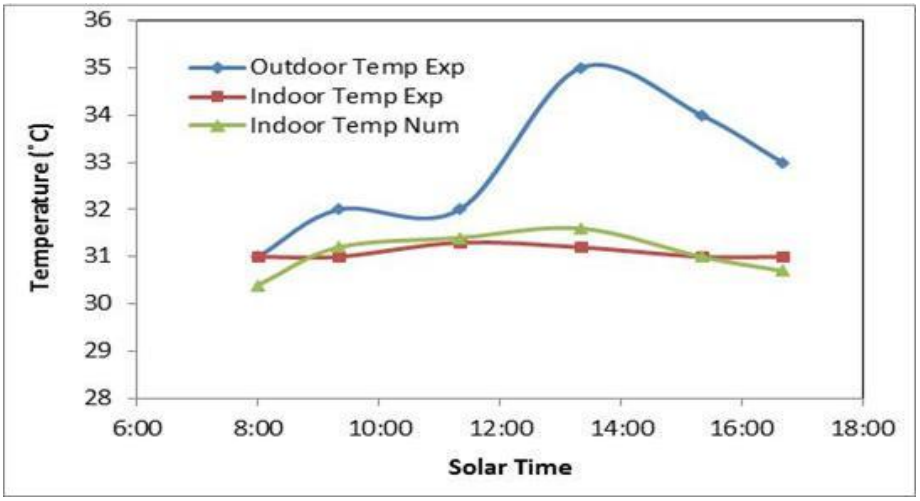

Figure 4.52 : Comparison between experimental and numerical results (CFD).

Table 4.11 : Experimental and numerical temperature values of the office

Time	Outdoor Temp Exp	Indoor Temp Exp	Indoor Temp. Num	The percentage of accuracy between the practical and experimental
8:00	30.5	31.0	30.4	1.9 %
9:20	31.5	31.0	31.2	0.6.%
11:20	32.4	31.3	31.4	0.3%
13:20	34.6	31.2	31.6	1.3.%
15:20	33.6	31.0	31.0	0.00%
16:40	32.6	31.0	30.7	0.97%

Air Velocity Profiles

Figure 4.53 shows a comparison between the numerical (CFD) and experimental measurement results of indoor air velocities profiles, as well as the average outdoor velocity and the relationship with solar time. The predicted air velocity was linear and parallel with the measured experimental values, thereby agreeing well with results throughout all solar times. Thus, the CFD simulations are acceptable and achievable.

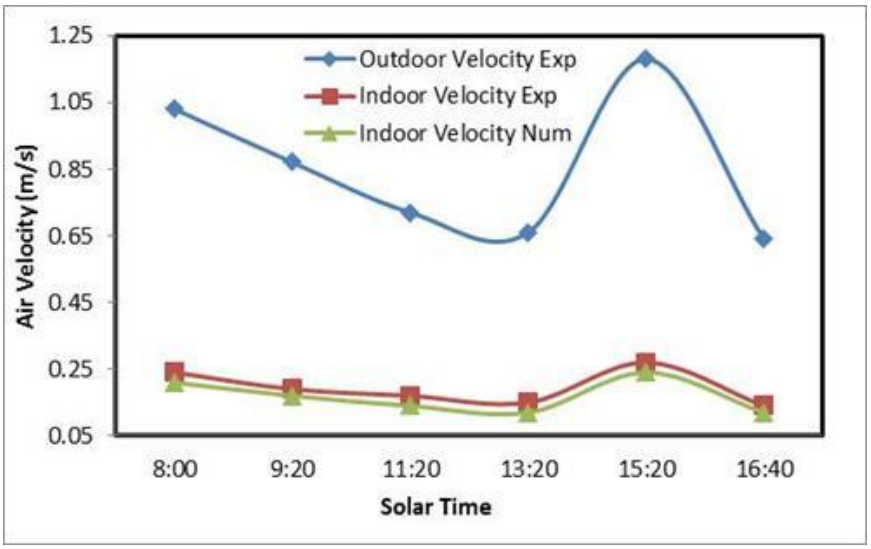

Figure 4.53 : Comparison between CFD and measurement results.

Table 4.12 shows the air velocities of numerical results (CFD), indoor and outdoor measurement data, and their accuracy. The outdoor air velocities were between 0.64 m/s to 1.18m/s, and the peak air velocity was measured at 3:20 pm.

Table 4.12 : Eexperimental and numerical air flow value of the office

Time	Outdoor Velocity Experimental	Indoor Velocity Experimental	Indoor Velocity Numerical	percentage of accuracy between CFD and Exp.
8:00	0.97	0.24	0.21	1.4 %
9:20	0.87	0.19	0.17	1.2%
11:20	0.72	0.17	0.14	2.1%
13:20	0.66	0.15	0.12	2.5%
15:20	1.18	0.27	0.24	1.3%
16:40	0.64	0.14	0.12	1.7%

4.5 Verification and Validation

The reliability of the CFD results is determined through verification followed by validation.

4.5.1 Verification

Verification is the process of assessing simulation numerical uncertainty U_{SN} and, when conditions permit, estimating the sign and magnitude δ^*_{SN} of the numerical error itself and the uncertainty ϵ_{SN} in that error estimator (Stern et al 2001).

$$\delta_{SN} = \delta_I + \delta_G + \delta_T + \delta_P \quad (4.1)$$

Where the subscript I,G,T, and P represent the iteration number, the grid size, the time step and other parameters, respectively. Considering that the errors are assumed independent, the simulation numerical uncertainty is then given by

$$U^2_{SN} = U^2_I + U^2_G + U^2_T + U^2_P \quad (4.2)$$

Given that only steady-state conditions are considered, the simulation numerical accuracy is dependent on only the iteration number and the grid size.

The residual convergence value used in this study is 10^{-4}. A smaller residual value does not significantly change of the calculated results but requires extensively more computation time. To achieve a solution that is independent of the time step size, the time step must be small enough so that a single step does not rotate the interface by a distance greater than the smallest cell size. As a result, the time step used was quite small, typically on the order of 1 second. In most cases, three revolutions of the rotor are required to reach a stable solution (each case requires 30 to 36 hours of computational time on a 2.8 GHz Core 2 Duo workstation with 4 GB RAM depending on the size of the mesh file). Figure 4.54 presented the iteration convergence obtained from this study's steady-state simulations (FLUENT V.6.3).

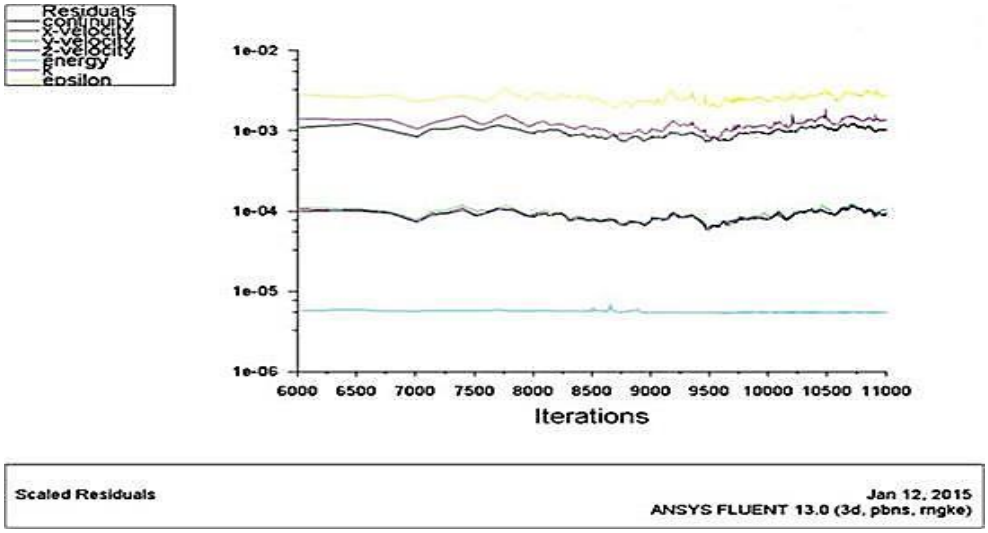

Figure 4.54 : Solution convergence; iteration obtained from steady-state simulation.

Stern et al. (2001) provides an estimate for the uncertainty in the case of an oscillatory convergence:

$$U = \frac{1}{2}\ (S_{up} - S_{low}) \tag{4.3}$$

Where; S_{up} and S_{Low} are the upper and lower bounds of the solution oscillation near the final iteration, respectively.

Transport equations of natural ventilation

In completing CFD analysis for the whole shape of the office room and windows, setting up the governing equations (momentum, continuity and energy) is necessary. For the specific case of heat flux effect and fluid flow through the office, the governing equations are solved with assumptions. On the basis of these assumptions, the energy, momentum, and continuity equations for this study can be written as stated by Hung et al. (2012)

The continuity equation:

$$\frac{\partial u}{\partial x} + \frac{\partial v}{\partial y} + \frac{\partial w}{\partial z} = 0 \tag{4.4}$$

The X-momentum equation:

$$\rho\left(u\ \frac{\partial u}{\partial x} + v\ \frac{\partial u}{\partial y} + w\ \frac{\partial u}{\partial z}\right) = -\frac{dp}{dx} + \mu\left(\frac{\partial^2 u}{\partial x^2} + \frac{\partial^2 u}{\partial y^2} + \frac{\partial^2 u}{\partial z^2}\right) \tag{4.5}$$

The Y-momentum equation:

$$\rho\left(u\,\frac{\partial v}{\partial x}+v\,\frac{\partial v}{\partial y}+w\,\frac{\partial v}{\partial z}\right)=-\,\frac{\mathrm{dp}}{\mathrm{dy}}+\mu\left(\frac{\partial^2 v}{\partial x^2}+\frac{\partial^2 v}{\partial y^2}+\frac{\partial^2 v}{\partial z^2}\right) \quad (4.6)$$

The Z-momentum equation:

$$\rho\left(u\,\frac{\partial w}{\partial x}+v\,\frac{\partial w}{\partial y}+w\,\frac{\partial w}{\partial z}\right)=-\,\frac{dp}{dx}+\mu\left(\frac{\partial^2 w}{\partial x^2}+\frac{\partial^2 w}{\partial y^2}+\frac{\partial^2 w}{\partial z^2}\right) \quad (4.7)$$

The energy equation:

$$\rho \mathrm{C}_{p.}\left(u\,\frac{\partial T_f}{\partial x}+v\,\frac{\partial T_f}{\partial y}+w\,\frac{\partial T}{\partial z}\right)=k\left(\frac{\partial^2 T}{\partial x^2}+\frac{\partial^2 T}{\partial y^2}+\frac{\partial^2 T}{\partial z^2}\right) \quad (4.8)$$

ρ effective density
c_p Heat capacity
μ Dynamic viscosity
k Thermal conductivity

4.5.2 Validation

Actual measurements and numerical simulations of the reference case, in which a comparison was performed between experimental results and simulations, were undertaken on the optimum model at solar noon (1:20 pm). The calculated air temperatures and air velocities by CFD simulation were examined and compared with the measurement data. For the experiment, only measurements at two positions (50 and 200 cm) were carried out from the window (inlet), whereas continuous measurements for the entire office were calculated in CFD. Model and boundary conditions were modified several times before the best representation of the indoor climate in the test office was achieved. Then, final comparisons were performed. Table 4.13 shows the average outdoor and indoor temperatures, air velocities, and humidity of the experimental measurements and the numerical simulation (CFD) results of Model 22%.

Table 4.13 : Comparison between experiment and numerical results (CFD)

Models	Outdoor Velocity	Indoor velocity	Outdoor Temperature	Indoor Temperature	Humidity	Δ T.
Model 22%	0.67 m/s	0.37 m/s	307.6	300.8	53%	6.8
Experiment reference case	0.62 m/s	0.33 m/s	307.3	301.5	56%	5.8

Figure 4.55 shows a comparison between the numerical simulation results (CFD) and the experimental measurement results of indoor temperatures with distance from window to the center of the office at solar noon (1:20 pm). The predicted air temperatures are linearly related with measured experimental values. The maximum difference between measured air temperatures and air temperatures calculated in CFD simulation deviations is 0.3 K.

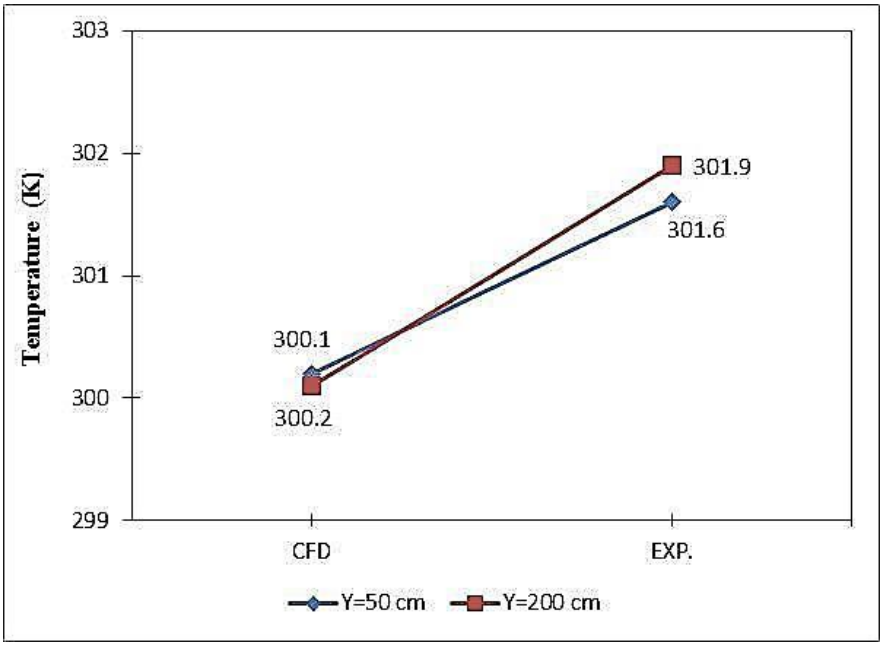

Figure 4.55 : Comparison between average temperatures of experimental and numerical results of Model WWR 22%.

Figure 4.56 shows a comparison between the numerical and experimental measurement results of indoor air velocities with distance from the windows to the center of the office 1.5 m above the floor, as well as the relationship with solar noon (1:20 pm). The maximum difference between measured air velocities and air velocities calculated in CFD simulation deviations was 0.02 m/s.

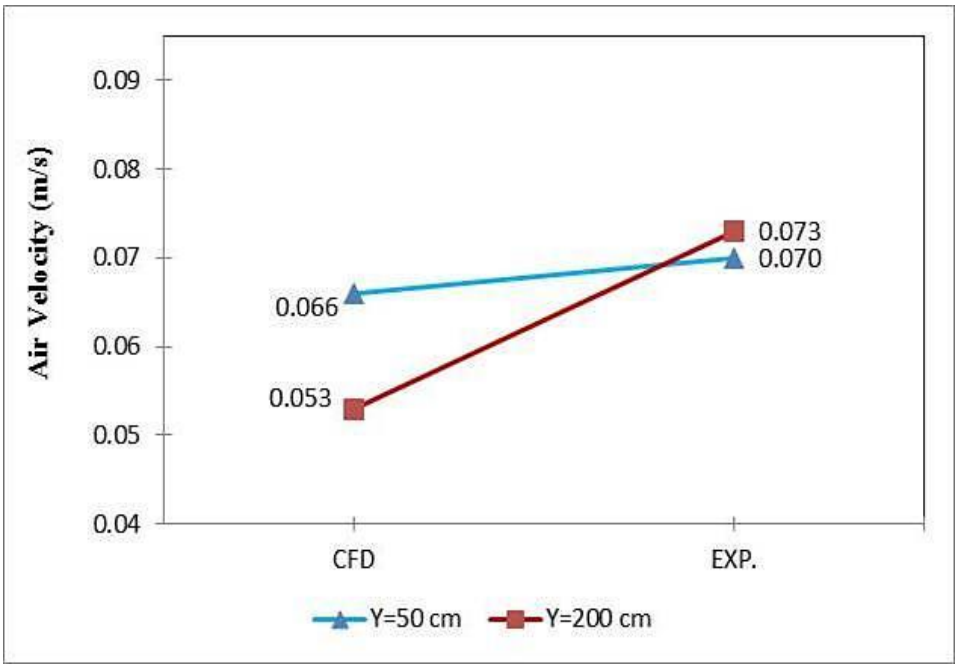

Figure 4.56 : Comparison between air velocities of the experimental and numerical results of Model WWR 22%

Figure 4.57 shows a comparison between the numerical simulation results and experimental measurement results of average indoor temperatures, as well as the relationship with solar noon (1:20 pm). Significant agreement was found between the numerical and experimental values. The percentage of accuracy between the numerical and experimental measurements of temperatures was 0.2%, which was minuscule and acceptable for engineering applications.

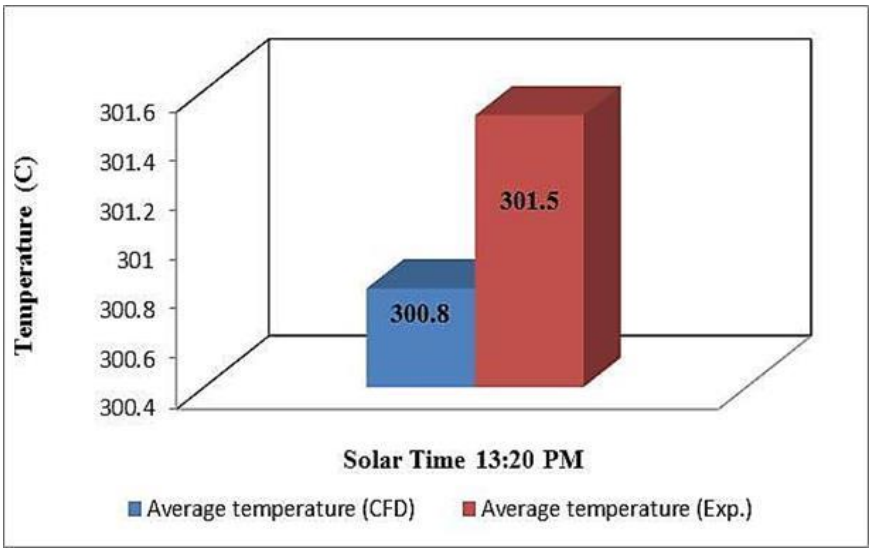

Figure 4.57 : Comparison between experimental and numerical results of Model WWR 22% (air temperature).

Figure 4.58 presents a comparison of the temperature difference between outdoor and indoor environments for the experimental and numerical procedures of model WWR 22%. The highest temperature difference was observed at 1:20 pm.

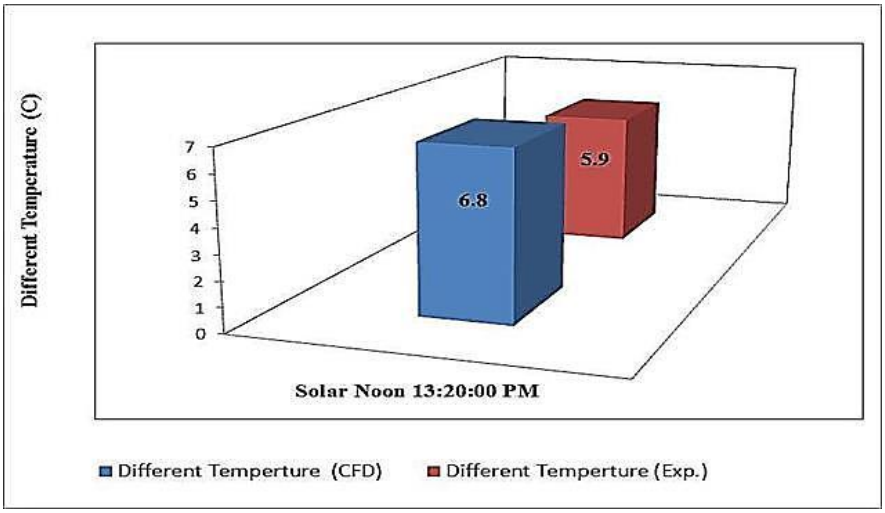

Figure 4.58 : Comparison between experimental and numerical results of Model 22% (temperature difference).

Figure 4.59 shows a comparison between the numerical and experimental measurement results of indoor average air velocities, as well as the relationship with solar time (13:20 PM) for Model WWR 22%. Results confirm that the CFD simulations are acceptable and achievable, and that the percentage of accuracy between the numerical and experimental measurements was 0.2%.

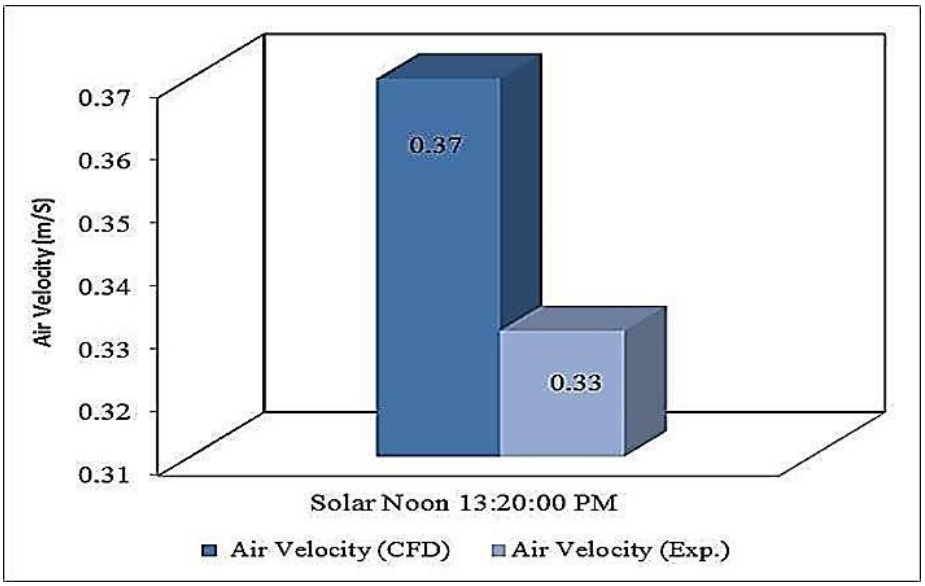

Figure 4.59 : Comparison between experimental and numerical results of Model 22% (average air velocity).

4.6 Results of PMV and PDD

The office was simulated in CFD software as a base case. Then, different models were simulated to improve the efficiency of natural ventilation. Different WWRs and window openings, such as front, top and bottom, were simulated. To evaluate the thermal comfort in optimum models, air temperature and relative humidity obtained from the simulations were analyzed by using two methods: Givoni (1992) and ASHRAE Standard 55 (2012). ASHRAE methods were applied to evaluate the thermal comfort conditions in the office. The office was occupied at 1:20 pm without an air conditioning system. The office has a 2.00 m x 0.90 m door and a WWR of 22% for a dry-hot climate and a warm-humid climate.

The factors for calculating PMV index, air temperature, and RH were obtained directly from interior measurements. Air flow was obtained from CFD simulation results, and the mean radiation temperature was set to be $\mathbf{2^0}$C above the interior air temperature based on CFD simulation results, Xiuzhang Fua and Dingxin Wuc (2015). The metabolic rate is set at 1.2 MET, and the clothing insulations of hot-dry climate and warm-humid are set at 0.6 and 0.5, respectively, ASHRAE Standard 55 (2012). PMV was computed by using the CBE Thermal Comfort Program software to calculate thermal comfort based on ASHRAE Standard 55 (2012). The outdoor and indoor climatic measurements in the naturally ventilated office are given in Table 4.14.

The method presented in ASHRAE 55 Standard 55 (2012) was applied. This method considers the acceptable indoor operative temperature based on the mean outdoor temperature. ASHRAE Standard 55 (2012) is a different method of determining the limits of thermal conditions in naturally ventilated offices.

Table 4.14 : Value of PMV and PDD for the Malaysian and Libyan models

No	$\mathbf{T_{Outdoor}}$	T_{Indoor}	Mean radiant Temperature. (C)	Air Velocity (m/s)	RH (%)	Metabolic met	Clothing insulation (clo)	PMV	PDD
Libya model WWR (22%)	34.8	28.1	30.4	0.4	30	1.2	0.6	0.3	7%
Malaysia model WWR (22%)	34.6	27.8	29.5	0.3	56	1.2	0.5	0.4	7%

The interior comfort temperature changes with different mean temperatures based on 80% and 90% acceptable ranges and the 80% acceptable ranges are used for normal thermal comfort assessments, and the 90% ranges may be used when a higher standard of thermal comfort is desired. For this study, the acceptability limit of 90% was adopted. Thus, the average outdoor air temperatures in Malaysia and Libya

were calculated. The indoor operative temperatures were obtained from the simulations. Comfort was calculated by using the simulation results, which were plotted in the charts of ASHRAE Standard 55. The result was the percentage of comfort and thermal comfort, as shown in Figure 4.60 in the Malaysian model and Figure 4.61 in the Libyan model.

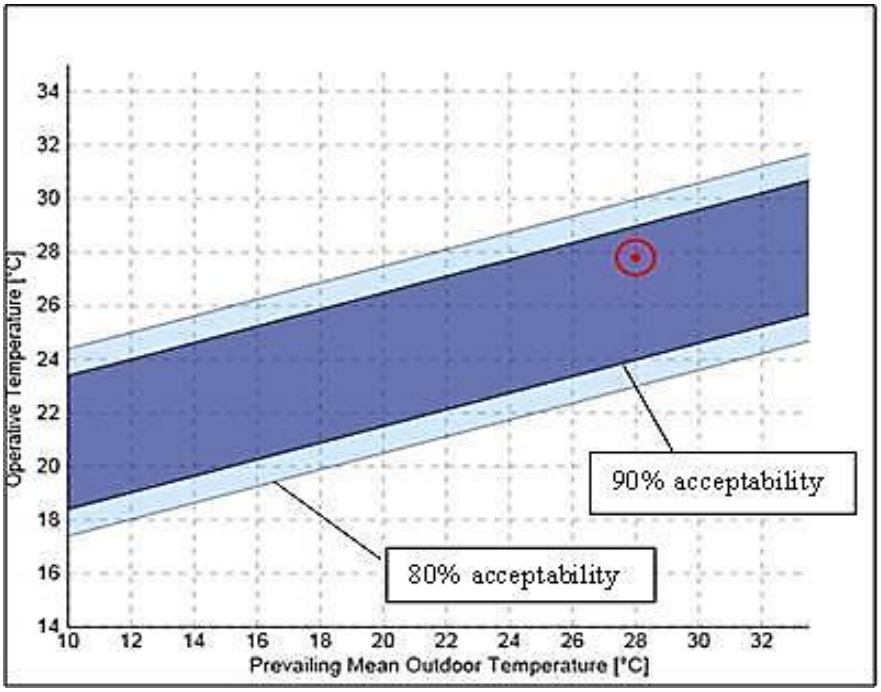

Figure 4.60 : Comfort bandwidths of the Malaysian model.

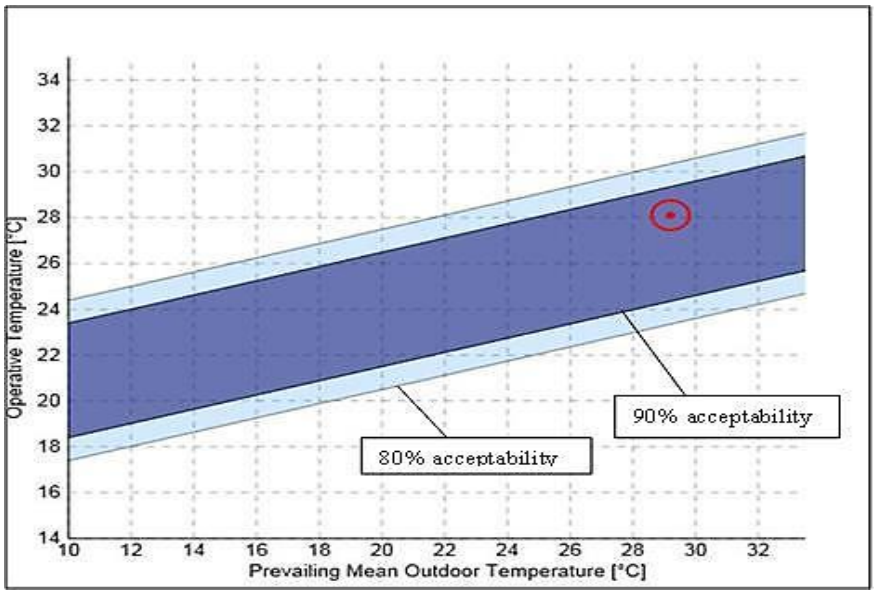

Figure 4.61 : Comfort bandwidths of the Libyan model.

Thermal comfort in the offices with an occupant was studied through experimental measurements and numerical results. The thermal comfort index (PMV) that formed the basis of the study is considered applicable within an environment for the following reasons: Fanger's investigation was based on a wide range of environmental conditions, including conditions when air temperature < 30 ℃ and relative humidity was between 40% and 55%. In addition, a moderate thermal environment is attained when PMV values range from −3 as cold to +3 as hot. Figure 4.62 shows the functional relationship between PMV and PPD inside two test offices. At PMV neutral (0), 0.3 of the occupant is satisfied.

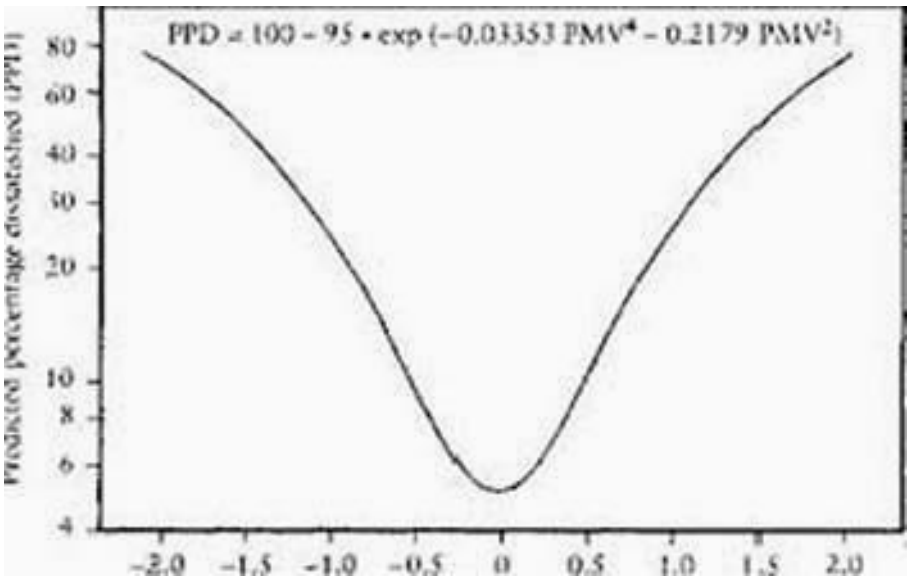

Figure 4.62 : Comfort bandwidths of the Malaysian window model.

4.7 Indoor Air Quality

This section focuses on IAQ indicators and pollutants, each of which is discussed in terms of characteristics, guidelines, ideal levels, and health effects. ASHRAE Standard 55 (2012) presents guidelines and recommendations for ensuring that at least 80% of the occupants would find the thermal conditions acceptable or comfortable.

The standard specifies that ideal indoor relative humidity levels should range between 50% and 70%. The concentration of carbon dioxide indoors varies based on the location, occupancy, and time of day, and tends to increase during the day. Typical office levels are in the range of 600–800 ppm (ASHRAE Standard 55-2012). In Ventilation for Acceptable Indoor Air Quality, a minimum ventilation rate of 10 L/s per person is recommended to ensure good IAQ in the office by using the ventilation rate procedure. Air temperature in the office should be < 28^0 C. Furthermore, the standard indicates that the eight-hour average exposure limit for carbon monoxide should not exceed 9 ppm. The Environmental Protection Agency recommends a PM_{10} standard of 50 $\mu g/m^3$ for annual exposure and 150 mg/m^3 for

24 hours. The size range of concern to human health and IAQ is 0.1–10 μm. Therefore, the window design that can provide an air temperature of 27 ℃ and air velocity of 0.34 m/s fulfills the conditions for a thermally acceptable office.

4.8 Summary

In this chapter, experiments and numerical results, verification and validation results, and the results of PMV, PDD, and IAQ conducted in Libya and Malaysia were presented. The results from the experiments along with the measurement data were compiled in tables and graphs. Measurements of the outside and interior air temperature, glass window temperature, relative humidity were collected. The data (air temperature, air velocity, and relative humidity) were obtained from meteorological stations from Hoon and Kuala Lumpur. The field data readings were collected and based on various conditions.

This chapter also presented the CFD results, grid independence tests, and validation, then compared the results with those obtained from the field study in Malaysia. The experimental and simulation results were presented in terms of air flow and air temperature profiles. The result can be utilized in many engineering and architecture applications to obtain an optimum ventilation level and reduce the temperature in buildings.

CHAPTER 5

DEVELOPMENT OF OPTIMUM DESIGN OF WINDOW CONFIGURATION

5.1 Introduction

This chapter focuses on the implementation of CFD software simulation. Air flow and air temperature from buildings were modeled by using 36 models from the WWRs. The experimental results were used to develop a numerical model. The stack effect is explained through cross ventilation experiments along with a description of the methods of physical modeling with CFD. The physical and numerical models were applied using results from experimental data.

5.2 Optimum Model

Increased air flow and decreased temperature difference through windows significantly affect the thermal comfort of an office. The Malaysia case was used to achieve the best WWR in a hot-humid climate. Predictions for a hot-dry climate in Libya were optimized by CFD using the results from Malaysia.

Finite element analysis and the optimum design of double glazed window were investigated using the CFD software and its parameterized modeling method. The optimum dimensions of the window were obtained and the air flow and air temperature distribution inside the office were found to be suitable. Table 5.1 shows the input data in FLUENT v6 for this thesis. The optimum dimensions of the Malaysia model are a height of 200 cm and a width of 40 cm (WWR=22%). The optimum dimensions of the Libya model are a height of 200 cm and a width of 80 cm (WWR=22%) at 15 cm above the floor.

Table 5.1 : Input data of simulation

Solver	Pressure Based
Time	Steady
Turbulent Model	Spalart - Allmaras model
Materials	Air, glass, aluminum and wood, façade wall
Operating Pressure	0 Pascal
Operating Temperature	307.6 K
Inlet Velocity	0.67 m/s
Convergence criterion	1E-06
Number of Iteration	Above 10000

Table 5.2 illustrates the output parameters used to optimize the model. The output parameters are optimized to determine the optimum double-glazed window for an office.

Table 5.2 : Output data of simulation

No	Parameters
1	Temperature Distribution
2	Air Velocity Distribution
3	Temperature Difference

The CFD modeling process, physical model, and assumptions that govern the model, as well as equations, code validation, boundary conditions and mesh number are presented in the following sections.

5.3 Physical Model and Assumptions

5.3.1 Physical Model

A schematic diagram of the office design at the Faculty of Engineering building at UPM that was used as a reference case is shown in Figure 5.1. The office is geometrically facing and oriented at 22 ° from north to true east. The east and west walls of the office are adjacent to other offices, and the north wall is on the exterior, whereas the south wall is located in the corridor. The shape of the office is rectangular with overall dimensions of 3.80 m × 2.85 m × 2.60 m (width, y-direction; length, x-direction; and height, z-direction, respectively). The office room is located on the fifth floor of the building; its location was chosen to reduce and effects of the ground and the office roof. This study was carried out using 36 models of windows by comparing average temperature and air velocity between models, as well as decreasing the WWR.

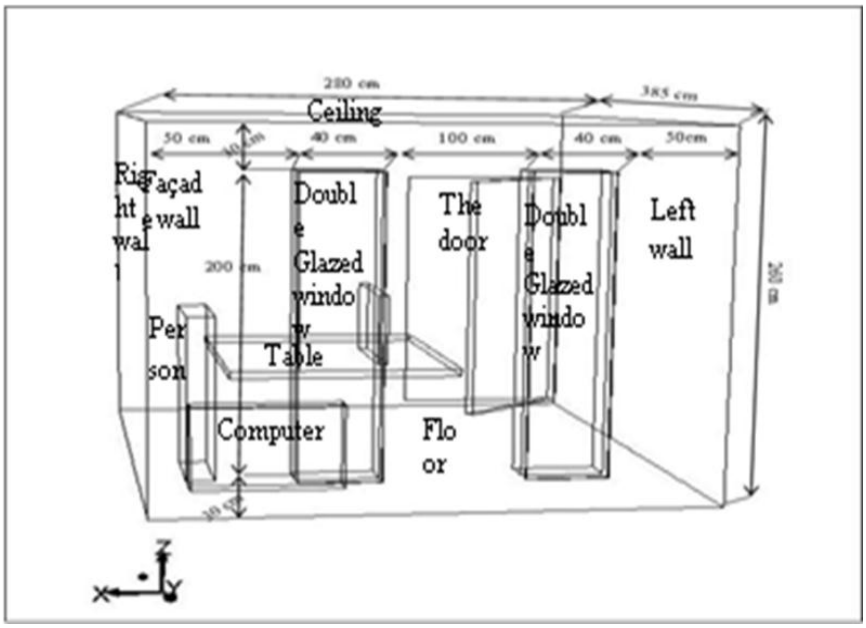

Figure 5.1 : Schematic diagram of the office.

The analysis includes values of the WWR, and these cases were simulated scenarios that consist of front (A), top (B), and bottom (C) window openings. The calculation of WWR for the given fa çade is as follows:

$$WWR = (a \times b) / (H \times W). \quad (5.1)$$

Where,
a: Height of window
b: Width of window
H: Height of fa çade wall
W: Width of fa çade of wall

The 36 models of dimensional analysis and the openings of designed window are shown in Tables 5.3 and 5.4.

The major assumptions involved in the investigations are as follows: the analysis is a 3D Cartesian coordinate system and steady-state condition, the fluid properties of material are constant, and flow is isothermal and incompressible. The numerical techniques were solved by using (Navier–Stokes). Continuity, energy, momentum and concentration equations were used for 3D analysis. Turbulent fluid flow was applied in CFD. Turbulence closure scheme RNG k-ε was used in the model and implemented in FLUENT (Stavrakakis 2008). The governing equations provide the steady-state conditions, and the general form was used as conducted by Markatos et

al. (1982). On the basis of these assumptions, the governing equations were calculated as shown below.

Table 5.3 : Summary of various opening window configurations with dimensional

Models	Method of Opening	High (a)	Width (b)	H	W	WWR $\frac{(a \times b)}{(H \cdot W)} \times 100\%$	WWR (2windows)	WFR $\frac{(a \times b)}{(H \cdot L)} \times 100\%$
1	Ahead Opening	1.5	0.3	2.6	2.85	6%	12%	8%
2		1.5	0.5	2.6	2.85	10%	20%	14%
3		1.5	0.8	2.6	2.85	16%	32%	22%
4		1.5	1.05	2.6	2.80	21%	43%	29%
5	Top Opening	1.5	0.3	2.6	2.85	6%	12%	8%
6		1.5	0.5	2.6	2.85	10%	20%	14%
7		1.5	0.8	2.6	2.85	16%	32%	22%
8		1.5	1.05	2.6	2.80	21%	43%	29%
9	Bottom Opening	1.5	0.3	2.6	2.85	6%	12%	8%
10		1.5	0.5	2.6	2.85	10%	20%	14%
11		1.5	0.8	2.6	2.85	16%	32%	22%
12		1.5	1.05	2.6	2.80	21%	43%	29%
13	Ahead Opening	2	0.4	2.6	2.85	11%	22%	15%
14		2	0.6	2.6	2.85	16%	32%	22%
15		2	0.8	2.6	2.85	22%	43%	30%
16		2	1.0	2.6	2.80	27%	54%	37%
17	Top Opening	2	0.4	2.6	2.85	11%	22%	15%
18		2	0.6	2.6	2.85	16%	32%	22%
19		2	0.8	2.6	2.85	22%	43%	30%
20		2	1.0	2.6	2.80	27%	54%	37%
21	Bottom Opening	2	0.4	2.6	2.85	11%	22%	15%
22		2	0.6	2.6	2.85	16%	32%	22%
23		2	0.8	2.6	2.85	22%	43%	30%
24		2	1.0	2.6	2.80	27%	54%	37%
25	Ahead Opening	2.5	0.5	2.6	2.85	17%	34%	23%
26		2.5	0.75	2.6	2.85	25%	51%	35%
27		2.5	1.0	2.6	2.85	34%	67%	46%
28		2.5	1.25	2.6	2.80	42%	84%	58%
29	Top Opening	2.5	0.5	2.6	2.85	17%	34%	23%
30		2.5	0.75	2.6	2.85	25%	51%	35%
31		2.5	1.0	2.6	2.85	34%	67%	46%
32		2.5	1.25	2.6	2.80	42%	84%	58%
33	Bottom Opening	2.5	0.5	2.6	2.85	17%	34%	23%
34		2.5	0.75	2.6	2.85	25%	51%	35%
35		2.5	1.0	2.6	2.85	34%	67%	46%
36		2.5	1.25	2.6	2.85	42%	84%	58%

Table 5.4 : Summary of various opening window configurations with dimension

Model-1 Ahead Open (H.W) 1.5 x 0.3	**Model-2** Top Open (H.W) 1.5 x 0.3	**Model-3** Bottom Open (H.W) 1.5 x 0.3	**Model-4** Ahead Open (H.W)1.5 x 0.5	**Model-5** Bottom Open (H.W)1.5 x 0.5	**Model-6** Ahead Opening (H.W)1.5 x 0.5
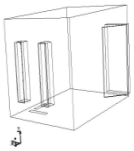	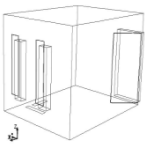	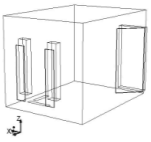	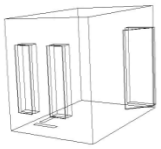	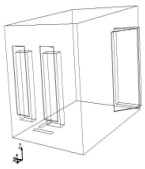	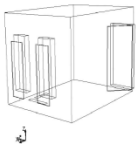
Model-7 Ahead Open (H.W) 1.5 x 0.8	**Model-8** Top Open (H.W) 1.5 x 0.8	**Model-9** Bottom Open (H.W) 1.5 x 0.8	**Model-10** Ahead Open (H.W)1.5 x 1.05	**Model-11** Top Open (H.W)1.5 x 1.05	**Model-12** Bottom Open (H.W)1.5 x 1.05
	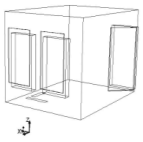	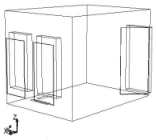	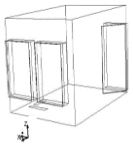	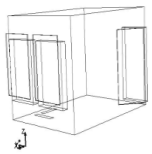	
Model-13 Ahead Open (H.W) 2 x 0.4	**Model-14** Top Open (H.W) 2 x 0.4	**Model-15** Bottom Open (H.W) 2 x 0.4	**Model-16** Ahead Open (H.W) 2 x 0.6	**Model-17** Top Open (H.W) 2 x 0.6	**Model-18** Bottom Open (H.W) 2 x 0.6
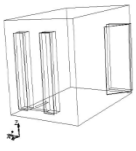	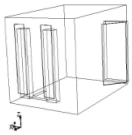	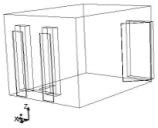	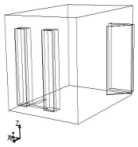	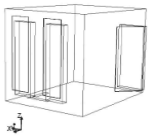	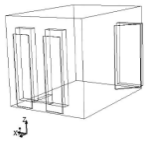
Model-19 Ahead Open (H.W) 2 x 0.8	**Model-20** Top Open (H.W) 2 x 0.8	**Model-21** Bottom Open (H.W) 2 x 0.8	**Model-22** Ahead Open (H.W) 2 x 1.0	**Model-23** Top Open (H.W) 2 x 1.0	**Model-24** Bottom Open (H.W) 2 x 1.0
			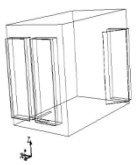	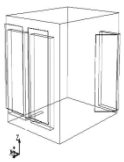	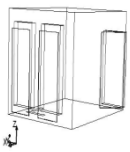
Model-25 Ahead Open (H.W) 2.5 x 0.5	**Model-**26 Top Open (H.W) 2.5 x 0.5	**Model-27** Bottom Open (H.W) 2.5 x 0.5	**Model-28** Ahead Open (H.W) 2.5 x 0.75	**Model-29** Top Open (H.W) 2.5 x 0.75	**Model-30** Bottom Open (H.W) 2.5 x 0.75
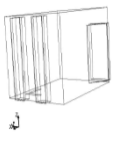		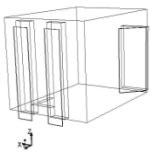		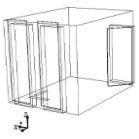	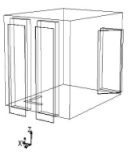
Model-31 Ahead Open (H.W) 2.5 x 1.0	**Model-32** Ahead Open (H.W) 2.5 x 1.0	**Model-33** Top Open (H.W) 2.5 x 1.0	**Model-34** Ahead Open (H.W) 2.5 x 1.25	**Model-35** Top Open (H.W) 2.5 x 1.25	**Model-36** Bottom Open (H.W) 2.5 x 1.25
	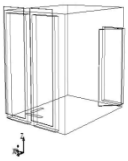	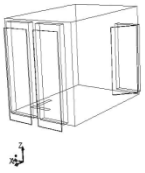	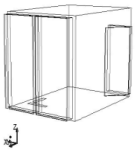	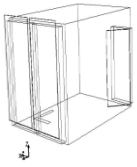	

5.3.2 Governing Equations

In completing CFD analysis for the whole shape of the office room and windows, setting up the governing equations (momentum, continuity and energy) is necessary. For the specific case of heat flux effect and fluid flow through the office, the governing equations are solved with assumptions. On the basis of these assumptions, the energy, momentum, and continuity equations for this study can be written as stated by Hung et al. (2012)

The continuity equation

$$\frac{\partial u}{\partial x} + \frac{\partial v}{\partial y} + \frac{\partial w}{\partial z} = 0 \tag{5.2}$$

The X-momentum equation:

$$\rho\left(u\,\frac{\partial u}{\partial x} + v\,\frac{\partial u}{\partial y} + w\,\frac{\partial u}{\partial z}\right) = -\frac{dp}{dx} + \mu\left(\frac{\partial^2 u}{\partial x^2} + \frac{\partial^2 u}{\partial y^2} + \frac{\partial^2 u}{\partial z^2}\right) \tag{5.3}$$

The Y-momentum equation:

$$\rho\left(u\,\frac{\partial v}{\partial x} + v\,\frac{\partial v}{\partial y} + w\,\frac{\partial v}{\partial z}\right) = -\frac{\mathrm{dp}}{\mathrm{dy}} + \mu\left(\frac{\partial^2 v}{\partial x^2} + \frac{\partial^2 v}{\partial y^2} + \frac{\partial^2 v}{\partial z^2}\right) \tag{5.4}$$

The Z-momentum equation:

$$\rho\left(u\,\frac{\partial w}{\partial x} + v\,\frac{\partial w}{\partial y} + w\,\frac{\partial w}{\partial z}\right) = -\frac{dp}{dx} + \mu\left(\frac{\partial^2 w}{\partial x^2} + \frac{\partial^2 w}{\partial y^2} + \frac{\partial^2 w}{\partial z^2}\right) \tag{5.5}$$

The energy equation:

$$\rho \mathrm{C}_{p.}\left(u\,\frac{\partial T_f}{\partial x} + v\,\frac{\partial T_f}{\partial y} + w\,\frac{\partial T}{\partial z}\right) = k\left(\frac{\partial^2 T}{\partial x^2} + \frac{\partial^2 T}{\partial y^2} + \frac{\partial^2 T}{\partial z^2}\right) \tag{5.6}$$

ρ_f effective density
$\mathrm{c}_{p.f}$ heat capacity
μ_f dynamic viscosity
k_f thermal conductivity
T_f temperature of coolant (℃)

5.3.3 Code validation

The code validation of this thesis depends on two experimental works, namely, Dahlan et al. (2011) and Wang Liping et al. (2007). These papers were chosen because of the authors' interest in natural ventilation of buildings and because of their similarity to the current study. All the code validation papers investigated the fluid flow and heat transfer characteristics in a rectangular room for an optimal

window model that was obtained from 36 models. The results and discussion of the numerical model show the code validation for the different temperature and air velocity flow profiles between outdoor and indoor conditions.

5.3.4 Boundary Conditions of the CFD Model

To represent the effect of boundary conditions, the surrounding environment was represented by the computational domain. The geometry used in the computations is shown in Figure 5.2 and Table 5.5, and is set equal to the experimental data. The inlet values of the air velocities and air temperature are set equal to the experimental conditions at solar time 1:20 pm. The average temperature is determined to represent the actual temperatures of a typical office, and the irradiation model is calculated by the CFD. Temperature from the person was assumed 310 K; the heat flux was taken as 68 W/ m^2 for the seated person, ASHRAE (2012). The heat flux by the computer and monitor is set to 75 and 10 W, respectively, ASHRAE (2012). The surface temperature of the glazed windows that face the front of the office was between 304 and 305.9 K. The internal side walls were set at 300 K and the floor and ceiling were measured at 300 and 299 K respectively. The door, chairs, and table were assumed to be adiabatic, Hajdukiewicz (2013). The emissivity and diffuse fraction of all surfaces inside the office were assumed to be 0.9 and 1.0, respectively (FLUENT 6.3 User's Guide).

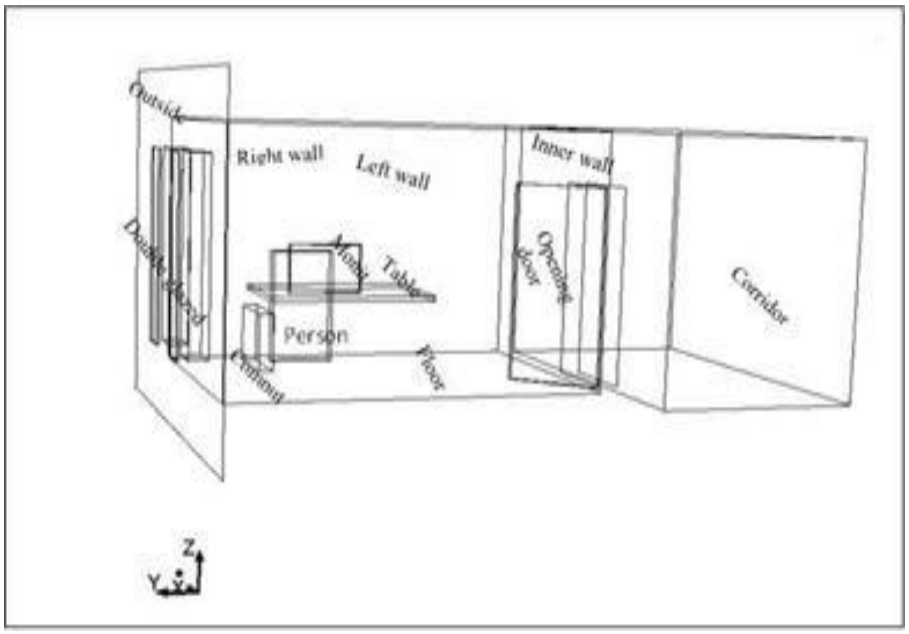

Figure 5.2 : Boundary conditions of the model.

Table 5.5 : Boundary conditions for the CFD model

Boundary	Type	Heat transfer	Mass & momentum	Radiation
Window gap	Inlet	T_o = 307.6 (K)	V_x=0.67 (m/s) V_y=0.74 (m/s)	
Outdoor	Outlet (opening)	T_o = 307.6 (K)	$P_{relative}$ = 0	ε = 0.9 DF = 1.0
External double glazed windows	Wall	T_{wall} = 304 (K)		ε = 0.9 DF = 1.0
internal double glazed windows	Wall	T_{wall} = 305.9 (K)		ε = 0.9 DF = 1.0
Internal sides walls	Wall	T_{wall} =298 K		ε = 0.9 DF = 1.0
Face wall (north)	Wall	Heat flux = 20W		ε = 0.9 DF = 1.0
Ceiling	Wall	T_{wall} = 298 K		ε = 0.9 DF = 1.0
Floor	Wall	T_{wall} =300 K		ε = 0.9 DF = 1.0
People sitting	Wall	generate heat = 68 W/m^2 T=310 K		ε = 0.9 DF = 1.0
Computer + Monitor	Wall	Heat flux =75w +10W		ε = 0.9 DF = 1.0
Tables, chairs	Wall	Adiabatic		ε = 0.9 DF = 1.0

5.3.5 Computational Domain and Grid of CFD Model

The computational domain and grid are constructed at a reduced rate (1:100) to be exactly similar to the office, including window size and wind flow geometry. The size of the entire computational domain in the vertical and wind flow directions depend on the represented area and on the boundary conditions used by Frank et al. (2010) and Ramponi (2012). The dimensions of the domain are 3.85 × 2.80 × 2.60 m^3 (W × D × H), which correspond to 385 × 280 × 260 m^3 in full scale. The grid must be designed in such a manner that it does not introduce overly large errors. The finite volume method is widely used in commercial CFD software. Thus, the resolution of the grid should be sufficiently fine to capture important physical phenomena, such as shear layers and vortices with sufficient resolution (Frank et al. 2010).

Many different types of mesh are available. Mesh selection depends on the problem and the solver's capabilities. The advantage of using unstructured mesh is that it reduces the numerical errors and improves the consistency of cross-domain solutions. The numerical grid consists of approximately 39030 unstructured elements, and the hexahedron-type mesh is used for the six shapes of window, office walls, corridor, table, computer, and human, as shown in Figure 5.3. The total number of mesh cells for the new model of windows and office is 1033440; the number of faces is 2537270.

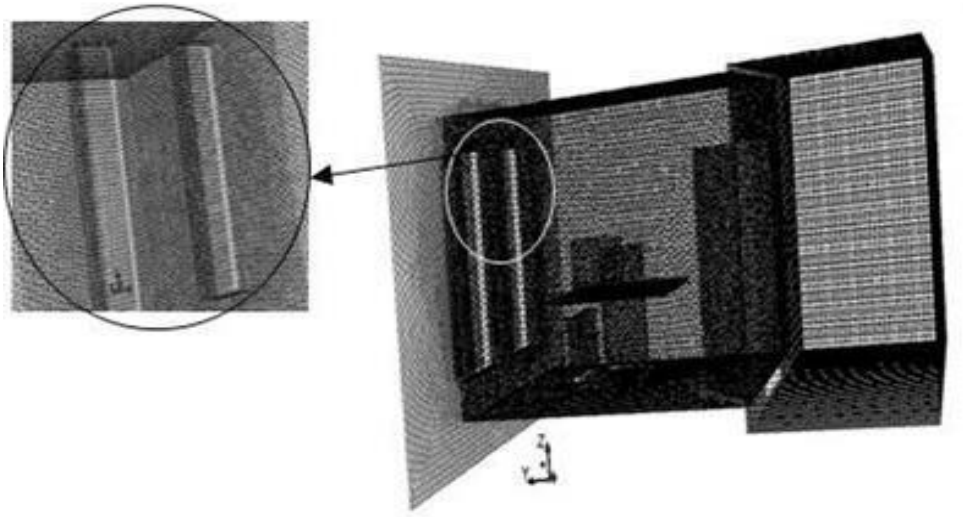

Figure 5.3 : Mesh of model window and office view

5.4 Model of CFD Process

The commercial CFD solver FLUENT V. 6.3 is used for modeling in this study. FLUENT allows the modeling of air flow and air temperature in complex geometries. With the software, we can complete the meshing with flexibility and solve flow problems with unstructured meshes that can be generated by complex geometries. The numerical techniques have been solved by using the momentum (Navier–Stokes), continuity, energy, and concentration equations for 3D analysis. Turbulent fluid flow was applied in CFD, the FLUENT 6.3 model, and the CFD model using the turbulence closure scheme RNG κ-ε and implemented in FLUENT, Stavrakakis (2008). The governing equations provide the steady-state conditions, and the general form was used and implemented based on Markatos et al. (1982). In each case, the simulation was performed in addition to the typical hour at 1:20 pm (the solar noon for Malaysia). The hottest day in August in the study year 2013 was selected for this study. The outdoor ambient temperature was $35\ ^{o}$C, air velocity was 0.67 m/s, and relative humidity was 63% on 22 August 2013 at 1:20 pm. The general procedure to solve any CFD problem is shown in Figure 3.6. The date and time of the simulation were August 22, 2013 at 1:20 pm, respectively. The simulation is set for internal and external conditions of the office, as shown in Table 5.6.

Table 5.6 : Internal and external conditions of the lecturer's office

Climate conditions	standard	Obtained
Latitude	3.0077 °N	MMD
Longitude	101.72 °E	MMD
Façade of building	North to 22^o East	MMD
Glazing type	22% transmittance	
Outdoor air speed	0.67 m/s	Measured
.Direction wind	70^o	MMD
Outdoor air temp	34.6^o (307.6 k)	Measured
Relative humidity	60%	Measured
Windows surface and walls side	assume	-

5.5 Physical properties of fluid

To conduct fluid simulation, the physical properties, such as specific heat, effective properties of density, viscosity, and thermal conductivity, were analyzed on the basis of mixing theory. Table 5.7 shows the physical properties of fluids and solids.

Table 5.7 : Physical properties of fluid and solid, Holman, J. P. (2002)

physical properties	Fluid	Solid
Cp (Specific Heat)	1006.43	871
Density (kg/m^3	1.225	2719
Thermal Conductivity (w/m k)	0.0242	202.4
Viscosity (kg/m-s)	1.7894e-05	-

5.6 Results and Discussion of the Numerical Model

The results obtained from 36 simulation runs were applied in CFD software and analyzed by using Microsoft Excel. The analysis of the numerical results and Microsoft Excel showed all the models for both air flow and indoor air temperatures within the office. The effects of window size were assessed with maximum temperature difference between models, and the effects of air flow were evaluated with maximum temperature difference with percentage of WWR and WFR. A reduced WWR for all 36 six models tested leads to a reduction in indoor air temperature and air flow within the office, as shown in Appendix E.

The effect of shading devices, such as double glazing on the test models, eliminates solar and conductive heat gains through the windows. The computational method can accurately predict air flow and air temperature within the office, which can be used to assess the effect of the window on indoor temperature. The windows are an important source of natural lighting with respect to WFR in the distribution of light within the office. Gutherie (1995) recommends a 10% to 25% WFR; thus, the chosen model in this study is suitable. Figure 5.4 illustrates the relationship between the

curves of the simulated static indoor air temperature, as well as air velocity results within the office with different window models. Peak temperature was 304.4^{o}K as shown in Model 43% and drop temperature was 300.8^{o} K, as shown in Model 22%.

Figure 5.5 illustrates the relationship between the curves of the average temperature difference and air velocity results within the office with different window models. The average difference in temperatures was between 3.2 and 6.8 K; the average air velocities within the office were 0.070 m/s to 0.11 m/s.

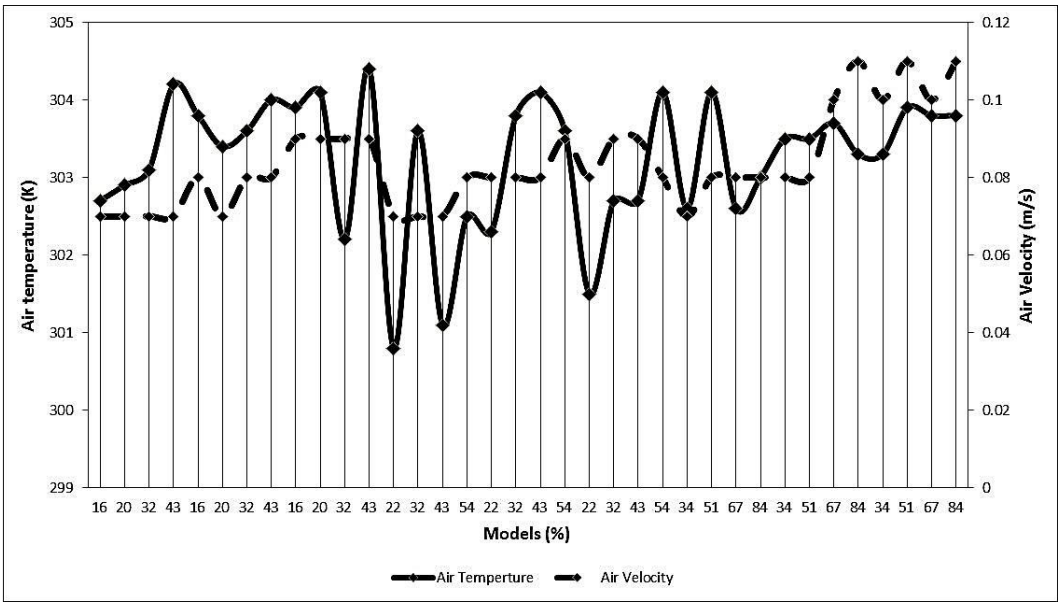

Figure 5.4 : Indoor temperature and air velocity of 36 models.

The peak average temperature difference in Model 22% was 6.8 K. Model 43% had a lower difference in temperature at 3.2 K. Average air velocities were 0.071 m/s to 0.087 m/s when the outdoor air temperature was 307.6 K and air velocity was 0.67 m/s.

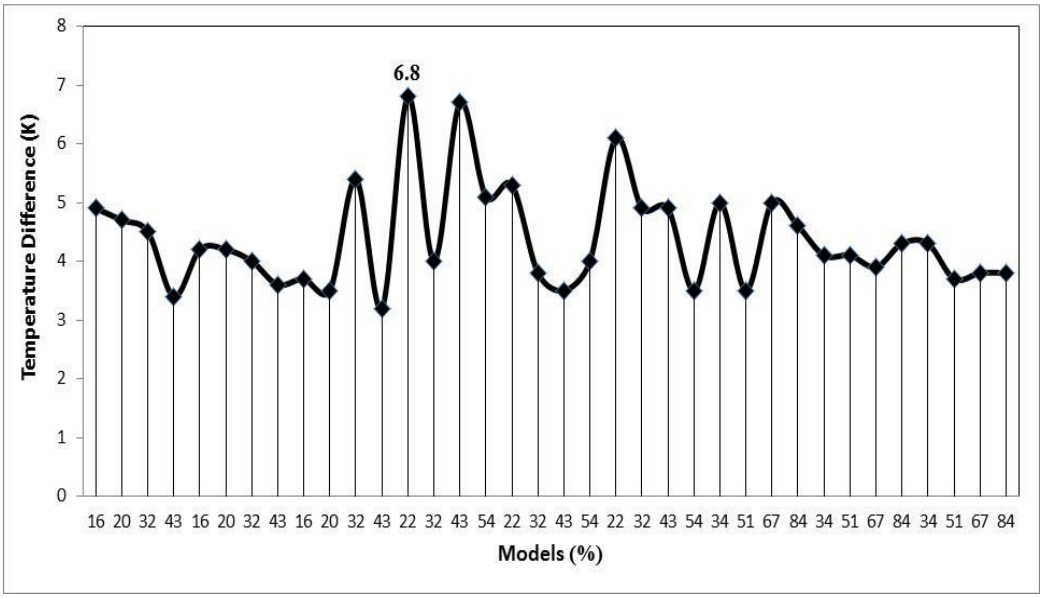

Figure 5.5 : Temperature differences of 36 models.

5.6.1 Selecting the Ideal Model Window in Warm-Humid Climates

The main parameter that affects the air velocity and air temperature within the office is window size, which is expressed as WWR in this study. Appendix E shows the temperature contours at the central xz, yz plane, and the velocity vectors at the yz plane for the twelve tested models of the 36 simulated models. Convergence was achieved with the RNG k–ε and the turbulence models. All twelve models were satisfactorily predicted in terms of the flow and type of layers of the fields of temperature. Figures 5.6 and 5.7 are displays the variation of average temperature and wind velocity respectively, inside the office with 12 different models with a window with three opening methods (ahead, top and bottom). The curves of air velocities within the office are almost the same for the 12 models window with three opening methods. The curves of air temperatures within the office increase depending on the size of the windows.

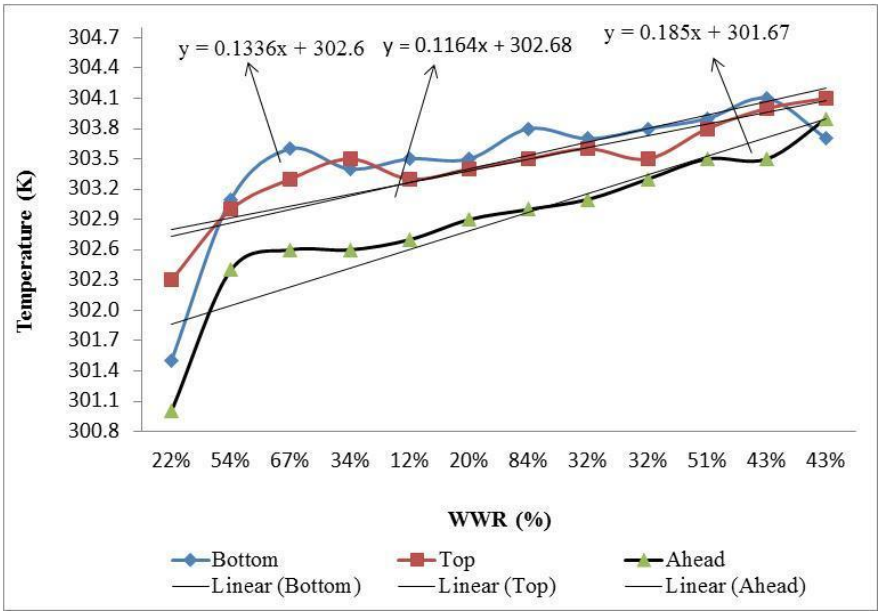

Figure 5.6 : Variation in air temperature according to window size

The developed model equations in Figures 5.6 and Figure 5.7 are calculated by f WWR= $f_{1=(T_i,e)}$ and$f_{1=(V,e)}$, (show Appendix H).

From WWR= $f_{1=(T_i,e)}$ and $f_{1=(V,e)}$ a generalized model such as $f_{1=(T,V,e)}$ and multiple equations of temperature and velocity are developed to obtain the equation (show Appendix H).

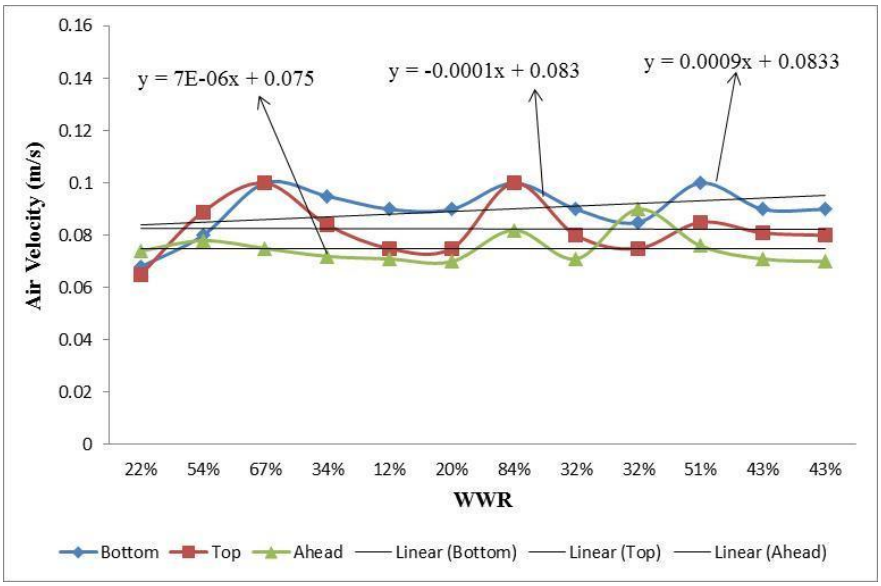

Figure 5.7 : Variation in air velocity according to window size

Figure 5.8 illustrates various average wind velocities and different temperatures between outdoors and indoors for seven models of WWR. The curves for temperature differences were from 4.9 K to 6.8 K. Of the nine models, the model with a WWR of 22% is the optimum. The average temperature difference was 6.8 K, and the average velocity was 0.070 m/s. The ratio of glazing area to floor area for daylighting was WFR 15%, as prescribed by Gutherie (1995), who evaluated the effect of WWR for different buildings and preferred a value between 17% and 22%.

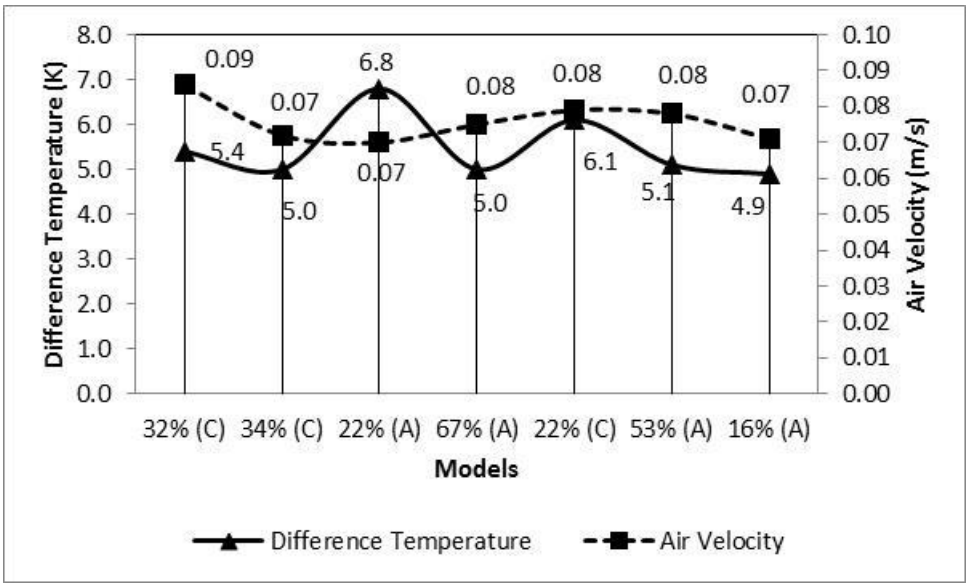

Figure 5.8 : Seven convergent models with differences in temperatures and velocities

Figure 5.9 illustrates the percentage curves of WWR and WFR for seven different models that were selected in this study. The model with WWR 20% and WFR 15% was the best model that provided a good temperature difference with sufficient daylighting in the test office.

Table 5.8 shows a summary of the results obtained from CFD and a comparison of results between models to obtain the best model. The distribution of average air temperature contours plot and average velocity for the plane YZ, as well as air temperature and air velocity at a height of (Z=1.5 m) from the floor and distances of 50 and 200 cm from the windows. The variations in temperature and air velocity from the window along horizontal plane y=50 cm and y=200 cm are between 300.8 K to 300 K. Air velocities are from 0.053 m/s to 0.078 m/s. The air temperature and air velocity of the vertical plane Z=1 m from the floor of the office are 302.3 and 0.36 m/s, respectively. The results from all three models that are presented in the table are close except for that from the model with WWR 22% and daylight WWF.

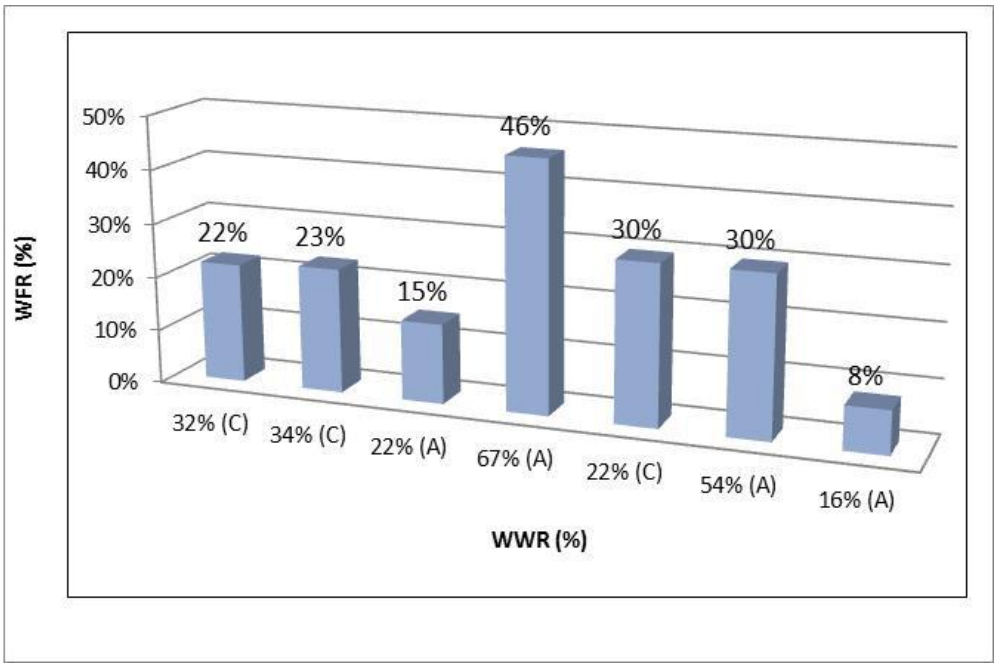

Figure 5.9 : Comparison between WWR and WFR of nine models.

Table 5.8 : Summary of results for WWR models

Models	Velocity			Temperature			Average P.	Average V.	Average T.	Δ T.
	Y=50 cm	Y=200 cm	Z= 1m	Y=50 cm	Y=200 cm	Z=1m				
Model (H.W) 2 x 0.4 (22%) C	0.078	0.075	0.29	299.8	301.5	302.7	0.0065	0.071	301.5	6.1
Model (H.W) 2x x 0.4 (22%) A	0.066	0.053	0.37	300.2	300.8	304.4	0.0044	0.070	300.8	6.8
Model (H.W) 2x 0.6 (32%) C	0.073	0.064	0.27	300.3	302.2	302.9	0.0044	0.073	302.2	5.4

Outdoor velocity=0.61m/s, Outdoor Temperature=307.6 K

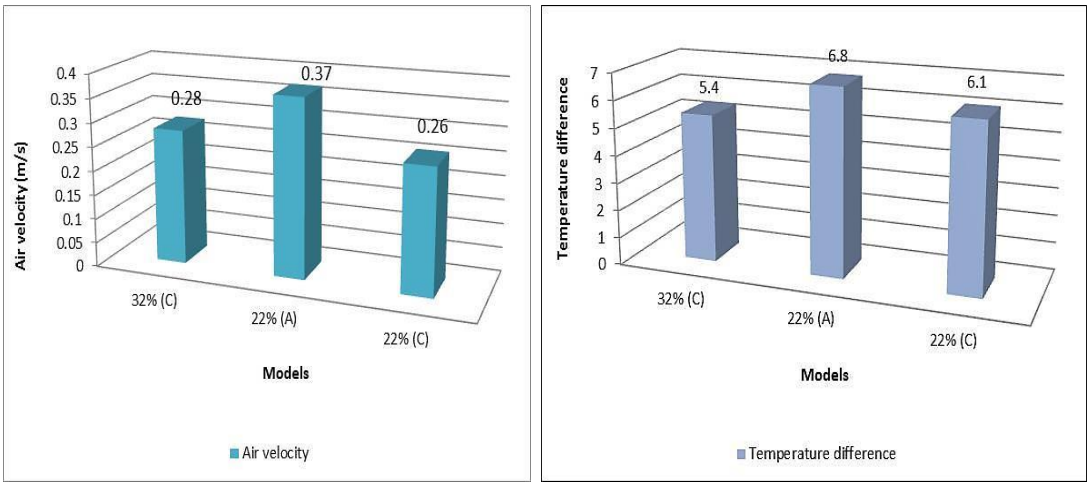

Figure 5.10 : Comparison of temperature difference and air velocity between models.

Figure 5.11 illustrate the trade-offs between air velocity, temperature difference, and lighting energy inside the office when three models are compared. The model with a WFR at 15% or less shows a relatively constant cooling energy and lighting energy that begins to rise steeply; this model can be applied in all climates.

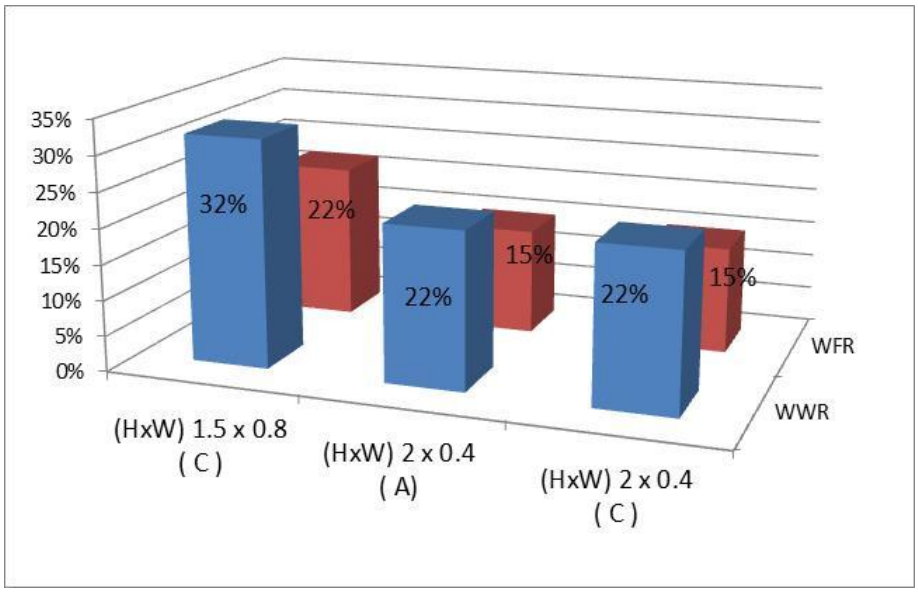

Figure 5.11 : Comparison of WWR and WFR between models

Figure 5.11 shows a new formula for WWR of 22% with an WFR of 15%. This model is superior to all other models in this study because it allows reduced air temperature in the office, decreased temperature difference, and increased airflow. The WFR in this model is an estimated 15%, which is adequate for Malaysia on the basis of Seyedehzahra et al. (2013).

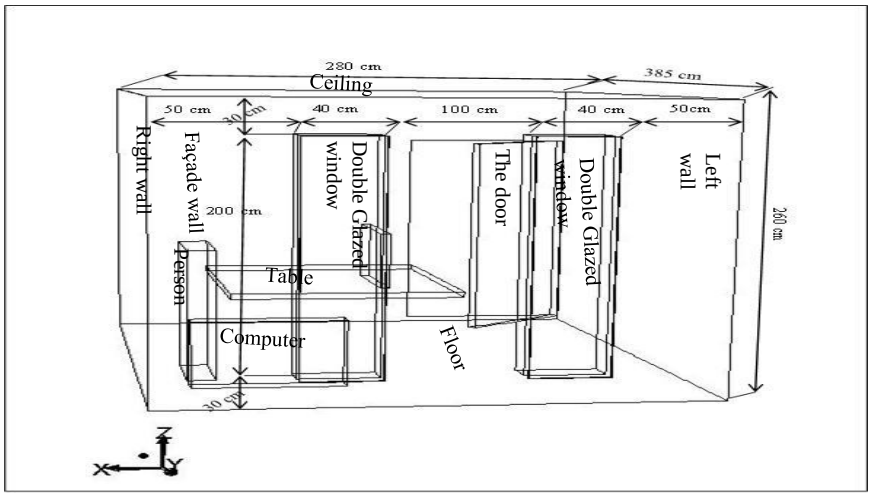

Figure 5.12 : Geometry of the model office room.

The CFD results within the office are presented in Table 5.9, and the temperature contours at the central xz, yz plane, and velocity vectors at yz plane are shown in Figure 5.12.

Table 5.9 : Summary of results for the best window model (Malaysia)

Models	Velocity			Temperature			Average P.	Average V.	Average T.	Δ T.
	Y=50 cm	Y=200 cm	Z= 1.5m	Y=50 cm	Y=200 cm	Z=1m				
Model 22%	0.066	0.053	0.070	300.2	300.1	304.4	0.0044	0.37	300.8	6.8

Outdoor velocity=0.67m/s, Outdoor Temperature=308K

The CFD results within the office for all 36 models are presented in Appendix F.

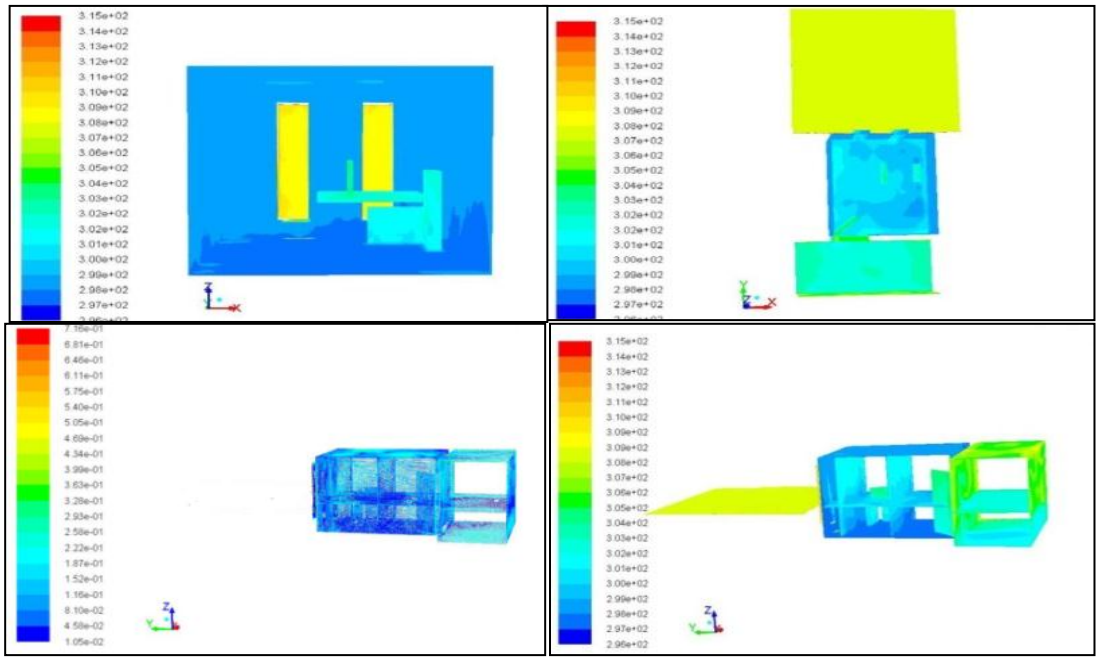

Figure 5.13 : Temperature contours at the central xyz, yx, yz, and velocity vectors.

5.7 Verification Optimum Model

On the basis of the above optimization models, CFD simulations are performed to verify the accuracy of the model. For validation, the optimal model is validated with experimental and simulation results of the reference office. Figure 5.13 shows the comparison of the results of Model 22% with the experimental and simulated CFD results.

Figure 5.14 shows a verification of Model 22% with previous studies by Dahlan et al. (2011) and Wang Liping et al. (2007). The curves show a vast temperature difference because of the differences in the size of window openings in terms of WWR, as well as those in the air flow velocity indoors.

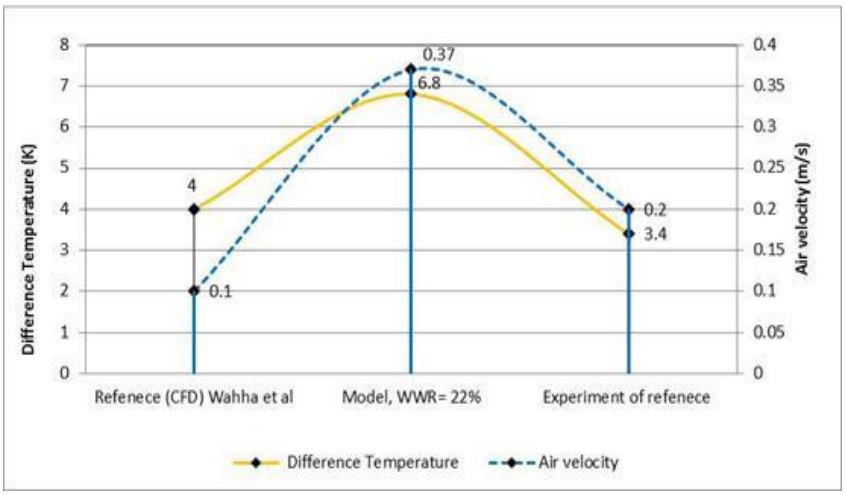

Figure 5.14 : Comparison of Model 22% with experimental work and CFD results.

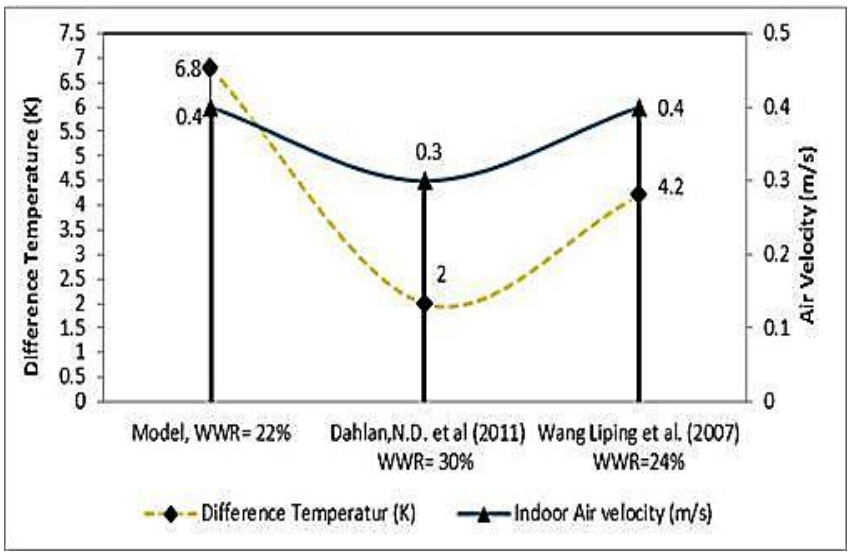

Figure 5.15 : Comparison of Model 22% with experiments in previous studies.

5.7.1 Selecting the Ideal Window Model in Hot–Dry Climate (Libya)

Figure 5.15 shows the schematic design of the Libyan test office. Its interior dimensions are 4.50 m × 3.80 m × 3.20 m (length × width × height), and its WWR is 22%. The results of the Libyan window models are shown in Table 5.10.

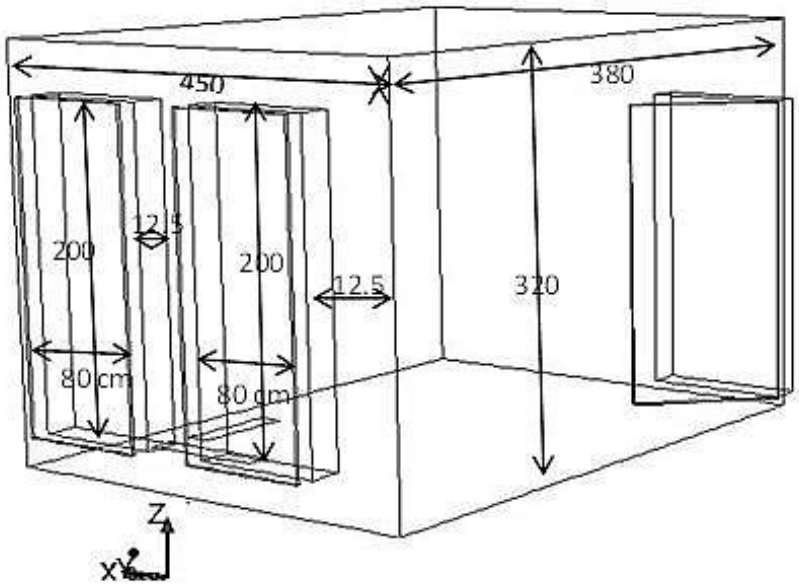

Figure 5.16 : Double-glazed window models in Libya (WWR 20%).

Figure 5.18 shows the temperature difference between the 12 best models. The peak temperature difference was 6.7 ℃ in the model WWR 22% (A). The results for the best Libyan model, WWR 22% (A) are shown in Table 5.11.

Table 5.10 : Summary of results for WWR models

Open method	Size of Window	WWR	Input Parameters		Output Parameters	
			Outdoor Temperature	Outdoor Wind speed (m/s)	Indoor Temperature	Difference Temperature
Ahead (A)	1.5 x 0.7	15%	307.5	6	302.7	4.8
Top (B)	1.5 x 0.7	15%	307.5	6	303.4	4.1
Bottom (C)	1.5 x 0.7	15%	307.5	6	303.9	3.6
Ahead (A)	2 x 0.8	22%	307.5	6	300.8	6.7
Top (B)	2 x 0.8	22%	307.5	6	302.3	5.2
Bottom (C)	2 x 0.8	22%	307.5	6	301.5	6.0
Ahead (A)	2.5 x 0.6	20%	307.5	6	302.9	4.6
Top (B)	2.5 x 0.6	20%	307.5	6	303.4	4.1
Bottom (C)	2.5 x 0.6	20%	307.5	6	304.1	3.4
Ahead (A)	2.5 x 0.9	31%	307.5	6	303.1	4.4
Top (B)	2.5 x 0.9	31%	307.5	6	303.6	3.9
Bottom (C)	2.5 x 0.9	31%	307.5	6	302.2	5.3

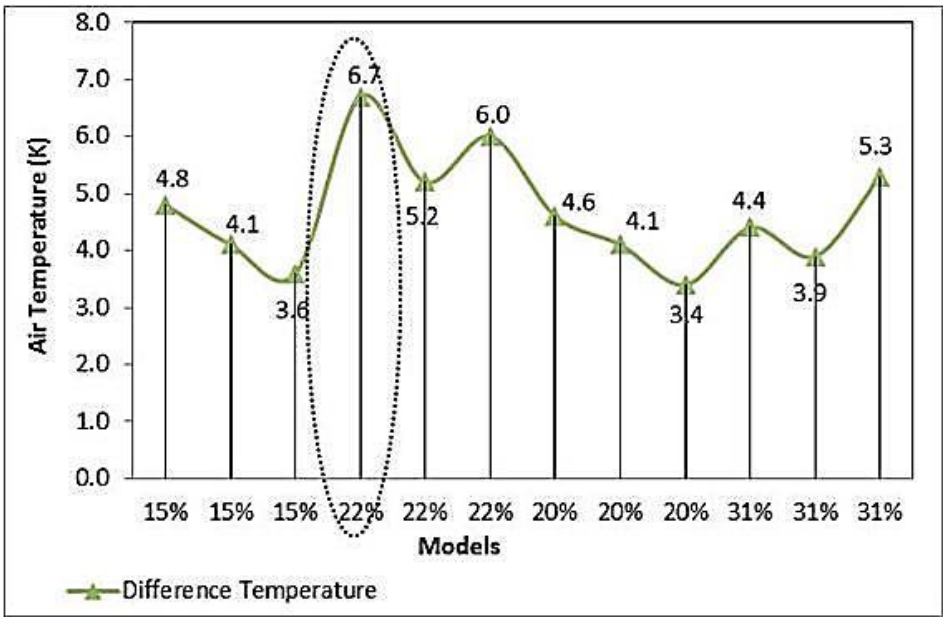

Figure 5.17 : Temperature difference between models.

Table 5.11 : Summary of results for the best window model (Libya)

Models WWR	Velocity			Temperature			Average P.	Average V.	Average T.	Δ T.
	Y=50 cm	Y=200 cm	Z= 1.5m	Y=50 cm	Y=200 cm	Z=1m				
Model 22%	0.066	0.053	0.070	300.2	300.1	304.4	0.0044	0.47	301.1	6.7

The CFD results in the Libyan office are presented in Table 5.12. The temperature contours at the central xz, yz plane, and the velocity vectors at yz plane are shown in Figure 5.19.

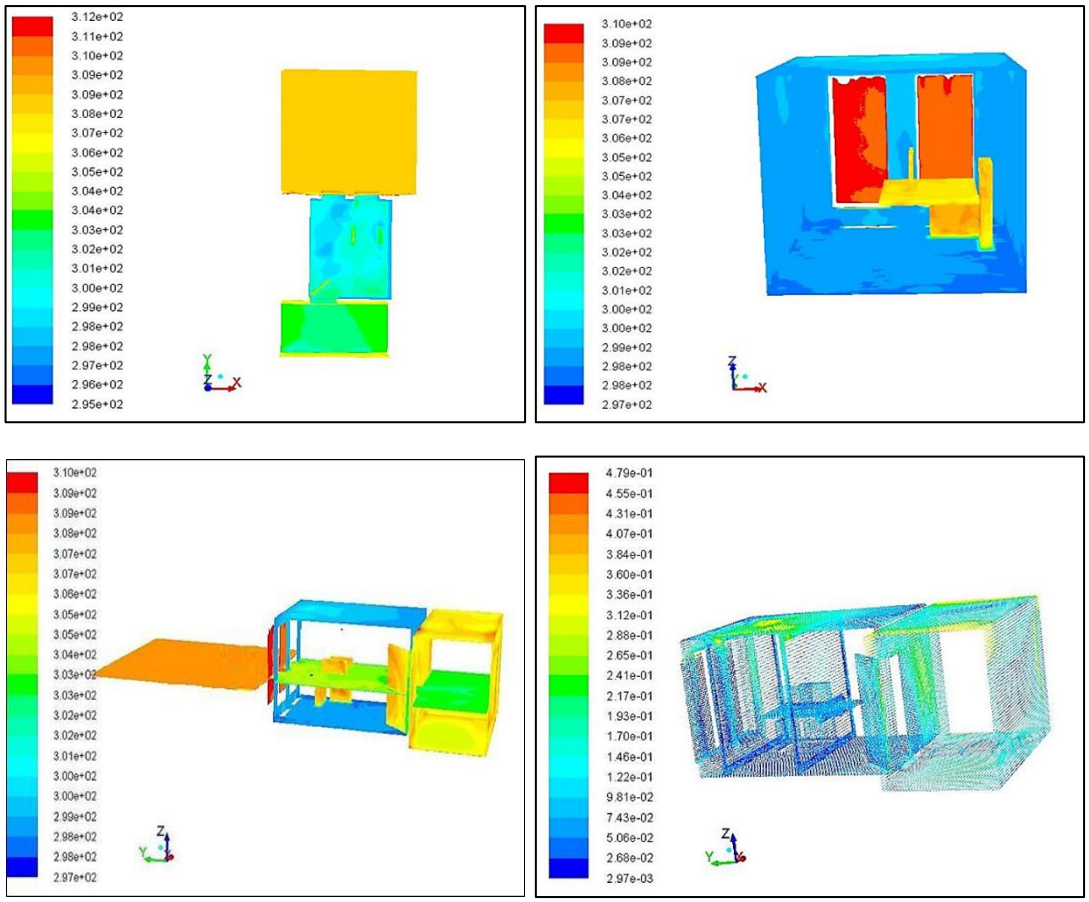

Figure 5.18 : Temperature contours at the central xz, yz, xyz, and velocity vectors at yz.

Table 5.12 shows a comparison between the Libyan and Malaysian models with WWR 22% in terms of building location and outdoor parameters.

Table 5.12 : Location buildings and outdoor parameters

Climate	Location of building	Ambient Temperature	Wind speed	Relative Humidity
Malaysia Model	North 20° East	307.6 K	5 m/s	60%
Libyan Model	North 22° East	307.8 K	6 m/s	43%

5.7.2 Comparison between Malaysian and Libyan Models

Table 5.13 and Figure 5.20 show a comparison between the Malaysian and Libyan models in terms of window dimensions and indoor parameters.

Table 5.13 : Comparison between Malaysia and Libyan models in terms of window WWR (22%)

Models	Dimensional window a x b	Dimensional wall H x W	WWR (%) $\frac{a.b}{H.W}$	WFR (%) $\frac{a.b}{\text{Floor area}}$	Indoor temperature K	Average indoor velocity (m/s)	Difference Temperature
Malaysia Model	2 x 0.4	2.6 x 2.80	22%	15%	300.8	0.070	6.8
Libyan Model	2 x 0.8	3.20 x 4.50	22%	19%	301.1	0.080	6.7

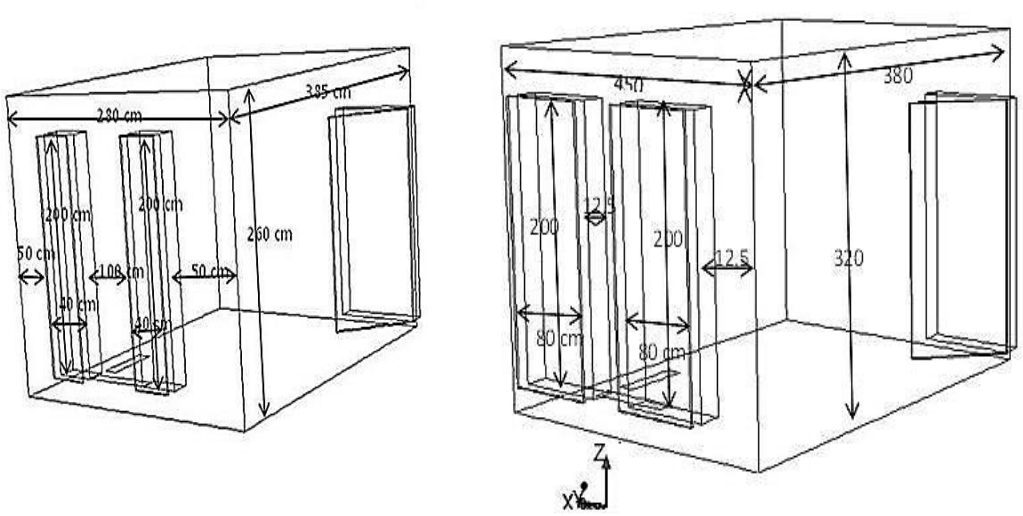

Malaysian Model

Libyan Model

Figure 5.19 : Comparison between Malaysian and Libyan models (WWR 22%).

Figures 5.21 and 5.22 show a comparison of indoor air temperature and temperature differences between the Libyan and Malaysian offices.

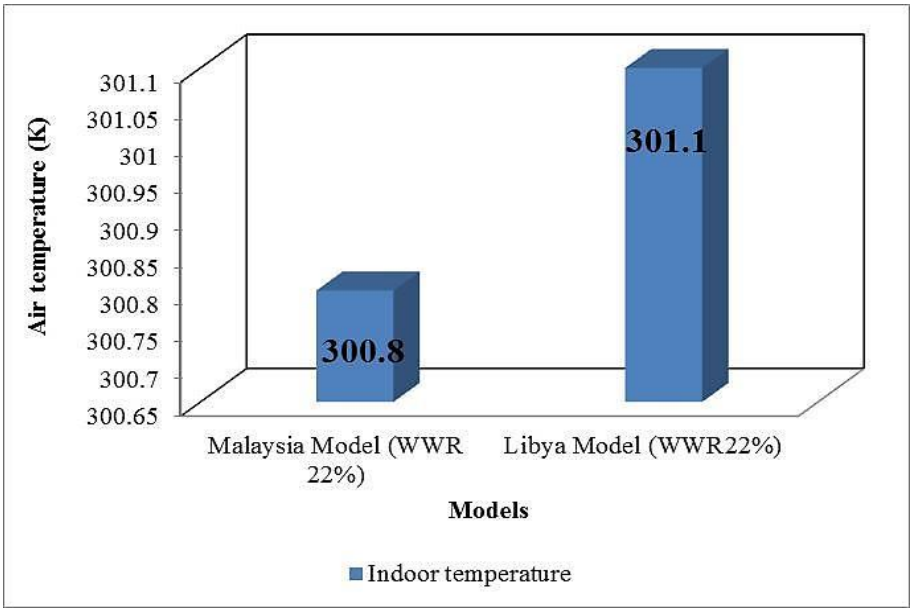

Figure 5.20 : Average indoor temperatures between models.

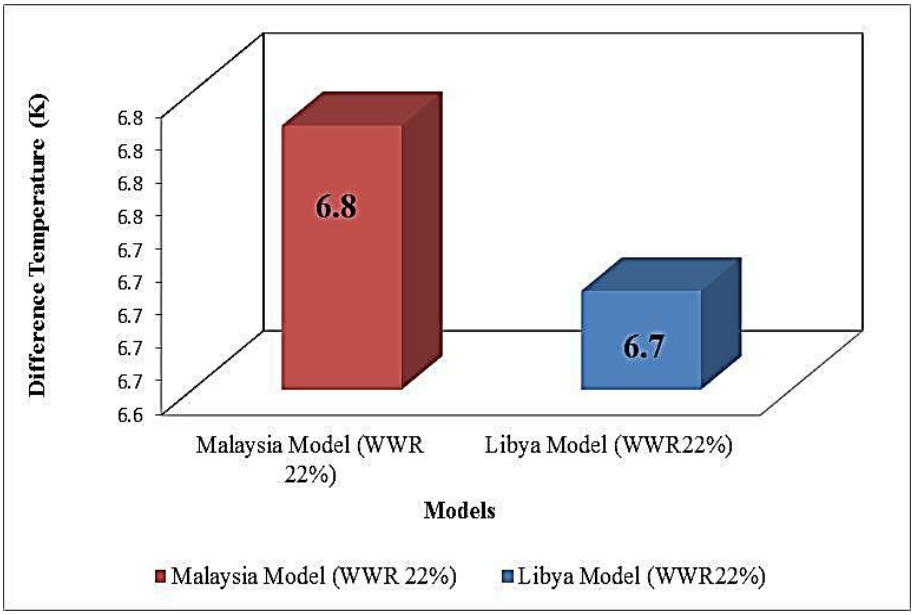

Figure 5.21 : Average temperature differences between models.

Figure 5.23 shows a comparison of indoor air velocity between the Libyan and Malaysian models.

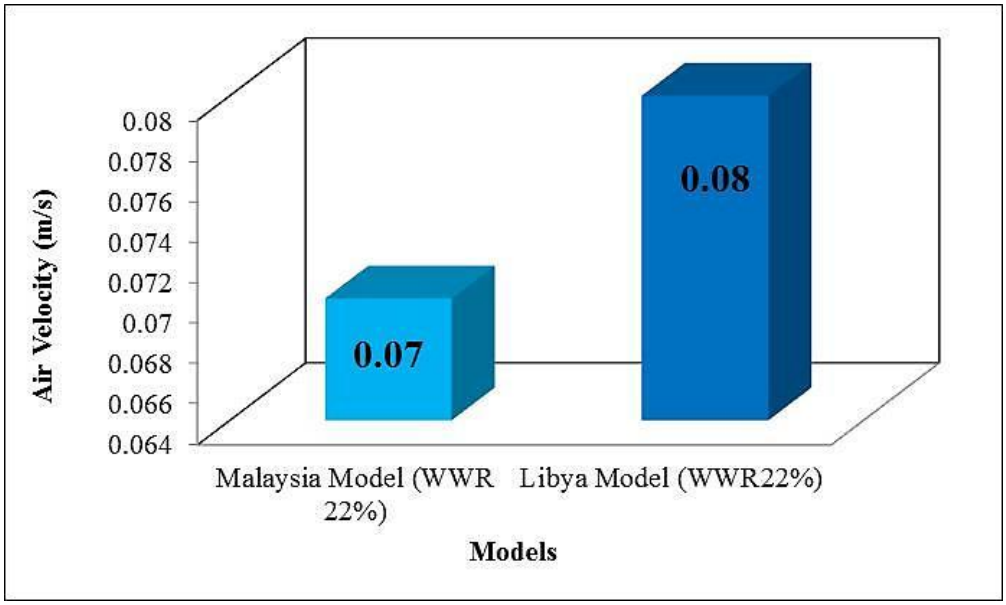

Figure 5.22 : Indoor air velocities between models.

CHAPTER 6

CONCLUSIONS AND RECOMMENDATIONS

6.1 Conclusions

This research is concerned with designing window size for the tropical hot wet climate under natural ventilation using computational fluid dynamics. The first objective of this thesis is to perform a double glazed window model design with the low E glazing windows and dimensions using CFD on data of Malaysia fieldwork. In this study, six models of 36 models have been chosen using CFD for the best suitable window size in the warm climate. Through this process, the result is a certain model with WWR value of 22% and WFR value of 15% in the size designed window for Malaysia with the corresponding dimensions of 2 m height and 0.4 m width. The temperature difference between outdoor and indoor office was 6.8 C and air velocity within office was 0.36 m/s at solar time in Malaysia 13:20 h. The predicted window size in Libya using the thirty- six models is model WWR value 22% and WFR value of 19%.

The second objective of this thesis is to predict pertinent parameters for thermal comfort inside building based on window size. The PMV and PPD are calculated inside the office using CBE Thermal Comfort Program software. A field measurements in naturally ventilated office in Malaysia found during solar noon time with WWR 22% size (high 2 m and width 0.4 m), a mean operative temperature of 27.8 C, mean RH of 56%, mean air velocity of 0.37 m/s, mean occupant clothing insulation level of 0.6 clo, and an average metabolic rate of 1.2 met. These conditions are within ASHRAE comfort zone.

The prediction in naturally ventilated office in Libya found during solar noon time with WWR 22% size (high 2 m and width 0.8 m), a mean operative temperature of 28.1 C, mean RH of 30%, mean air velocity of 0.47 m/s, mean occupant clothing insulation level of 0.6 clo, and an average metabolic rate of 1.2 met. The mean thermal comfort vote on a seven-point scale was observed to be +0.3, which was between neutral and Satisfied and able to remove the indoor pollution effectively. This condition is also within neutral comfort zone presented by ASHRAE (2012).

Determine parameters that must be considered for designing windows. The window to wall ratio (WWR) for minimizing heat transfer and the window to floor area ratio (WFR) for daylighting were the first selection criteria along with measured parameters of outdoor wind velocity, outdoor temperature, outdoor relative humidity, indoor air temperature, indoor air velocity, relative humidity and solar irradiation value.

The turbulent RANS (Reynold Average Navier Stokes) governing equations for RAG k-ε differencing was applied for the CFD work and hexahedron cell was chosen for Finite Volume Method.

The natural ventilation in the tropical region, such as Malaysia, where the weather is warm with high relative humidity. This study illustrates the types of windows used in Malaysia and their properties and the characteristics of the ideal window. The field study has been evaluated in the Department of Aerospace Engineering at Universiti Putra Malaysia (UPM) as reference office. The parameters experiments were airflow velocity within the office and temperature difference. The experimental results were measured and compared with simulated results.

6.2 Recommendations

This study has given way to other studies that occurs, and discuss improvements the air flow and reducing the temperatures within the buildings. The following recommendations could be made for future work:

1. Conduct experiments using the proposed optimum window design in actual building
2. Compare model of double glazed window with single glazed window using numerical analysis.
3. The authors Pérez et al. (2005), Manz, H (2004) and Hamza (2008) recommend the use glazed with high properties such as low-e coating, for the glazed areas of the offices which facing double glazed window. The double glazed window minimize heat in cavity and low-e reduces the radiative the heat from double glazed window, while Silvana et al (2015) showed that well-designed double glazed window can reduce the summer energy consumption of buildings, even using West double glazed facade in sunny climates.

REFERENCES

Abdul Rahman AM., Ismail 2008. Future design in an energy efficient building as an identity of a Malaysian tropical architecture with emphasis on photovoltaic technology and passive solar building design elements: Project report, USM, pp. 440-449

Abdul Majid Ismail, Prospect of Wind-Driven Natural Ventilation in Tall Buildings.

Adel Akair / László Bánhidi, Thermal comfort investigation in Libya, Mechanical Engineering, 51/1 (2007) 45–51 http://www.hbp.usm.my/ventilation/winddesign.htm

Ansys, Ansys, Inc., 2012. [Online]. Available: http://www.ansys.com.

ASHRAE Standard 55-2004, American Society of Heating, Refrigerating, and Air Conditioning Engineers, April 16, 2004, pp. 4–5.

ASHRAE, 2004. ANSI/ASHRAE Standard 55-2004: Thermal Environmental Conditions for Human Occupancy. Atlanta, 2004.

Ahmed, A. Rizka, and Gregor, P. Henze (2010). Improved airflow around multiple rows of buildings in hot arid climates, Energy and Buildings 42 (2010): 1711–1718.

Allocca, C., Chen, Q., and Glicksman, L. R. 2003. Design analysis of single-sided natural ventilation. Energy and Buildings, 35(8), 785-795.

Assem, E. O., Al-Mumin, A. A. 2010. Code compliance of fully glazed tall office buildings in hot climate, Energy and Buildings (42) PP.1100–1105.

Allard, F., Santamouris, M., Alvarez, S., Dascalaki, E., Guarracino, G., Maldonado, E., Sciuto, and S., Vandaele, L. (1998). Natural ventilation in buildings - a design handbook. London: James and James (Science Publishers).

Anastasia, D., Stavridou, Panagiotis, E., Prinos 2013. Natural ventilation of buildings due to buoyancy assisted by wind: Investigating cross ventilation with computational and laboratory simulation. Building and Environment 66: PP 104-119.

Standard ANSI/ASHRAE 55 (2004). Thermal environment conditions for human occupancy Atlanta.

Awbi, H. B. (1996). Air movement in naturally-ventilated buildings, Renewable Energy: 241-247.

Ardalan, A., Norhayati, M., Zakaria, A., Cheikh, M., Mohamad, B. (2015). A review on natural ventilation applications through building facade components and

ventilation openings in tropical climates. Energy and Buildings 101: 153–162

Ayad Samir S. (1999). Computational study of natural ventilation. Journal of Wind Engineering and Industrial Aerodynamics 82: 49-68.

ASHRAE. Handbook of fundamentals. Atlanta, USA: American Society ofHeating, Refrigerating, and Air-Conditioning Engineers; 2013.

Bangaleea, M. Z.I., Lina, S.Y., Miaua, J. J. (2012). Wind driven natural ventilationBuildings 45: 317–32.

Binggeli, C., 2003. Building Systems for Interior Designers. 1st Edn. John Wiley and Sons Inc., New Jersey, ISBN: 0-471-41733-5, pp: 452.

BBin Su Building Environmental Design, bsu@unitec.ac.nz, (accepted 2014)

Building Envelope Design Guide – Windows (WBDG). National Institute of Buliding Sciences. https://www.wbdg.org/design/env_fenestration_win.php Carmody, J., Selkowi, S., Bariush Arasten and Heschong, L. 2000. Residential Windows. A Guide to New Technologies and EnergyPerformance, 2nd Edition, Norton, New York.

Christine, W., Gang, T., Leon, G. (2011). Reduced-scale building model and numerical investigations to buoyancy-driven natural ventilation Original Research Article Energy and Buildings, Volume 43, Issue 9: 2404-2413

Chapter APTER 3, Window design for day lighting, ventilation and to reduce solar heat gains, accepted 2013.

Chen Q. Comparison of different k –ε models for indoor air flow computations. Numerical Heat Transfer 1995; 28 (Part B):353-69.

Chen Q. Prediction of room air motion by Reynolds-stress models. Building and Environment 1996;31(3):233–44.

Commercial Buildings Energy Consumption Survey (CBECS) (1995), U.S. Energy Information Administration, (accepted 2013)

CBE Thermal Comfort Tool ASHRAE-55, Berkeley University of California Berkeley http://comfort.cbe.berkeley.edu/

Dahlan, N.D., Jones, P.J., Alexande, D. (2011). Operative temperature and thermal sensation assessments in non-air-conditioned multi-storey hostels in Malaysia Original Research Article Building and Environment, Volume 46, Issue 2: 457-467

Durrani, S. M. A., et al., (2004). Dielectric/Ag/dielectric coated energy-efficient glass windows for warm climates, Energy and Buildings, 36 (9): 891-898.

Dascalaki, E., Santamouris, M., Argiriou, A., Helmis, C., Asimakopoulos, N., Papadopoulos, K., Soilemes, A. (1995). Predicting single sided natural ventilation rates in buildings, Solar Energy 55: 327–341.

EN ISO 7730. Moderate thermal environments – Determination of the PMV and PPD ˇ indices and specification of the conditions for thermal comfort, Prague, 1997

El-Agouz, S. A. (2008). The effect of internal heat source and opening locations on environmental natural ventilation, Energy and Buildings 40(4): 409-418.

Etzion, Y. and Erell, E. (2000). Controlling the Transmission of Radiant Energy Through Windows: a Novel Ventilated Reversible Glazing System, Journal of Building and Environment, 35: 433- 444.

Elisabeth Gratia and Andre De Herde (2004). Natural cooling strategies efficiency in an office building with a double-skin fa çade Energy and Buildings, Volume 36, Issue (11): 1139–1152.

Eftekhari, M. M. (1995). Single-sided natural ventilation measurements. Building Service Engineering Research Technology 16(4): 221–235.

Energy Information Administration, State Energy Data Report 1995, Tables 3.

Energy Efficiency and Renewable Energy Clearinghouse, U.S. Department of Energy 1997.

Franke, J., Hellsten, A., Heinke, E., Schlunzen, Bertrand C. (2010). The Best Practise Guideline for the CFD simulation of flows in the urban environment .The Fifth International Symposium on Computational Wind Engineering, North Carolina, USA: 23-27.

FLUENT Inc., FLUENT 6.3 User's Guide, 2006.

Ferziger, J. H. and Perić, M. (1999). Computational methods for fluid dynamics. Berlin etc: Springer, (Vol. 2).

Fanger P.O.(1972) Thermal comfort, analysis, and applications in environmental engineering. McGraw-Hill, New York.

Gutherie, P., (1995). The Architect's Portable Handbook: First Step Rules of Thumb for Building Design. Mc-Graw-Hill, New York.

Guohui, Gan (2000). Effective depth of fresh air distribution in rooms with single-sided natural ventilation. Energy and Buildings, Volume 31(1): 65-73.

Gan, G. 2010. Simulation of buoyancy-driven natural ventilation of buildings-impact of computational domain, Energy and Buildings 42:1 PP. 290-300.

Guohui, Gan. (2010). Interaction between Wind and Buoyancy Effects in Natural Ventilation of buildings Technology Journal 4:134-145.

Gebremedhin KG, Wu BX. Characterization of flow field in a ventilated space and simulation of heat exchange between cows and their environment. Journal of Thermal Biology 2003;28(4):301–19.

Hajdukiewicz, M., Geron, M., Keane, M. (2013). Formal calibration methodology for CFD models of naturally ventilated indoor environments. Building and Environment 59: 290-302.

Heiselberg, P. and Svidt, K. (2001). Characteristics of airflow from open windows. Building and Environment 36: 859-869.

Heiselberg, P. (2004). Natural ventilation design. International Journal of Ventilation, vol. 2, No. 4: 295-312.

Hassan, M. A. and Guirguis, N. M. (2007). Investigation of effects of window combinations on ventilation.

Holman, J. P. (2002). Heat Transfer. 9th Edition, Mc Graw Hill. New York

Jianhua Fan. An office model for indoor aiar flow simulation. Course lection note, Department of Civil Engineering, Technical University of Denmark 2010

Jiang, Yi Qingyan, Chen (2002). Wind direction on cross natural ventilation in buildings from large eddy simulation Building and Environment (37): 379 – 386.

Jong, T., de, and Bot, G. P. A. 1992. Flow characteristics of one-side-mounted windows, Energy and Buildings, 19 PP. 105-112.

James, O.P., Cheung, C., Ho, Liu. (2011). CFD simulations of natural ventilation behaviour in high-rise buildings in regular and staggered arrangements at various spacing, Energy and Buildings (43):1149–1158.

Jiang, b., Alexander, D., Jenkins, H., Arthur, R., Chen, Q. (2003). Natural ventilation in buildings: measurement in a wind tunnel and numerical simulation with Large Eddy Simulation, J. Wind Eng. Ind. Aerodyn. (91): 331–353.

Jong, T. and Bot, G. P. A. (1992). Flow characteristics of one-side-mounted windows. Energy and Buildings, 19: 105-112.

Jennifer, R., Gosselin, Q., Yan, Chen (2008). A computational method for calculating heat transfer and airflow through a dual-airflow window, Energy and Buildings (40): 452–458.

Joel H., Ferziger and Milovan Peric. (1999). Computational Methods for Fluid Dynamics. Springer-Verlag Berlin Heidelberg New York. ISBN 3-540-65373-2

James J Lo and Atila Novoselac. (2015). Localized air-conditioning with occupancy control in an open office 2014. Energy and Buildings 42: 1120–1128

Klote, J.H., (1991). A general routine for analysis of stack effect. National Institute of Standards and Technology, Report, United States Department of Commerce, Gaithersburg: 28.

Katunsky, Dusan Azra Korjenic, Jana Katunska, Martin Lopusniak, Sinan Korjenic, Saeed Doroudiani. (2013). Analysis of thermal energy demand and saving in industrial buildings: a case study in Slovakia Build Environ, 67: 138–146

Kamal Abdel Radi Ismail, Fátima Aparecida Morais Lino, Raquel da Cunha Ribeiro da Silva, Carlos T. Salinas. (2014). Models for Thermally Efficient Double Glass Windows, European International Journal of Science and Technology Vol. 3: No. 3

Malaysia Meteorological Department. (2013). General climate of Malaysia. Retrieved on August 22, 2013

Montazeri, H. and Blocken, B. (2013). CFD simulation of wind-induced pressure coefficients on buildings with and without balconies: Validation and sensitivity analysis, Building and Environment (60): 137-149.

Mokhtarzadeh, and Dehghan, M. R. (2011). Numerical simulation and comparison with experiment of natural convection between two floors of a building model via a stairwell Original Research Article. International Journal of Heat and Mass Transfer, Volume 54, (1–3): 19-33.

Montazeri, H., Blocken, B. (2013). CFD simulation of wind-induced pressure coefficients on buildings with and without balconies: Validation and sensitivity analysis, Building and Environment (60): 137-149

Nielsen V. P. Termisk Komfort ved brug af et ventilati on sloft – Widex domicil. Måling og simulering. 2009

Olufowobi, M.B. and Adenuga, O.A. (2012). Towards the Specification of Windows Sizes for Natural Ventilation in Classrooms in a Warn Climate, NIGERIA. Journal of Building Performance ISSN, Volume 3 Issue 1: 2180-2106.

Ooi, S., Badruddin, I.A., Zainal, Z.A., Narayana, A. (2007). Airflow analysis in an air conditioning room. Building and Environment, 42: 1531-1537.

Oesterle E, Lieb R, Lutz M, Heusler W. (2001). Double-skin facades-integrated planning. Munich: Prestel Verlag.

PHOENICS 3.2 (software package). London, UK: CHAM; 1999.

Papakonstantinou, K. A., Kiranoudis, C.T., N.C Markatos N.C. (2000). Numerical simulation of air flow field in single-sided ventilated buildings, Energy and BuildingsVolume 33: 41–48

Parsons, K. (2003) Human thermal environments: the effects of hot, moderate, and cold environments on human health, comfort, and performance, 2nd ed., London, Taylor, 527 p.

Mat Santamouris and Peter Wouters, 2006, Building Ventilation: The State of the Art. by (Editor)

Rajapaksha I. (2004). Passive Cooling in the Tropics: A Design Proposition for Natural Ventilation, The 21st Conference on Passive and Low Energy Architecture. Eindhoven, the Netherlands. University of Moratuwa, Moratuwa, Sri Lanka

Ramponi, R. and Blocken, B. (2012) CFD simulation of cross-ventilation flow for different isolated building configurations: Validation with wind tunnel measurements and analysis of physical and numerical diffusion effects, Journal of Wind Engineering and Industrial Aerodynamics, Volumes 104–106: 408-418.

Roetzel, A., Tsangrassoulis, D., Sabine, B. (2010). A review of occupant control on natural ventilation, Renewable and Sustainable Energy Reviews (14): 1001–1013.

Rouaud O, Havet M. Computation of the airflow in a pilot scale clean room using k–ε turbulence models. International Journal of Refrigeration 2002;25(3):351–61.

Rahman AMA. (1995). Housing design in relation to environmental comfort (2005) Buil Res Inform; 23(1): 49-54.

Slah Driss, Zied Driss and Imen Kallel Kammoun (2016) Computational study and experimental validation of the heat ventilation in a living room with a solar patio system. Volume 119, 1 May 2016, Pages 28–40, Energy and Buildings

Seyedehzahra Mirrahimi, Nik Lukman Nik Ibrahim, M. Surat (2013). Effect of daylighting on student health and performance. Computational Methods in science and Engineering. ISBN: 978-1-61804-174-6

Stern, F., Wilson, R.V., Coleman, H. W. and Paterson, E.F. Comprehensive approach to verification and validation of CFD simulations - part 1: Methodology and procedures. Journal of Fluids Engineering, 123:793–802, December 2001.

Sinha, S.L., Arora, R.C., Roy, Subhransu (2002). Numerical prediction of the laminar two dimensional room air flows with and without buoyancy. Fluid Mechanics and Fluid Power: 563–568.

Sarah L., Hara, O., Miche`le, Clarke, L., Mokhtar, S., Elatrash 2006. Field measurements of desert dust deposition in Libya, Atmospheric Environment, Volume 40, (21), PP. 3881-3897

Shafqat Hussain, Patrick H. Oosthuizen and Abdulrahim Kalendar, Evaluation of various turbulence models for the prediction of the airflow and temperature distributions in atria. Journal of Energy and Buildings, Volume 48, May 2012, Pages 18–28.

Siewa, C. C., Che-Anib, A. I., Tawilb, N. M., Abdullahb, N. A. G., Mohd-Tahirb, M. (2011). Classification of Natural Ventilation Strategies in Optimizing Energy Consumption in Malaysian Office Buildings. Procardia Engineering 20: 363-371. The 2nd International Building Control Conference

Stavrakakis, G. and Koukou, M. (2008). Natural cross-ventilation in buildings: building scal experiments, numerical simulation and thermal comfort evaluation, Energy and Buildings 40 (9): 1666–1681.

Selkowitz, S. (2004) Head of Building Technologies, Lawrence Berkeley National Laboratories, California, USA) – private communication

The, K., Li, S.L. (1996) Two-dimensional numerical study of airflow through large openings, Indoor Air; 1027-1032

Tahir, A., Ertuğrul Ç., Osman, Y. (2007). Adaptive neuro-fuzzy inference systems (ANFIS) application to investigate potential use of natural ventilation in new building designs in Turkey. Energy Conversion and Management Volume 48, Issue 5: 1472–1479

United States Environmental Protection Agency (1970). https://www.epa.gov/indoor. Founded: December 4.2016.

Wong, N. H., and Li, S. (2007). A study of the Effectiveness of Passive Climate Control in Naturally Ventilated Residential, Journal of Building and Environment 42: 1395-1405

Wang, Liping† and Wong Nyuk Hien. (2007) Applying Natural Ventilation for Thermal Comfort in Residential Buildings in Singapore, Architectural Science Review Volume 50 (3): 224-233.

Wong, P. C., Prasad, D., Behnia, M. (2008). New type of double-skin facade configuration for the hot and humid climate, Energy and Buildings (40): 1941–1945

Wong, N. H. and Li, S. (2007). A study of the effectiveness of passive climate control in naturally ventilated residential buildings in Singapore, Building and Environment 42: 1395–1405

Windows for High-performance in a building. http://www.commercial windows.org/wwr.php

Xam ána, J., P érez-Nucamendi, J., Hinojosa, J., Álvarez, G., Zavala-Guill éna. (2014). Thermal analysis for a double pane window with a solar control film for using in cold and warm climates. Energy and Buildings (76): 429–439.

Xiuzhang Fua , Dingxin Wuc (2015) Comparison of the efficiency of building hybrid ventilation systems with different thermal comfort models. Energy Procedia 78 (2015) 2820 – 2825

Yongsona, Ooi Irfan Anjum Badruddina, Zainala, Z.A., Aswatha Narayanab, P.A. (2007). Airflow analysis in an air conditioning room' Building and Environment 42: 1531–1537

Yang, L., Miao, Y., Bao-Jie h. (2014). CFD simulation research on residential indoor air quality. Science of the Total Environment 472: 1137–1144

Zain-Ahmed A. (2008). Integrating sustainable energy in buildings: a case study in Malaysia: in FAU conference 2008. Copenhagen Denmark: 78-91.

Zöllner, A., winter, E. F., Viskanta, R. (2002). Experimental studies of combined heat transfer in turbulent mixed convection fluid flows in double-skin-façades. International Journal of Heat and Mass Transfer 45: 4401

Vasanth, S., Tauseef, S.M., Tasneem Abbasi,. Abbasi, S.A (2013) Assessment of four turbulence models in simulation of large-scale pool fires in the presence of wind using computational fluid dynamics (CFD), Journal of Loss Prevention in the Process Industries, Volume 26, Issue 6, November 2013, Pages 1071–1084.

Window-to-wall ratio (WWR) Windows for High, http://www.commercialwindows org/wwr.php

APPENDICES

APPENDIX A

Outdoor environment parameters in 2009 (Source: Libyan Meteorological Department)

Year	Jan	FEB	Mar	Apr	May	Jun	Jul	Aug	Sep	Oct	Nov	Dec
Solar radiation	341	455	577	677	729	792	808	740	498	494	371	308
Humidity	47.2	41.7	36.6	30.3	27.9	27.5	30.3	32.3	35	38	40.1	45.1
Temperature	11.8	13.2	16.9	21.6	26.1	29.3	29.7	37	37	30	18.1	13.2
Velocity	4.6	5.0	5.2	5.5	5.7	5.3	5.1	5.0	5.0	4.9	4.5	4.5

Hourly Outdoor Variables for Typical Design in Southern Libya (Libyan meteorological Station) (15-August-2009)

Days	Air Dry Temperature	Air wet Temperature	Air velocity	humidity
1	29.8	18	5.1	31
2	29.6	18.2	5.4	36
3	30.2	19.2	4.5	37
4	30.7	15.8	5.8	28
5	31.3	16.5	4.6	21
6	30.6	21.0	8.9	31
7	28.8	19.6	8.3	45
8	28.9	19.5	8.3	43
9	28.7	18.5	9.0	42
10	27.5	19.5	6.4	49
11	28.6	19.2	5.8	45
12	30.1	20.2	7.8	38
13	30.2	20.1	9.8	33
14	29.6	19.5	7.0	43
15	32.1	20.5	5.3	30
16	32.9	21.8	9.0	32
17	31.6	19.6	8.5	33
18	30.2	21	10.1	38
19	28.6	20.2	7.9	47
20	28.1	19	3.5	47
21	29.8	19.9	7.0	37
22	28.2	18.2	12.1	42
23	27.5	20.3	7.3	46
24	28.0	17.5	2.5	43
25	29.6	17.1	7.0	34
26	29.4	18	7.1	33
27	28.8	18	5.4	36
28	29.2	18	4.6	35
29	29.7	18.2	9.3	41
30	31.4	19.5	9.1	30
31	32.9	18.6	6.9	26

Average Hourly Outdoor Variables for Typical Design Day in 15-August - 2009 in Southern Libya (Libyan meteorological Station)

Time	Air Dry Temperature (◦C)	Air wet Temperature(◦C)	Humidity (%)	Air Velocity (m/s)	Solar irradiation (W/m^2
9:00	32	21	32	0.22	299
12:00	38	25	33	0.43	350
15:00	39	22	18	5	209
18:00	37	23	25	5	134

Heat Transfer Coefficient and Heat Flux near Windows

Time	Heat transfer coeff. (outer surface) EXP	Heat transfer coeff. (inner surface) EXP.	Heat flux on the outer surfaces	Heat flux on the inner surfaces
9:00	1.76	1.79	20	20
12:00	2.16	2.20	48	49
15:00	1.97	2.02	33	34
18:00	1.98	1.78	33	20

APPENDIX B

Interior Temperature Measurements within office in Libyan work (15-August-2009)

Time	A.p1	A.p2	A.p3	A.p4	A.p5	A.p6	A.p7	A.p8	A.p9	A.p10	A.p11	A.p12
09:00	23.7	23.65	23.94	23.49	23.43	23.46	23.33	23.35	23.35	23.26	23.26	23.17
09:30	24.8	24.86	25.54	25.64	24.45	24.50	25.35	25.29	24.39	24.26	24.78	24.77
10:00	24.9	24.97	25.65	25.67	24.60	24.63	25.44	25.36	24.41	24.32	24.81	24.80
10:30	25.2	25.21	25.79	25.87	24.84	24.85	25.50	25.40	24.49	24.36	24.83	24.82
11:00	25.4	25.54	26.19	26.46	24.94	24.98	25.61	25.47	24.54	24.41	24.89	24.86
11:30	25.9	25.88	26.45	26.59	25.14	25.21	25.88	25.73	24.58	24.55	24.90	24.90
12:00	25.9	25.99	26.59	26.64	25.33	25.35	25.99	25.77	24.64	24.58	24.92	24.92
12:30	26.1	26.15	26.77	26.74	25.43	25.55	26.31	25.88	24.69	24.63	24.98	24.98
13:00	26.5	26.47	26.80	26.79	25.74	25.75	26.78	25.29	24.84	24.77	25.08	25.09
13:30	26.5	26.52	26.94	26.97	25.97	25.99	26.86	25.43	24.88	24.81	25.09	25.14
14:00	26.6	26.55	27.13	27.20	25.58	25.44	26.77	25.47	24.86	24.80	24.90	24.92
14:30	25.9	26.15	26.87	27.05	25.48	25.33	26.20	25.24	24.62	24.68	24.80	24.81
15:00	24.9	24.89	25.04	24.50	24.39	24.30	24.33	24.35	24.26	24.25	24.34	24.32
15:30	24.4	24.40	24.95	24.27	24.31	23.80	24.24	24.27	23.40	24.22	24.30	23.38
16:00	23.9	23.98	24.47	23.67	23.94	23.53	23.54	23.92	23.30	23.48	23.52	23.28
16:30	23.5	23.62	23.90	23.42	23.44	23.51	23.40	23.36	23.21	23.20	23.34	23.19
17:00	23.4	23.52	23.80	23.33	23.40	23.30	23.36	23.27	23.15	23.16	23.26	23.13
17:30	23.4	23.44	23.61	23.42	23.32	23.30	23.34	23.31	23.12	23.10	23.20	23.11
18:00	23.3	23.34	23.39	23.28	23.29	23.28	23.32	23.30	23.10	23.04	23.18	23.05

Average interior temperature in an office (All temperature ℃) (15-August-2009)

Time	A.p 1	A.p2	A.p3	A.p4	A.p5	A.p6	A.p7	A.p8	A.p9	A.p10	A.p11	A.p12	Ave
9:00	23.6	23.7	23.7	23.4	23.5	23.5	23.3	23.4	23.4	23.3	23.3	23.3	23.4
12:00	25.9	25.9	26.6	25.6	25.6	25.7	25.4	25.5	25.6	24.6	24.7	24.9	25.5
15:00	24.5	24.5	25.1	24.4	24.4	24.5	24.3	24.4	24.4	24.3	24.3	24.3	24.4
18:00	23.3	23.33	23.42	23.2	23.3	23.3	23.2	23.2	23.3	23.2	23.2	23.2	23.3

APPENDIX C

Average temperature of eight points above internal surface window in (℃) (15-August-2009)

Time	$W_{1-in.}$	$W_{2-in.}$	$W_{3-in.}$	$W_{4-in.}$	$W_{5-in.}$	$W_{6-in.}$	$W_{7-in.}$	$W_{8-in.}$	Average T. internal
9:00	24.51	24.36	24.54	24.35	24.62	24.58	24.92	24.81	25
12:00	28.67	28.19	28.77	28.18	28.90	28.95	28.71	28.51	29
15:00	27.50	27.09	27.26	27.09	27.16	27.54	27.19	27.40	27
18:00	25.22	25.41	25.57	25.51	25.42	25.46	25.04	25.33	25

Average temperature of eight points above external surface window (in ℃) (15-August-2009)

Time	W_{1-e}	W_{2-e}	W_{3-e}	W_{4-e}	W_{5-e}	W_{6-e}	W_{7-e}	W_{8-e}	Average T. external
9:00	33.1	34.4	34.5	34.4	34.3	34.6	35.4	34.8	34
12:00	41.7	41.2	42.8	42.2	41.9	43.0	42.0	42.6	42
15:00	40.8	42.6	42.3	42.4	42.2	44.3	42.7	42.3	42
18:00	39.3	40.5	40.7	40.5	40.4	41.8	39.3	38.2	40

Average Inner Surface Temperature, Outer Surface Temperature and Difference Temperature between Glasses (15-August-2009)

Time	inner surface temperature C	Solar irradiation (W/m^2	Outer surface Temperature C	Difference Temperature between glasses C
09:00	25	299	34	9
12:00	29	350	42	13
15:00	27	209	42	15
18:00	25	134	40	15

Average internal air temperature and ambient temperature and Difference Temperature (15-August-2009)

Time	Office Temperature	Ambit Temperature	Difference Temperature
9:00	23	32	9
12:00	26	38	12
15:00	24	39	15
18:00	23	37	14

Comparison of average distribution of interior temperature with distance from window (15-August-2009)

Average interior temperature (℃)	Distance (cm)
28.6	0.05
24.6	0.50
24.4	1.00
24.8	2.00

Comparison Between average distribution interior temperature with office height (15-August-2009)

Office height (cm)	Average Air Internal Temperature (℃)
200	24.3
100	24.6
0.50	24.7

Comparison Between Experimental and CFD Of Temperature Results

Time	EXP.	CFD
9:00	296	297
12:00	299	298
15:00	297	299
18:00	296	298

Comparison Between Experimental and CFD of inner Heat Transfer

Time	Heat transfer coeff.(inner surface) EXP.	Heat transfer coeff.(inner surface)CFD
9:00	1.79	1.15
12:00	2.20	2.27
15:00	2.02	1.12
18:00	1.78	1.24

Comparison of Experimental and CFD of Outer Heat Transfer

Time	Heat transfer coeff.(outer surface) EXP	Heat transfer coeff.(outer surface) CFD
9:00	1.76	1.74
12:00	2.16	2.61
15:00	1.97	1.70
18:00	1.98	1.59

Comparison of Experimental and CFD Results of Heat Transfer Flux

Time	Total heat Flux (EXP)	Total heat Flux (CFD)
9:00	3.5	4.6
12:00	8.6	6.9
15:00	5.9	5.5
18:00	5.9	3.5

APPENDIX D

The outdoor measurements results of Malaysia meteorological Station in year (2013)

Months of Year 2009	Solar globe radiation(KW/m^2)	Humidity (%)	Air Dry Temperature(o_C)	Air wet Temperature(o_C)	Velocity (m/s)
January	14.26	80.9	27.0	24.4	6.8
February	20.33	77.3	28.3	25.0	5.01
March	18.82	80.9	28.0	25.3	10.3
April	19.53	82.2	28.3	25.8	8.5
May	20.33	78.0	29.0	25.8	10.8
June	18.71	78.1	29.2	25.6	6.8
July	18.17	74.3	28.9	25.3	8.0
August	17.81	78.1	28.3	25.3	5.0
September	18.59	77.2	28.4	25.2	5.0
October	17.93	80.3	27.9	25.1	4.9
November	16.49	83.1	27.5	25.2	4.5
December	15.05	81.7	27.5	25.0	4.5

The outdoor measurements of Malaysia meteorological Station (August-2013)

Date of Day	humidity	Mean wet bulb temperature	Mean Dry bulb temperature	Date of Day	Direction	Air velocity
1	69.3	25.2	29.5	1	130	7.5
2	69.2	25.6	30	2	130	7.1
3	76.5	25.7	29.1	3	140	7.2
4	84.8	24.8	26.8	4	230	5.8
5	77.5	25.5	28.7	5	340	6.1
6	76.7	26	29.3	6	260	9.7
7	77.2	25.8	28.9	7	250	8.6
8	74.4	25.8	29.5	8	190	6.6
9	73.5	25.6	29.4	9	90	9.2
10	85.1	24.8	26.8	10	270	10
11	72.3	25.1	29.1	11	240	6.5
12	79	25.2	28.2	12	120	11.6
13	84.8	24.9	27.2	13	120	7.1
14	83.7	25.3	27.5	14	240	10.1
15	82.1	24.7	27.2	15	60	7.7
16	73.8	25.1	28.9	16	140	6
17	75.4	25.1	28.7	17	140	7.3
18	76.8	25.4	28.8	18	60	5.5
19	74	25.5	29.5	19	60	6.3
20	82.8	24.4	26.6	20	130	8.5
21	77.7	25.1	28.3	21	120	9
22	81.8	25.4	27.8	22	70	10.6
23	79.7	25	27.7	23	230	6
24	81	25.5	28.2	24	240	8.6
25	78.9	25.1	28	25	260	9.2
26	84.7	24.9	26.9	26	240	7.4
27	76.3	25.1	28.4	27	240	6.8
28	76.2	25.4	28.7	28	250	8.2
29	82.3	24.5	27	29	260	7
30	74.4	25.5	29.2	30	120	6.4
31	78.5	25.9	28.8	31	240	13.5

APPENDIX E

Measurement data

Indoor Measurements (3/August/2013)

Solar Time	Aver. Indoor Temperature (C)	Relative Humidity (%)	Wind speed (m/s)	Air Pressure
8:00	-	-	-	-
8:40	-	-	-	-
9:20	-	-	-	-
10:00	-	-	-	-
10:40	30.90	59%	0.43	0.01612
11:20	31.90	56%	0.13	0.04107
12:00	32.10	50%	0.14	0.01329
12:40	32.50	64%	0.15	0.01162
13:20	32.80	60%	0.15	0.03532
14:00	31.40	59%	0.13	0.02129
14:40	30.60	62%	0.1	0.01489
15:20	-	-	-	-
16:00	-	-	-	-
16:40	-	-	-	-

Measurement surfaces of windows 3-8-2013

Solar Time	**Glazed window (G-1)**	**Glazed wall (G2)**	**Glazed window (G-3)**
8:00			
8:40			
9:20			
10:00			
10:40	32.5	34.2	32.5
11:20	33.3	33.8	33.3
12:00	33.2	34.3	33.2
12:40	32.3	33.3	32.3
13:20	32.6	33.3	32.6
14:00	32	32.2	32
14:40	31	31.5	31
15:20			
16:00			
16:40			

Outdoor Measurements (3/ August/2013)

Solar Time	Ambient Temperature (C)	Wind speed (m/s)	Relative Humidity (%)	Solar Irradiance (W/m^2)
8:00	-	-	-	-
8:40	-	-	-	-
9:20	-	-	-	-
10:00	-	-	-	-
10:40	33	0.5	48%	407.7
11:20	33.4	0.3	46%	883.9
12:00	33.9	0.3	42%	620.3
12:40	34.3	0.3	41%	600.5
13:20	**35.7**	0.3	39%	544.6
14:00	34.6	0.3	41%	508.7
14:40	34.4	0.3	38%	667.1
15:20	-	-	-	-
16:00	-	-	-	-
16:40	-	-	-	-

Outdoor Measurements (4/August /2013)

Solar Time	Ambient Temperature (C)	Wind speed (m/s)	Relative Humidity (%)	Solar Irradiance (W/m^2)
8:00	26.0	0.83	84%	331.2
8:40	25.7	0.89	86%	439.5
9:20	26.8	0.93	82%	551.5
10:00	30.6	0.70	89%	756.6
10:40	33.1	0.73	78%	541.5
11:20	33.7	0.66	65%	640.1
12:00	34.4	0.4	69%	684.3
12:40	36.1	0.73	72%	675.2
13:20	34.8	0.69	66%	617.1
14:00	35.6	0.87	78%	491.4
14:40	34.0	0.84	78%	429.7
15:20	33.1	1.11	70%	443.6
16:00	32.7	0.	66%	538.8
16:40	29.1	0.69	72%	418.0

Indoor Measurements (4/ August/2013)

Solar Time	Aver. Indoor Temperature (C)	Relative Humidity (%)	Wind speed (m/s)	Air Pressure
8:00	30.4	70%	0.2	0.01003
8:40	30.7	75%	0.31	0.020057
9:20	31.4	77%	0.34	0.03218
10:00	31.7	82%	0.30	0.03407
10:40	32.1	65%	0.05	0.00727
11:20	32.4	60%	0.64	0.0131
12:00	32.9	63%	0.42	0.0272
12:40	31.3	67%	0.26	0.01162
13:20	**31.8**	**64%**	**0.24**	**0.03532**
14:00	31.5	83%	0.15	0.02129
14:40	30.4	62%	0.10	0.01489
15:20	30.2	56%	0.15	0.01854
16:00	29.7	60%	0.10	0.015015
16:40	27.5	62%	0.08	0.00987

Measurement surfaces of windows 4-8-2013

Solar Time	Glazed window (G-1)	Glazed wall (G2)	Glazed window (G-3)
8:00	31.6	31.3	31.6
8:40	34.1	31.8	34.1
9:20	34.6	33.2	34.6
10:00	34.2	34	34.2
10:40	32.5	34.2	32.5
11:20	33.3	33.8	33.3
12:00	33.2	34.3	33.2
12:40	32.3	33.3	32.3
13:20	32.6	33.3	32.6
14:00	32	32.2	32
14:40	31	31.5	31
15:20	30.4	30.3	30.4
16:00	29.8	30.6	29.8
16:40	27.6	28	27.6

Outdoor Measurements (6-/August /2013)

Solar Time	Ambient Temperature (C)	Wind speed (m/s)	Relative Humidity (%)	Solar Irradiance (W/m^2)
8:00	-	-	-	-
8:40	-	-	-	-
9:20	-	-	-	-
10:00	30.0	0.90	71%	497.5
10:40	31.0	0.86	70%	497.6
11:20	33.0	0.79	55%	577.0
12:00	34.1	0.67	52%	512.1
12:40	34.4	0.60	59%	749.1
13:20	**35.4**	0.56	**56%**	**730.3**
14:00	34.8	0.59	50%	486.2
14:40	33.5	0.62	64%	374.3
15:20	34.3	**0.71**	60%	741.1
16:00	32..8	1.10	59%	258.8
16:40	-	-	-	-

Indoor Measurements (6/ August/2013)

Solar Time	Aver. Indoor Temperature (C)	Relative Humidity (%)	Wind speed (m/s)	Air Pressure
8:00	-	-	-	-
8:40	-	-	-	-
9:20	-	-	-	-
10:00	31.8	47%	0.14	0.02202
10:40	31.6	52%	0.11	0.01734
11:20	32.5	41%	0.17	0.02706
12:00	31.8	50%	0.14	0.02257
12:40	32.9	47%	0.12	0.0183
13:20	32.4	61%	0.07	0.00835
14:00	31.2	48%	0.1	0.01415
14:40	30.3	53%	0.25	0.3906
15:20	29.6	62%	0.08	0.00987
16:00	28.7	66%	0.07	0.00898
16:40	-	-	-	-

Measurement surfaces of windows 6-8-2013

Solar Time	**Glazed window (G-1)**	**Glazed wall (G2)**	**Glazed window (G-3)**
8:00			
8:40			
9:20			
10:00	34.2	34	34.2
10:40	32.5	34.2	32.5
11:20	33.3	33.8	33.3
12:00	33.2	34.3	33.2
12:40	32.3	33.3	32.3
13:20	32.6	33.3	32.6
14:00	32	32.2	32
14:40	31	31.5	31
15:20	30.4	30.3	30.4
16:00	29.8	30.6	29.8
16:40			

Outdoor Measurements (8/August/2013)

Solar Time	Ambient Temperature (C)	Wind speed (m/s)	Relative Humidity (%)	Solar Irradiance (W/m^2)
8:00	30.0	0.92	53%	426.9
8:40	32.9	0.91	55%	564.5
9:20	33.4	0.79	53%	679.8
10:00	34.3	0.67	49%	782.1
10:40	36.1	0.60	45%	850.7
11:20	36.5	0.77	46%	789.5
12:00	36.5	0.61	46%	600.5
12:40	37.3	0.80	55%	971.4
13:20	**37.3**	**0.91**	**44%**	**874.8**
14:00	36.3	1.10	41%	635.7
14:40	34.5	0.96	49%	550.1
15:20	33.5	1.00	46%	578.6
16:00	-	-	-	-
16:40	-	-	-	-

Indoor Measurements (8/ August/2013)

Solar Time	Aver. Indoor Temperature (C)	Relative Humidity (%)	Wind speed (m/s)	Air Pressure
8:00	28.4	60%	0.15	0.01324
8:40	30	55%	0.10	0.01112
9:20	31	60%	0.13	0.01864
10:00	32.7	57%	0.15	0.023325
10:40	33.2	58%	0.14	0.03322
11:20	33.1	61%	0.21	0.03359
12:00	33.2	59%	0.38	0.06178
12:40	33.2	62%	0.22	0.03609
13:20	**32.3**	**63%**	**0.22**	**0.03749**
14:00	32.1	64%	0.1	0.01229
14:40	33.5	58%	0.19	0.02762
15:20	32.7	56%	0.16	0.02655
16:00	-	-	-	-
16:40	-	-	-	-

Measurement surfaces of windows 8-8-2013

Solar Time	Glazed window (G-1)	Glazed wall (G2)	Glazed window (G-3)
8:00	32	30.9	31.2
8:40	36.8	34	36.3
9:20	37.1	35.2	36.6
10:00	37.6	36.6	36.8
10:40	37.8	38.2	36.5
11:20	36.8	37.9	37.4
12:00	37	37.9	36.8
12:40	37.9	39.3	38.3
13:20	38.6	38.8	38.1
14:00	37.6	37	36.8
14:40	35.9	35.6	35.1
15:20	34.3	33.6	33.7
16:00			
16:40			

Outdoor Measurements (13/ August/2013)

Solar Time	Ambient Temperature (C)	Wind speed (m/s)	Relative Humidity (%)	Solar Irradiance (W/m^2)
8:00	-	-	-	-
8:40	-	-	-	-
9:20	-	-	-	-
10:00	-	-	-	-
10:40	-	-	-	-
11:20	-	-	-	-
12:00	-	-	-	-
12:40	31.9	0.88	50%	432.0
13:20	31.5	1.09	48%	368.6
14:00	30.6	0.77	61%	268.7
14:40	31.3	0.34	57%	204.3
15:20	29.9	0.31	54%	292.5
16:00	29.7	0.52	53%	193.0
16:40	29.6	0.39	50%	116.4

Indoor Measurements (13/ August/2013)

Solar Time	**Aver. Indoor Temperature (C)**	**Relative Humidity (%)**	**Wind speed (m/s)**	**Air Pressure**
8:00	-	-	-	-
8:40	-	-	-	-
9:20	-	-	-	-
10:00	-	-	-	-
10:40	-	-	-	-
11:20	-	-	-	-
12:00	-	-	-	-
12:40	29.1	70%	0.72	0.06759
13:20	29.3	66%	0.74	0.071682
14:00	29.4	72%	0.61	0.058181
14:40	29.7	72%	0.64	0.052134
15:20	29.4	71%	0.73	0.076372
16:00	28.1	74%	0.77	0.071285
16:40	28.6	70%	0.72	0.06759

Measurement surfaces of windows 13-8-2013

Solar Time	Glazed window (G-1)	Glazed wall (G2)	Glazed window (G-3)
8:00			
8:40			
9:20			
10:00			
10:40			
11:20			
12:00			
12:40	32.5	33.9	32.9
13:20	32.8	33	32.3
14:00	31.9	31.3	31.1
14:40	32.7	32.4	31.9
15:20	30.7	30	30.1
16:00	30.2	30.6	29.8
16:40	29.9	30.1	29.7

Outdoor Measurements (16/ August/2013)

Solar Time	Ambient Temperature (C)	Wind speed (m/s)	Relative Humidity (%)	Solar Irradiance (W/m^2)
8:00	30.8	0.92	64.90	421.1
8:40	31.5	0.91	58.30	564.5
9:20	32.8	0.68	54.40	604.5
10:00	33.4	0.78	57.20	437.6
10:40	34.1	0.68	55.70	433.2
11:20	34.3	0.89	42.70	641.3
12:00	34.5	0.83	38.60	687.3
12:40	34.5	0.94	39.80	675.2
13:20	34.6	0.93	53.40	964.6
14:00	34.1	0.83	52.20	617.1
14:40	33.4	1.11	45.00	839.2
15:20	33.4	0.67	49.90	433.6
16:00	32.7	0.57	60.10	538.8
16:40	31.8	0.64	59.90	418.0

Indoor Measurements (16/ August/2013)

Solar Time	Aver. Indoor Temperature (C)	Relative Humidity (%)	Wind speed (m/s)	Air Pressure
8:00	29.0	58%	0.38	0.02978
8:40	30.1	51%	0.51	0.04730
9:20	30.4	49%	0.25	0.02710
10:00	30.6	45%	0.24	0.02903
10:40	30.9	47%	0.6	0.05784
11:20	31.1	48%	1.08	0.10514
12:00	31.4	46%	0.39	0.05780
12:40	31.4	45%	0.27	0.02899
13:20	30.6	52%	1.12	0.11253
14:00	30.1	44%	0.78	0.07653
14:40	30.5	43%	0.52	0.04965
15:20	29.7	61%	0.32	0.02935
16:00	29.5	58%	0.38	0.02978
16:40	28.7	51%	0.51	0.04730

Measurement surfaces of windows 16-8-2013

Solar Time	Glazed window (G-1)	Glazed wall (G2)	Glazed window (G-3)
8:00	32.8	31.7	32
8:40	35.4	32.6	34.9
9:20	36.1	34.2	35.6
10:00	36.7	35.7	35.9
10:40	36.8	37.2	35.5
11:20	37	38.1	37.6
12:00	36.8	37.7	36.6
12:40	37.3	38.7	37.7
13:20	37.5	37.7	37
14:00	37.2	36.6	36.4
14:40	37.2	36.9	36.4
15:20	34.2	33.5	33.6
16:00	33.7	34.1	33.3
16:40	31.1	31.3	30.9

Outdoor Measurements (20-August-2013)

Solar Time	Ambient Temperature (C)	Wind speed (m/s)	Relative Humidity (%)	Solar Irradiance (W/m^2)
8:00	30.7	0.94	53	287.5
8:40	31.3	0.83	55	303.2
9:20	32.7	0.89	53	488.4
10:00	32.8	0.93	49	405.7
10:40	33.3	0.83	45	412.9
11:20	34.2	0.65	46	825.2
12:00	34.5	0.66	46	674.3
12:40	34.4	0.67	55	802.1
13:20	34.8	0.78	44	905.4
14:00	34.1	0.67	41	847.2
14:40	33.6	0.83	49	226.7
15:20	33.2	0.81	46	641.5
16:00	32.3	1.13	49	158.8
16:40	31.1	0.94	47	155.3

Indoor Measurements (20-August-2013)

Solar Time	Aver. Indoor Temperature (C)	Relative Humidity (%)	Wind speed (m/s)	Air Pressure
8:00	30.4	69%	0.24	0.01048
8:40	30.5	64%	0.14	0.02341
9:20	31.5	54%	0.19	0.03841
10:00	31.5	57%	0.15	0.03552
10:40	31.1	55%	0.22	0.05427
11:20	31.2	57%	0.23	0.05051
12:00	31.2	54%	0.34	0.02541
12:40	31.3	57%	0.20	0.04741
13:20	31.3	60%	0.15	0.03671
14:00	31.2	65%	0.32	0.02441
14:40	31.2	64%	0.2	0.02234
15:20	31.0	70%	0.27	0.01254
16:00	30.2	75%	0.09	0.01048
16:40	29.5	69%	0.14	0.01048

Measurement surfaces of windows 20-8-2013

Solar Time	Glazed window (G-1)	Glazed wall (G2)	Glazed window (G-3)
8:00	32.71	31.61	31.91
8:40	35.2	32.4	34.7
9:20	35.4	33.5	34.9
10:00	35.1	34.1	34.3
10:40	35	35.4	33.7
11:20	35.2	36.3	35.8
12:00	36	36.9	35.8
12:40	36.4	37.8	36.8
13:20	37.6	37.8	37.1
14:00	36.7	36.1	35.9
14:40	33	32.7	32.2
15:20	34	33.3	33.4
16:00	31.8	32.2	31.4
16:40	31.4	31.6	31.2

APPENDIX F

Data of models

Cases	Dimensional H x W	Total Size of one window (m)	Size of two window (m)	WWR (%)	WFR (%)	Temperature K	Velocity (m/s)	Difference Temperature
A	1.5 x 0.3	0.6	1.2	12%	11%	302.7	0.07	4.9
A	1.5 x 0.5	0.75	1.5	20%	14%	302.9	0.07	4.7
C	1.5 x 0.8	1.2	2.4	32%	22%	303.7	0.07	4.5
A	1.5 x 1.05	1.6	3.2	43%	30%	303.5	0.07	3.4
B	1.5 x 0.3	0.6	1.2	12%	11%	303.3	0.08	4.2
C	1.5 x 0.5	0.75	1.5	20%	14%	303.4	0.07	4.2
A	1.5 x 0.8	1.2	2.4	32%	22%	303.1	0.08	4.0
B	1.5 x 1.05	1.6	3.2	43%	30%	304.0	0.08	3.6
C	1.5 x 0.3	0.6	1.2	12%	11%	303.5	0.09	3.7
A	1.5 x 0.5	0.75	1.5	20%	14%	302.9	0.09	3.5
B	1.5 x 0.8	1.2	2.4	32%	22%	302.8	0.09	5.4
C	1.5 x 1.05	1.6	3.2	43%	30%	304.1	0.09	3.2
A	2x 0.4	0.8	1.6	22%	15%	300.8	0.07	6.8
B	2x 0.6	1.2	2.4	32%	14%	303.8	0.07	4.0
C	2x 0.8	1.6	3.2	43%	22%	303.7	0.07	6.7
A	2x 1.0	2	4	54%	37%	302.4	0.08	5.1
B	2x 0.4	0.8	1.6	22%	15%	301.5	0.08	5.3
C	2x 0.6	1.2	2.4	32%	14%	303.3	0.08	3.8
A	2x 0.8	1.6	3.2	43%	22%	303.9	0.08	3.5
B	2x 1.0	2	4	54%	37%	303.1	0.09	4.0
C	2x 0.4	0.8	1.6	22%	15%	301.5	0.08	6.1
A	2x 0.6	1.2	2.4	32%	22%	303.8	0.09	4.9
B	2x 0.8	1.6	3.2	43%	22%	303.5	0.09	4.9
C	2x 1.0	2	4	54%	37%	304.1	0.08	3.5
A	2.5x0.5	1.25	2.5	43%	23%	303.9	0.07	5.0
B	2.5x0.75	1.9	3.8	51%	35%	303.8	0.08	3.5
C	2.5x 1.0	2.5	5	67%	46%	303.3	0.08	5.0
A	2.5x 1.25	3	3.2	84%	30%	303.0	0.08	4.6
B	2.5x0.5	1.25	2.5	43%	23%	303.5	0.08	4.1
C	2.5x0.75	1.9	3.8	51%	35%	303.9	0.08	4.1
A	2.5x 1.0	2.5	5	67%	46%	302.6	0.10	3.9
B	2.5x 1.25	3	6	84%	30%	303.8	0.11	4.3
C	2.5x0.5	1.25	2.5	43%	23%	303.3	0.10	4.3
A	2.5x0.75	1.9	3.8	51%	35%	303.5	0.11	3.7
B	2.5x 1.0	2.5	5	67%	46%	303.6	0.10	3.8
C	2.5x 1.25	3	3.2	84%	30%	303.7	0.11	3.8

Distribution air Temperature in Office (CFD)

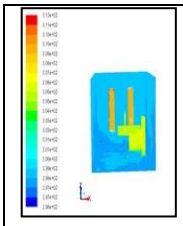	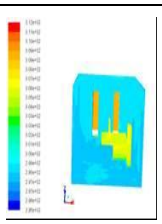	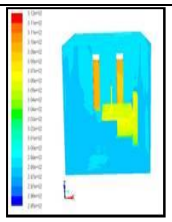	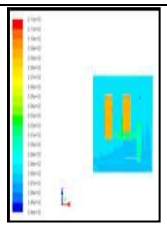	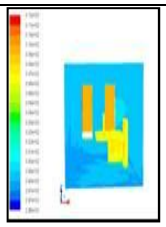	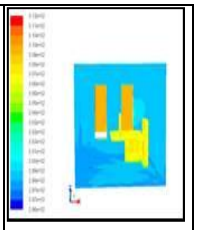
Model-7 Ahead Open (H.W) 1.5 x 0.8	**Model-8** Top Open (H.W) 1.5 x 0.8	**Model-9** Bottom Open (H.W) 1.5 x 0.8	**Model-10** Ahead Open (H.W)1.5 x 1.05	**Model-11** Top Open (H.W)1.5 x 1.05	**Model-12** Bottom Open (H.W)1.5 x 1.05
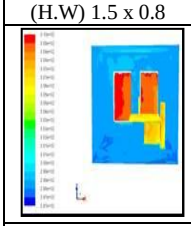	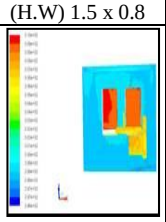	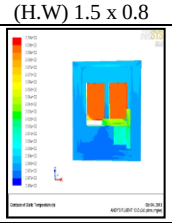	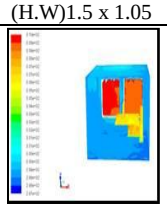	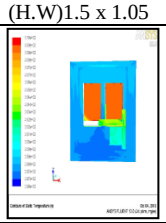	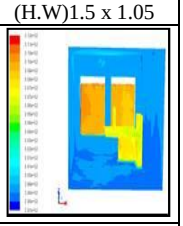
Model-13 Ahead Open (H.W) 2 x 0.4	**Model-14** Top Open (H.W) 2 x 0.4	**Model-15** Bottom Open (H.W) 2 x 0.4	**Model-16** Ahead Open (H.W) 2 x 0.6	**Model-17** Top Open (H.W) 2 x 0.6	**Model-18** Bottom Open (H.W) 2 x 0.6
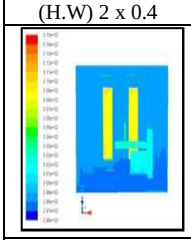	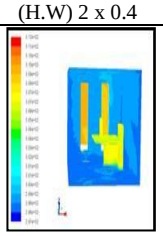	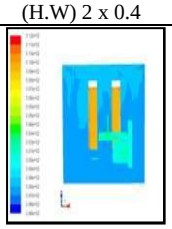	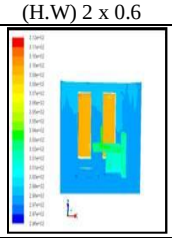	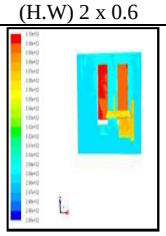	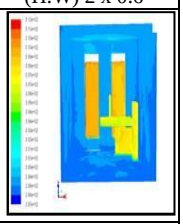
Model-19 Ahead Open (H.W) 2 x 0.8	**Model-20** Top Open (H.W) 2 x 0.8	**Model-21** Bottom Open (H.W) 2 x 0.8	**Model-22** Ahead Open (H.W) 2 x 1.0	**Model-23** Top Open (H.W) 2 x 1.0	**Model-24** Bottom Open (H.W) 2 x 1.0
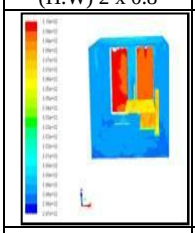	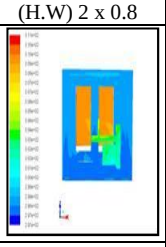	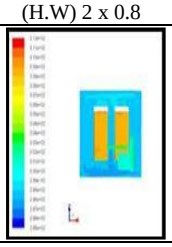	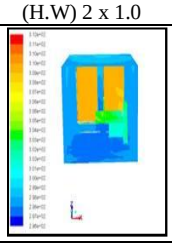	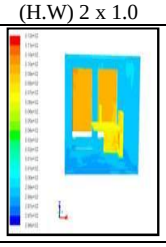	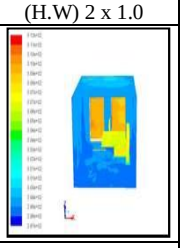
Model-25 Ahead Open (H.W) 2.5 x 0.5	**Model-26** Top Open (H.W) 2.5 x 0.5	**Model-27** Bottom Open (H.W) 2.5 x 0.5	**Model-28** Ahead Open (H.W) 2.5 x 0.75	**Model-29** Top Open (H.W) 2.5 x 0.75	**Model-30** Bottom Open (H.W) 2.5 x 0.75
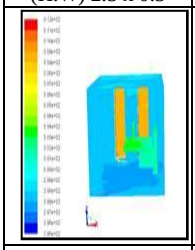	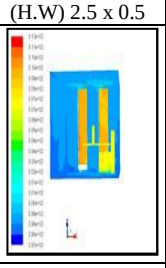	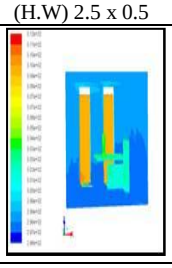	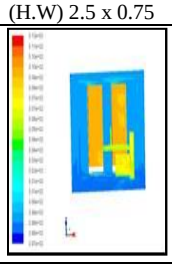	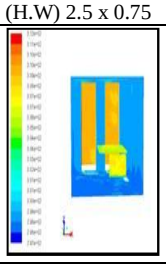	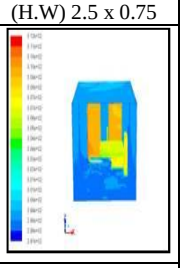
Model-31 Ahead Open (H.W) 2.5 x 1.0	**Model-32** Ahead Open (H.W) 2.5 x 1.0	**Model-33** Top Open (H.W) 2.5 x 1.0	**Model-34** Ahead Open (H.W) 2.5 x 1.25	**Model-35** Top Open (H.W) 2.5 x 1.25	**Model-36** Bottom Open (H.W) 2.5 x 1.25
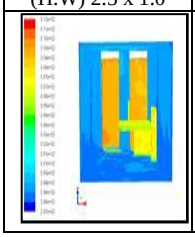	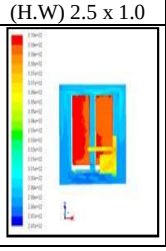	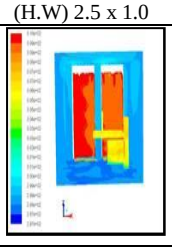	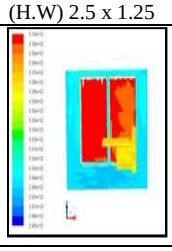	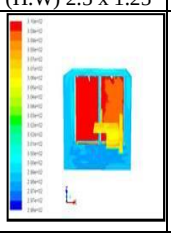	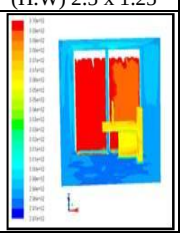

APPENDIX G

Table 5.4: The outdoor Measurements (22-August-2013)

Solar Time	Ambient Temperature (C)	Wind speed (m/s)	Relative Humidity (%)	Solar Irradiance (W/m^2)
8:00	30.5	0.83	55	201.4
8:40	30.7	0.89	53	203.2
9:20	31.5	0.93	49	388.4
10:00	31.3	0.83	45	405.7
10:40	31.7	0.65	46	412.9
11:20	32.4	0.66	46	525.2
12:00	32.8	0.67	55	674.3
12:40	33.7	0.78	44	702.1
13:20	34.6	0.67	41	750.4
14:00	34.1	0.83	49	840.2
14:40	33.2	0.81	46	726.7
15:20	33.6	1.13	49	441.5
16:00	32.7	0.94	47	358.8
16:40	32.4	0.94	53	255.3

External Convection Heat Transfer Coefficient and Heat Flux near wall glazed window (22-Aug.2013)

Solar Time	Heat transfer coefficient (outer surface)	Heat flux (outer surfaces)
8:00	11.5	10
8:40	12.3	13
9:20	14.3	26
10:00	15.4	35
10:40	15.0	31
11:20	13.2	18
12:00	12.9	18
12:40	14.4	29
13:20	13.2	20
14:00	10.4	7
14:40	13.2	20
15:20	11.3	10
16:00	11.3	10
16:40	9.4	5

APPENDIX H

PMV = [0.303.exp (-0.036.M) + 0.028].
$\{(M - W) - 3.05\ 10^{-3} . [5733 - 6.99\ (M - W) - p_a]$
$- 0.42\ [M - W) - 58.15]\} - 1.7 . 10^{-5}\ M\ (5868 - p_a)$
$- 0.0014 . M\ (34 - t_a) - 3.96 .\ 10^{-8} . f_{cl}[(t_{cl} + 273)^4$
$- (t_r + 273)^4] - f_{cl} . h_c . (t_{cl} - t_a)]$
t_{cl} = 35.7 – 0.028(M-W) - I_{cl} {3.96. 10^{-8} . f_{cl} [$(t_{cl} + 273)^4$
$- (t_r + 273)^4$] + f_{cl} . h_c $(t_{cl}$ - t_a)}

PDD = 100 -95. Exp (-0.03353 PMV^4 – 0.2179..PVM^2)

Metabolic rates of different activities

Activity	Metabolic rate	
	W/m^2	met
Reclining	46	0.8
Seated, relaxed	58	1.0
Standing relaxed	70	1.2
Sedentary activity (Office, dwelling, school;. laboratory	70	1.2
Standing, light activity (shopping, laboratory, light industry	93	1.6
Standing, medium activity (shop assistant, domestic work, machine work	116	2.0

Thermal insulation

Ensemble Description	I_{cl} (clo)
Walking shorts, short-sleeved shirt	0.36
Trousers, short-sleeved shirt	0.57
Trousers, long-sleeved shirt	0.61
Same as above, plus suit jacket	0.96
Same as above, plus vest and T-shirt	0.96
Trousers, long-sleeved shirt, long-sleeved sweater, T-shirt	1.01
Same as above, plus suit jacket and long underwear bottoms	1.30
Sweat pants, sweat shirt	0.74
Long-sleeved pajama top, long pajama trousers, short 3/4 sleeved robe, slippers	0.96
Knee-length skirt, short-sleeved shirt, panty hose, sandals	0.54
Knee-length skirt, long-sleeved shirt, full slip, panty hose	0.67
Knee-length skirt, long-sleeved shirt, half slip, panty hose, long-sleeved sweater	1.10
Knee-length skirt, long-sleeved shirt, half slip, panty hose, suit jacket	1.04
Ankle-length skirt, long-sleeved shirt, suit jacket, panty hose	1.10
Long-sleeved coveralls, T-shirt	0.72
Overalls, long-sleeved shirt, T-shirt	0.89
Insulated coveralls, long-sleeved thermal underwear, long underwear bottoms	1.37

Excel equations of models:

The temperature (T) with (ahead) opening is

$$Y = 0.185\ WWR + 301.7$$

The air velocity (v) with (Ahead) opening was,

$$Y = 7E\text{-}0.6\ WWR + 0.0075$$

The temperature (T) with (top) opening is

$$Y = 0.117\ WWR + 302.7$$

The air velocity (v) with (top) opening is

$$Y = -0.0001\ WWR + 0.0083$$

The temperature (T) with (bottom) opening is

$$Y = 0.1336\ WWR + 302.6$$

The air velocity (v) with (bottom) opening is

$$Y = -0.00009\ WWR + 0.0833$$

Generalized model such as $f_{1=(T,V,e)}$ and multiple equations of temperature and velocity

Ahead, $T.V = WWR^2\ (0.0000013) + (22.6)$
Top $T.V = WWR^2\ (0.000012) + (25.1)$
Bottom $T.V = WWR^2\ (0.00012) + (26.3)$

BIODATA OF STUDENT

Ali Mohamed A. Wahhad was born in Tripoli, Libya on 26th May 1963. He completed his primary school, secondary school in Libya, and high school education in Libya. The B.Sc Degree was completed in Naval Academy-Split-Yugoslavia from1982-1988, specialization marine Engineering (Mechanics Department). From 1988 to 1993 was Assistant mechanical engineer in maintenance Basin. From 1993 to 1997 was Assistant Mechanical engineer in the ship. From 1997 to end 2003 was a responsible marine engineer student inside and outside Libya. In 5th January 2003, he traveled to Malaysia and joined to ELS Institute for ten months. Then he gets permeation to continue his study in Mechanical Engineering in Master of Science at Universiti Putra Malaysia on January 2004-2007. He continued his high study (PhD) in same a university from 2010 until now.

LIST OF PUBLICATIONS

A.M. Whaad, N.M. Adam, S.M. Sapuan and R.Saidur) 2010), EFFECT OF SELECTED SHADING DEVICES ON OFFICE ROOM TEMPERATURE, International Journal of Mechanical and Materials Engineering (IJMME), Vol.5 (2010), No.2, 236-243

Ali M. Wahhad, Nor Mariah Adam, Mohd S. Salit and Ahmed A. Alarabi (2011), EVALUATING THE THERMAL PERFORMANCE OF GLAZED WINDOWS IN WARM-HUMID CLIMATE, GCREEDER 2011, Amman-Jordan, April 26th – 28th 2011

Ali M. Wahhad, Nor Mariah Adam, S. M. Sapuan and Fatah Omran Al Ghuol (2014), MODERN OFFICE BUILDINGS IN A DESERT CLIMATE, Journal of Food, Agriculture & Environment Vol.12 (2): PP.1 1 5 3 - 1 1 5 8. (2 0 1 4)

A.M. Wahhad[1], N. M. Adam[1] and S.M. Sapuan[1,2*] COMPARISON OF NUMERICAL SIMULATION AND EXPERIMENTAL STUDY ON AIR IN DOOR QUALITY OF AIR-CONDITIONED OFFICE BUILDING IN DESERT CLIMATE. International Journal of Automotive and Mechanical Engineering (IJAME), ISSN: 2229-8649 (Print); ISSN: 2180-1606 Volume 12, pp. 3109-3124, July-December 2015

Fatah Omran Al Ghuol*, Kamaruzzaman Sopian Shahrir Abdullah and Ali M. Wahhad PREDICTION OF SPHERICAL PHASE CHANGE MATERIAL TEMPERATURE USING RBFNN MODEL. Applied Mechanics and Materials Vol. 704 (2015) pp. 63-69 Submitted: 21.10.2014 (2015)

Fatah. O. A Ghuol[1] ,K. Sopian[1] , Shahrir Abdullah[1] , Mohammed Al – Ghoul[1] & Ali Whaad[2] . HEAT TRANSFER ENHANCEMENT TECHNIQUES FOR SOLAR AIR COLLECTOR HEAT: Review. Modern Applied Science, Vol.9 No 9, 2015, ISSN 1913-1844

UNIVERSITI PUTRA MALAYSIA

STATUS CONFIRMATION FOR THESIS / PROJECT REPORT AND COPYRIGHT

ACADEMIC SESSION : _____

TITLE OF THESIS / PROJECT REPORT :

DEVELOPMENT OF OPTIMUM WINDOW SIZE IN TROPICAL CLIMATE USING COMPUTATIONAL FLUID DYNAMICS AND EXPERIMENTAL WORKS

NAME OF STUDENT: ALI MOHAMED WAHHAD

I acknowledge that the copyright and other intellectual property in the thesis/project report belonged to Universiti Putra Malaysia and I agree to allow this thesis/project report to be placed at the library under the following terms:

1. This thesis/project report is the property of Universiti Putra Malaysia.
2. The library of Universiti Putra Malaysia has the right to make copies for educational purposes only.
3. The library of Universiti Putra Malaysia is allowed to make copies of this thesis for academic exchange.

I declare that this thesis is classified as :

*Please tick (√)

☐ **CONFIDENTIAL**	(Contain confidential information under Official Secret Act 1972).
☐ **RESTRICTED**	(Contains restricted information as specified by the organization/institution where research was done).
☐ **OPEN ACCESS**	I agree that my thesis/project report to be published as hard copy or online open access.

This thesis is submitted for :

☐ **PATENT** Embargo from _____ (date) until _____ (date)

Approved by:

_____	_____
(Signature of Student)	(Signature of Chairman of Supervisory Committee)
New IC No/ Passport No.:	Name:
Date :	Date :

[Note : If the thesis is CONFIDENTIAL or RESTRICTED, please attach with the letter from the organization/institution with period and reasons for confidentially or restricted.]